

**Polymer Sensors and Actuators:  
Synthesis and Characterization of  
Polythiophenes Modified with  
Benzospiropyran Derivatives**

Michele Zandoni M.Sc.

Thesis submitted for the Degree of Doctor of Philosophy

Supervisor: Professor Dermot Diamond



School of Chemical Sciences

Dublin City University

*Ad Alessandra,  
sole e gioia della mia vita!  
Ai miei genitori e a mia nonna,  
da sempre e per sempre miei sostenitori*

***All the interests of my reason, speculative as well as practical, combine in  
the three following questions: 1. What can I know? 2. What ought I to  
do? 3. What may I hope?***

***Immanuel Kant***

I hereby certify that this material, which I now submit for assessment on the programme of study leading to the award of the Degree of Doctor of Philosophy is entirely my own work, and that I have exercised reasonable care to ensure that the work is original, and does not to the best of my knowledge breach any law of copyright, and has not been taken from the work of others save and to the extent that such work has been cited and acknowledged within the text of my work.

Signed: \_\_\_\_\_ (Candidate) ID No.: 58114149\_ Date: \_\_\_\_\_

## General Declaration

I hereby declare that this thesis contains no material which has been accepted for the award of any other degree or diploma at any university or equivalent institution and that, to the best of my knowledge and belief, this thesis contains no material previously published or written by another person, except where due reference is made in the text of the thesis.

This thesis includes 4 original manuscripts published in peer-reviewed journals and 1 manuscript in preparation. The core theme of the thesis is the preparation of a new family of spiropyran-functionalised poly-thiophenes. The ideas, development and writing up of all the manuscripts in the thesis were the principal responsibility of myself, the candidate, working within the School of Chemistry under the supervision of Professor Dermot Diamond.

The inclusion of co-authors reflects the fact that the work came from active collaboration between researchers and Universities and acknowledges input into team-based research. For each of the chapters presented, the main contributions of the collaborators are as follows:

1. **Chapter 2** the synthesis of the terthiophene derivatives, of the first spiropyran-terthiophene (BSP2) and the polymerization was firstly done at IPRI, University of Wollongong, New South Wales, Australia by local experts, and then repeated at DCU. The spectrochemical characterization and the photochemistry were equally divided between DCU and IPRI.
2. **Chapter 3** IPRI researchers synthesised terthiophene while the novel spiropyran molecule (BSP3) was prepared at DCU by the candidate. All spectroscopy and characterization was completed at DCU.
3. **Chapter 4** the AFM tip was functionalized at IPRI and all experiments were devised and performed in close collaboration with the local experts during the first research visit of the candidate at IPRI.
4. The molecule presented in **Chapter 5** (TSP4) was initially prepared in IPRI and then characterized by means of spectroscopy in the laboratories of DCU.
5. **Chapter 6** the molecule called BSP6 was firstly isolated in IPRI. The other spiropyran derivatives (BSPe and BSP7) were prepared and analysed by the candidate at DCU. The electrochemical analysis and spectroscopy were carried out at DCU. All the protonation study and kinetics were done at DCU.

In the case of Chapters Two, Three, Four, Five and Six my contribution to the work involved the following:

<b>Thesis chapter</b>	<b>Publication title</b>	<b>Publication status</b>	<b>Nature and extent of candidate's contribution</b>
2	A Multiswitchable Poly(terthiophene) Bearing a Spiropyran Functionality: Understanding Photo- and Electrochemical Control	Published. JACS 2011	Co-Author, data collection and analysis, manuscript development.
3	Physicochemical Study of Spiropyran-terthiophene Derivatives: Photochemistry and Thermodynamics	Published. PCCP, 2012	First Author, initiation, manuscript development Data collection / analysis.
4	Optical switching of protein interactions on photosensitive–electroactive polymers measured by atomic force microscopy	Published. J. Mat. Chem. B, 2013	Co-Author, initiation, key ideas, experimental design, data collection and analysis, manuscript development and writing up.
5	A merocyanine-based conducting polymer	Published. J. Mat. Chem. C Comm. 2013	Co-Author, data collection and analysis, manuscript development.
6	New class of spiropyran-terthiophene multi-switches: photochromic, halochromic and electrochromic properties	In preparation, 2013	First Author, initiation, key ideas, experimental design, data collection and analysis, manuscript development and writing up.

**Signed:** ..... **Date:**.....

Mr. Michele Zandoni, ID No.: 58114149

**Signed:** ..... **Date:**.....

Professor Dermot Diamond

## Acknowledgements

The past years in Dublin and in particular here at DCU have been fantastic, rich of fun and scientifically challenging. This experience has been incredible and precious for my personal formation. For these reasons there are a lot of people that I would like to thank and I would like to begin with the people that contributed to this project.

First of all, I would like to thank Prof. Dermot Diamond for all his help and support during the last 4 years, because in each brain storming session and during the months in Australia, his constant support, his valuable contribution and his hilarious spirit have been a strong motivation to complete this challenge. Thank you for your advice and for giving me the opportunity to grow as a scientist and a critical researcher.

I owe the same gratitude to Dr. Kevin J. Fraser, who became a friend and assisted me in the bad moments of these years and contributed massively to the completion of my work. A special thank goes to Dr. Robert Byrne, because the starting ideas of this project came from his Formula 1 powered brain.

I would like to gratefully thank all the people I met in Australia during my permanence at the Intelligent Polymer Research Institute, University of Wollongong. In particular a special thank goes to Prof. Gordon G. Wallace, because he has always supported and welcomed me in his institute like a member of the team. Special thanks go to Prof. David L. Officer for his priceless scientific support and for being a guide during these years of strong collaboration. Another big thanks goes to Dr. Klaudia and Pawel Wagner, because you are the most awesome couple of scientists I have ever met. I want to thank also Dr. Sanjeev Gambhir for the work you put into this project. It was a privilege to collaborate and learn from you guys. I cannot forget to thank Dr. Stephen Beirne and his wife Sara, because our friendship will go much further than this PhD (luckily!). Thank you Robin, because it is very rare to meet somebody so enthusiastic of his job and at the same time so nice with the other people. I hope that our little research project will be a winner one! During my stay there I had also many memorable moments with lots of people: Joseph, Mark, Gia, Eoin, Paul, Bin-Bin, Amy, Peter, Julia, Andy and Enrico.

My years here at DCU would not be the same without my lab mates and all the people of the ASG group, but a particular thank goes to all the guys of the SG07 crew: Bartosz, Monika, Vincenzo, Mercedes, Giusy, Claudio, Andy, Simon Gallagher, Simon Coleman, Silvia, Larisa and our internal students Aoife, Aoibheann, Sinead, Raffaella,

Marcela, Stephane, Jannick, Nuria, Isabel, Sergio and Mathilde. Our laughter's and our jokes together are unbeatable and unforgettable. A big thanks goes also to all the people of N205 (Deirdre, Cormac, Dylan, Tom, Fiachra, Eoghan, John and Damien).

A huge thanks goes to my Italian friends, because even if I was here in Ireland they did not forget about me and in particular Matteo and Lavinia, Andrea, Maurizio, Giovanni and Alice, Tommy and Enrica, Federico and Natalia, Stefano and Alice, Claudio and Laura, Andrea and Elisa, Enrico, Manlio and Vincenzo. I will always be there for you!

Un grazie speciale va ai miei amici italiani, perchè anche se ero qui in Irlanda non vi siete mai dimenticati di me ed in particolare Matteo e Lavinia, Andrea, Maurizio, Giovanni and Alice, Tommy ed Enrica, Federico e Natalia, Stefano ed Alice, Claudio e Laura, Andrea ed Elisa, Enrico, Manlio e Vincenzo. Io ci sarò sempre per voi!

A big, huge, massive thanks goes to my family: to my grandmother Pina, my mother Sergia and my father Maurizio because you always supported me during my travels and for my efforts. A big thanks goes to my uncles, my aunts and my cousins, but in particular my aunt Celeste and my cousins Lorenzo (with Silvia), Elettra (with Giovanni), Niccolò, Irene, Cecilia, Erica, Gabriele, Chiara, Laura, Daniela and Marco. You are the best family I could ever dream! A special thanks to Alessandro and Angiolina for your support, you are the wonderful family of my only love!

Un immenso e grandissimo grazie va alla mia famiglia: a mia nonna Pina, mia mamma Sergia e a mio papà Maurizio, perchè mi avete sempre supportato durante i miei viaggi e nei miei sforzi. Un grosso grazie va anche ai miei zii, e ai parenti tutti, ma in particolare a mia zia Celeste e ai miei cugini Lorenzo (con Silvia), Elettra (con Giovanni), Niccolò, Irene, Cecilia, Erica, Gabriele, Chiara, Laura, Daniela e Marco. Siete la migliore famiglia che si possa desiderare. Un grazie speciale ad Alessandro ed Angiolina per il vostro aiuto, siete i genitori stupendi del mio unico amore!

The principal thanks goes to the most important person of my life, my wonderful fiancée Alessandra. You are my first my last, my everything, I thank every moment we are spending together! The tomorrow belongs to us. I love you my life!

Il mio ringraziamento principale va alla persona più importante della mia vita, la mia splendida fidanzata Alessandra. Sei tutto per me e ringrazio ogni momento che viviamo insieme! Il domani appartiene a noi! Ti amo mia vita!

**Thanks to all of you!**

## List of Publications:

### Peer-Reviewed Journal Articles:

[6] M. Zanoni, K. Wagner, R. Byrne, S. Gambhir, K.J. Fraser, P. Wagner, G. G. Wallace, D. L. Officer and D. Diamond, "Spiropyran-Terthiophene multi-modal molecular switches: photochromic, acidochromic and electrochromic properties", *In preparation June 2013*.

[5] K. Wagner, M. Zanoni, A.B.S. Elliott, P. Wagner, R. Byrne, L.E. Florea, D. Diamond, K.C. Gordon, G.G. Wallace, D.L. Officer, "A merocyanine-based conducting polymer", *Journal of Material Chemistry C*, **2013**, 10.1039/c3tc30479e.

[4] A. Gelmi, M. Zanoni, M.J. Higgins, S. Gambhir, D.L. Officer, D. Diamond and G.G. Wallace, "Optical switching of protein interactions on photosensitive–electroactive polymers measured by atomic force microscopy", *Journal of Material Chemistry B*, **2013**, 1 (16), 2162–2168.

[3] M. Zanoni, S. Coleman, K.J. Fraser, R. Byrne, K. Wagner, S. Gambhir, D. L. Officer, G. G. Wallace and D. Diamond, "Physicochemical Study of Spiropyran-terthiophene Derivatives: Photochemistry and Thermodynamics", *Physical Chemistry Chemical Physics*, **2012**, 14, 9112-9120.

[2] K. Wagner, R. Byrne, M. Zanoni, S. Gambhir, L. Dennany, R. Breukers, M. Higgins, P. Wagner, D. Diamond, G.G. Wallace, and D.L. Officer, "A Multiswitchable Poly(terthiophene) Bearing a Spiropyran Functionality: Understanding Photo- and Electrochemical Control", *Journal of the American Chemical Society*, **2011**, 133 (14), 5453–5462.

[1] A. Jaina, G. Gazzola, A. Panzera, M. Zanoni, E. Marsili, "Visible spectroelectrochemical characterization of *Geobacter sulfurreducens* biofilms on optically transparent indium tin oxide electrode", *Electrochimica Acta*, **2011**, 56 (28), 10776-10785.

## **Conference Contributions:**

### **Oral Presentations:**

[4] *Dual Control Molecular Switches: a Journey into the Nanoworld of Spiropyran-Functionalized Terthiophene Polymers*, Michele Zanoni, Klaudia Wagner, Amy Gelmi, Michael Higgins, Pawel Wagner, Sanjeev Gambhir, Gordon G. Wallace, David L. Officer, and Dermot Diamond, ACES meeting, 13-15 February **2013**, iC Science Centre, University of Wollongong, NSW, Australia.

[3] *Mutli Modal Stimuli Responsive Molecular Switches*, M. Zanoni, K.J. Fraser, K. Wagner, R. Byrne, S. Gambhir, A. Gelmi, P. Molino, M. Higgins, P. Wagner, G.G. Wallace, D.L. Officer, and D. Diamond, CIMTEC 2012 4th International Conference Smart Materials Structures Systems, 10-13 June **2012**, Montecatini Terme (PT), Italy.

[2] *Spiropyran – Terthiophene Polymers as Multi – Stimuli – Responsive Platforms for Biochemical Interactions*, M. Zanoni, A. Gelmi, M. Higgins, K.J. Fraser, R. Byrne, K. Wagner, S. Gambhir, D.L. Officer, G.G. Wallace, D. Diamond, conference oral presentation at the Materials Research Society (MRS) Spring Meeting **2012**, April 9-13 2012, San Francisco, California, USA

[1] *Physico-Chemical Properties of New Stimuli Responsive Molecular Switches*. M. Zanoni, R. Byrne, K. Wagner, S. Gambhir, L. Dennany, R. Breukers, M. Higgins, P. Wagner, D.L. Officer, G.G. Wallace, and D. Diamond, 63<sup>rd</sup> Chemistry Colloquium 24th June **2011**, UCD, Dublin, Ireland.

### **Poster Presentations:**

[5] *Dual Control Molecular Switches: a Journey into the Nanoworld of Spiropyran-Functionalized Terthiophene Polymers*, Michele Zanoni, Klaudia Wagner, Amy Gelmi, Michael Higgins, Pawel Wagner, Sanjeev Gambhir, Gordon G. Wallace, David L. Officer <sup>b</sup>, and Dermot Diamond, ACES meeting, 13-15 February **2013**, iC Science Centre, University of Wollongong, NSW, Australia.

[4] *Dual-Control Molecular Actuators for Biomedical Applications*. M. Zanoni, R. Byrne, M.J. Higgins, A. Gelmi, P. Molino, S. Beirne, K. Wagner, P. Wagner, S. Gambhir, D.L. Officer, G.G. Wallace and D. Diamond. ACES meeting, 9-11 February **2011**, iC Science Centre, University of Wollongong, NSW, Australia.

[3] *Electrochromic Properties of Spiropyran-Terthiophene adaptive polymers*. M. Zanoni, R. Byrne, D. Diamond. MACRO-2010 RSC Conference in Glasgow, 12-16 July **2010**, Glasgow (UK).

[2] *Spiropyran and Thiophene Hybrid Materials: the New Frontier for Sensor Compounds*. M. Zanoni, R. Byrne, D. Diamond. EMRS European Materials Research Society, 7-11 June **2010**, Strasbourg (F).

[1] *Photo/Electro – Responsive Hybrid Materials Based on Spiropyran Dyes and Terthiophene*. M. Zanoni, R. Breukers, R. Byrne, G. Wallace, D.L. Officer and D. Diamond, SPIE Smart Structures/NDE 2010, 7-11 March **2010**, San Diego, Cal. (USA).

#### **Awards:**

[1] Outstanding Oral Presentation at 63<sup>rd</sup> Chemistry Colloquium 2011, UCD, Dublin, Ireland for the presentation titled *Physico-Chemical Properties of New Stimuli Responsive Molecular Switches*.

#### **Collaborations:**

##### **[2] Applications of Terthiophene-Spiropyran Polymers into Portable Analytical Devices.**

Intelligent Polymer Research Institute, University of Wollongong, Australia, *January – March 2013 (8 weeks)*.

##### **[1] Investigations on Terthiophene Inherently Conducting Polymers Doped with Spiropyran Derivatives: Surface Study and Biochemical Interactions.**

Intelligent Polymer Research Institute, University of Wollongong, Australia, *November – February (2010 – 2011, 12 weeks)*.

## Abstract

The aim of this thesis is to understand the basic physico/chemical behaviour of novel nitrospiropyran-substituted-(poly)terthiophene materials. Attractive characteristics that distinguish these materials include electrochemical/photochemical-switching processes. Understanding the fundamental behaviour of these new derivatives is the key to taking advantage of these characteristics. The stimuli induced isomerisation between the colourless spiropyran and the highly coloured merocyanine is the key-process studied in this research.

**Chapter 2** reports the electrochromic behaviour of spiropyran, through irreversible electrooxidative isomerisation in at least two merocyanine isomers. The molecular photophysical processes of the electrochemically-generated polymer are reported and the properties studied.

In **Chapter 3** a new monomer, which differs by a single methylene group in the linking ester-linker functionality from the previous one, will be introduced. A nitrospiropyran was used as a reference, and a detailed spectroscopy analysis will help in the description of the thermodynamic properties.

**Chapter 4** highlights how the polymeric molecular switches can bind an important extracellular protein, fibronectin, and explores by means of microscopy the on-demand tuning of the protein adhesion.

A new derivative is presented in **Chapter 5**, wherein a spiropyran moiety is intercalated between two thiophenes. The electrochemical and optical switching of the spiropyran and thiophene groups were investigated.

In **Chapter 6** three new spiropyran-based derivatives are presented, and routes to multi-modal switching behavior are explored via photochemical, electrochemical and chemical stimuli, such as pH. Their reversibility and their properties are investigated using both spectroscopic and electroanalytical methods.

The final chapter outlines future work and initial progress related to the integration of spiropyran-thiophene polymers into photo-electro active portable analytical devices.

## List of Abbreviations

3-EDSPA	3-ethoxydimethylsilylamine
Acet	Acetone
ACN	Acetonitrile
AcTTh	4,4''-didecyloxy-2,2':5',2''-terthiophene-3'-acetic acid <b>(Chapters 3 and 6)</b>
AFM	Atomic Force Microscopy
APS	Ammonium persulfate
BDMC	Merocyanine isomer of Bis(dithiophene)-substituted spiropyran
BDSP	Bis(dithiophene)-substituted spiropyran
BSP	General abbreviation for 'Benzospiropyran'
BSP1	1-(2-hydroxyethyl)-3,3-dimethylindoline-6'- nitrobenzospiropyran
BSP2	2-(3,3''-Dimethylindoline-6'- nitrobenzospiropyranylethyl)4,4''-didecyloxy-2,2':5',2''- terthiophene-3'-acetate
BSP3	Ethyl (3,3''-dimethylindoline-6'-nitrobenzospiropyranylethyl)- 4,4''-didecyloxy-2,2':5',2''-terthiophene-3'carboxylate
BSP5	1-(2-hydroxyethyl)-3,3-dimethylindoline-6'- hydroxylspiropyran
BSP6	1',3',3'-trimethylspiro(chromene-2,2'-indolin)-6-yl-4,4''- bis(decyloxy)-(2,2':5',2''-terthiophene))-3'-acetate
BSP7	1',3',3'-trimethylspiro[chromene-2,2'-indolin]-6-yl-4,4''- bis(decyloxy)-(2,2':5',2''-terthiophene))-3'-carboxylate
BSPe	1',3',3'-trimethylspiro(chromene-2,2'-indolin)-6-yl acetate
CbTTh	4,4''-didecyloxy-2,2':5',2''-terthiophene-3'-carboxylic acid <b>(Chapters 3 and 6)</b>
CDCl <sub>3</sub>	deuterated-Chloroform
CP	Conducting Polymer
CuCN	Copper Cyanide
CV	Cyclic Voltammetry
DAPI	4',6'-Diamidino-2-Phenylindole

DCC	Dicyclohexylcarbodiimide
DCM	Dichloromethane
DFT	Density Functional Theory Calculations
DMAP	4-(Dimethylamino)pyridine
DMF	Dimethylformamide
$\Delta G^\ddagger$	Variation of the Gibbs free Energy of the transition state
$\Delta H^\ddagger$	Variation of Enthalpy of the transition state
$\Delta S^\ddagger$	Variation of Entropy of the transition state
$E_a$	Activation Energy
ECHs	Electrochemically Conductive Hydrogels
ET(30)	Empirical Values of Solvent Polarity
Et <sub>2</sub> O	Diethyl Ether
EtOH	Ethanol
FN	Fibronectin
FTIR	Fourier Transform Infrared spectroscopy
FT-Raman	Fourier Transform Raman spectroscopy
GAH	Gluteraldehyde
HCl	Hydrochloric acid
HOMO	Highest occupied molecular orbital
HPLC	High Performance Liquid Chromatography
HRMS	High Resolution Mass Spectroscopy
ICT	Intramolecular Charge Transfer
ILs	Ionic Liquids
IR	Infrared
ISNBP	Indolinespiro nitro-benzopyran
ISBP	Indolinespirobenzopyran
ITO	Indium Tin Oxide
$K^\ddagger$	Equilibrium of activation
KOH	Potassium Hydroxide
LED	Light-emitting diode
LUMO	Lowest unoccupied molecular orbital
MC	Merocyanine form
MCH <sup>+</sup>	Protonated merocyanine form
M <sup>n+</sup>	Cationic form of a general Divalent Metal Ion

MeOH	Methanol
NIPAAm	<i>N</i> -isopropyl acrylamide
NMR	Nuclear magnetic resonance
OTTLE	Optically Transparent thin-layer Electrochemical Cell
PBS	Phosphate Buffer Saline
PEDOT	Poly(3,4-ethylenedioxythiophene)
p-BSP2	Abbreviation for the polymer (3,3''-Dimethylindoline-6'-nitrobenzospiropyranyl)ethyl4,4''-didecyloxy-2,2':5',2''-terthiophene-3'-acetate in <b>Chapter 2</b>
p-MC2	Abbreviation for the merocyanine isomer of the polymer (3,3''-Dimethylindoline-6'-nitrobenzospiropyranyl)ethyl4,4''-didecyloxy-2,2':5',2''-terthiophene-3'-acetate in <b>Chapter 2</b>
PEDOT	Poly(3,4-ethylenedioxythiophene)
PMMA	Polymethylmethacrylate
pNIPAM	Poly( <i>N</i> -isopropylacrylamide)
pThs	Poly-Thiophenes
pTTh-MA	Abbreviation for the polymer poly-(Methyl 4,4''-didecyloxy-2,2':5',2''-terthiophene-3'-acetate) in <b>Chapters 2 and 4</b>
pTTh-MC	Abbreviation for the polymer poly-(3,3''-Dimethylindoline-6'-nitrobenzospiropyranyl)ethyl4,4''-didecyloxy-2,2':5',2''-terthiophene-3'-acetate in <b>Chapter 4</b>
pTTh-SP1	Abbreviation for the polymer poly-(3,3''-Dimethylindoline-6'-nitrobenzospiropyranyl)ethyl4,4''-didecyloxy-2,2':5',2''-terthiophene-3'-acetate in <b>Chapter 4</b>
pTTh-SP	Abbreviation for the polymer poly-(3,3''-Dimethylindoline-6'-nitrobenzospiropyranyl)ethyl4,4''-didecyloxy-2,2':5',2''-terthiophene-3'-acetate in <b>Chapter 2</b>
p-TThoxMC2ox	Abbreviation for the oxidized merocyanine version of the polymer poly-(3,3''-Dimethylindoline-6'-nitrobenzospiropyranyl)ethyl4,4''-didecyloxy-2,2':5',2''-terthiophene-3'-acetate in <b>Chapter 2</b>
SAMs	Self Assembled Monolayers

SEM	Scanning electron microscopy
TBA	Tributylamine
TBAP	Tetrabutylammonium Perchlorate
TFA	Trifluoroacetic Acid
THF	Tetrahydrofuran
TMC4	Merocyanine isomer of 5',6-Bis(4-decyloxythien-2-yl)- 1',3'-dihydro-1,3',3'-trimethyl-spiro[2 <i>H</i> -1-benzopyran-2,2'- [2 <i>H</i> ]indole]
Tol	Toluene
TSP4	5',6-Bis(4-decyloxythien-2-yl)-1',3'-dihydro-1,3',3'- trimethyl-spiro[2 <i>H</i> -1-benzopyran-2,2'-[2 <i>H</i> ]indole]
TTh	General abbreviation for the 'Terthiophene' moiety
TThAA	4,4''-Didecyloxy-2,2' :5',2''-terthiophene-3'-acetic acid
TThMA	4,4''-Didecyloxy-2,2' :5',2''-terthiophene-3'-acetic acid methyl ester
UV	Ultraviolet
<i>Vis</i>	Visible

# TABLE OF CONTENTS

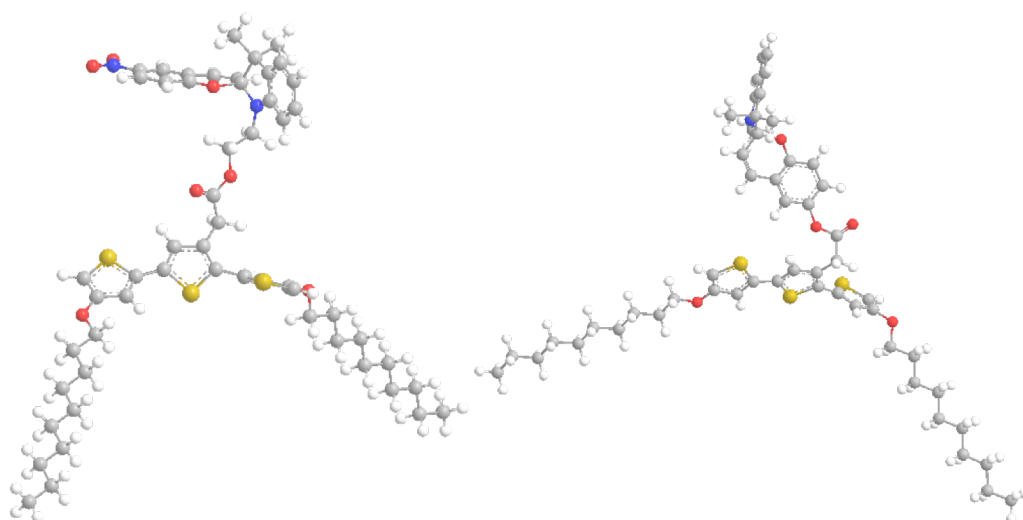
<b>CHAPTER 1 INTRODUCTION</b>	<b>1</b>
1.1 Materials Science	2
1.2 A Brief History of Electrochemical Science	2
1.3 Conducting Polymers	3
1.3.1 Poly-Thiophenes-based Synthetic Metals	5
1.3.2 Synthesis of Substituted Terthiophene Monomers	7
1.3.3 Electropolymerisation and Electrochemical Properties of the Thiophene - Based Polymers	8
1.3.4 Optical and Chromic Properties of Poly-Thiophenes	11
1.3.5 Conducting Polymers as Biomaterials	12
1.4 AFM and Fibronectin	15
1.5 Molecular Photo-Switches	18
1.5.1 Photochromism	18
1.5.2 Physico-Chemical Aspects of Spiropyrans: Dynamics of Conversion to the Merocyanine Form	24
1.5.3 Solvatochromism	25
1.5.4 Photochemical Behaviour of Spiropyrans	27
1.5.5 Thermochromism	34
1.5.6 Synthesis of Benzospiropyran (BSP)	35
1.5.7 Protonation and Acidichromism	36
1.5.8 Electrochemistry of Benzospiropyran	38
1.6 Spiropyran As a Chelating Agent of Metal Ions	39
1.7 Applications of Spiropyran Moieties	41
1.8 General Aims of This Research	42
1.9 References	45
<b>CHAPTER 2 MULTISWITCHABLE POLY-(TERTHIOPHENE) BEARING A SPIROPYRAN FUNCTIONALITY: UNDERSTANDING PHOTO- AND ELECTROCHEMICAL CONTROL</b>	<b>51</b>
Abstract	52
2.1 Introduction	53
2.2 Experimental	54
2.2.1 Monomer Synthesis	54
2.2.2 Electrochemical Polymerization of BSP-2 and TThMA	57
2.2.3 UV-vis Spectroelectrochemistry	57
2.2.4 Conductivity measurement	58
2.3 Results and Discussion	58
2.3.1 Synthesis of the monomers	58
2.3.2 Electrochemistry and Spectroelectrochemistry of BSP-1	60
2.3.3 Electrochemical Polymerization of pBSP-2	63
2.3.4 UV-Visible Spectroelectrochemistry of poly-BSP2.	66
2.3.5 Light Control of BSP1 Isomerisation	72

2.3.6 Physical Properties of p-BSP2	74
2.4 Conclusion	76
2.5 References	77
<b><u>CHAPTER 3 PHYSICO-CHEMICAL STUDY OF SPIROPYRAN-TERTHIOPHENE DERIVATIVES: PHOTOCHEMISTRY AND THERMODYNAMICS</u></b>	<b>80</b>
Abstract	81
3.1 Introduction	82
3.2 Experimental	85
3.2.1 Materials	85
3.2.2 Photochemical Methods	86
3.3 Results and Discussion	89
3.3.1 Material synthesis	89
3.3.2 Photochromic properties	89
3.3.3 Kinetics of photo-induced ring opening	90
3.3.4 Kinetics and thermodynamics of ring closure	93
3.3.5 Solvatochromic effects	96
3.3.6 Fluorescence spectroscopy	99
3.4 Conclusions	102
3.5 Acknowledgements	103
3.6 References	103
<b><u>CHAPTER 4 OPTICAL SWITCHING OF PROTEIN INTERACTIONS ON PHOTSENSITIVE-ELECTROACTIVE POLYMERS MEASURED BY ATOMIC FORCE MICROSCOPY</u></b>	<b>106</b>
Abstract	107
4.1 Introduction	108
4.2 Materials and Methods	111
4.3 Results and Discussion	112
4.3.1 UV-Vis Spectra	112
4.3.2 Contact Angle Measurements	113
4.3.3 Protein Adhesion	113
4.4 Conclusion	118
4.5 Acknowledgements	119
4.6 References	119
<b><u>CHAPTER 5 A MEROCYANINE-BASED CONDUCTIVE POLYMER</u></b>	<b>123</b>
Abstract	124
5.1 Introduction	125
5.2 Results and Discussion	125
5.3 Conclusions	133
5.4 Acknowledgements	133

5.5 References	134
<b><u>CHAPTER 6 SPIROPYRAN-TERTHIOPHENE MULTI-MODAL MOLECULAR SWITCHES: PHOTOCHROMIC, ACIDOCROMIC AND ELECTROCHROMIC PROPERTIES</u></b>	<b>136</b>
Abstract	137
6.1 Introduction	138
6.2 Experimental	140
6.3 Results and Discussion	140
6.3.1 Synthesis of BSPe, BSP 6 & BSP7	140
6.3.2 Photochemistry study	142
6.3.3 Kinetics of protonation	149
6.3.4 Thermodynamics of protonation	152
6.3.5 Electrochemistry	154
6.3.6 Photonic response of the polymers	160
6.3.7 Surface properties	161
6.4 Conclusions	164
6.5 Acknowledgments	165
6.6 References	165
<b><u>CHAPTER 7 THESIS CONCLUSIONS AND FUTURE WORK</u></b>	<b>169</b>
7.1 Thesis Conclusions	170
7.2 Future Work	172
7.2.1 Poly-Spiropyran-Terthiophenes Incorporated into Micro Total Analytical Systems ( $\mu$ TAS)	173
7.2.2 Living Cell Adhesion on Photo-Switchable Conducting Polymers	174
7.2.3 Bi-Modal Uptake and Release of Metal Ions from Diluted Solutions of Photo-Switchable Conducting Polymers	176
7.3 References	177
<b><u>APPENDIX A MULTISWITCHABLE POLY-(TERTHIOPHENE) BEARING A SPIROPYRAN FUNCTIONALITY: UNDERSTANDING PHOTO- AND ELECTROCHEMICAL CONTROL</u></b>	<b>A1</b>
A-1 Electrochemical Deposition of p-BSP2	A2
A-2 Spectroelectrochemistry of p-TThMA	A3
A-3 Spectroelectrochemistry of p-TThMA	A3
A-4 Photo-regeneration of p-BSP2	A4
A-5 AFM analysis of the polymer	A5
<b><u>APPENDIX B PHYSICO-CHEMICAL STUDY OF SPIROPYRAN-TERTHIOPHENE DERIVATIVES: PHOTOCHEMISTRY AND THERMODYNAMICS</u></b>	<b>B1</b>
B-1 Analytical characterization of BSP-3	B2
B-2 Thermal Relaxation Profile of MC-2 in Acetonitrile	B2
B-3 Thermal Relaxation Profile of MC-1	B3

B-4 Solvatochromic effect on MC-2	B3
B-5 Thermal Relaxation Profiles of MC-2 and MC-3 in The Molecular Solvents Studied	B4
<b><u>APPENDIX C A MEROCYANINE–BASED CONDUCTIVE POLYMER</u></b>	<b>C1</b>
C-1 Synthesis of 5',6-Bis(4-decyloxythien-2-yl)-1',3',3'-Trimethyl-Spiro[2H-1-Benzopyran- 2,2'-[2H]Indole] (TSP4)	C2
C-2 Electrochemical Polymerization of TSP4	C3
C-3 UV-vis Spectroscopy	C4
C-4 Conductivity Measurement.	C6
C-5 Elementary Analysis.	C6
C-6 SEM Imaging.	C7
C-7 Fourier-Transform Raman	C7
C-8 Computational Modelling	C9
C-9 References	C10
<b><u>APPENDIX D SPIROPYRAN-TERTHIOPHENE MULTI-MODAL MOLECULAR SWITCHES: PHOTOCHROMIC, ACIDOCHROMIC AND ELECTROCHROMIC PROPERTIES</u></b>	<b>D1</b>
D-1 Synthesis of the New Spiropyran (BSPe) and Spiropyran-Terthiophene Moieties (BSP6 and BSP7)	D2
D-2 Reagents and Analytical techniques	D5
D-3 Analytical methods for the protonation experiments	D6
D-5 Kinetics and thermodynamic analysis	D8
D-6 Electropolymerization and Electrochemical experiments	D9
D-7 Conductivity measurement	D9
D-8 Electrochemistry and spectroelectrochemistry of BSPe	D9
D-9 UV-vis spectroelectrochemistry of the polymers	D9
D-10 Photochemistry of pBSP6 and pBSP7	D10
D-11 Atomic force microscopy (AFM) and scanning electron microscopy (SEM)	D10
D-12 UV- <i>vis</i> Characterization of BSPe 10 <sup>-4</sup> M in Acetonitrile	D11
D-13 UV- <i>vis</i> Overnight Protonation of BSP6 and BSP7 10 <sup>-4</sup> M in Acetonitrile	D12
D-14 UV- <i>vis</i> Overnight Protonation of BSP6 and BSP7 10 <sup>-4</sup> M in Acetonitrile	D12
D-15 Protonation Experiment of AcTTh and CbTTh	D13
D-16 Kinetics of Protonation for BSP7 and BSPe	D14
D-17 UV- <i>vis</i> Spectral Response at Constant Wavelength of pBSP6, pBSP7 and pAcTTh	D15
D-18 Photochemical Actuation of pBSP6	D15
D-19 SEM Pictures of pBSP7	D16
D-20 AFM Pictures of pBSP7	D16





# CHAPTER 1

# INTRODUCTION

## 1.1 Materials Science

Materials science is a broad interdisciplinary field that spans many areas of scientific research with exciting developments arising from the ever-increasing ability to control the behaviour of bulk materials through actions at the molecular level. New approaches to stimuli-responsive materials that lead to new ion-selective systems, advanced drug-release devices and bio-interfaces are needed, for example based on photonic or electronic mediated control of surface charges/polarity. Their versatility offers a variety of possible applications and attracts an always-increasing attention, particularly because of the biocompatibility of many of these materials and because of the accessible preparatory conditions.<sup>1</sup> They also need to be cost-efficient to the end-user whilst improving efficiency. Materials science is now able to offer an opportunity to link research in advanced materials with molecular biology and bionics, thus allowing the development of new devices that allow growth of specific cell lines or tissue regeneration depending on the particular stimulus transmitted to the scaffold, with remarkable potential and high impact in modern society and the quest for new therapies.<sup>1</sup>

## 1.2 A Brief History of Electrochemical Science

Electrochemistry can be defined as the science which studies the electron transfer at the solution/electrode interface. Electrochemistry plays an important role in a wide number of fundamental and applied researches. These include the synthesis and exploration of new inorganic and organic compounds, the analysis of mechanisms of action of biochemical and biological systems, corrosion, energy applications involving fuel cells and solar cells, and nanoscale investigation.<sup>2</sup>

The scientific community was interested by this fascinating discipline in the 19th Century with Coulomb, who developed the law of electrostatic attraction in 1785.<sup>3</sup> The Italian scientist Alessandro Volta was the inventor of the battery (voltaic pile, 1800), but its most important concepts were defined by Faraday in 1832, and in 1835 when he provided a definition for such common experimental terms as: electrode, cathode, anode and electrolyte.<sup>3</sup>

The positive and negative mathematical convention for electrical charge is attributed to Benjamin Franklin, although this had already been theorized years earlier by Charles-

François de Cisternay du Fay.<sup>3</sup> Svante Arrhenius, with his thesis published in 1884 titled “*Recherches sur la conductibilité galvanique des électrolytes*” (Investigations on the galvanic conductivity of electrolytes), could conclude from his results that electrolytes, when dissolved in water, become to varying degrees split or dissociated into electrically opposite positive and negative ions.<sup>3</sup> In 1888 Walther Hermann Nernst described the electromotive force (voltage) and then in 1889 he demonstrated the equation, known as the Nernst equation, which related the voltage of a cell to its properties and can be used to calculate both the equilibrium reduction potential of a half-cell in an electrochemical cell and the voltage for a full electrochemical cell.<sup>3</sup>

The field of electrochemistry encompasses a huge array of different phenomena (e.g., electrophoresis and corrosion), devices (electrochromic displays, electroanalytical sensors, batteries and fuel cells) and technologies (the electroplating of metals and the large scale production of aluminium and chlorine).<sup>3</sup>

To conclude this brief survey on the most important events in the history of electrochemistry, a special mention must be made on the discovery of conducting polymers using electrochemistry in 1978 as reported by C.K. Chiang *et al.*,<sup>4</sup> materials that are nowadays used in a wide number of applications and devices, and which will be discussed in more detail.

### 1.3 Conducting Polymers

Conducting polymers can be described as having high  $\pi$ -conjugation and high-order crystal architecture (extrinsic effects), which allow elevated charge transport properties such as “hopping conduction”.<sup>5</sup> Hopping conduction is defined as the process in which charge carriers conduct the electric current by thermally activated tunnelling from an occupied site to an empty site. The thermal energy that is required for the process to occur is gained from the phonon system. Conwell, Mott and Pines first suggested the concept of ‘hopping’ in 1956 and this property alone has made these materials the subject of intensive studies.<sup>5-7</sup> In addition to this property, there are also intrinsic properties that are important to describe the transport of electrons. The electron-phonon coupling present in low-dimensional carbon-based systems can produce self-localization of the charge-carrier, which means the formation of polarons.

The concept of polaron was firstly proposed by Holstein,<sup>8</sup> describing charge transport in molecular crystals. As a result of electron-lattice interaction, the surrounding lattice particles will be displaced to new equilibrium positions. The induced displacements

provide a well for the electron. If the well is sufficiently deep, the electron will occupy a bound state unable to move unless accompanied by the well. The unit consisting of the electron together with its induced lattice deformation is termed “the polaron”. In this model the crystal is described as a regular one-dimensional (1-D) array of diatomic molecules.

In these systems,  $\pi$ -conjugation order plays an important role in the processes involving charge transfer. This is a disordered process, which can be described by wavefunctions and a portion of this disorder is energetic (appears as fluctuations). Transport properties depend strongly on the amount of this type of disorder as well as the spatial correlations in the values of the on-site energies between sites.

In a crystal, the polaron can be localized by a gain in energy caused by the intramolecular geometrical response to the energy that results from electronic intermolecular reactions,  $J$ . Depending on the relative strength of these two interactions, one can describe the intrinsic transport in three different categories:

**(1)** when  $J \ll$  localization energy ( $E_l$ ), weak intermolecular interactions arise, the so-called small Holstein polaron localized to a single molecule is stable. As the electronic state is localized, transport occurs through hopping from one molecule to the next (non-adiabatic process that implies slow carrier motion when compared with the molecular relaxation time and the mobility depends quadratically on the intermolecular interaction strength). With these conditions  $E_l$  is approximately identical to the formation energy of the polaron and the barrier for polaron hopping is  $E_l/2$ .

**(2)** When  $J \sim E_l$  the polaron is delocalized over several molecular units and the electron probability density can sample an even larger region in space. Under external electric fields the charge density moves associated with the polaron to the direction of the field and in an adiabatic way, generating a modification of the molecular geometry as the carrier drifts along the system. With these conditions the activation energy is small and the mobility is weakly dependent on the strength of the intermolecular interactions.<sup>29</sup>

**(3)** Finally, for  $J \gg E_l$  the lattice (a regular repeated three-dimensional arrangement of atoms, ions, or molecules in a metal or other crystalline solid) relaxation can be neglected and transport is based on band theory and can be described by relaxation time approximation.<sup>9</sup>

The polaron concept was further developed together with the idea of doped systems: it

has been shown that the electrical conductivity increases in doped conjugated polymers.<sup>9</sup> Furthermore in heavily doped samples a metallic-similar structure is likely to be more appropriate to describe the disposition of the components of the system in the ordered regions. Recent studies have shown that at undoped states the number of charge carriers is small and the consequent transport is more dependent on the mobility of charge carriers. This indicates how important in terms of conductivity, the purity of the system and the order of the structure is.<sup>9</sup>

### 1.3.1 Poly-Thiophenes-based Synthetic Metals

Poly-thiophenes are important families of organic polymers able to conduct electrical stimulus. They offer a high number of possibilities to couple analyte receptor interactions, as well as nonspecific interactions, into observable (transducible) response. A key advantage of CP-based sensors over devices using small molecule (chemosensor) elements is the potential of the CP to exhibit collective properties that are sensitive to very minor perturbations. In particular, the CP's transport properties, electrical conductivity or rate of energy migration, provide amplified sensitivity towards analytes of interest.<sup>10-12</sup> Their suitability for these applications results from their unique electronic and optoelectronic properties.<sup>13-27</sup> When poly-thiophene (a non-degenerate polymer) is oxidized, the resultant radical cation, a positive polaron, is defined by both the charged excitation and the structural defect that it induces (a domain of quinoid-type bond sequence).<sup>7</sup> These charged defects are localised over several monomer units. If further oxidation is able to produce the di-cation, then a second polaron forms and two of these species can combine to form a spinless bipolaron, a process dependent on the length of the oligomer.<sup>13, 14, 28, 29</sup> There remains some uncertainty over which type of charged defect, polarons or bipolarons, is principally responsible for the conductivity observed in non-degenerate conjugated polymers. In addition, the precise mechanism of conduction is still unclear, most notably, the path of the charge carriers through the polymer.

CPs generally exhibit semi-conductive to insulating levels of conductivity in their pure state but can be made conductive by doping. The term doping is derived in analogy to semiconductor systems. However, in contrast to semiconductor systems, doping does not refer to the replacement of atoms in the material's framework. Doping in the case of a CP refers to the oxidation or reduction of the  $\pi$ -electronic system, p-doping and n-

doping, respectively, and can be effected chemically or electrochemically. To maintain electroneutrality, doping requires the incorporation of a counter ion.

Poly-thiophene stimuli responsive materials are widely studied, developing and improving the synthesis of new multifunctional derivatives with innovative properties. These materials have been investigated for a large variety of applications including energy storage and electrochemical or bioelectrochemical sensors.<sup>26</sup> So far the large majority of conducting polymers have been synthesised by electropolymerization of a precursor, usually a monomer or a short-chain oligomer, previously substituted with specific functional groups bearing desired properties such as hydrophobicity/hydrophilicity and molecular recognition.<sup>15-17</sup>

Several approaches have been explored for the composition of the desired thiophene-based building blocks and the most suitable procedure applied was the Stille coupling.<sup>16-21</sup> This technique (Figure 1.1) allows the formation of a versatile C-C bond with very few limitations on the R-groups lying on the scaffold. It is given by the combination of halides and stannanes and it is an improvement of the Suzuki reaction (from an average yield of 40% up to 70%).<sup>15-21</sup> Roncali and co-workers<sup>16-21</sup> successfully applied this synthetic pathway to achieve their aim of producing more thiophene-based derivatives and the identification of their major properties.<sup>16-21</sup>

The intrinsic conductivity of organic semiconductors based on  $\pi$ -conjugated systems depends on the concentration and mobility of the charge carriers. The performance of the semiconductor depends on both intermolecular factors and on the structure of the conjugated system. Thus the leading concept for the construction of these new materials has been the preparation of monomers and oligomers bearing conjugated features readily on the functional unit.

For the purpose of this thesis, two different terthiophene derivatives have been synthesised and characterised following a procedure reported elsewhere and discussed in further detail in **Chapter 2**.

### 1.3.2 Synthesis of Substituted Terthiophene Monomers

The electronic properties of thiophene oligomers and polymers may be tuned by introducing functionality onto the polymer chain in the form of aromatic substituents. Thus, poly (3-arylthiophenes) have improved doping capacity and redox cycling characteristics when compared to traditional poly-thiophenes. Aromatic substituents have also been attached to thiophene as styryl groups.<sup>30</sup> Although electrochemical homo polymerisation of 3-styrylthiophene resulted in a nonconductive material, conductive polymers have been obtained by copolymerisation of styryl-substituted thiophenes with thiophenes. However, whilst these co-polymerisations undoubtedly lead to improvement in desired polymer properties, their irregular structure makes it difficult to deconvolute the role of the substituent.<sup>22</sup>

In this project one of the biggest challenges was the incorporation of a photochromic unit onto a conductive surface (e.g. CP). While the required structure for monolayer and bilayer formation does not affect the function of the photo-molecules, one of the challenges in using polymers is that the building unit used to synthesise the polymer, and the polymerisation process itself, must be compatible with the photo- / electroactive switching units. In addition, the incorporation of the photoresponsive functionality must not affect the polymerisation of the monomer. Figure 1.1 shows the synthesis steps leading to the isolation of mono and di-substituted terthiophenes.<sup>30</sup>

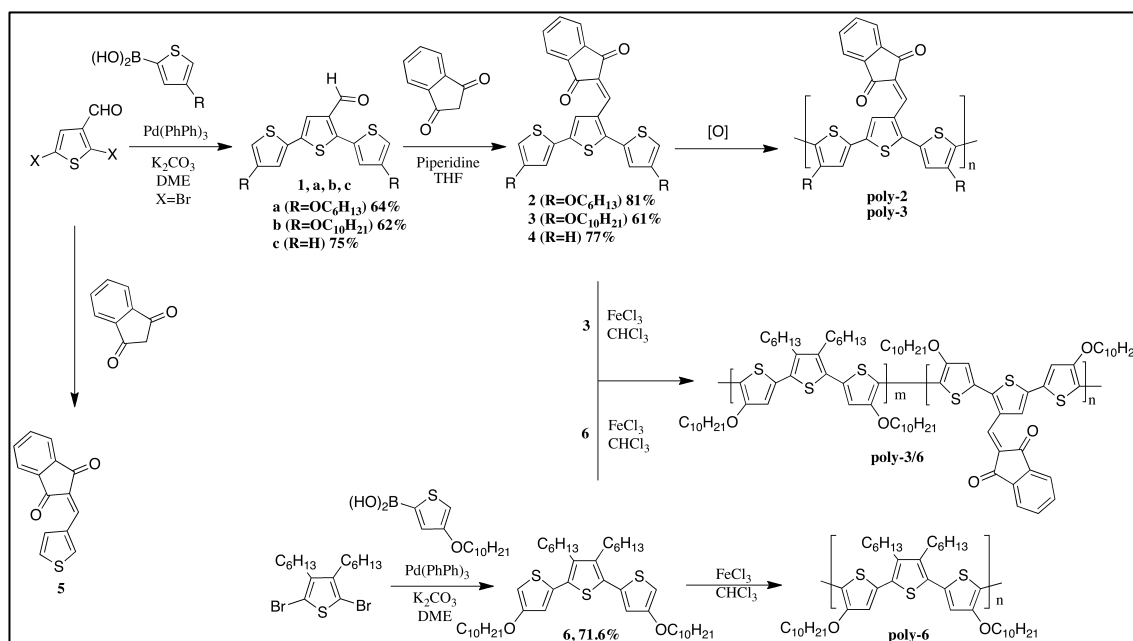
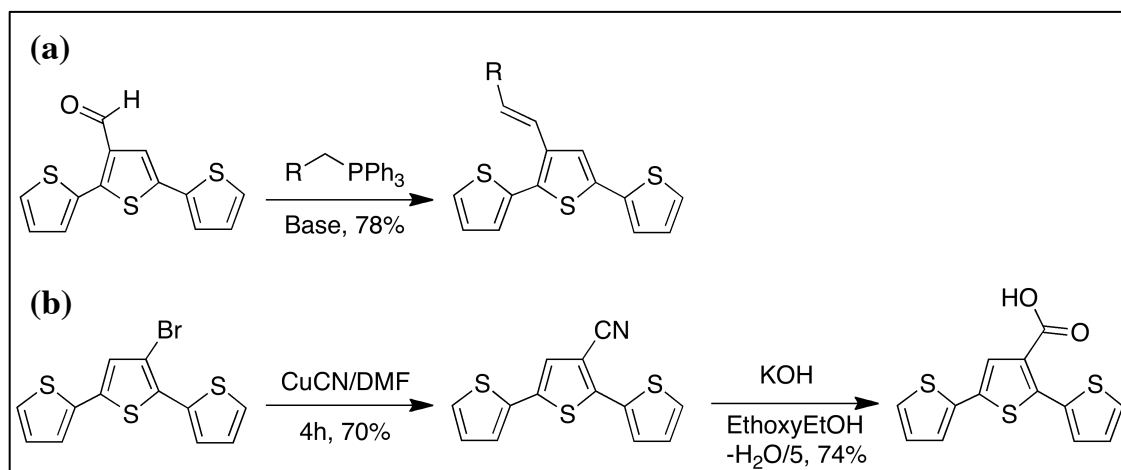


Figure 1.1: Synthesis of mono and di-substituted terthiophene.<sup>30</sup>

An efficient method developed for the synthesis of substituted thiophene derivatives is the building block approach. The single units were composed with Suzuki reactions and

then condensed together under Wittig and Horner – Emmons conditions<sup>23, 24</sup> (Figure 1.2a).



**Figure 1.2:** (a) Procedure to isolate functionalised terthiophenes.<sup>23</sup> (b) Synthesis of terthiophene-3'-carboxylic acid.<sup>24</sup>

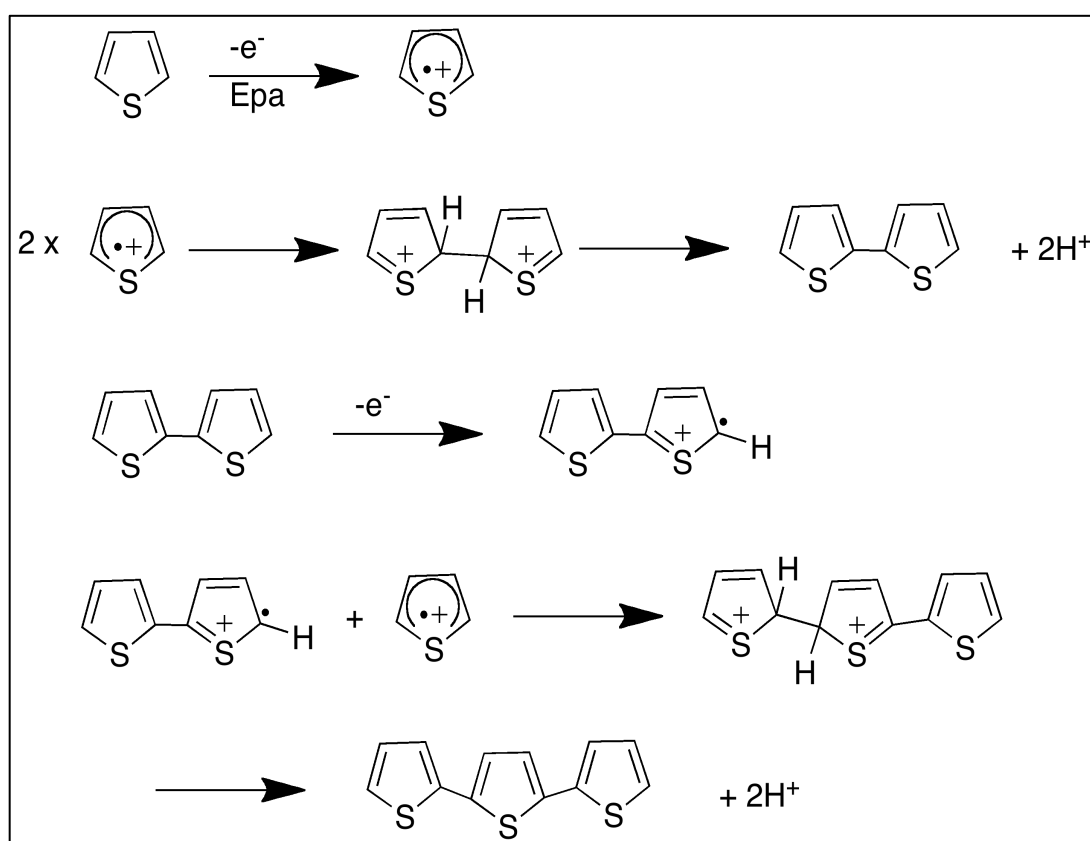
Lee *et. al.*<sup>16</sup> who were able to attach a reactive and an environmental stable functional group on terthiophene developed alternative synthetic routes. One example of this substitution is shown in Figure 1.2 (b) (position 3' a carboxylic acid). The choice of this particular site inside the three heterocyclic ring system has two main advantages: in comparison with the 3-substituted thiophene, the terthiophene monomeric unit functionalized on its 3'-position allows rapid polymerisation, evidencing steric hindrance caused by the bulky functional group around the reaction site for polymerisation. Secondly, the conducting polymers prepared from terthiophene exhibit both high environmental stability and high conductivity.

With these advantages, a similar functional group (acetic acid at 3'), which bears similar characteristics, was synthesised. A more detailed description of the steps involved in this part of the work is reported in **Chapter 2**.

### 1.3.3 Electropolymerisation and Electrochemical Properties of the Thiophene - Based Polymers

Polythiophene derivatives are of particular interest due to their stability and relative ease of synthesis and functionalization. Owing to the reversibility of the transition between the neutral and the oxidized (p-doped) or reduced (n-doped) states, p-thiophenes are highly electroactive materials. They can be applied in a broad range of devices: from simple solar cells to complex electroluminescent devices.

The most applied and efficient technique used for the preparation of poly-terthiophene based materials is the electrochemically-controlled growth from diluted solutions of monomers. The mechanism occurring during this process is depicted in Scheme 1.1 and was proposed by Genies *et. al.*<sup>26, 31</sup> The first passage follows the oxidation of the monomer to its radical cation. A high concentration of the generated radicals is kept constantly around the electrode surface by the fast electron-transfer reaction (quicker than the diffusion of the monomer from the bulk solution). The second step consists in the coupling of two radicals, which generates a dihydro dimer that rapidly loses two protons and re-aromatize. This passage is the rate-determining step of the reaction. Since the dimer is easier to oxidize than the monomer, the system proceeds to a further coupling passage with a freestanding monomeric radical. The electropolymerisation proceeds until the oligomer becomes insoluble in the electrolyte and precipitates onto the electrode surface.



**Scheme 1.1:** Mechanism of electropolymerisation of five-membered heteroatomic aromatic rings.<sup>26, 31</sup>

The electronic character of attached functional groups typically affects the electron density of the thiophene rings in the polymer. The energy gap ( $E_g$ ) is related to the electrical and optical properties of the polymer and has often been lowered by extending the  $\pi$ -electron delocalization over the whole backbone chain or by using electron donors

or electron acceptors as substituents, which induce minimally twisted arrangements in the conjugated polymers.<sup>32</sup> This kind of donor- $\pi$ -acceptor (D- $\pi$ -A) arrangement in oligomers or polymers can permit a high degree of intramolecular charge transfer (ICT). ICT interaction can provide low-band-gap polymers with broad absorption bands that extend into the near-infrared spectral range, high electron affinity and low ionization potential, efficient photo-induced charge transfer and separation, and ambipolar charge transport with high mobility. The electrochemical profile of a similar polymer is shown in Figure 1.3 (a) and (b).<sup>30</sup>

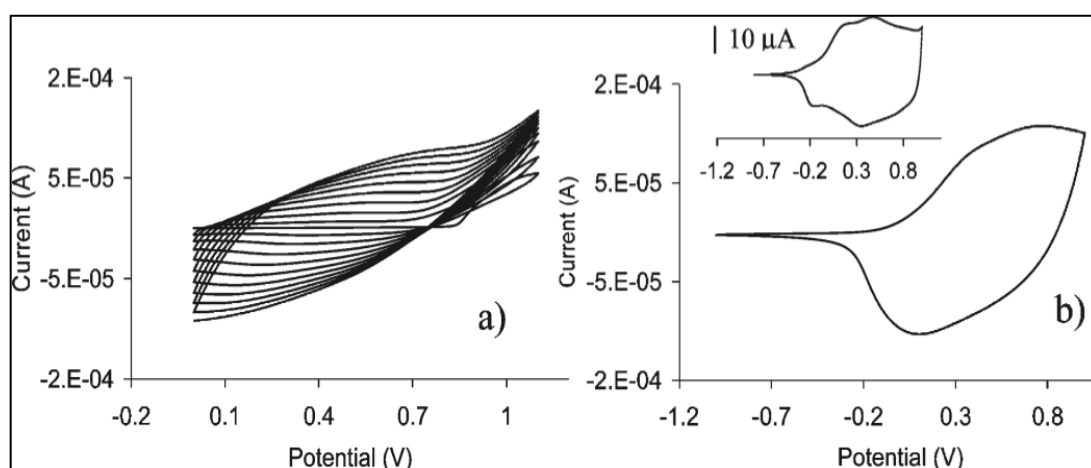


**Figure 1.3:** (a) Electrochemical polymerization and (b) post CV of poly-2e (fig 1.1); scan rate 100 mV/s (inset: 10 mV/s).<sup>30</sup>

The activity of the derivatives presented in Figure 1.2 (b), is addressed to precursors for nanoporous electroactive materials potentially applicable in the field of sensors and energy storage systems, as the insertion of functional groups on the central thiophene unit will improve the absorbance spectrum of the polymer in the visible region, thus favouring light-harvesting capability.<sup>30</sup>

Thiophene monomers and polymers can be modified by the incorporation of functionality to alter the solubility, surface properties, and biodegradability of the polymer films. This offers a number of advantages due to the changes in solubility, allowing for easy processing of the polymers into various structures such as films and fibers, circumventing the limited processability of many conducting polymers such as polyaniline and polypyrrole. The inherent variability of the polymer materials produced can be further enhanced by doping with a wide range of anions thus facilitating the development of a suitable conducting polymer structure for *in vitro* engineering of specific cell lines.<sup>33</sup>

### 1.3.4 Optical and Chromic Properties of Poly-Thiophenes

UV-*vis* spectroscopy has been established as a versatile and powerful technique for the characterisation of conjugated polymers. Determination of the extension of the  $\pi$ -orbital in conjugated systems, for example, can be calculated.<sup>27,35</sup> The extent of the conjugation is directly proportional to the maximum absorption for such systems. Since the energy of the HOMO and LUMO are closely related to the reversible half-wave oxidation and reduction potentials corrected by the solvation energies, electrochemical techniques can provide important information regarding the magnitude of the energy gap and the extent of the conjugated  $\pi$ -systems in CP's. This is the manifestation of the  $\pi$ - $\pi^*$  transition (HOMO / LUMO or bandgap) therefore UV-*vis* allows one to describe the conformational state and structure of conjugated polymers.

Regio-regular poly-thiophenes show a red shift in the  $\lambda$  max compared to the regio-irregular poly-thiophenes, indication of a lower  $\pi$ - $\pi^*$  transition for the regio-regular p-thiophenes and, therefore, a longer conjugation length. The reason for this increase in orbital overlap is the more planar conformation in solution for the regio-regular ones, while the regio-irregular p-thiophenes are more coils like, twisting the orbitals away from interaction (Figure 1.4). This behaviour is highly influenced by the substituents and their positions on the ring.<sup>34,35</sup>

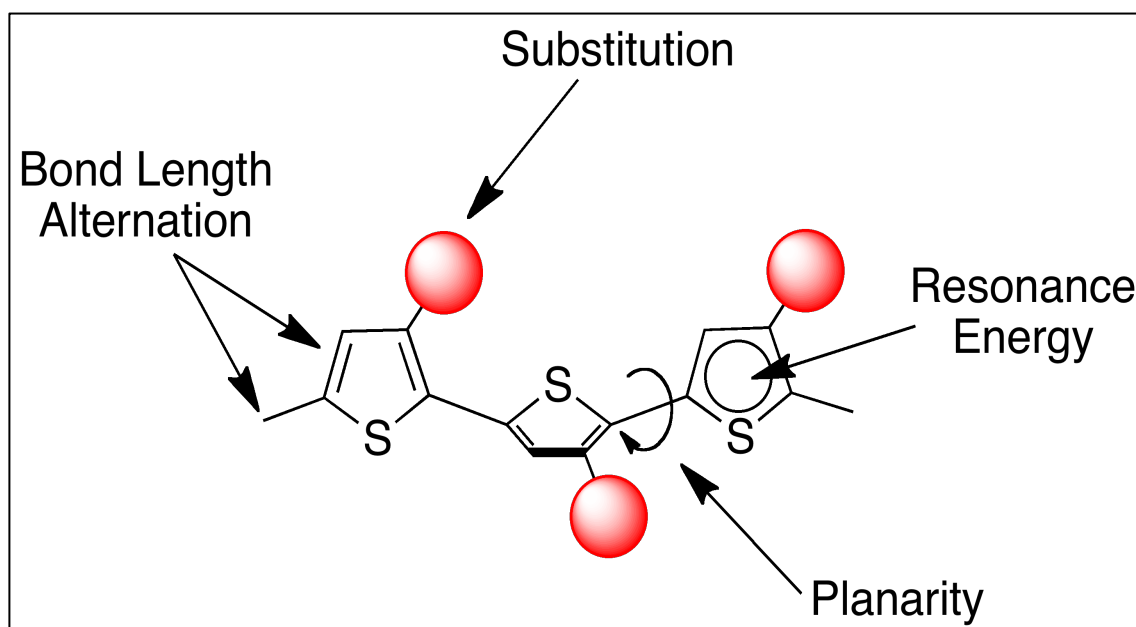


**Figure 1.4:** Structural factors determining the band gap of materials bearing linear  $\pi$ -conjugated systems.<sup>35</sup>

Other interesting studies demonstrated the effect of electron-donating groups that produced a *hypsochromic* shift to higher wavelengths. However a smaller *bathochromic* shift has been detected when electron-withdrawing groups are substituted on the polymer chains.<sup>30</sup>

The possible effects that can be observed using UV-*vis* spectrometry on thiophene-based conjugated polymers are the following: thermochromism (with a decrease in temperature, aggregation of the polymers increase, with a resulting blue-shift in the spectrum). Solvatochromism (which translates itself in a red or blue shift depending on the extent of solvation of each moiety in different solvents), electrochromism (red or blue shift which depends on the potential applied to the polymer) and finally photochromism (generated by exposure to different wavelengths) are important properties of interest in the characterisation of poly-thiophene moieties.

The electrochemical and optical properties of films obtained with various monomer concentrations and electrical conditions show that the increase in conductivity is correlated to a decrease of the oxidation potential and to a bathochromic shift of the absorption maximum, changes that are indicative of an extension of conjugation.

A variety of side-chain functionalized polymers also exhibit chromic responses in the presence of external stimuli. A large majority of poly-thiophenes are not soluble in common solvents and this problem requires an expedient to allow their analysis with traditional spectrometers. A possible alternative pathway could be the electrodeposition of the polymers on optical transparent surfaces such as ITO, which will permit the *in situ* analysis with the well-known spectrochemical and spectroelectrochemical techniques. The chromic properties are induced by exposition to different potentials conditions and, for a terthiophene based polymer, they traditionally shift from the red (reduced state) to the blue (oxidized) region of the spectra.

### 1.3.5 Conducting Polymers as Biomaterials

Conducting polymers (CPs), thanks to their adaptive nature, are impacting on a wide variety of bioapplications such as neural interfaces,<sup>36-39</sup> biosensors or biodegradable platforms.<sup>40-42</sup> In particular, CPs have exciting potential as scaffolds for tissue engineering and they can be applied in the regenerative medicine field. This discipline holds the promise of treating or curing a wide range of conditions such as burned skin, damaged muscle tissue and spinal cord injury.<sup>43</sup> The fundamental goal of tissue engineering is to regenerate or replace defective, diseased, or missing tissues and

organs.<sup>43</sup> The concept involves the formation of porous polymeric scaffold where cells can intercalate and slowly start the reproduction of the tissue. ‘Scaffolds’ for medicine applications are defined in the tissue engineering and biomaterials community as ‘tissue substitute’. These substitutes are grafts or porous substrates that interact with different cell lines to promote and maintain during time their differential state, contributing to form a precise functional tissue. The structure of the polymer scaffold can be selectively template by means of electrosynthesis and growing conditions (Figure 1.5).<sup>44</sup>

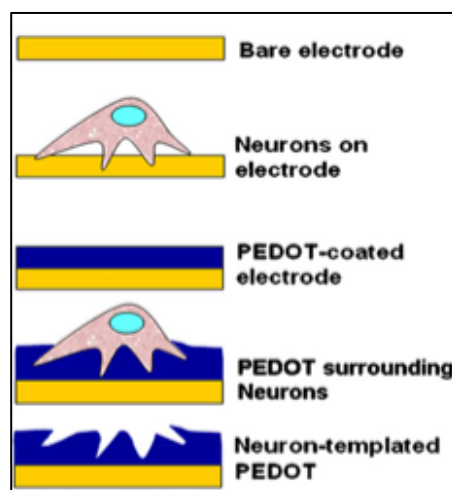


**Figure 1.5:** Model representing the different conditions for electrodes with or without PEDOT coating.<sup>44</sup>

Three ‘classical’ tissue-engineering approaches can be listed as follows: (i) the use of an instructive environment (e.g., bioactive material) to recruit and guide host cells to regenerate tissue, (ii) delivery of repair cells and/or bioactive factors into the damaged area, and (iii) cultivation of cells on a biomaterial scaffold in a culture system (bioreactor), under conditions designed to engineer a functional tissue for implantation (Figure 1.6).<sup>43</sup> However, scaffolds for muscle and nerve cell regeneration would also benefit from electrical conductivity, which has been shown to provide enhanced cell growth and differentiation. The optimal physical and biological characteristics of a scaffold for tissue engineering include tissue-like mechanical properties, a hydrated environment, and biocompatibility (preferably enhancing the cell growth).<sup>38, 45</sup>

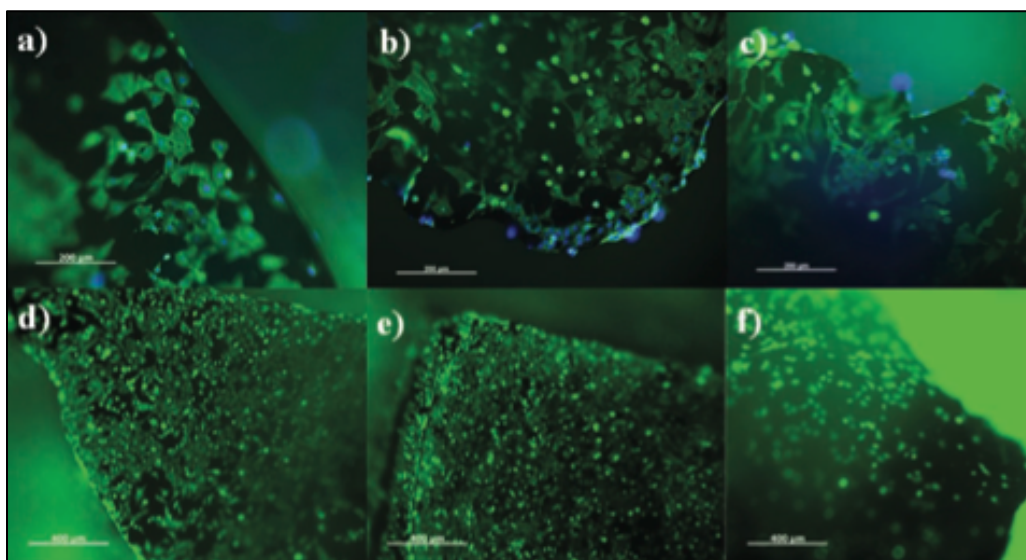


**Figure 1.6:** Fluorescent images of myoblast cells on hydrogel substrates following 72h incubation. (a–c) Cells are stained with Phalloidin-Alexa 488 (green) to visualize F-actin filaments (d–f), and DAPI (blue) to visualize nuclei.<sup>46</sup>

Unfunctionalized polythiophenes are normally prepared from organic solvents, and they spontaneously de-dope to the more insulating form under physiological conditions (pH 7) due to the aqueous environment, rendering them less suitable for bionic electrodes. However, polythiophenes can be readily modifiable by attaching selected functional groups in mild chemical conditions to modify solubility, their de-doping and electrochemical properties.<sup>25,32</sup> The polythiophene backbone is more readily functionalized than the polypyrroles or the polyanilines, and with polythiophenes the functionalization can often result in improved processability with a concomitant improvement in mechanical and electronic properties. Their increasing role in the field of biomaterials for poly-thiophenes is witnessed by the already available quantity of informations in literature regarding PEDOT derivatives and this availability is going to increase quite fast.<sup>44</sup>

Another class of materials which has proved to be an excellent candidate for tissue scaffolds is the hydrogels family.<sup>46</sup> While there is no defined level of conductivity required for tissue engineering scaffolds, it can be seen that all these materials exhibit, at best, moderate conductivities. As stated by Bendrea *et al.*,<sup>43</sup> despite the low conductivity, CP-based materials should still be able to pass the low currents that are potentially required for cell stimulation (in the range of 10 to 100  $\mu\text{A}$ ). Electrochemically conductive hydrogels (ECHs) are important candidates to fulfill this role.<sup>46</sup> Largely, however, ECHs are polymeric composites fabricated from two components: a hydrogel component that provides a highly hydrated environment and a

CP component that provides electrical conductivity. Gilmore *et. al.*<sup>47</sup> was the first to report the fabrication of such a composite, a material based on polypyrrole directly electropolymerized on a preformed polyacrylamide hydrogel and recently Mawad *et. al.* obtained a remarkable success in preparing a poly-thiophene based cross-linked hydrogel, where the chemical composition was simplified by eliminating the polyacrylamide from the structure and the capability to swell in water was retained.<sup>46</sup>

To sum up, poly-thiophenes are attracting increasing attention in the recent years thanks to their accessible properties and to their stability. It is vital that the resulting scaffold is able to resist of all the biochemical conditions of the cell development process, like the initial sterilization and the removal of the re-grown tissue from the surface, without releasing contaminants and keeping their biocompatibility throughout the various procedural steps. Finally, these materials should also be prone to be easily incorporated into different types of devices.<sup>38</sup>

## 1.4 AFM and Fibronectin

Atomic force microscopy (AFM) is recognized as a powerful nanoscale imaging tool in materials and nanotechnology research though it has had an equivalent impact in many bioapplications, especially by providing molecular insight into the intermolecular and biological specific forces governing the interactions between proteins and surfaces.<sup>48</sup> This technology is widely used to 3D probe conducting polymers surfaces, by measuring forces between a sharp probe (<10 nm) and a surface at very short distance (0.2 – 10 nm). The probe is supported on a flexible cantilever and is generally made of ‘Si’ derivatives and can present different sizes. The tip, with the probe placed on the very end of the cantilever, during the measurement gently touches the surface and records the little force between the probe and the surface.<sup>49-57</sup> AFM measures the amount of force between the probe and sample, which is dependent on the spring constant (stiffness) of the cantilever and the distance between the probe and the sample surface. Hooke’s law describes this force (equation (1.1)).

$$F = -Kx \quad (1.1)$$

Where ‘F’ is the force, ‘K’ is the spring constant and ‘x’ is the cantilever deflection.

The deflection is monitored when the constant of the cantilever (typically ~ 0.1 – 1 N/m) is less than the one of the surface, as this condition allows the cantilever to bend.

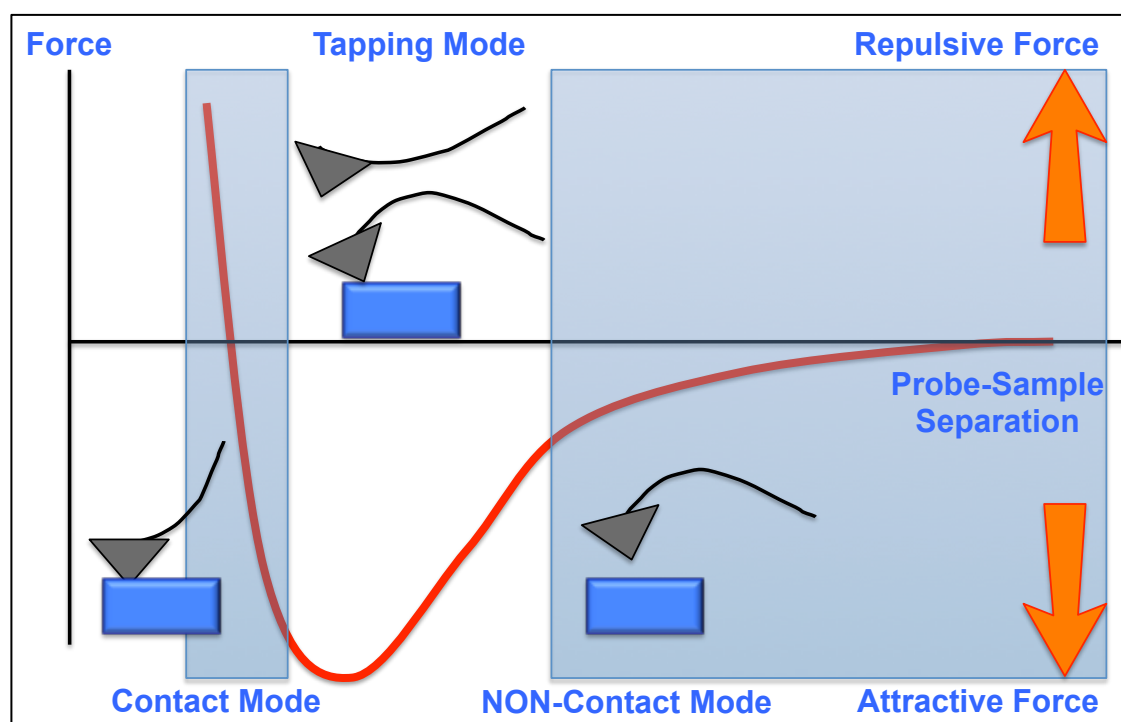
The forces resulting range between nN ( $10^{-9}$ ) to  $\mu$ N ( $10^{-6}$ ) in the open air. The dominant interactions at short probe-sample distances in the AFM are usually Van der Waals interactions. The measurements proceed as depicted in Scheme 1.2. The contact

phase is when the probe deals with the repulsive Van der Waals forces (contact mode). This leads to the tip deflection and, as the tip moves further away from the surface, attractive Van der Waals forces become dominant (non contact mode).

The imaging modes are:

- 1) Contact mode (repulsive Van der Waals): if the deflection of the cantilever is kept constant, the force between the probe and the sample remains constant and an image of the surface is obtained.
- 2) Intermittent mode: the cantilever is oscillated at its resonant frequency. By keeping this frequency constant, the image of the surface is drawn.
- 3) Non-contact mode: the cantilever oscillates over the fluid that covers the surface during the scanning.

In addition to raster scanning the probe across the surface to build up a three-dimensional topographic image, approaching and retracting the tip at a single x-y position while monitoring the displacement of the cantilever enables forces such as adhesion to be measured as a function of the distance from the surface (i.e., force-distance curve), hardness, elasticity, rupture of bond lengths and other chemical and mechanical properties. The measurements can be conducted in fluids, thus opening up the exploration of biomolecular and protein interactions in near physiological and biologically relevant environments.<sup>49-57</sup>



**Scheme 1.2:** Plot of the force as a function of probe-sample separation.

This analytical device can be used to measure the physical properties of a new material together with inter-intra molecular interactions, commonly recognized as stimulus sources for influencing cell behaviour, including topography, roughness and Young's modulus.<sup>51</sup> In 2000 Schönherr and co-workers, following methodologies already reported in literature for AFM-tip functionalization, described for the first time the substitution of reacting groups on an AFM tip for the titration of a polymeric surface thus validating reactions of surface chemistry.<sup>50, 56</sup> Following this intriguing strategy and applying mild chemical conditions, also bio-molecules can be covalently substituted on the surface of an AFM-tip (Figure 1.7).<sup>52, 58, 59</sup> In **Chapter 4** we focused on the effect of optical stimulation on the effect of optical stimulation on polymer pBSP-2 (Figure 1.22) to investigate the ability to control fibronectin (FN) adhesion, which is an important interaction within extracellular matrix for mediating cell adhesion. In order to support cell adhesion and signalling via  $\alpha_5\beta_1$  integrin binding receptors to RGD sites within FN, the protein must be in the appropriate conformation whilst possessing adhesion to the substrate. FN binding to cell integrin receptors triggers the formation of actin stress fibres that promotes cell adhesion and proliferation. Subsequent cell signalling is modulated through a continuum of mechanical forces (i.e. mechanotransduction) and thus is dependent on the strength of FN adhesion to a surface.

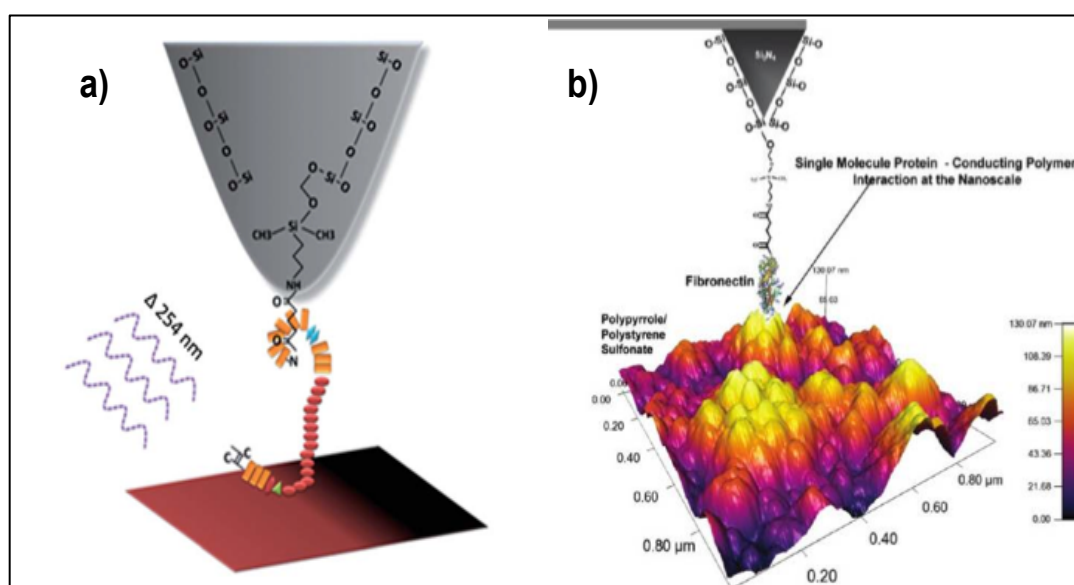


**Figure 1.7:** (a) Schematic diagram of AFM tip functionalised with FN interacting with a chromophoric surface stimulated with UV light (wavelength 254 nm).<sup>60</sup> (b) Schematic 3D picture of the surface interactions between a functionalised AFM tip with FN and a polypyrrole substrate.<sup>61</sup>

## 1.5 Molecular Photo-Switches

There are many classes of compounds that undergo colour change due to external stimuli (such as heat, light, electrical current and pH) such as polyaniline,<sup>62</sup> PEDOT<sup>63</sup> and 1,2-dithienylethene,<sup>64</sup> however some molecules are also known to switch in the presence of metal ions (benzospiropyran being the most pertinent example).<sup>65</sup>

The colour change phenomena can be classified according to the different causes determining them. Some examples are: photochromism (induced by light), thermochromism (generated by heat), electrochromism (induced by voltage), solvatochromism (solvent polarity), ionochromism (presence of ions) and finally halochromism (pH changes).<sup>65</sup>

Colour changes provide an important signal that can be used to communicate information about the surrounding environment in a fast and effective way. Furthermore, when the colour variation is reversible, the possibility of applications become more significant, sensors and biosensors being examples.

### 1.5.1 Photochromism

Photochromism is the reversible interconversion of a single chemical species between two states with different absorption spectra when irradiated with light.<sup>65, 66</sup> The changes may be induced by ultra-violet, visible and infra-red radiation. The isomers generated by photonic radiation differ not only in the absorption spectra but also in various physical and chemical properties such as refractive index, dielectric constant and geometrical structure.<sup>65</sup>

Organic photochromic compounds are molecules of considerable interest as they have potential to offer routes to new functional materials that take advantage of polarity and geometrical changes induced by irradiation. Photochromic molecules can be used to produce platforms with switchable behaviour where light irradiation can be used to induce reversible conformational transitions.<sup>67</sup> The colour changes induced by photoirradiation leads to their use in various photo responsive devices such as light sensitive eyewear<sup>68</sup>, optical memory<sup>69</sup>, molecular devices<sup>70</sup> and optical sensing applications, such as transport of metal ions<sup>71</sup> and metal detection.<sup>72-74</sup>

Well-known families of photochromic compounds include the benzospiropyrans, spironaphtooxazine, naphthopyran, diarylethenes and furylfulgides. All these families of photochromic compounds undergo reversible photo-isomerisation behaviour: one

isomer can be transformed to the other which then reverts back to the initial form in the dark (thermodynamically) or under a different light irradiation.

There has been increasing interest in organic photochromic compounds as they represent bi-stable molecular systems, that exist in two stable molecular forms which can be converted from one to another with a wide range of potential applications in electronic, photonics and computing.<sup>74</sup> Molecular sized switches incorporated into a nanoscaled logic circuit are able to detect events and transmit signals in response to environmental stimulation.<sup>75, 76</sup>

Benzo and naphthopyrans or chromenes are an important type of thermo-reversible photochromic compounds that have found application in the variable optical transmission materials field, specifically ophthalmic lenses. Their development into commercially useful materials has been fairly recent, within the last ten years. The broad absorption bands exhibited by the open forms of the naphthopyrans (Figure 1.8) and the heteroannallated naphthopyrans are somewhat complementary to the absorption bands of the naphthoxazines, leading to colour neutralization when they are used together. Their resistance to photo-oxidation is also good relative to most other families of photochromic compounds. In this respect they are comparable to the spirooxazines, which again adds to the complementary character of the two families. The colour of the opened forms can be tuned over a large range of the visible spectrum, by substituents on the naphthyl moiety or on the aromatic groups present on the  $sp^3$  carbon atom of the pyran ring.<sup>76</sup>

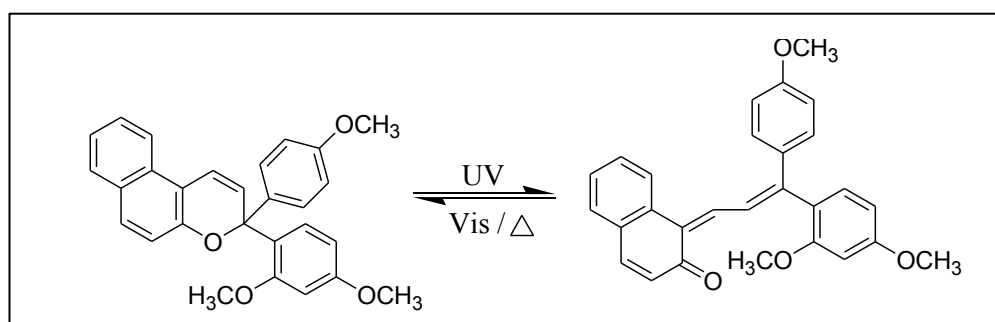


**Figure 1.8:** Photo-isomerization of naphthopyran.

The diarylethenes with heteroaryl groups, for example the bis-heteroaryl ethenes (Figure 1.9), are photochromic compounds similar to the fulgides in that the coloured or cyclized forms are thermally stable. Decolouration is again driven photochemically. Increasing the thermal stability of the coloured has been a major goal of the research on this family as their targeted use is information storage.<sup>76</sup>

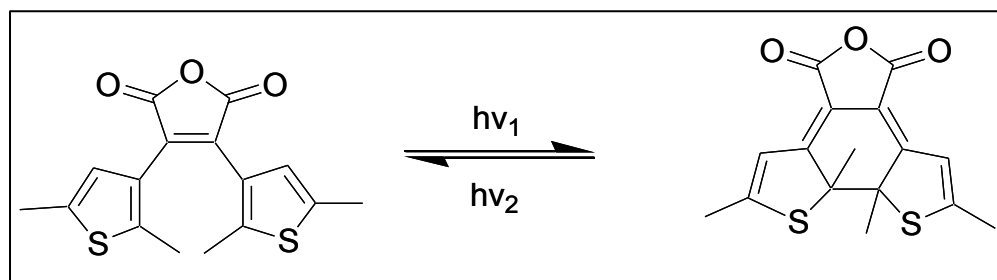


**Figure 1.9:** Photo-isomerization of diarylethenes.

Azobenzene is a diazene ( $\text{HN}=\text{NH}$ ) derivative where phenyl groups replace both hydrogens. This moiety can exist either in the *cis* or *trans* configuration. The *trans* to *cis* isomerization is induced by irradiation with UV-visible light or mechanical stress. This process is extremely fast and it is completed on picosecond timescales. The *cis* to *trans* conversion occurs in the dark due to the thermodynamically stability of the *trans* isomer (Figure 1.10). An important application of this class of chromophores is the photochemical control of the behaviour of modern liquid-crystals-based devices and it is strictly related to the large geometry change associated with azobenzene isomerization.<sup>77</sup>

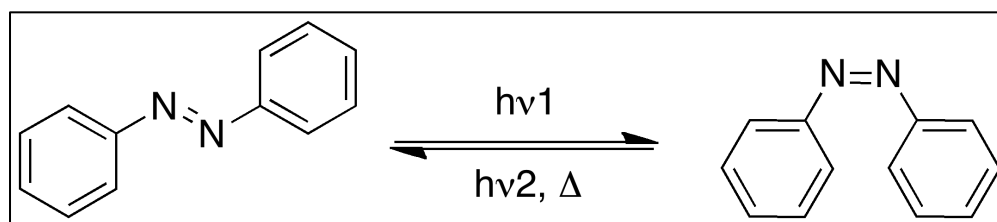


**Figure 1.10:** Photo-isomerization of azobenzenes.

The photochromic properties of benzospiropyrans were first discovered by Fischer and Hirschberg in 1952<sup>78</sup> where they observed that irradiation of several solutions of benzospiropyrans with UV-light (not exceeding 450 nm) were changing colour that could be reversed by exposing the same solutions to yellow light (containing no radiation below 500 nm).

An interesting study concerning a series of spiroconjugated compounds was made by Maslak *et al.*: these molecules differed in the structure of the  $\pi$  systems of the two halves of the molecule connected through the common insulating tetrahedral carbon.<sup>79</sup>

They named one half “the donor” (substituted diamines, like Figure 1.11 structure **4**) and the other “the acceptor”, (indandione moieties, like Figure 1.11 structure **1**) and they synthesized a series of spiro compounds formed by combinations of different diamines and indandione units in order to study the influence of the molecular structure of the two  $\pi$  arrangements in the spiro conjugation effect. The donor and the acceptor part have been

chosen on the basis of the determination of the energy and the symmetry of their orbitals using MOPAC calculations.<sup>74</sup>

Only acceptors with an antisymmetric LUMO and donors with antisymmetric HOMO will generate interactions, which will give rise to new spiro conjugated orbitals spanning the entire spiro molecule. The new lower energy orbital (HOMO) corresponds to the bonding combination between the two halves and the higher energy one (LUMO) corresponds to the antibonding combination.

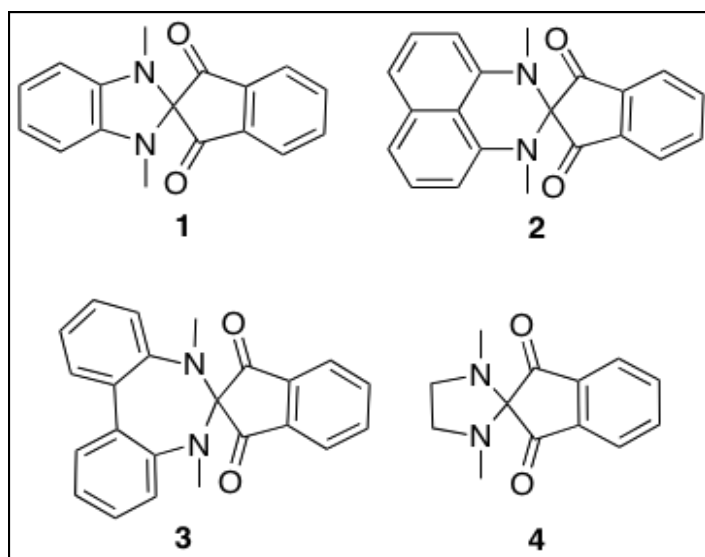


**Figure 1.11:** Structures of four spirocompounds synthesized by Maslak *et al.* with different interactions between the donor (1,3-indandione) and acceptor moiety (different N,N-dimethyl amines).<sup>79</sup>

This demonstrated that spiro conjugation occurs most readily when the symmetry of the LUMO of the acceptor and one of the HOMO of the donor are antisymmetric versus both molecular planes of the spiro orthogonal structure. When this condition is satisfied, the HOMO energy is lowered compared to isolated donor part and the LUMO energy is increased compared to the isolated acceptor, so that the difference between the two energy levels is lower. Orbital overlap then occurs and new bands in the visible region of the absorption spectra appear, while when considering the two isolated molecules that correspond to the two halves of the spiro-compound they do not show any appreciable band above 370 nm.

The intramolecular nature of the charge transfer is confirmed by the fact that the new bands in the visible region follows the Lambert-Beer law and that the  $\lambda$  max value and the extinction coefficient remain constant over dilution.

These spirocompounds are composed of 1,3-indandione moieties as an acceptor (kept constant) in which the  $\pi$  system has an antisymmetric LUMO, and different aromatic and non-aromatic N,N-dimethyl amines as donor (Figure 1.9(a) and (b)) The generated

compounds present a new absorption band in the visible region, although the presence and the entity of the charge transfer phenomenon due to spiro conjugation varies, depending on the symmetry of the orbital of the donor and acceptor part.

These molecules prepared by Maslak *et al.* demonstrate how in spiro moiety the charge transfer phenomenon depends both on the symmetry of the orbitals and on the strength of the donor and the acceptor.<sup>79</sup>

Among the different families of photochromic compounds, benzospiropyrans are probably the most widely studied<sup>80</sup> due to their high photosensitivity, clear colour change and rapid switching kinetics between the two isomers, one of which has a guest binding site for certain metal ions.<sup>47</sup> When the photochromic behaviour is combined with the possibility of switchable guest binding, in principle the binding behaviour can be switched “on” and “off” using external light stimulation. In the “off” state, binding sites are passivized hence the active surface is deactivated, whereas in the “on” state the surface binding sites are activated and available.

Benzospiropyrans refer in general to (substituted) *2H-1-benzopyrans* having a second ring system, usually (but not necessarily) heterocyclic, attached to the 2-carbon atom of the pyran in a spiro manner with a common tetrahedral carbon atom.<sup>78</sup> The two halves of the molecule co-join two orthogonal planes (Figure 1.12).

The benzopyran part is the common structure to all spiroopyrans (Figure 1.12), except for different substitutions on the aromatic ring, while the heterocyclic part is variable and often built upon mono or bi-heteroatomic azaheterocycles saturated or benzofused.<sup>81</sup>

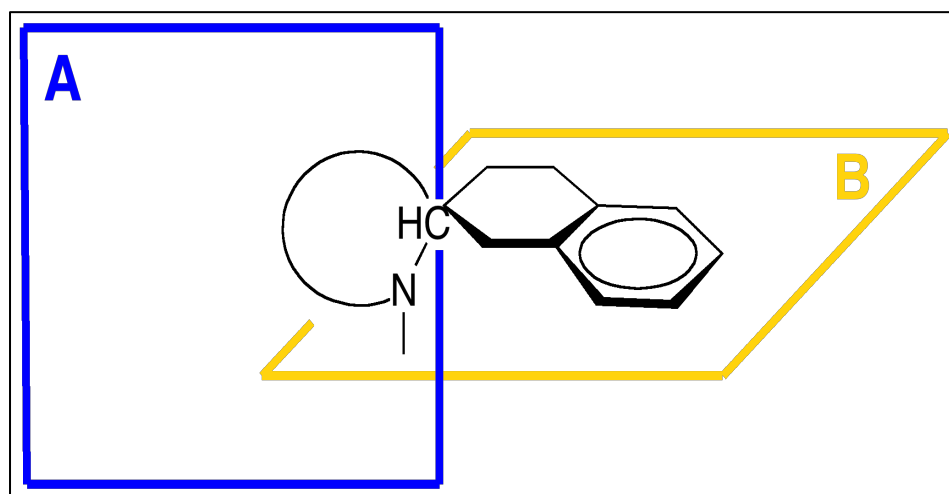


**Figure 1.12:** (a) Schematic representation of a Benzospiropyran in its closed aplanar form (two planes, A and B).<sup>67</sup>

Upon irradiation of UV light, the C<sub>spiro</sub>-O bond in the **BSP** form is cleaved heterolytically process during which the sp<sup>3</sup>-hybridised “spiro” carbon achieves sp<sup>2</sup> hybridisation and becomes planar. The aromatic group rotates, aligns its  $\pi$ -orbitals with the rest of the molecule and it forms the conjugated system of the merocyanine form, with ability to absorb photons of visible radiation, and therefore strongly coloured. When the UV source is removed, the molecules immediately relax to their ground state, the carbon-oxygen reforms, the spiro carbon atom becomes sp<sup>3</sup> hybridised again and the molecule returns to its colourless state.

In solution the **BSP** form presents an absorption spectrum in the UV range (200-400 nm) with an actinic band situated between 320-380 nm. The absorption around this band causes conversion to the **MC** form, in which the conjugation between the two halves of the molecule results in a shift of the absorption band from the UV to the visible region of the spectrum.<sup>65, 82, 83</sup>

The **MC** is a negative solvatochromic dye,<sup>74</sup> *i.e.* with increasing solvent polarity the adsorption band undergoes a hypsochromic (blue) shift (Figure 1.13). Studies on the solvent effect on the **MC** have shown that when the absorption maxima of **MC** are plotted against solvent polarity parameters, such as ET(30) values,<sup>84</sup> Kosower’s Z values,<sup>84</sup> Brooker’s Xb values<sup>85</sup> and Brownstein’s values,<sup>86</sup> that reasonable linear plots are obtained.

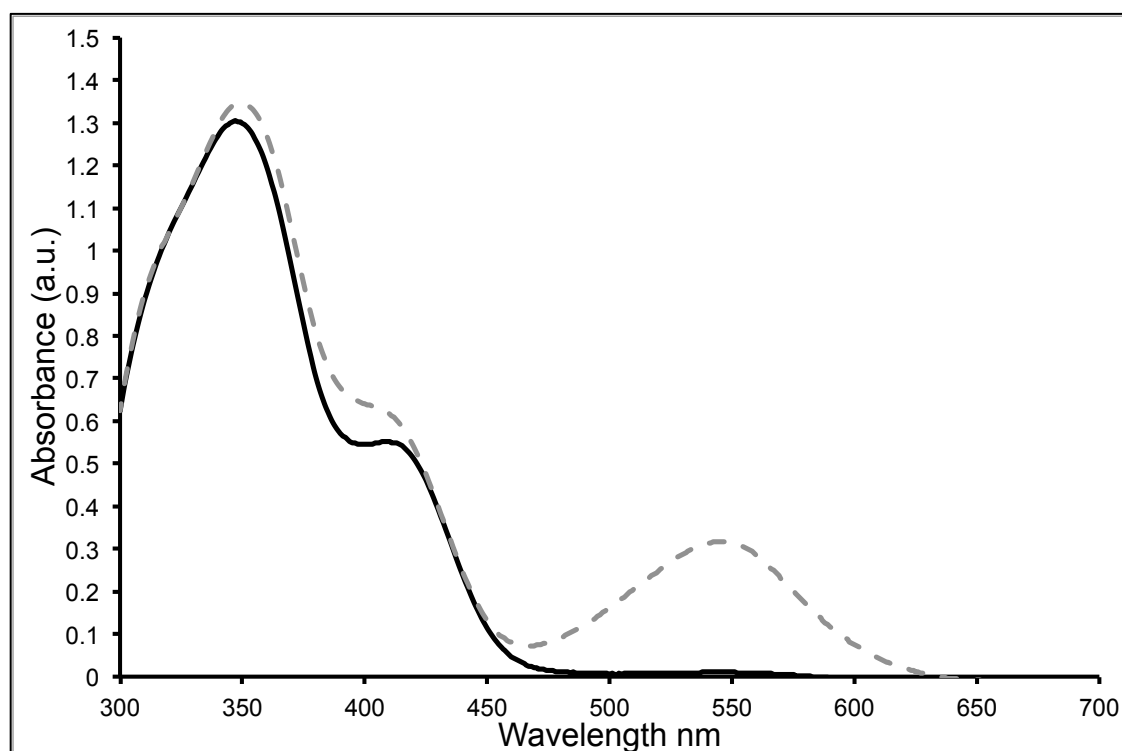


**Figure 1.13:** UV-*vis* spectra of **BSP** (black line) and photonicallly generated **MC** isomer (dashed line).

Generally benzospiropyrans undergo “positive” photochromism, as the thermodynamically less stable state is more deeply coloured. Upon UV irradiation the solution acquires a strong coloration that then fades thermally back to the original colourless **BSP** state. Benzospiropyrans containing hydroxyl, carboxyl and amine groups, exhibit so called “negative” photochromism as their solutions appear moderately coloured in the dark and reversibly fade under UV light exposure.<sup>74</sup>

Besides photochromism, many benzospiropyrans also exhibit thermochromism and their solutions become coloured when heated. In general the photochromic property of benzospiropyrans depends on the structure of the derivative, the solvent and the temperature.

### **1.5.2 Physico-Chemical Aspects of Spiropyrans: Dynamics of Conversion to the Merocyanine Form**

As previously mentioned, spiropyrans have two perpendicular  $\pi$ -electron systems linked through a spiro tetrahedral carbon atom. Molecules having similar structure can be subjected to spiro-conjugation: i.e. there could be an overlap between the  $\pi$  orbitals accompanied by electron delocalization which leads to the appearance of a characteristic band in the visible region of the spectrum, due to intermolecular charge transfer between the two halves of the molecule.<sup>74</sup>

Spiro-conjugation is verified when two halves of the spiro compound, linked by the spiro atom, consist of an electron-donor and electron-acceptor part, whose frontier orbitals (the LUMO of the acceptor and the HOMO of the donor) are anti-symmetric with respect to the two planes generated by the two halves of the molecule separated by the spiro carbon (Figure 1.14).

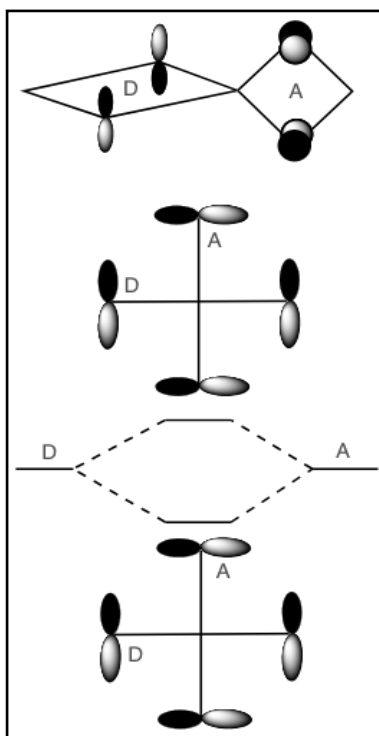


**Figure 1.14:** Schematic representation of the  $\pi$  orbitals of the two-allyl systems connected through a tetrahedral spiro carbon centre. In this spiro-conjugated system D is the donor part (substituted diamines) and A is the acceptor part (indandione moiety).<sup>74</sup>

This symmetry leads to a non-zero overlap which is required for intramolecular interactions and the electronic transition between these two orbitals correspond to a charge transfer transition.<sup>87</sup>

From the calculations, only acceptors with an anti-symmetric LUMO and donors with anti-symmetric HOMO will generate interactions that will give rise to new spiro conjugated orbitals spanning the entire spiro molecule. The new lower energy orbital (HOMO) corresponds to the bonding combination between the two halves and the higher energy one (LUMO) corresponds to the antibonding combination.

The intramolecular nature of the charge transfer is confirmed by the fact that the new bands in the visible region follows the Lambert-Beer law and that the  $\lambda$  max value and the extinction coefficient remain constant over dilution.

### 1.5.3 Solvatochromism

The solvatochromic behaviour of spiropyran depends on the polarity of the medium that it is in. This change is exhibited with pronounced changes in the position and intensity of the UV-*vis* absorption bands. These changes are caused by intermolecular interactions between the solute and solvent that modify the energy gap between the

ground and excited state of the absorbing species.<sup>83,74</sup> Consequently, variations in the position, intensity, and shape of the absorption spectra can be direct measures of the specific interactions between the solute and solvent interactions.

The solvatochromism of spiropyrans depend on three main factors: 1) solvent polarity, 2) nature of the substituent groups and 3) concentration of the solution. The solvatochromism effect of spiropyran may be governed by two mechanisms: the first is related to the shifting of the equilibrium between the **BSP** and the **MC** form when the molecule is placed in a solvent with different polarity. This effect is manifested by a shift in the absorption bands. The second is governed by the interactions that may occur between solvent and solute in solvents with different physical and chemical properties.

In general for nitro-benzospiropyrans, as the polarity of the solvent increases, the maximum absorbance to shorter wavelengths (*hypsochromic* or blue shift) is observed, while the opposite is true for a decrease in polarity (*bathochromic* or red shift).

The coloured **MC** form is highly conjugated and characterised by strong polar features, due to its zwitterionic character that strongly contributes to the electronic distribution of the ground state. As a consequence **MC** is stabilised by polar solvents, which decrease the thermal relaxation rate constant and the reversion **MC-BSP** (Figure 1.15).

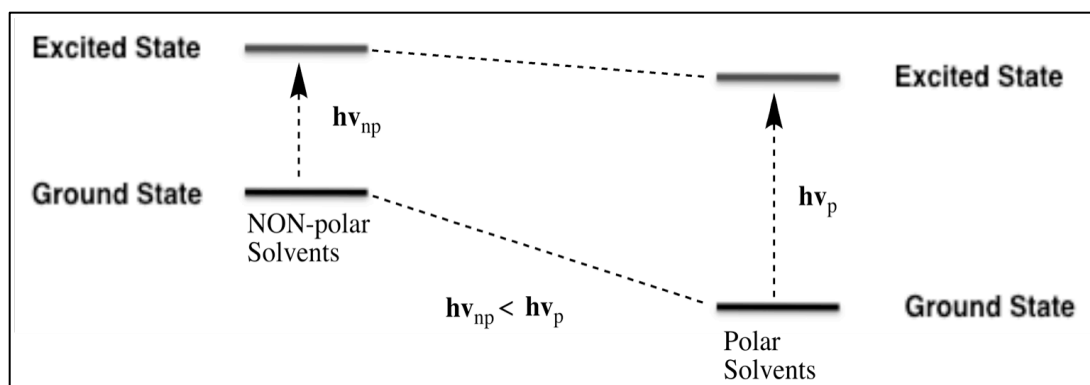


**Figure 1.15:** Schematic representation of the energy difference between the ground and the excited state of the MC form in polar and non-polar solvents.<sup>83</sup>

Advances in the understanding of the mechanisms involved in the solvatochromic process have been achieved by Byrne *et. al.* who studied the **BSP-MC** isomerisation in alternative solvents, such as ionic liquids.<sup>88-90</sup> Ionic liquids (**ILs**) are classified as salts that have a melting point below 100 °C, thus forming liquids that are comprised entirely of cations and anions. A subclass of **ILs** known as room temperature ionic liquids (**RTILs**), in particular have the most applicable characteristics for solvent use compared to traditional organic solvents (low vapour pressure, majority of **ILs** are non flammable

and can be tailored for a specific system). In recent years, **ILs** have been shown to act as recyclable solvents and have replaced molecular solvents in catalysis, electrochemistry and synthesis.<sup>91</sup> The combination of this particular solvent (**ILs**) with **BSP** moieties was aimed to probe the structure of ion - ion interactions as the **BSP-MC** isomerisation can reveal a significant amount of information about its surrounding molecular environment: (1) at equilibrium an estimation of polarity can be calculated from the value  $K_e$ , the population of non-polar **BSP** versus the highly polar **MC**, (2) the **MC** isomer exhibits a large negative solvatochromic shift with increasing polarity, (3) the **MC** isomer possesses a large polarisable-electron system, suitable for the registration of dispersion interaction, (4) the phenolate oxygen on the **MC** exhibits a highly basic, electron pair donor, suitable for interaction with hydrogen bond donors and Lewis acids.

#### 1.5.4 Photochemical Behaviour of Spiropyrans

The photochemical activity of spiropyrans depends on: the polarity of the  $C_{\text{spiro}}\text{-O}$  bond, the charge distribution on the benzopyran ring (in particular the presence of electronegative groups on the benzene ring) and the degree of interactions between the indoline and the benzopyran sections.<sup>74</sup>

Ground state interactions between two halves of the spiropyran molecule around the spiro carbon occur as a consequence of stereo electronic phenomena arising from negative hyperconjugation and the anomeric effect.<sup>92</sup> Negative hyperconjugation can be described as the donation of electron density from filled  $n_\pi$  orbitals (non bonding orbitals) containing a lone pair electron to a  $\sigma$  bond or  $\sigma^*$  antibonding orbital, resulting in building a  $\pi$  character into bonds that nominally possesses only  $\sigma$  character.<sup>92</sup>

The anomeric effect was initially used to explain the tendency of the heteroatomic substituents to prefer an axial instead of the equatorial orientation in a cyclohexane ring. Generally speaking this conformational phenomenon occurs in a system wherein a carbon is linked to a heteroatom with a lone electron pair on one side, and to an electronegative atom on the other.

In spiropyran the spiro carbon is covalently joined to the indoline nitrogen and to the benzopyran oxygen. The nitrogen orbitals have a pyramidal structure with the lone electron pairs perpendicular to the plane formed by  $C_{8a}$  and  $C_{\text{spiro}}$  ( $C_{22}$  Figure 1.16 (a)), with the plane formed by  $N\text{-}C_{\text{spiro}}\text{-}C_3$ , forming a dihedral angle approximately  $23\text{-}30^\circ$ . This structure reduces the conjugation between the lone pair electron of the N and the  $\pi$  system of the benzene ring.<sup>74</sup> On the other side, the electron density of the lone pair

electron on the oxygen occupies a *trans* position relative to that of the unshared electron pair of the nitrogen. This conformation causes specific interactions between the lone pair electron orbital on the nitrogen ( $\eta_N$ ) and the antibonding orbital between the  $C_{\text{spiro}}$  and the electronegative oxygen atom ( $\sigma^*_{\text{C-O}}$ ), and defines the anomeric effect.

Considering that the electronegativity of the oxygen is greater than that of the nitrogen, the energy level of the electron pair in the  $\eta_O$  is lower than the  $\eta_N$  and the antibonding orbital  $\sigma^*_{\text{C-O}}$  is lower in energy than the  $\sigma^*_{\text{C-N}}$ . As a result, interactions between the  $\eta_N$  and the  $\sigma^*_{\text{C-O}}$  occurs, leading to a strengthening of the  $C_{\text{spiro-O}}$  bond<sup>74</sup> (Figure 1.16 (b)). Studies on the length of these bonds shows that the  $C_{\text{spiro-N}}$  bond is in the range of 1.432-1.453 Å, shorter than the normal length of a general  $C_{\text{sp}^3} - N_{\text{sp}^3}$  bond (1.47-1.48 Å)<sup>74</sup>, while the  $C_{\text{spiro-O}}$  bond is remarkably longer than usual, being in the range of 1.452-1.497 Å, instead of 1.41-1.43 Å.<sup>74</sup>

This variation in the  $C_{\text{spiro-O}}$  bond length is critical in determining the overall photo behaviour of the spiropyran, as it has been found that under continuing irradiation of their solutions, all spiropyrans with  $C_{\text{spiro-O}}$  bond length longer than 1.42 Å undergo photochromism, while spiropyrans with  $C_{\text{spiro-O}}$  shorter than 1.42 Å do not.<sup>74</sup>

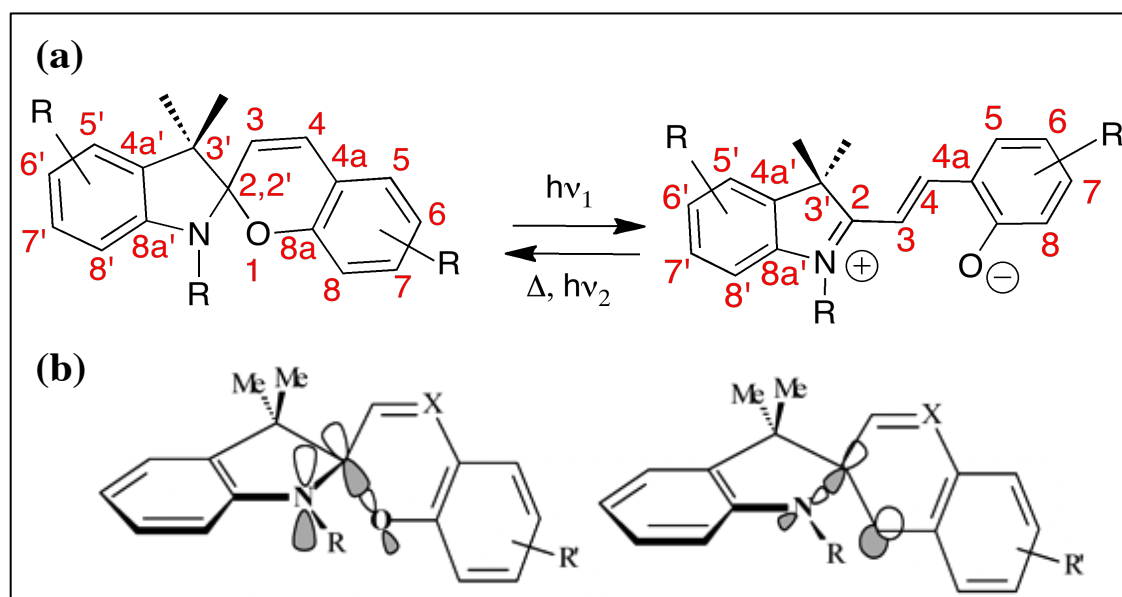
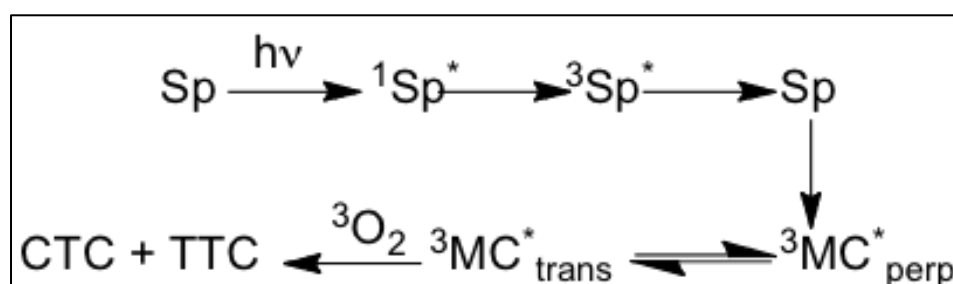


**Figure 1.16:** (a) schematic representation of indolinespirobenzopyran moiety's numbers.<sup>74</sup> (b) Figure representing the two spatial interactions which may occur between the lone pair electrons on the nitrogen and oxygen and the  $\sigma^*$  antibonding between the  $C_{\text{spiro}}$  and the two heteroatoms. As the electronegativity of the oxygen is greater than one of the nitrogen, the energy of the unshared electron pair in the  $\eta_N$  is greater than the one in the  $\eta_O$  and the energy level of the  $\sigma^*_{\text{C-O}}$  is lower than the  $\sigma^*_{\text{C-N}}$ . For these reasons the interaction between the  $\eta_N$  electrons and the  $\sigma^*_{\text{C-O}}$  (A) is favoured compared to the lone pair  $\eta_O$  electrons interactions with  $\sigma^*_{\text{C-N}}$  (B), determining a weakening of the  $C_{\text{spiro-O}}$  bond and a strengthening of the  $C_{\text{spiro-N}}$  bond.<sup>74</sup>

The presence of electronegative substituents on the benzene ring linked to the pyran cycle further increased the photochemical properties of the spiropyran molecule. For example, the presence of electron accepting substituents on the benzopyran ring, such as nitro groups ( $\text{NO}_2$ ) leads to an increase in delocalisation due to electron transfer from the lone pair of electrons located on the oxygen  $\pi$  system of the benzene ring, thus further weakening the  $\text{C}_{\text{spiro}}\text{-O}$  bond. The stabilisation effect of the **MC** form is also verified once the  $\text{C}_{\text{spiro}}\text{-O}$  bond has been cleaved by vibrational excitation as the electronegative nitro group enhances delocalisation by resonance of the negative charge on the oxygen, when cleavage occurs.<sup>83,74</sup>

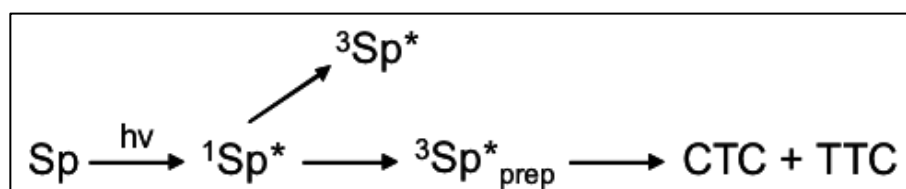
In Scheme 1.3 is depicted the proposed mechanism involving nitrospiropyrans with the nitro group in position 6 (Figure 1.16 (a)) and with or without a functionality in position 8. This involves intersystem crossing to the short-lived triplet state of the ring closed isomer  $^3\text{Sp}^*$ , which serves as the precursor to the triplet so called ‘perpendicular’ merocyanine form  $^3\text{MC}^*_{\text{perp}}$ . This conformation is in equilibrium with the triplet of the trans isomer, observed as a short lived transient with absorption maxima at 420-440 and 560-590nm and a lifetime  $< 10$  ms. The reaction ends with quenching the triplet with oxygen and establishing a thermal equilibrium between the most stable merocyanine isomers, presumably CTC and TTC (Figure 1.14). The presence of oxygen in solution strongly influences the dynamic of the overall photo-induced reaction of isomerization and in particular the quantum yields of the population of the merocyanine triplet state.<sup>93</sup>



**Scheme 1.3:** Photochemical ring opening reaction of nitro containing spiropyrans and the intermediates involved in the process.

The position of  $\text{NO}_2$  on the pyran ring is crucial for the stabilisation of the open **MC** form. Only *para* and *ortho* nitro substituted benzene rings show this stabilisation effect of the **MC** form due to mesomeric effect.<sup>74</sup> A nitro group in spiropyran has a dual effect on their photochromic capacity. On the one hand, it strongly enhances the quantum yield of the photocolouration (up to 0.7 - 0.9 in solvents of low polarity), and on the other hand, it also enhances the quantum yield of the intersystem crossing, which

facilitates formation of singlet molecular oxygen from the triplet excited state and  $^3\text{MC}^*$ , thus, photodegradation of spiropyran via oxidation by singlet oxygen. The adverse influence of the inclusion of highly reactive triplet states (both  $^3\text{Sp}^*$  and  $^3\text{MC}^*$ ) of spiropyran into the mechanism of the ring opening on their fatigue resistance properties has been recognized by many authors.<sup>93</sup> It was found that the quantum yields of irreversible photodegradation of various spiropyran are virtually independent of the nature of their ‘left-half’ heterocyclic moiety and are directly correlated with the lifetime of the triplet-state intermediate formed upon excitation. For spiropyran without nitro groups in the benzopyran rings, the quantum yields of the photocoloration are essentially independent of solvent polarity and are substantially lower than those for spiropyran with nitro groups. In contrast to the latter, spiropyran without nitro groups display photochromism only in the excited singlet manifold.



**Scheme 1.4.** Photochemical ring-opening reaction of spiropyran not containing nitro group and the intermediates involved in the mechanism.

The mechanism of the photochemical process is schematically represented in Scheme 1.4, where the structure of the singlet excited-state intermediate  $^1\text{Sp}^*_{\text{prep}}$  corresponds to that formed upon immediate cleavage of the  $\text{C}_{\text{spiro}}\text{-O}$ . According to the CASSCF<sup>1</sup> modeling of this process, the structure similar to  $^1\text{Sp}^*_{\text{prep}}$  in Figure 1.17 does not conform to a real intermediate but rather a crossing point, i.e., a conical intersection between the lowest singlet excited-state and ground-state energy surfaces. At this point, two reaction valleys are generated, one of which leads to ring closing to the initial spirocyclic form and the other one to the formation of the *cis-cisoid* (CCC) ring-opened form, to be compared with Figure 1.19. The existence of this intermediate, usually called the X-form, was first proposed on the basis of the studies of the photochemistry of spiropyran in low-temperature matrices.

The cleavage of the  $\text{C}_{\text{spiro}}\text{-O}$  due to photo-excitation leads to the formation of an opening excited state in a time scale of femtoseconds while a small fraction reforms the broken  $\text{C}_{\text{spiro}}\text{-O}$  bond (also in the femtoseconds time scale), its major fraction

<sup>1</sup> Complete Active Space-Self Consistent Field

vibrationally relaxes with a constant time of picoseconds (strictly depending on the medium), undergoing subsequent isomerisation which leads to the formation of the coloured isomer, a conjugated **MC** form, which strongly absorbs in the visible region due to delocalization of the  $\pi$ -electronic system. These transient isomers can be represented as different resonance forms of a twisted cisoid (which appears just after the  $C_{\text{spiro}}\text{-O}$  bond breaks) and planar transoid stereoisomers, which are more stable, as it minimises the non-bonding interactions (Figure 1.17).<sup>83</sup>

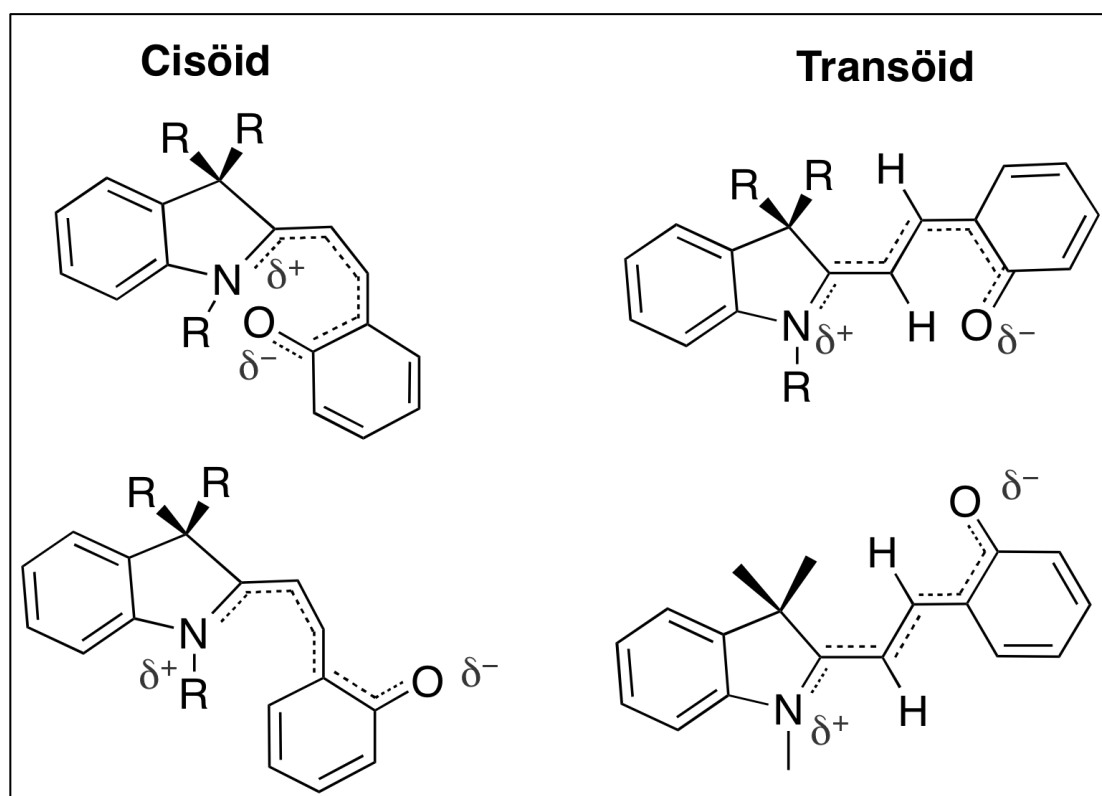


**Figure 1.17:** Examples of possible cisoid and transoid of the **MC** form.<sup>83</sup>

As the structure of the transoid stereoisomers is similar to one of Brooker's merocyanine dyes,<sup>94</sup> the ring open form of indolinebenzospiropyrans has been named after it.

Brooker's merocyanine dyes exist in two forms, a covalent quinone and a zwitterionic form, and the equilibrium between these two depends on the surrounding environment. In a similar way, the spiropyran photo-merocyanine in the more stable transoid isomers can be described as a resonance hybrid between a quinonic and a dipolar zwitterionic form (Figure 1.18).

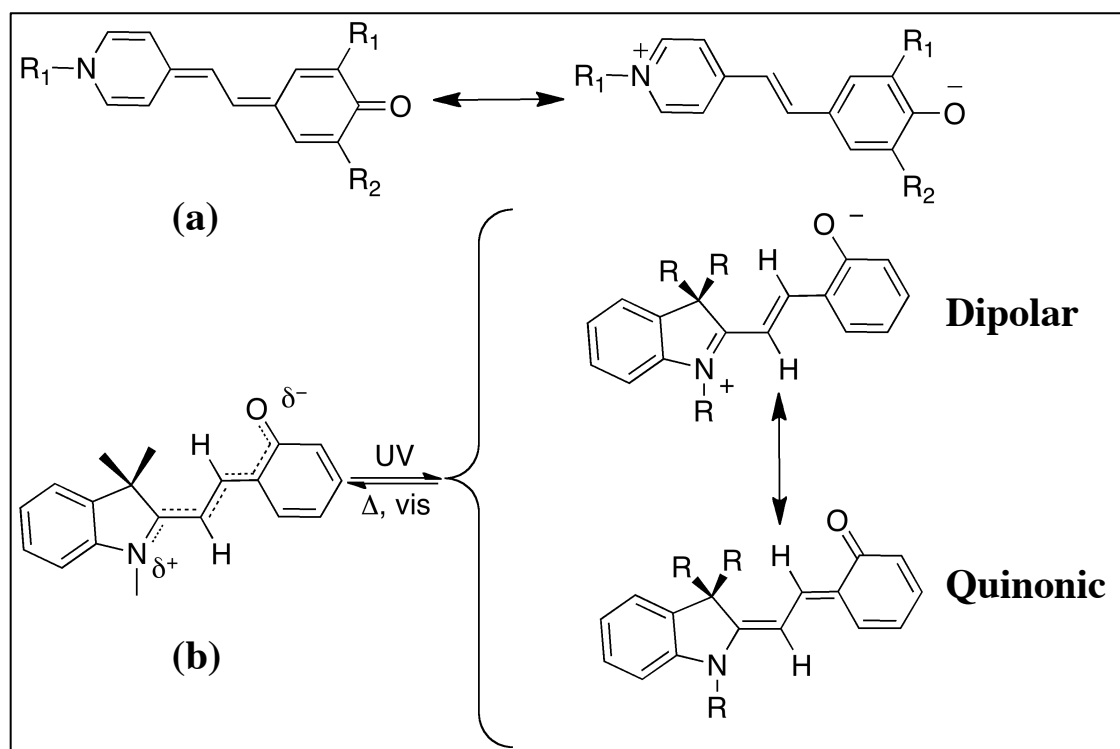


**Figure 1.18:** (a) Brooker's merocyanine equilibrium isomers; (b) Quinonic and dipolar resonance hybrids of a transoid structure of the ring-open BSP merocyanine form.<sup>94</sup>

The ring opening reaction which starts with cleavage of the C<sub>spiro</sub>-O bond initially leads to the formation of a sterically strained intermediate which is higher in energy as the two halves of the molecule are still orthogonal to each other. This rapidly converts to the more stable, planar transoid isomers<sup>74</sup>.

Different **MC** isomers have been identified using transient spectroscopy methods. They all differ for the geometrical arrangements along the central chain of the three conjugated C-C bonds (C<sub>22</sub>, -C<sub>3</sub>, -C<sub>4</sub>, -C<sub>4a</sub>, referred to Figure 1.19 (a)), defining three dihedral angles. All three carbon bonds have a partial double-bond character, and their dihedral angles can be closer either to 0° or to 180°, which correspond to cisoid and transoid configurations.

These cisoid or transoid configurations have been labelled by a sequence of three C or T letters indicating the setting of the three dihedral angles (Figure 1.17). Only the isomers having a central transoid segment represent a local energy minimum and are stable **MC** isomers. The other cisoid configurations are at a relatively higher energy level due to internal steric hindrance. The structures of the most stable isomers have been reported as TTC and CTC conformers (Figure 1.19) as these possess a larger dipole moment according to theoretical modelling calculations.<sup>74</sup>

Upon light excitation, C<sub>spiro</sub>-O bond cleavage is induced with formation of a cisoid intermediate, which through subsequent rotation around the C<sub>spiro</sub>-N bond leads to the

**MC** isomer **CTC** which undergoes isomerisation through rotation of the C-C bond leading to the formation of the more stable **TTC** isomer (Figure 1.19).

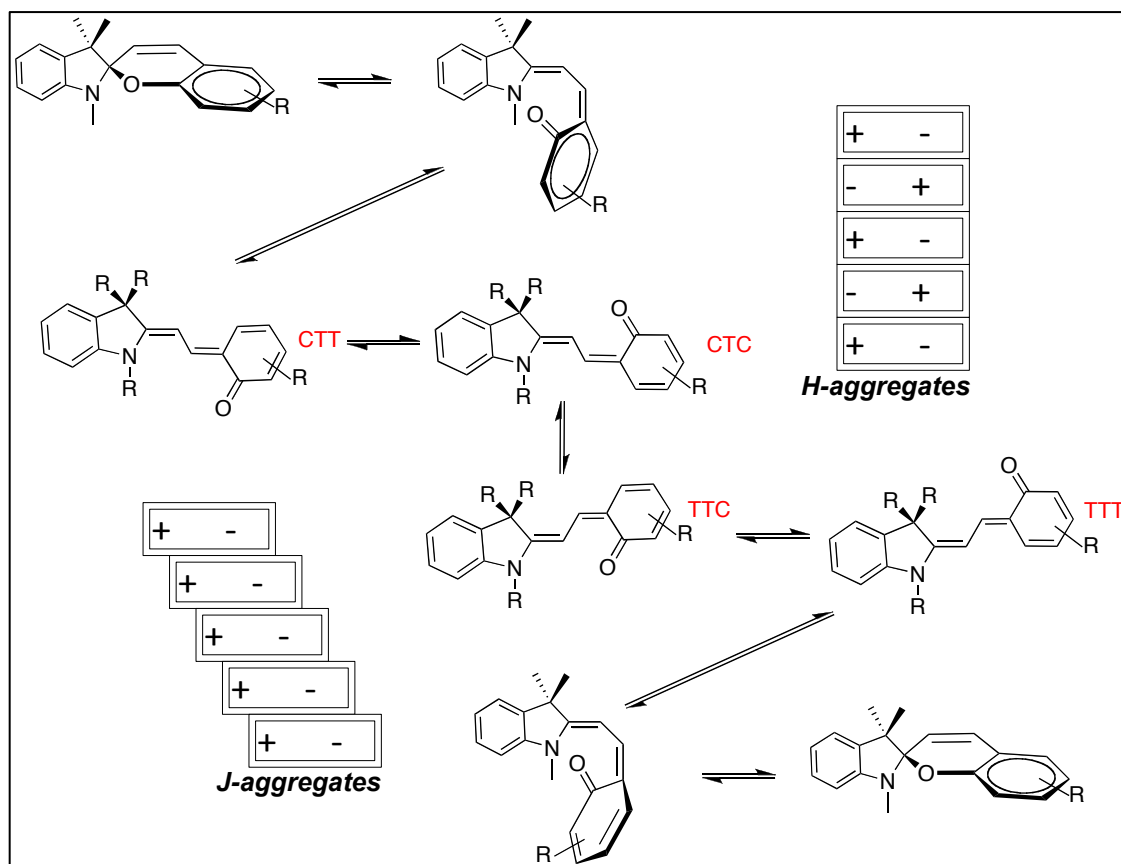
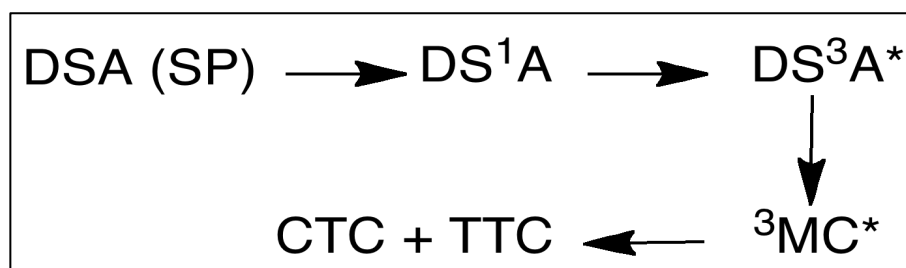


**Figure 1.19:** Schematic representation of different possible intermediate isomers induced by photo excitation of the ring closed **BSP** form.<sup>74</sup>

The nature of the excited states is strongly dependent on substitution of the parent spirobenzopyran ring<sup>74</sup>. For compounds containing a nitro group studies performed using resonance Raman spectroscopy, laser photolysis and quenching have shown that the ring-opening mechanism follows a triplet state pathway, with the excitation inducing the formation of an open cisoid singlet state which converts by intersystem crossing to a triplet state (enhanced by the presence of the nitro group)<sup>74</sup>. This is the precursor of a triplet **MC**, which is quenched in the presence of oxygen to form a more stable **CTC** and **TTC** transoid conformer (Scheme 1.5). In contrast the excitation of spirocyan without a nitro group follows a singlet pathway.



**Scheme 1.5:** Schematic representation of the triplet excitation pathway followed by nitro substituent spiropyran. DSA represents a general spiropyran with a nitro group in the benzopyran ring (A) which is linked to a D indoline through a spiro carbon atom (S).<sup>94</sup>

After removal of UV-light irradiation, the enhanced coloration slowly reverts back to the original ring closed colourless spiro form. The relaxation time at room temperature depends significantly on the structure of the spiropyran and on the solvent polarity. This thermal decolouration of the MC has been demonstrated to follow a first order decay rate.<sup>95</sup>

In summary, indolinespirobenzopyran derivatives are strongly affected by solvent polarity and by the presence of oxygen. Upon UV irradiation they undergo strong colour changes and they will be of important focus in this thesis.

### 1.5.5 Thermochromism

In solutions of non-polar solvents, most spiropyran exist as ring-closed isomers, but upon dissolving in polar solvents they can undergo thermal ring opening to the corresponding merocyanine forms. The position of the established complex equilibrium depends on many factors, primarily solvent polarity, the nature of the substituents, and the concentrations of the solution. Thermal equilibrium established in solutions of spiropyran is depicted in Figure 1.19, with indolinospirobenzopyran by way of example. The ring-opening reaction starts with cleavage of the C-O bonds in the stereoisomers to give rise to sterically strained chiral intermediates, which rapidly convert to nearly planar merocyanine isomers, labelled according to the configurations of the molecular fragments relative to the two double bonds (*cis*, *trans*: **C** and **T**) and a partially double bond, neutral quinoid or the zwitterionic oxygen (*s-cis*, *s-trans*: **C**, **T**). Because *s-cis* conformers are significantly higher in energy than their *s-trans* isomers, Figure 1.16 is restricted to the interconversion of the latter. The presence of more than one merocyanine isomer in solutions of spiropyran has been shown in several studies using transient spectroscopy, <sup>1</sup>H, <sup>13</sup>C and time-resolved resonance Raman spectroscopy experiments.<sup>96</sup> The structure of the most stable isomers was determined as TTC and

CTC conformers. This finding is in accord with the conclusions made on the basis of theoretical modelling of the equilibria.<sup>97</sup>

The dependence of the relative stability of the ring-closed and ring-opened forms of spiropyran on the structure of their indoline section and the type of annulation of the 2H-pyran moiety with benzene ring(s) was studied in much detail. Electron-withdrawing substituents in 2*H*-chromene moieties of spirobenzopyran favor the stabilization of the ring-opened forms. The maximal effect is attained when strong electron-accepting groups, such as nitro or arylazo groups, are placed in the *p*- or/and *o*-position relative to the phenolate oxygen of the merocyanine acquiring the zwitterionic character. Solutions of these compounds in polar solvents at room temperature contain measurable amounts of the ring-opened forms.

As shown in Figure 1.19 the polar merocyanine forms of spiropyran tend to associate into stack-like aggregates.<sup>98</sup> This tendency is very strong, and rather stable associates are formed in very dilute solutions and even in polymeric films. Absorption spectra of *J*-aggregates, which have a head-to-tail arrangement of the molecular dipoles, are shifted to longer wavelengths relative to the spectra of the isolated merocyanine molecules. For *H*-aggregates having a head-to-head arrangement of the molecular dipoles, the spectra are shifted to shorter wavelengths. An important property of the *J*-aggregates produced by irradiation of solutions in non-polar solvents is that their spectra consist of very narrow absorption bands (absorption peak widths are a few tens of nanometers), which is a necessary condition for design of wavelength-multiplexed memory systems. It has also been shown that the formation of the spiropyran aggregates causes very large changes in the refractive indices and, thus, provides a new approach towards the synthesis of tuneable photonic gap materials.

### 1.5.6 Synthesis of Benzospiropyran (BSP)

BSP's are commonly prepared from a Fisher base (heterocyclic ammonium salt in basic medium) and 2-hydroxysalicylaldehyde derivatives. The Fisher base is generally a 2-ethylene-1,3,3-substituted indoline. The solvent is generally anhydrous ethanol, or benzene when a substrate in the reaction is labile or possesses other reactive functions (Figure 1.20).

The reaction mechanism involves the formation of a carbanion by the mesomeric effect from the Fisher base, and this species carries out a nucleophilic attack to the carbonyl group of the substituent 2-hydroxysalicylaldehyde. This is followed by ring

closure through intramolecular addition of the phenolic oxygen to the ammonium group which gives, under elimination of water, the spiro compound (Figure 1.20).<sup>99</sup>

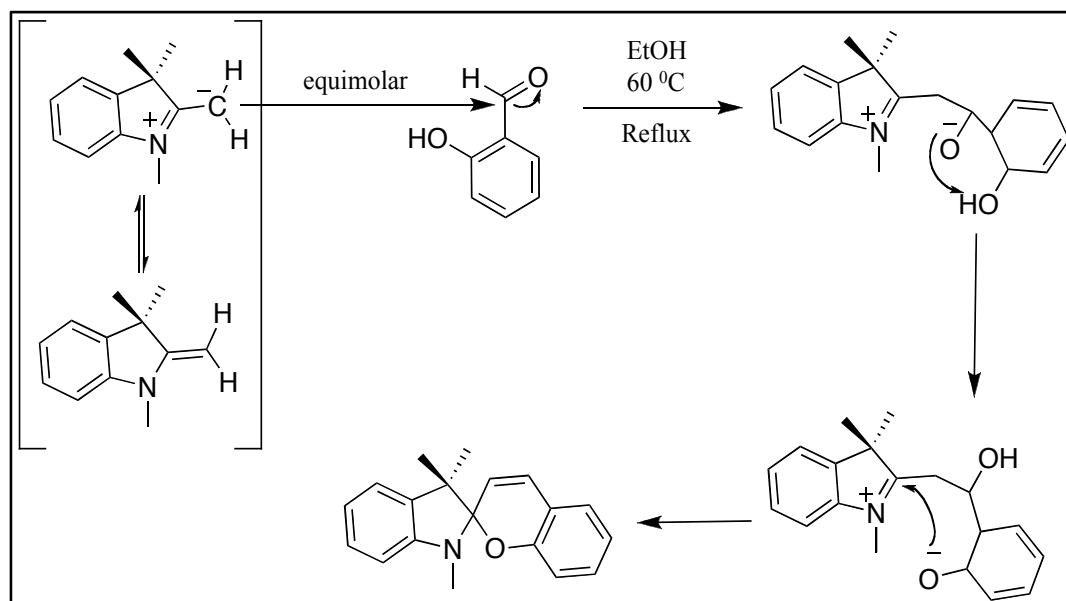


**Figure 1.20:** Schematic representation of the reaction mechanism between the Fischer base and the 2-hydroxysalicylaldehyde derivatives to produce a general indoline benzopyran molecule. The two most commonly used methods consist of the condensation of a heterocyclic quaternary salt with an alkyl group in a vicinal position with respect to the heteroatom or the corresponding methylene base with 2-hydroxyarenealdehydes or their heterocyclic analogues. Due to the ready availability of 1,3,3-trimethyl-2-methyleneindoline (Fischer's base) and its derivatives, and due to the particularly valuable properties of spiroopyrans containing their fragments, the reaction already employed for the preparation of many hundreds of 1,3-dihydrospiro (2H-1-benzopyran-2,2''-(2H)-indoles (final product in the figure) may undoubtedly be regarded as the most important in the chemistry of spiroopyrans. Generally, the reaction occurs smoothly upon refluxing ethanol solutions of equimolar amounts of the components to afford the desired moiety in 70-98% yields.<sup>99</sup>

### 1.5.7 Protonation and Acidichromism

The phenolate ion derived from the isomerisation of indolinespirobenzopyran into its **MC** is also able to interact with protons in solution.<sup>100, 101</sup>

The protonation of **MC** has been observed when strong acids are added to organic solutions of spiroopyran. The resulting protonated phenolate results in a *hypsochromic* shift of the **MC** band. A direct effect of the protonation of **MC** is a stabilisation of this polar isomer by a non-thermal, non-photochemical route, and creates a stable positive charge upon the molecular unit at the phenolate group (Figure 1.21 (a) and (b)).<sup>102</sup>

This aspect is of particular interest from the material science point of view as through protonation, it is possible to create a stable charge that can be easily reversed by irradiation of visible light.

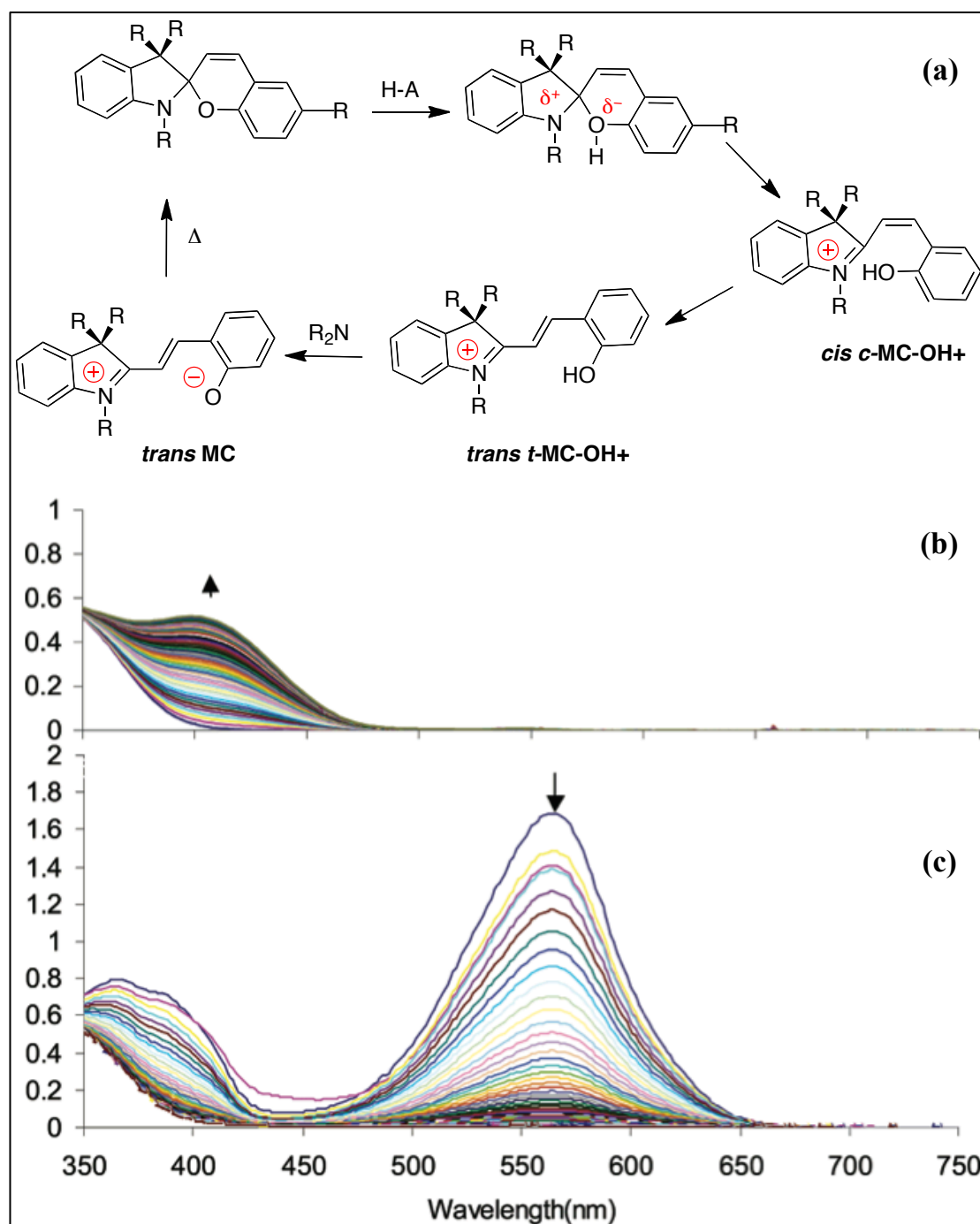


**Figure 1.21:** (a) Schematic representation of the mechanism of protonation of a spiro-moiety. (b) Stacked absorption vs. wavelength plots depicting two distinct thermal processes. SP-1  $\Rightarrow$  MC-OH<sup>+</sup> in the presence of [TFA]  $5 \times 10^{-4}$  M, in acetone at 25 °C, time interval) 600 s; (c) thermal reversion of MC to SP after treatment of MC-OH<sup>+</sup> with tributylamine, [TBA] ( $5 \times 10^{-4}$  M, time interval 30s).<sup>102</sup>

As long as a slightly acidified solution of spiro-pyrane is kept under blue light illumination, the neutral isomer is the prevalent form (because of the predominant SP form). When the solution is kept in the dark, it becomes positively charged, because of the protonation of the phenolate group of the MC isomer. This process can be repeated over a prolonged time.<sup>102</sup> This principle is vastly exploited in the preparation of pH-

active hydrogels and ionogels, a particular class of spiropyran-based stimuli responsive materials, which has recently gained an increasing relevance as micro-actuator and fluid handling valves in microfluidic devices.<sup>103-105</sup>

### 1.5.8 Electrochemistry of Benzospiryran

An important target of this research is the description of the electrochemical properties of indolinespirobenzopyran moieties in order to better understand the behaviour of the hybrid materials that will be discussed in **Chapters 2** and **6**. In our case attention will be focused on derivatives **BSP-1** and **BSPe** (Figure 1.24), as their electrochemical properties have not been fully described in the literature. Nevertheless, Willner *et. al.* successfully and firstly exploited the properties of the photo-switchable spiropyran substituted over several types of gold electrodes or glucose oxidases-structured biochemical sensors.<sup>106-108</sup> Their work does not investigate the electrochemical mechanism involved in the transduction of the signal, but it “simply” takes advantage of the photo-induced amperometric variation produced by their elegant molecular sensor.

The electrochemistry of **BSP-1** analogues has been previously reported, whereas **BSPe** was synthesised *ad hoc* as a complementary source of information and for a full comprehension of the behaviour of the new hybrid molecules isolated.<sup>109-111</sup> Zhi *et. al.*<sup>110</sup> discussed the electrochemistry and spectroelectrochemistry of a specific N-methyl-nitrobenzospiryran, but focusing only on the reduction behaviour of this moiety and describing only marginally the oxidation of spiropyran. Their studies were also performed in low vapour tension, polar and high viscosity solvent (DMF), which favours some spiropyran processes among others.<sup>112</sup> For these reasons and for others that will be presented in **Chapter 2** the results here discussed did not reproduce the same conditions, but explored different and undisclosed properties with a new approach from what could be found in the literature. They reported brief comments about the oxidation voltammograms and only the first scan of that experiment. Recently Jukes *et. al.*<sup>113</sup> provided a study concerning **BSP-1**, with their attention focused on the importance of the reduction process on the subsequent oxidation phase of the moiety. In **Chapter 2** will be discussed the proposed mechanism for the electrochemical generation of **MC-1**, whilst in **Chapter 6** will be presented the results regarding **BSPe**.

## 1.6 Spiropyran As a Chelating Agent of Metal Ions

Metallochromic ligands are molecules that bind metal ions and form coloured species. This colour change is important for the recognition of binding events at the molecular scale. When the binding molecules are also photochromic, like members of the spiropyran family, the possible analytical implications increase, as the formation of the complex can be externally modulated by simple illumination with a specific wavelength. The absorption in the 200-400 nm range produces the desired and colourful cleavage of the benzospiropyran bond that involves the spirocarbon and the oxygen atom generating a new zwitterion isomer among others (MC). This isomerization does not produce any disruption of the aromatic system, but it generates a highly coloured species with a redshift in the visible region resulting in a coloured solution.<sup>114, 115</sup> This exciting property of the system can also be exploited to form complexes with certain d- and f- elements in low polarity solvents and the complexation causes a blue shift in the MC visible absorption band. The mechanism of the complex formation between a spiropyran and the transition phase metals was suggested by Goerner *et al.*<sup>80</sup> Particularly for spiropyran bearing the  $-\text{NO}_2$  functionality, the complex formation involves the merocyanine *cis* and *trans* isomers. Therefore, the formation of the complex in solvents of medium or high polarity is accompanied by a major absorption band in the visible region allowing the system to become inherently self-indicating.<sup>115</sup> The ratio of the complexes formed is commonly 2 (MC) : 1 ( $\text{M}^{\text{n}+}$ ), meaning that two phenolates belonging to two distinct merocyanines are necessary to bind one metal ion in solution (Figure 1.22 and 1.23).<sup>116, 117</sup>

In the literature the ion-complex behaviour of many MC derivatives have been evaluated in different media and with a wide range of transition metals and in particular, impressive results have been obtained with copper and zinc.<sup>80, 115, 118</sup>

In a different strategic approach, more complex photochemical systems are more effective as metal ion ligands as they incorporate crown ether functionalities as the binding site.<sup>119, 120</sup> These interesting structures are also sensitive to alkaline earth metals like  $\text{Ca}^{2+}$  and  $\text{Mg}^{2+}$ . Although the selectivity for the ions indicated was higher than the previously reported spiropyran, the complexation process was difficult to control photochemically.

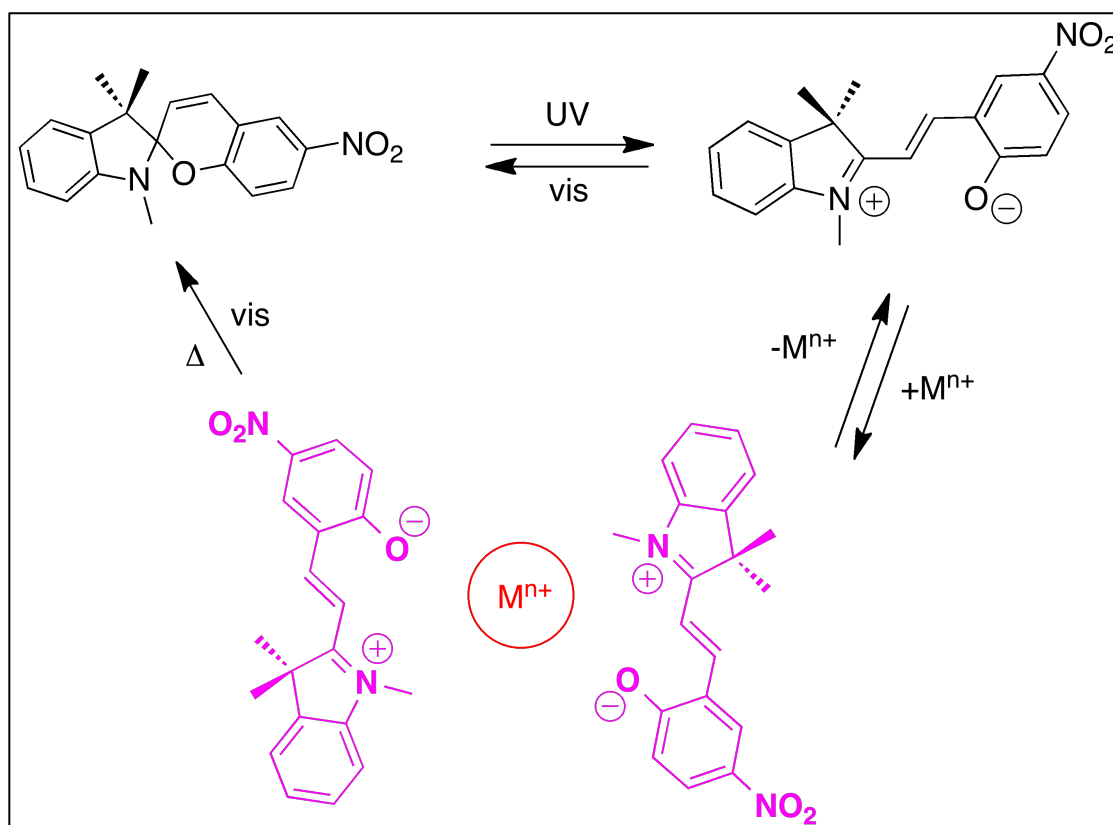


**Figure 1.22:** general mechanism proposed for the reversible conversion between a closed, uncharged, non-planar, inactive and colourless spiro (BSP) form to the planar, open, active and highly coloured merocyanine (MC) isomer upon UV illumination. This MC can now bind metal ions and release them when illuminated with a visible light source.<sup>113</sup>

In addition new polymeric matrixes containing BSP functionalities that retain the analytical-relevant binding capability have been investigated. Some examples are the functionalization of PMMA (through the formation of an amide group over carboxylic functionalities)<sup>116, 117</sup> or preparation of silica nanobeads (similar esterification of carboxylic groups).<sup>121</sup> These systems allowed ease of light-activation by LED, and accessible synthesis procedures. The relatively mild chemical conditions helped to increase the lifetime of the photogenerated merocyanine isomeric form by retarding the dark back reaction and hindering the photodegradation pathways.

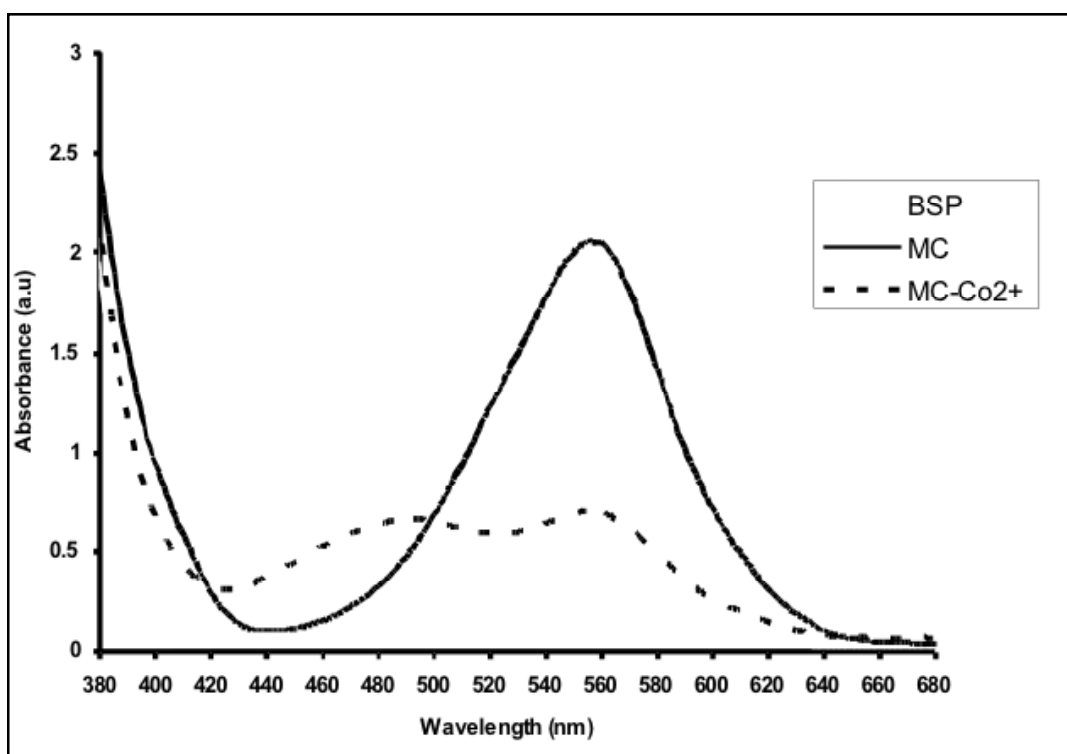


**Figure 1.23:** UV-vis spectra of BSP equilibrated in the dark, after 1 minute irradiation at 360 nm (MC), and after equal molar equivalent addition of cobalt (II) chloride to merocyanine solution (MC-Co<sup>2+</sup>). All measurements were done in acetonitrile.<sup>116</sup>

To conclude, complexation of spiropyrans with metal ions in solution arises from two coupled reactions: (i) formation of merocyanine-type ligand and (ii) substitution of the solvent (coordinated at the metal ion) by the ligand (Figure 1.23). The overall rate of thermal complexation is limited by the rate of thermally activated ring opening, whereas the rate of light-induced complexation is determined by the rate of thermal substitution. The complexation reactions of photochromic spiropyran have been successfully employed in the potential development of a new family of chemosensors for metals ions and for other important applications.

## 1.7 Applications of Spiropyran Moieties

Two general types of applications can be defined:

1. Applications directly dependent upon the colour change caused by the molecular and electronic structures of the two species (BSP and MC) and their corresponding absorption spectra. Examples of this would be variable-transmission optical materials such as the photochromic ophthalmic lenses; fluid flow visualization; and authentication systems (security printing inks);

2. Applications dependent upon changes in the physical or chemical properties that occur along with the more easily observed color change during the photochromic reaction. Examples of such properties are conductivity, refractive index, electrical moment, dielectric constant, chelate formation, ion dissociation, phase transitions, solubility, and viscosity. Optoelectronic systems (semi-conductors modulated by photochromic pigments) such as those found in reversible holographic systems, optical switches, photochemically switchable biomimetic systems, (platforms for biomolecular interactions;<sup>122</sup>) and photo-active dynamic gels and ionogels;<sup>103</sup> are of particular interest for the aims of this research.

The applications based on the spiropyran family of compounds allow new approaches to multi-switchable uptake and release of molecular guests and photo-electro-actuated separations.<sup>123</sup> This concept for chemical sensing is based on the following principles:

- The sensor surface should be in an inactive or passive state when a measurement is not being conducted.
- The surface is converted into an active state under an external light stimulus principally interacting with the **BSP** → **MC** interconversion.
- The photo-activated surface binds with the target species and generates a signal that enables the analytical measurement to be made.
- Once the measurement is completed, the target species is expelled by an external photonic or electrochemical stimulus and the surface returns to its inactive form.

## 1.8 General Aims of This Research

The unique chemical profile and electrochemical behaviour of novel conducting polymers functionalised with spiropyran on their backbone requires a detailed study of the chemical properties and will be outlined as follows:

- In **Chapter 2** the synthesis and the characterization of the electrochemical properties of spiropyran-doped poly-terthiophene family 2-(3,3''-Dimethylindoline-6'-nitrobenzospiropyranyl)-ethyl-4,4''-didecyloxy-2,2':5',2''-terthiophene-3'-acetate Figure 1.21, **BSP-2**) will be presented and discussed. A detailed insight of

the electrochemical features of the photochromic precursor 1-(2-hydroxyethyl)-3,3-dimethylindoline-6'-nitrobenzospiropyran (Figure 1.24, **BSP-1**) will be reported.

- The photochemical and physical properties of these compounds shall be further discussed in **Chapter 3** where also a new molecule will be presented, Ethyl-(3,3''-dimethylindoline-6'-nitrobenzospiropyran-4,4''-didecyloxy-2,2':5',2''-terthiophene-3'-carboxylate (Figure 1.24, **BSP3**).
- In **Chapter 4** the photoinduced interactions between the surface of **pBSP2** and an important mediator for the tissue regrowth fibronectin will be studied by means of AFM techniques. The protein was chemically substituted on the cantilever and the surface of the polymer was photonicly actuated under different wavelengths. The varying electrostatic conditions were monitored through atomic force microscopy.
- **Chapter 5** will describe the synthesis / properties of a new stimuli responsive bithiophenespiropyran, named 5',6-Bis(4-decyloxythien-2-yl)-1',3'-dihydro-1',3',3'-trimethyl-spiro[2*H*-1-benzopyran-2,2'-[2*H*]indole] (**TSP4**), a novel conducting polymer with a merocyanine molecule incorporated into the polymer backbone (Figure 1.25).
- **Chapter 6** will present three new derivatives, 1',3',3'-trimethylspiro(chromene-2,2'-indolin)-6-yl-4,4''-bis(decyloxy)-(2,2':5',2''-terthiophene))-3'-acetate (**BSP6**), 1',3',3'-trimethylspiro[chromene-2,2'-indolin]-6-yl-4,4''-bis(decyloxy)-(2,2':5',2''-terthiophene))-3'-carboxylate (**BSP7**) and their electrochemically grown polymers) and the *ad hoc* synthesised, for comparative reasons, 1',3',3'-trimethylspiro(chromene-2,2'-indolin)-6-yl acetate (**BSPe**) (Figure 1.24). These molecules are designed to bear the spiropyran unit with a different orientation over the terthiophene backbone. Their photochemistry and electrochemistry are investigated.

In order to achieve the main aims of this research project, three different spiropyran moieties have been used and two of them, one nitro-benzopyran and one hydroxyl-spiro-derivative, were successfully substituted on two different terthiophene's backbones to obtain adaptive structures with interesting and innovative electrochromic and photochromic behaviour (Figure 1.24). The nitro-spiropyran (**BSP-1**) presents a nitro-group in position 6 and a hydroxyethyl substituent on the indoline nitrogen in order to allow the attachment of the chromophore on the different substrates.

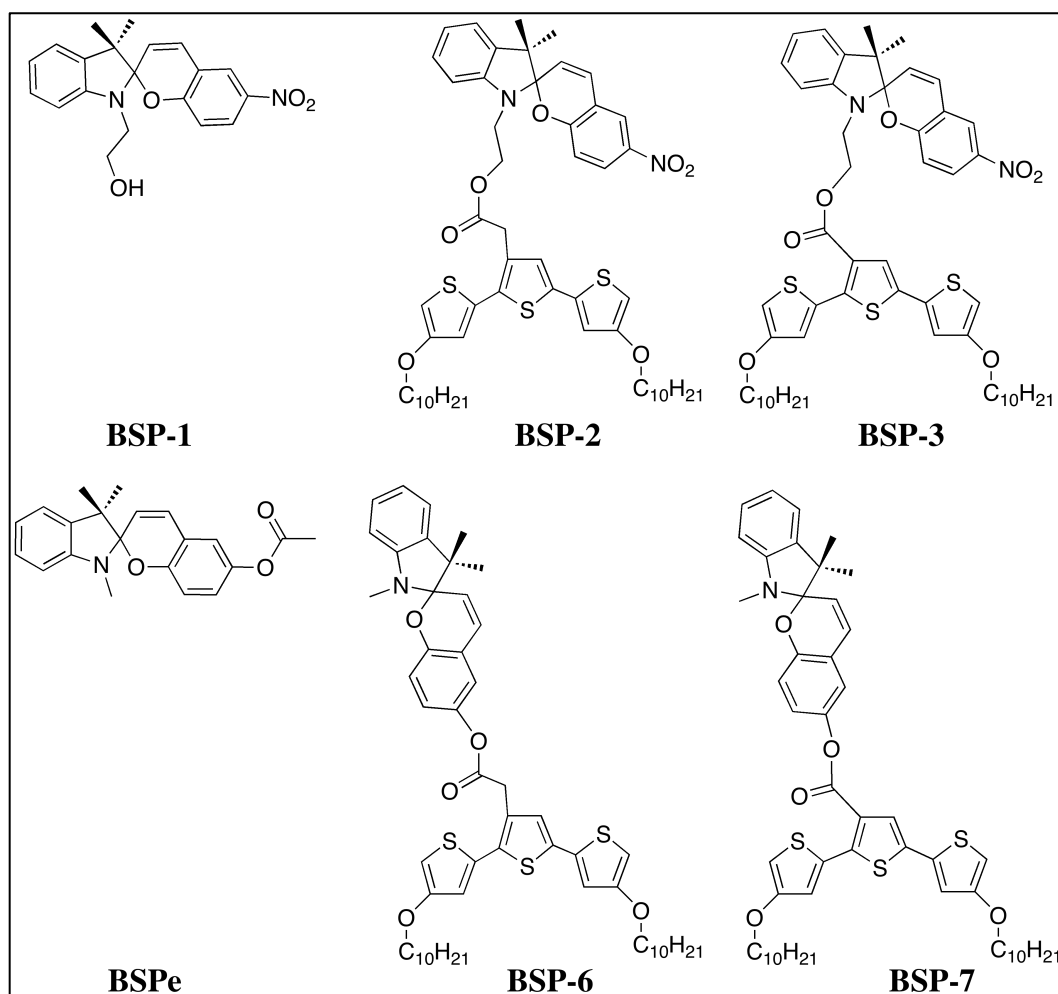


**Figure 1.24:** Molecular structures of the different derivatives studied in this thesis.

In this work, the focus was on two benzospiropyrans (**BSP-1** and **BSPe**) chromophore linked to two different terthiophene derivatives, which will generate **BSP-2**, **BSP-6** over the **AcTTh** terthiophene, and **BSP-3** and **BSP7** for the substitution over the **CbTTh** moiety, Figure 1.24), as this family of compounds is the basis for the development of new stimuli - responsive materials.

In Figure 1.25 is reported the chemical structure of the **TSP4** moiety and its photochemically generated **TMC4**.

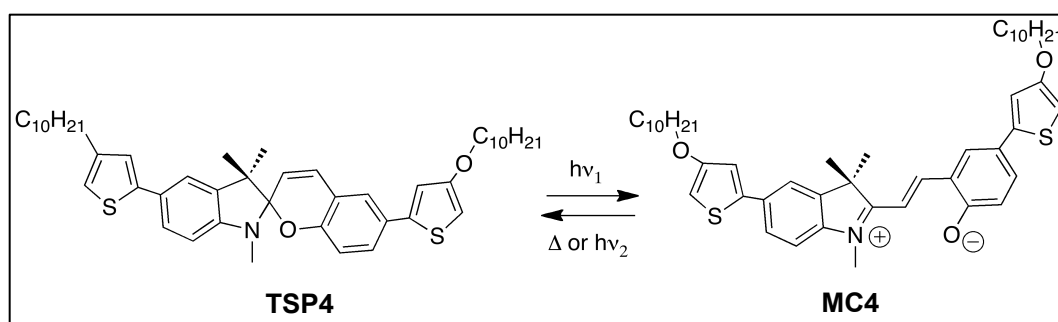


**Figure 1.25:** Molecular structure of **TSP4** and photochemical isomerization to **MC4**.

## 1.9 References

1. G. G. Wallace, P. R. Teasdale, G. M. Spinks and L. A. Kane-Maguire, *Conductive electroactive polymers: intelligent polymer systems*, CRC press, 2008.
2. A. J. Bard and L. R. Faulkner, *Electrochemical methods: fundamentals and applications*, Wiley New York, 1980.
3. C. G. Zoski, *Handbook of electrochemistry*, Elsevier Science Limited, 2007.
4. C. K. Chiang, M. A. Druy, S. C. Gau, A. J. Heeger, E. J. Louis, A. G. MacDiarmid, Y. W. Park and H. Shirakawa, *Journal of the American Chemical Society*, 1978, **100**, 1013-1015.
5. E. M. Conwell, *Physical Review*, 1956, **103**, 51.
6. N. Mott, *Canadian Journal of Physics*, 1956, **34**, 1356-1368.
7. D. Pines, *Canadian Journal of Physics*, 1956, **34**, 1379-1394.
8. T. Holstein, *Annals of Physics*, 1959, **8**, 325-342.
9. T. A. Skotheim and J. Reynolds, *Conjugated polymers: theory, synthesis, properties, and characterization*, CRC press, 2006.
10. T. M. Clarke, K. C. Gordon, D. L. Officer and D. K. Grant, *Journal of Physical Chemistry A*, 2005, **109**, 1961-1973.
11. A. Pron and P. Rannou, *Progress in Polymer Science*, 2002, **27**, 135-190.
12. W. Gazzotti, A. Nogueira and E. Girotto, *Handbook of advanced electronic and photonic materials and devices (vol 10)*, 2001.
13. S. Irle and H. Lischka, *Journal of Chemical Physics*, 1997, **107**, 3021-3031.
14. J. van Haare, E. E. Havinga, J. L. J. van Dongen, R. A. J. Janssen, J. Cornil and J. L. Bredas, *Chemistry a European Journal*, 1998, **4**, 1509-1522.
15. F. Piron, P. Leriche, G. Mabon, I. Grosu and J. Roncali, *Electrochemistry Communications*, 2008, **10**, 1427-1430.
16. P. Leriche, P. Frere, A. Cravino, O. Aleveque and J. Roncali, *Journal of Organic Chemistry*, 2007, **72**, 8332-8336.
17. A. Cravino, S. Roquet, O. Aleveque, P. Leriche, P. Frere and J. Roncali, *Chemistry of Materials*, 2006, **18**, 2584-2590.
18. B. Jouselme, P. Blanchard, M. Allain, E. Levillain, N. N. Dias and J. Roncali, *Journal of Physical Chemistry A*, 2006, **110**, 3488-3494.
19. S. Roquet, P. Leriche, I. Perepichka, B. Jouselme, E. Levillain, P. Frere and J. Roncali, *Journal of Materials Chemistry*, 2004, **14**, 1396-1400.
20. I. F. Perepichka, S. Roquet, P. Leriche, J. M. Raimundo, P. Frere and J. Roncali, *Chemistry a European Journal*, 2006, **12**, 2960-2966.
21. F. Moggia, H. Brisset, F. Fages, P. Blanchard and J. Roncali, *Electrochemistry Communications*, 2006, **8**, 533-538.
22. P. Wagner, A. C. Partridge, K. W. Jolley and D. L. Officer, *Tetrahedron Letters*, 2007, **48**, 6245-6248.
23. G. E. Collis, A. K. Burrell and D. L. Officer, *Tetrahedron Letters*, 2001, **42**, 8733-8735.
24. T. Y. Lee, Y. B. Shim and S. C. Shin, *Synthetic Metals*, 2002, **126**, 105-110.
25. A. K. Burrell, J. Chen, G. E. Collis, D. K. Grant, D. L. Officer, C. O. Too and G. G. Wallace, *Synthetic Metals*, 2003, **135**, 97-98.
26. J. Roncali, *Chemical Reviews*, 1992, **92**, 711-738.
27. A. O. Patil, A. J. Heeger and F. Wudl, *Chemical Reviews*, 1988, **88**, 183-200.
28. J. J. Apperloo, R. A. J. Janssen, P. R. L. Malenfant, L. Groenendaal and J. M. J. Frechet, *Journal of the American Chemical Society*, 2000, **122**, 7042-7051.

29. Y. Gao, C. G. Liu and Y. S. Jiang, *Journal of Physical Chemistry A*, 2002, **106**, 5380-5384.
30. K. Wagner, L. L. Crowe, P. Wagner, S. Gambhir, A. C. Partridge, J. C. Earles, T. M. Clarke, K. C. Gordon and D. L. Officer, *Macromolecules*, 2010, **43**, 3817-3827.
31. E. M. Genies, G. Bidan and A. F. Diaz, *Journal of Electroanalytical Chemistry*, 1983, **149**, 101-113.
32. P. Wagner and D. L. Officer, *Synthetic Metals*, 2005, **154**, 325-328.
33. R. D. Breukers, K. J. Gilmore, M. Kita, K. K. Wagner, M. J. Higgins, S. E. Moulton, G. M. Clark, D. L. Officer, R. M. I. Kapsa and G. G. Wallace, *Journal of Biomedical Materials Research Part A*, 2010, **95A**, 256-268.
34. D. K. Grant, K. W. Jolley, D. L. Officer, K. C. Gordon and T. M. Clarke, *Organic & Biomolecular Chemistry*, 2005, **3**, 2008-2015.
35. J. Roncali, *Macromolecular Rapid Communications*, 2007, **28**, 1761-1775.
36. R. A. Green, N. H. Lovell, G. G. Wallace and L. A. Poole-Warren, *Biomaterials*, 2008, **29**, 3393-3399.
37. D.-H. Kim, J. A. Wiler, D. J. Anderson, D. R. Kipke and D. C. Martin, *Acta Biomaterialia*, 2010, **6**, 57-62.
38. S. E. Moulton, M. J. Higgins, R. M. I. Kapsa and G. G. Wallace, *Advanced Functional Materials*, 2012, **22**, 2003-2014.
39. D. M. Taylor, *Science*, 2002, **296**, 1829-1832.
40. L. Kumpumbu-Kalemba and M. Leclerc, *Chemical Communications*, 2000, 1847-1848.
41. D. Officer, G. Swiegers, C. Too and G. Wallace, *Electrochimica Acta*, 2002.
42. M. A. Rahman, D.-S. Park, S.-C. Chang, C. J. McNeil and Y.-B. Shim, *Biosensors and Bioelectronics*, 2006, **21**, 1116-1124.
43. A.-D. Bendrea, L. Cianga and I. Cianga, *Journal of Biomaterials Applications*, 2011, **26**, 3-84.
44. S. M. Richardson-Burns, J. L. Hendricks, B. Foster, L. K. Povlich, D.-H. Kim and D. C. Martin, *Biomaterials*, 2007, **28**, 1539-1552.
45. T. M. Brushart, R. Jari, V. Verge, C. Rohde and T. Gordon, *Experimental Neurology*, 2005, **194**, 221-229.
46. D. Mawad, E. Stewart, D. L. Officer, T. Romeo, P. Wagner, K. Wagner and G. G. Wallace, *Advanced Functional Materials*, 2012, **22**, 2692-2699.
47. K. Gilmore, A. J. Hodgson, B. Luan, C. J. Small and G. G. Wallace, *Polymer Gels and Networks*, 1994, **2**, 135-143.
48. D. Leckband, *Annual Review of Biophysics and Biomolecular Structure*, 2000, **29**, 1-26.
49. G. Binnig and C. F. Quate, *Physical Review Letters*, 1986, **56**, 930-933.
50. C. D. Frisbie, L. F. Rozsnyai, A. Noy, M. S. Wrighton and C. M. Lieber, *Science*, 1994, **265**, 2071-2074.
51. A. Gelmi, M. J. Higgins and G. G. Wallace, *Biomaterials*, 2010, **31**, 1974-1983.
52. K. Gilmore, M. Kita, Y. Han, A. Gelmi, M. Higgins, S. Moulton, G. Clark, R. Kapsa and G. G. Wallace, *Biomaterials*, 2009, **30**, 5292-5596.
53. M. Grandbois, *Science*, 1999, **283**, 1727-1730.
54. C.-A. Lamontagne, C. M. Cuerrier and M. Grandbois, *Pflügers Archiv - European Journal of Physiology*, 2007, **456**, 61-70.
55. D. A. Lamprou, J. R. Smith, T. G. Nevell, E. Barbu, C. Stone, C. R. Willis and J. Tsibouklis, *Applied Surface Science*, 2010, **256**, 5082-5087.
56. H. Schönherr, M. T. van Os, G. J. Vancso, R. Förch, W. Knoll, Z. Hruska, J. Kurdi and F. Arefi-Khonsari, *Chemical Communications*, 2000, 1303-1304.

57. S. K. Sinniah, A. B. Steel, C. J. Miller and J. E. ReuttRobey, *Journal of the American Chemical Society*, 1996, **118**, 8925-8931.
58. P. Y. Meadows, J. E. Bemis and G. C. Walker, *Langmuir*, 2003, **19**, 9566-9572.
59. G. Mitchell, C.-A. Lamontagne, R. Lebel, M. Grandbois and F. Malouin, *Biochemical and Biophysical Research Communications*, 2007, **364**, 595-600.
60. A. Gelmi, M. Zaroni, M. J. Higgins, S. Gambhir, D. L. Officer, D. Diamond and G. G. Wallace, *Journal of Materials Chemistry B*, 2013, **1**, 2162-2168.
61. M. J. Higgins, P. J. Molino, Z. Yue and G. G. Wallace, *Chemistry of Materials*, 2012, **24**, 828-839.
62. T. Kobayashi, H. Yoneyama and H. Tamura, *Journal of Electroanalytical Chemistry*, 1984, **161**, 419-423.
63. N. Sakmeche, S. Aeiyaeh, J.-J. Aaron, M. Jouini, J. C. Lacroix and P.-C. Lacaze, *Langmuir*, 1999, **15**, 2566-2574.
64. N. Katsonis, M. Lubomska, M. M. Pollard, B. L. Feringa and P. Rudolf, *Progress in Surface Science*, 2007, **82**, 407-434.
65. P. Banfield, *Chromic Phenomena-Technological Applications of Colour Chemistry*, 2001.
66. H. Dürr and H. Bouas-Laurent, *Photochromism: Molecules and Systems: Molecules and Systems*, Access Online via Elsevier, 2003.
67. S. Stitzel, R. Byrne and D. Diamond, *Journal of Materials Science*, 2006, **41**, 5841-5844.
68. J. C. Crano, T. Flood, D. Knowles, A. Kumar and B. VanGemert, *Pure and Applied Chemistry*, 1996, **68**, 1395-1398.
69. A. S. Dvornikov, J. Malkin and P. M. Rentzepis, *Journal of Physical Chemistry*, 1994, **98**, 6746-6752.
70. J. D. Winkler, K. Deshayes and B. Shao, *Journal of the American Chemical Society*, 1989, **111**, 769-770.
71. G. E. Collins, R. E. Morris, J. F. Wei, M. Smith, M. H. Hammond, V. Michelet, J. D. Winkler, P. M. Serino and Y. Guo, *Energy & Fuels*, 2002, **16**, 1054-1058.
72. L. Evans, G. E. Collins, R. E. Shaffer, V. Michelet and J. D. Winkler, *Analytical Chemistry*, 1999, **71**, 5322-5327.
73. T. Suzuki, T. Kato and H. Shinozaki, *Chemical Communications*, 2004, 2036-2037.
74. V. I. Minkin, *Chemical Reviews*, 2004, **104**, 2751-2776.
75. F. M. Raymo and S. Giordani, *Journal of the American Chemical Society*, 2001, **123**, 4651-4652.
76. J. C. Crano and R. J. Guglielmetti, *Organic Photochromic and Thermochromic Compounds: Volume 2: Physicochemical Studies, Biological Applications, and Thermochromism*, Springer, 1999.
77. H. M. D. Bandara and S. C. Burdette, *Chemical Society Reviews*, 2012, **41**, 1809-1825.
78. E. Fischer and Y. Hirshberg, *Journal of the Chemical Society*, 1952, 4522-4524.
79. P. Maslak and A. Chopra, *Journal of the American Chemical Society*, 1993, **115**, 9331-9332.
80. H. Gerner and A. K. Chibisov, *Journal of the Chemical Society-Faraday Transactions*, 1998, **94**, 2557-2564.
81. S. Gopalakrishnan, D. F. Liu, H. C. Allen, M. Kuo and M. J. Shultz, *Chemical Reviews*, 2006, **106**, 1155-1175.
82. R. M. Chriotte, *Colour Chemistry*, 2001.
83. H. Dürr, L. H. Bouas, *Photochromism-molecules and systems*, Elsevier, 2003.
84. C. J. Drummond and D. N. Furlong, *Journal of the Chemical Society-Faraday Transactions*, 1990, **86**, 3613-3621.

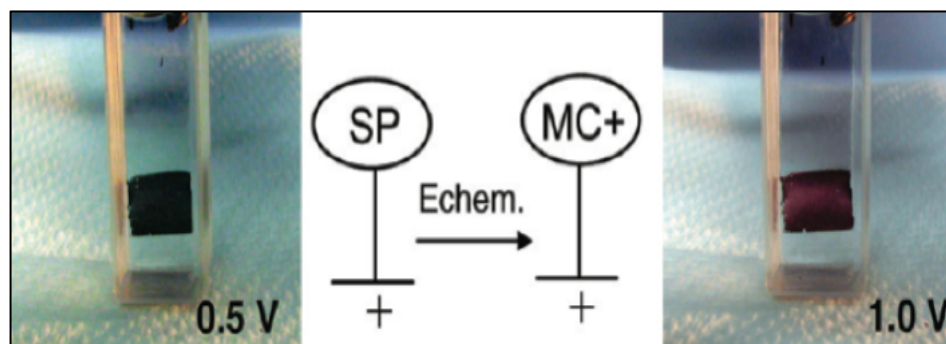
85. L. G. S. Brooker, A. C. Craig, D. W. Heseltine, P. W. Jenkins and L. L. Lincoln, *Journal of the American Chemical Society*, 1965, **87**, 2443-2450.
86. S. Brownstein, *Canadian Journal of Chemistry-Revue Canadienne De Chimie*, 1960, **38**, 1590-1596.
87. P. Maslak, A. Chopra, C. R. Moylan, R. Wortmann, S. Lebus, A. L. Rheingold and G. P. A. Yap, *Journal of the American Chemical Society*, 1996, **118**, 1471-1481.
88. R. Byrne, S. Coleman, K. J. Fraser, A. Raduta, D. R. MacFarlane and D. Diamond, *Physical Chemistry Chemical Physics*, 2009, **11**, 7286-7291.
89. R. Byrne, K. J. Fraser, E. Izgorodina, D. R. MacFarlane, M. Forsyth and D. Diamond, *Physical Chemistry Chemical Physics*, 2008, **10**, 5919-5924.
90. S. Coleman, R. Byrne, S. Minkovska and D. Diamond, *Journal of Physical Chemistry B*, 2009, **113**, 15589-15596.
91. M. Galinski, A. Lewandowski and I. Stepniak, *Electrochimica Acta*, 2006, **51**, 5567-5580.
92. *IUPAC Compendium of Chemical Terminology-The Gold Book*, 2009.
93. H. Gorner, *Chemical Physics Letters*, 1998, **288**, 381-390.
94. J. O. Morley, R. M. Morley, R. Docherty and M. H. Charlton, *Journal of the American Chemical Society*, 1997, **119**, 10192-10202.
95. H. Gorner, *Physical Chemistry Chemical Physics*, 2001, **3**, 416-423.
96. J. Hobley and V. Malatesta, *Physical Chemistry Chemical Physics*, 2000, **2**, 57-59.
97. Y. Abe, R. Nakao, T. Horii, S. Okada and M. Irie, *Journal of Photochemistry and Photobiology a-Chemistry*, 1996, **95**, 209-214.
98. G. Berkovic, V. Krongauz and V. Weiss, *Chemical Reviews*, 2000, **100**, 1741-1753.
99. R. C. Bertelson, *Techniques of Chemistry III*, Wiley-Interscience, New York, 1971.
100. C. J. Drummond, D. N. Furlong and G. Georgaklis, *Journal of the Chemical Society, Faraday Transactions*, 1990, **86**, 3913.
101. C. J. Roxburgh, P. G. Sammes and A. Abdullah, *Dyes and Pigments*, 2009, **82**, 226-237.
102. J. T. C. Wojtyk, A. Wasey, N.-N. Xiao, P. M. Kazmaier, S. Hoz, C. Yu, R. P. Lemieux and E. Buncl, *The Journal of Physical Chemistry A*, 2007, **111**, 2511-2516.
103. F. Benito-Lopez, R. Byrne, A. M. Răduță, N. E. Vrana, G. McGuinness and D. Diamond, *Lab on a Chip*, 2010, **10**, 195-201.
104. T. Satoh, K. Sumaru, T. Takagi and T. Kanamori, *Soft Matter*, 2011, **7**, 8030-8034.
105. T. Satoh, K. Sumaru, T. Takagi, K. Takai and T. Kanamori, *Physical Chemistry Chemical Physics*, 2011, **13**, 7322-7329.
106. I. Willner, R. Blonder, E. Katz, A. Stocker and A. F. Buckmann, *Journal of the American Chemical Society*, 1996, **118**, 5310-5311.
107. I. Willner, A. Doron, E. Katz, S. Levi and A. J. Frank, *Langmuir*, 1996, **12**, 946-954.
108. I. Willner, M. LionDagan and E. Katz, *Chemical Communications*, 1996, 623-624.
109. S. Gambhir, K. Wagner and D. L. Officer, *Synthetic Metals*, 2005, **154**, 117-120.
110. J. F. Zhi, R. Baba, K. Hashimoto and A. Fujishima, *Journal of Photochemistry and Photobiology a-Chemistry*, 1995, **92**, 91-97.
111. M. Campredon, G. Giusti, R. Guglielmetti, A. Samat, G. Gronchi, A. Alberti and M. Benaglia, *Journal of the Chemical Society-Perkin Transactions 2*, 1993, 2089-2094.

112. Z. Jin Fang, R. Baba, K. Hashimoto and A. Fujishima, *Journal of Photochemistry and Photobiology A: Chemistry*, 1995, **92**, 91-97.
113. R. T. F. Jukes, B. Bozic, F. Hartl, P. Belser and L. De Cola, *Inorganic Chemistry*, 2006, **45**, 8326-8341.
114. Y. Hirshberg and E. Fischer, *Journal of Chemical Physics*, 1953, **21**, 1619-1620.
115. M. Natali and S. Giordani, *Chemical Society Reviews*, 2012, **41**, 4010-4029.
116. R. J. Byrne, S. E. Stitzel and D. Diamond, *Journal of Materials Chemistry*, 2006, **16**, 1332-1337.
117. A. Radu, S. Scarmagnani, R. Byrne, C. Slater, K. Tong Lau and D. Diamond, *Journal of Physics D: Applied Physics*, 2007, **40**, 7238-7244.
118. G. E. Collins, L.-S. Choi, K. J. Ewing, V. Michelet, C. M. Bowen and J. D. Winkler, *Chemical Communications*, 1999, **0**, 321-322.
119. J. Filley, M. A. Ibrahim, M. R. Nimlos, A. S. Watt and D. M. Blake, *Journal of Photochemistry and Photobiology A: Chemistry*, 1998, **117**, 193-198.
120. S. Yagi, S. Nakamura, D. Watanabe and H. Nakazumi, *Dyes and Pigments*, 2009, **80**, 98-105.
121. S. Scarmagnani, Z. Walsh, C. Slater, N. Alhashimy, B. Paull, M. Macka and D. Diamond, *Journal of Materials Chemistry*, 2008, **18**, 5063-5071.
122. A. Higuchi, A. Hamamura, Y. Shindo, H. Kitamura, B. O. Yoon, T. Mori, T. Uyama and A. Umezawa, *Biomacromolecules*, 2004, **5**, 1770-1774.
123. D. Diamond, S. Coyle, S. Scarmagnani and J. Hayes, *Chemical Reviews*, 2008, **108**, 652-679.



# CHAPTER 2

## Multiswitchable Poly-(Terthiophene) Bearing a Spiropyran Functionality: Understanding Photo- and Electrochemical Control



**Publication status: PUBLISHED**

K. Wagner, R. Byrne, **M. Zanoni**, S. Gambhir, L. Dennany, R. Breukers, M. Higgins, P. Wagner, D. Diamond, G. G. Wallace and D. L. Officer, "A Multiswitchable Poly-(terthiophene) Bearing a Spiropyran Functionality: Understanding Photo- and Electrochemical Control" *Journal of the American Chemical Society*, 133, 5453-5462 (2011). DOI: 10.1021/ja1114634.

*For the supplementary information section see Appendix A*

## Abstract

An electroactive nitrospiropyran-substituted polyterthiophene, poly(2-(3,3''-dimethylindoline-6'-nitrobenzospiropyranyl)-ethyl-4,4''-didecyloxy-2,2':5'2''-terthiophene-3'-acetate), has been synthesized for the first time. The spiropyran, incorporated into the polymer backbone by covalent attachment to the alkoxyterthiophene monomer units, leads to multiple coloured states as a result of both photochemical and electrochemical isomerizations of the spiropyran moiety to merocyanine forms as well as electrochemical oxidation of the polyterthiophene backbone and the merocyanine substituents. While electrochemical polymerization of the terthiophene monomer can take place without oxidation of the spiropyran, increasing the oxidation potential leads to complex electrochemistry that clearly involves this substituent. To understand this complex behaviour, the first detailed electrochemical study of the oxidation of the precursor spiropyran, 1-(2-hydroxyethyl) 3,3-dimethylindoline-6'-nitrobenzospiropyran, was undertaken, showing that, in solution, an irreversible electrochemical oxidation of the spiropyran occurs leading to reversible redox behaviour of at least two merocyanine isomers. With these insights, an extensive electrochemical and spectroelectrochemical study of the nitrospiropyran-substituted polyterthiophene films reveals an initial irreversible electrochemical oxidative ring opening of the spiropyran to oxidized merocyanine. Subsequent reduction and cyclic voltammetry of the resulting nitromerocyanine-substituted polyterthiophene film gives rise to the formation of both merocyanine  $\pi$ -dimers or oligomers and  $\pi$ -radical cation dimers, between polymer chains. Although merocyanine formation is not electrochemically reversible, the spiropyran can be photochemically regenerated, through irradiation with visible light. Subsequent electrochemical oxidation of the nitrospiropyran-substituted polymer reduces the efficiency of the spiropyran to merocyanine isomerization, providing electrochemical control over the polymer properties. SEM and AFM images support the conclusion that the bulky spiropyran substituent is electrochemically isomerized to the planar merocyanine moiety, affording a smoother polymer film. The conductivity of the freestanding polymer film was found to be  $0.4 \text{ S cm}^{-1}$ .

## 2.1 Introduction

The immobilisation of light-responsive molecules on electroactive surfaces provides an exciting opportunity for the development of smart materials and devices.<sup>1</sup>

The exploitation of such light-responsive molecules<sup>1-8</sup> in devices typically requires immobilisation on a surface through an appended functionality that does not interfere with the light switching behaviour. This has been achieved for photoswitchable molecules by formation of self-assembled monolayers (SAMs)<sup>9</sup> and bilayers<sup>10</sup> and incorporation into polymer films<sup>11,12</sup> and beads.<sup>6</sup> While the required structure for monolayer and bilayer formation does not usually affect the functionality of the photomolecules, one of the challenges in using polymers is that the monomer used to synthesise the polymer, and the polymerisation process itself, must be compatible with the photo-/electroactive switching units. In addition, the incorporation of the photoresponsive functionality must not affect the polymerisation of the monomer. Wesenhagen *et al.* recently reported the incorporation of a photo-/electrochromic dithienylcyclopentene moiety into a polymer by oxidative electro- polymerisation of a methoxystyryl monomer attached to the photoactive unit.<sup>13</sup> The electroactive polymer was formed as only a thin film, the thickness of several monolayers as the result of limited conductivity.

The photoswitchable moiety can be appended to the polymer backbone or incorporated into it with quite different effects. In the latter case, the incorporated photoswitchable unit can affect the nature of the polymer backbone. Hugel *et al.* have demonstrated that incorporation of azobenzene units into the backbone of the polymer chain modifies the modulus of elasticity of the polymer.<sup>14</sup> The nature of the polymer backbone can also influence the kinetics of open/closed ring isomerisation of the photoactive units, affect the stability, or even lead to enhancement of photo degradation.<sup>15</sup>

While the introduction of photoswitchable molecules into polymers has proved valuable, the use of conducting polymers opens up a new avenue for electrochemical control of these multifunctional materials. In this regard, poly-(terthiophene) derivatives are of particular interest due to their stability and relative ease of synthesis and functionalization,<sup>16</sup> and they have been applied in a broad range of devices, from traditional solar cells<sup>17</sup> to complex electroluminescent devices.<sup>18</sup> This exciting potential of combining photo-switchability and electroactivity together was first recognised by Areephong *et al.* who reported the ability to control the electropolymerizability of an oligothiophene by the introduction of a photoswitchable dithienylethene unit into the

monomer.<sup>19</sup> Most recently, the first spiropyran-functionalized polythiophene was obtained by chemical copolymerisation of a thiophene monomer with covalently attached spiropyran and 3-hexylthiophene.<sup>20</sup> In that paper, it was demonstrated that both the fluorescence of this photoswitchable conductive copolymer and its interactions with cyanide ions could be controlled through **BSP** to **MC** photoconversion. However, the real benefit of combining the photoactivity and electrochemical activity of these materials was not explored.

The introduction of large functionalities onto a polythiophene can have a significant steric effect on the polymer backbone, adversely affecting the optical and electronic properties of the polymer as well as the polymer processability.

The use of dialkoxy-3-substituted terthiophenes as a precursor for developing novel substituted poly-(terthiophene)s provides reduced steric interactions between polymer backbone and substituent, allows better control of polymer regiochemistry, and the alkoxy side chains activate the monomer for polymerisation and ensure better polymer processability.<sup>21,22</sup> We have been exploring successfully the polymerisation of functionalized dialkoxyterthiophene monomers to avoid these problems.<sup>23</sup> Incorporation of the spiropyran moiety into a dialkoxyterthiophene monomer appeared to provide a good opportunity to investigate the potential for electrochemical control of photoresponsive functionality in a conducting polymer system. This chapter reports the synthesis and properties of spiropyran-functionalized poly-(terthiophene)s. The spiropyran unit is covalently linked to the monomer, which is then electropolymerized. The resulting film is electroactive and shows multiswitchable behaviour. In this exciting new material, we have electrochemical control of both, the polymer redox and the photochemical properties, as well as the ability to convert the **BSP** to **MC** form with potential and light. To the best of our knowledge, this is the first report of the synthesis and photo-electrochemical control of electropolymerized conductive polymer film.

## 2.2 Experimental

### 2.2.1 Monomer Synthesis

#### Methyl 4,4''-didecyloxy-2,2':5',2''-terthiophene-3'-acetate (TThMA)

2,5-Dibromothiophene-3-acetic acid methylester (1.72 g, 5.0 mmol) was dissolved in 1,2-dimethoxyethane (34 ml) followed by addition of K<sub>2</sub>CO<sub>3</sub> solution (1M, 17 ml) and Pd(PPh<sub>3</sub>)<sub>4</sub> (516 mg, 0.45 mmol) with stirring. 4.0 g, 4.1 mmol of 3-decyloxy thiophene-

2-boronic acid was initially added. After stirring for 4 hrs at 80 °C, a second aliquot of boronic acid (750 mg, 2.6 mmol) was added. The reaction was stirred for an additional 2 hours maintaining the temperature. The reaction was monitored with TLC, which showed the presence of only 2 main spots. Dichloromethane (50 ml) was added on cooling the reaction and separating the organic phase. On extracting the contents again with dichloromethane (50 ml), MgSO<sub>4</sub> was added for drying and the solvent was removed. This was purified on silica column (1'x14'') eluting with hexane: dichloromethane (7 : 3) resulting the clear separation of the impurity first, followed by yellow band which yielded the desired product on solvent evaporation (3.17 g, 94 %), mp 35-35.4 °C.

**<sup>1</sup>H NMR** (400 MHz)  $\delta$  7.06 (s, 1H, H4'); 6.86 (d, 1H, J = 1.7 Hz, H3); 6.83 (d, 1H, J = 1.7 Hz, H3''); 6.23 (d, 1H, J = 1.7 Hz, H5); 6.12 (d, 1H, J = 1.7 Hz, H5''); 3.94 (m, 4H, 2OCH<sub>2</sub>), 3.73 (2H, -CH<sub>2</sub>COOCH<sub>3</sub>), 3.725 (3H, -CH<sub>2</sub>COOCH<sub>3</sub>) 1.80-0.86 (16CH<sub>2</sub>, 2CH<sub>3</sub>). **<sup>13</sup>C NMR** (100.6 MHz)  $\delta$  171.1, 157.6, 136.2, 135.0, 133.3, 132.5, 130.6, 126.3, 119.0, 116.2, 98.0, 96.5, 70.1, 52.2, 34.6, 31.9. **IR** (KBr)  $\nu_{\max}/\text{cm}^{-1}$  2920 (s), 2851 (s), 1736 (s), 1722 (s), 1565 (s), 1533 (s), 1471 (s), 1452 (s), 1417 (s), 1371 (s), 1332 (m), 1216 (s), 1199 (s), 1170 (s), 1263 (m), 1170 (s), 1051 (s), 1029 (s), 962 (w), 894 (w), 883 (w), 867 (w), 812 (s), 740 (s), 719 (s), 676 (s), 613 (s), 563 (s), 477 (w). Anal. calcd. for C<sub>35</sub>H<sub>52</sub>O<sub>4</sub>S<sub>3</sub>: C, 66.41; H, 8.28; S, 15.20. Found: C, 65.69; H, 8.54; S, 14.99.

**MS** m/e (relative intensity, %): 631 (4), 632 (M+ 100), 633 (43), 634 (24), 635 (8). **HRMS** Calcd. for C<sub>35</sub>H<sub>52</sub>O<sub>4</sub>S<sub>3</sub>, 632.30278. Found: 632.30263. **Electronic spectrum** (CH<sub>2</sub>Cl<sub>2</sub>)  $\lambda_{\max}/(\log \epsilon)$  354 (4.41), 257 (4.13).

#### **4,4''-Didecyloxy-2,2':5',2''-terthiophene-3'-acetic acid (TThAA)**

4,4''-Didecyloxy-2,2' :5',2''-terthiophene-3'-acetic acid methylester (1.2 g, 1.9 mmol), was first dissolved in ethanol (95 %, 50 ml) with stirring and heating. Potassium hydroxide (1.2 g, 21.4 mmol) was dissolved in water (5 ml) and the solution was added to the reaction flask and the temperature was raised to 80 °C with stirring. Initially the contents were not soluble but as the reaction continued, contents went into the solution. After 4 hrs of stirring at 80 °C, reaction was worked-up by adding water (10 ml) and reaction contents were put on rotary evaporator. Ethanol was removed under vacuum and water (40 ml) followed by dichloromethane (DCM) (40 ml) was added to dissolve the compound. Contents were acidified with HCl (2 M) to pH~4. The Organic phase was separated and dried on MgSO<sub>4</sub> and solvent was removed on rotary evaporator

resulting in a dark brown colour crude product. This was purified on silica column (1.5'x10'') eluting with ethyl acetate: DCM (3:7) resulting in a bluish-yellow solid, (1.14 g, 97%), m.p.70-71 °C.

<sup>1</sup>H NMR (400 MHz, CDCl<sub>3</sub>) δ 7.07 (s, 1H, H4'); 6.87 (d, 1H, J = 1.7 Hz, H3); 6.83 (d, 1H, J = 1.7 Hz, H3''); 6.23 (d, 1H, J = 1.7 Hz, H5); 6.12 (d, 1H, J = 1.7 Hz, H5''); 3.94 (m, 4H, 2OCH<sub>2</sub>), 3.77 (2H, -CH<sub>2</sub>COOH) 1.81-0.86 (16CH<sub>2</sub>, 2CH<sub>3</sub>). <sup>13</sup>C-NMR (100.6 MHz) δ 176.7, 157.6, 157.4, 136.3, 134.9, 133.0, 132.9, 129.8, 126.2, 119.1, 116.3, 98.1, 96.6, 70.1, 34.5, 31.9, 29.5, 29.4, 29.3, 29.2, 26.0, 22.7, 14.1. IR (KBr) λ<sub>max</sub>/cm<sup>-1</sup> 3108 (m), 2954 (m), 2919 (s), 2852 (s), 1696 (s), 1571 (s), 1535 (s), 1472 (s), 1455 (m), 1390 (s), 1350 (s), 1214 (m), 1168 (s), 1031 (s), 810 (s), 719 (m), 676 (s). Electronic spectrum (CH<sub>2</sub>Cl<sub>2</sub>) λ<sub>max</sub> nm: 354, 258. Anal. calcd. for C<sub>34</sub>H<sub>50</sub>O<sub>4</sub>S<sub>3</sub>: C, 65.98; H, 8.14; S, 15.54. Found: C, 65.17; H, 8.29; S, 15.27. MS m/e (relative intensity, %): 616 (8), 617 (15), 618 (M+ 100), 619 (72), 620 (36), 621 (17). HRMS calcd. for C<sub>34</sub>H<sub>50</sub>O<sub>4</sub>S<sub>3</sub>, 618.28713. Found: 618.28785.

**2-(3,3''-Dimethylindoline-6'-nitrobenzospiropyranylethyl)4,4''-didecyloxy-2,2':5',2''-terthiophene-3'-acetate (BSP-2)**

(0.084 g, 0.136 mmol), dicyclohexylcarbodiimide (DCC) (0.03 g, 0.143 mmol) and 4-dimethylaminopyridine (0.0013 g, 0.011 mmol) were dissolved in DCM (12 ml) at 0 °C. 1-(2-hydroxyethyl)-3,3-dimethylindoline-6'-nitrobenzospiropyran, **BSP-1** (0.04 g, 0.11 mmol) in DCM (10 ml) was added drop wise over 30 mins to the stirring solution. After **BSP-1** was completely added, the reaction mixture was allowed to reach 20 °C. After a further 90 minutes, 50% of the DCM was removed under reduced pressure, cold ether (10 mls) was added to precipitate the urea salt of DCC. This precipitate was removed by filtration and the filtrate was reduced to give a brown oil, which was purified on a silica column, eluting with DCM. The resulting product was a brown-yellowish oil, which solidified on standing (0.081 g, 77 %).

<sup>1</sup>H NMR (400 MHz, CDCl<sub>3</sub>) δ 7.98 (dd, 1H, J = 8.9 and 2.8 Hz, 7-H of benzopyran); 7.90 (d, 1H, J = 2.8 Hz, 5-H of benzopyran); 7.17 (m, 1H, 6'-H of indoline); 7.06 (dd, 1H, J = 1.3 and 7.3 Hz, 4'-H of indoline) 6.93 (s, 1H, H4'); 6.88 (dt, 1H, J = 7.3 and 0.8 Hz, 5'-H of indoline); 6.83 (d, 1H, J = 1.7 Hz, H3); 6.81 (d, 1H, J = 1.7 Hz, H3''); 6.75 (d, 1H, J = 10 Hz, 4-H of benzopyran); 6.71 (d, 1H, J = 8.9 Hz, 8-H of benzopyran); 6.61 (d, 1H, J = 7.7 Hz, 7'-H of indoline); 6.21 (d, 1H, J = 1.7 Hz, H5); 6.14 (d, 1H, J = 1.7 Hz, H5''); 5.67 (d, 1H, J = 10 Hz, 3-H of benzopyran); 4.29 (m, 2H, NCH<sub>2</sub>); 3.94 (m, 4H, 2OCH<sub>2</sub>); 3.71 (2H, CH<sub>2</sub>COO); 3.42 (m, 2H, COOCH<sub>2</sub>); 1.81-0.86 (16CH<sub>2</sub>,

4CH<sub>3</sub>). <sup>13</sup>C-NMR (100.6 MHz)  $\delta$  170.5, 159.5, 157.6, 146.6, 141.0, 136.3, 135.8, 134.7, 133.1, 132.6, 130.3, 128.8, 128.2, 127.8, 126.2, 125.8, 122.7, 121.8, 121.7, 119.9, 118.9, 118.5, 116.3, 115.4, 106.5, 98.0, 96.6, 70.2, 68.1, 63.1, 52.7, 42.5, 34.8, 31.9, 30.3, 29.7, 29.5, 29.4, 29.3, 29.2, 28.9, 26.0, 25.7, 22.7, 19.7, 14.1, 14.0. HRMS calcd. for C<sub>54</sub>H<sub>68</sub>N<sub>2</sub>O<sub>7</sub>S<sub>3</sub>, m/z: 952.4261. Found m/z: 952.4232. Spectrum (CH<sub>2</sub>Cl<sub>2</sub>)  $\lambda_{\text{max}}$  nm: 357, 258, 579.

## 2.2.2 Electrochemical Polymerization of BSP-2 and TThMA

**Poly-BSP2** films were electrochemically grown on a platinum disc working electrode, with the surface area 0.02 cm<sup>2</sup> (Bioanalytical System) or on optically transparent ITO (Indium Tin Oxide) coated glass (Delta Technologies, Limited, resistivity R<sub>s</sub> = 4-8  $\Omega$ ) by cyclic voltammetry or chronoamperometric deposition at constant potential 0.8 V from a solution of anhydrous dichloromethane and acetonitrile (2:3) containing 0.1 M tetrabutylammonium perchlorate (TBAP) and the monomer at a concentration of 8 mM. **P-TThMA** films were electrodeposited from the solution of 20 mM **TThMA** in 0.1 M TBAP in anhydrous dichloromethane. Pt mesh and Ag / Ag<sup>+</sup> electrode were used as the counter electrode and quasi-reference electrode respectively. Half-wave potential was measured for 1 mM ferrocene, E<sub>1/2</sub> = 0.165 V, vs. Ag / Ag<sup>+</sup> reference electrode. All solutions were degassed prior to the measurements under nitrogen.

## 2.2.3 UV-vis Spectroelectrochemistry

Absorbance spectra were recorded using a Shimadzu UV-1800 spectrophotometer. In situ spectroelectrochemical measurements were performed using optically transparent thin-layer electrochemical (OTTLE) cell, equipped with a Pt minigrad working and auxiliary electrode, Ag wire pseudo reference electrode, and CaF<sub>2</sub> window, optical path length (0.2 mm). **p-BSP2** was electrochemically grown on ITO-coated glass by chronoamperometric deposition at constant potential 0.8 V during 40 s or by cyclic voltammetry in the potential range 0 V to 0.8 V from a solution of anhydrous dichloromethane and acetonitrile (2:3) containing 0.1 M tetrabutylammonium perchlorate (TBAP) and the monomer at a concentration of 8 mM. The spectroelectrochemistry of the polymer films deposited on ITO electrode was investigated in solutions of 0.1 M TBAP in acetonitrile vs. Ag wire for the reference electrode. These applied voltages for the OTTLE cell and for the Ag wire used for spectroelectrochemical experiments on ITO modified electrodes were rescaled vs.

Ag/Ag<sup>+</sup> by using ferrocene. The controlled-potential measurements were carried out with an eDAQ system controlled by EChem software.

In the photochemistry experiments, the **p-BSP2** and **p-TThMA** films were irradiated with an ultraviolet lamp at  $\lambda = 254$  nm or exposed to visible-IR light ( $>570$  nm).

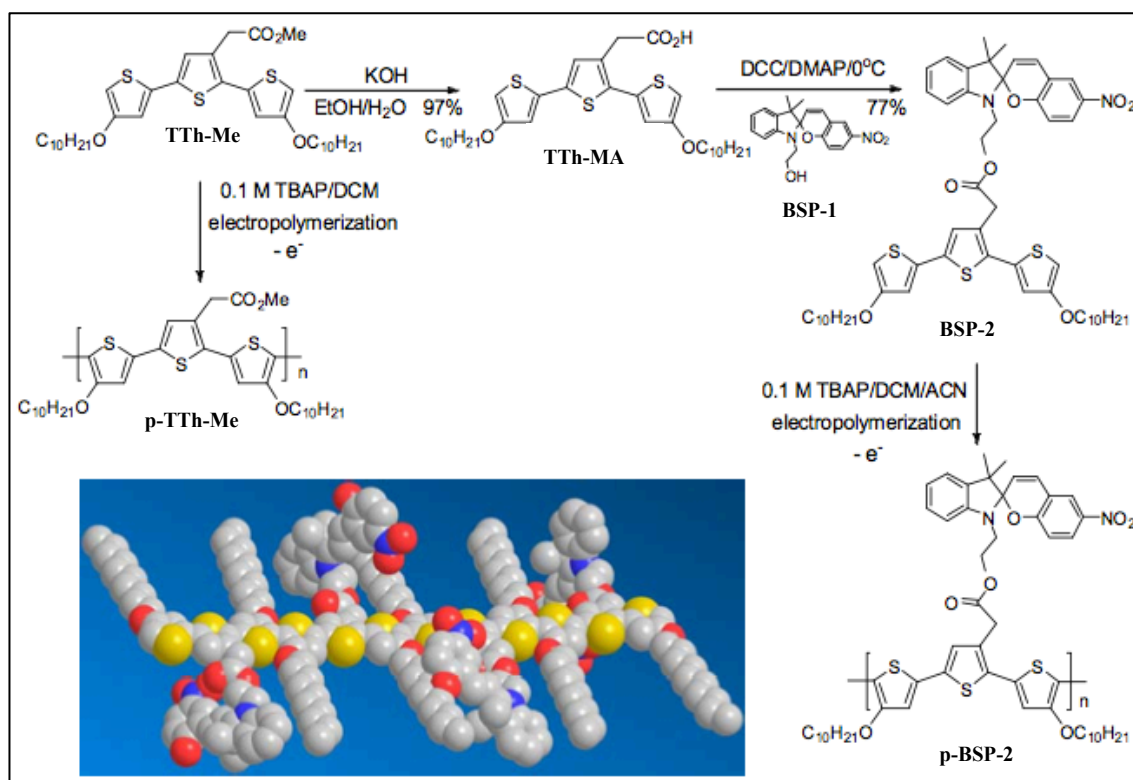
### 2.2.4 Conductivity measurement

4 point resistivity meter (JANDEL Model RM2), with spacing in square array 0.635 mm, was used in conductivity measurements. **p-BSP2** was electrochemically grown on optically transparent ITO- coated glass by chronoamperometric deposition at constant potential 0.8 V during 1 hour. The polymer was then peeled off the electrode and the conductivity measurement was performed on the freestanding film.

## 2.3 Results and Discussion

### 2.3.1 Synthesis of the monomers

The dialkoxyterthiophene acetic acid **TThMA** was chosen in this study as the terthiophene monomer to functionalise with the SP group because favourable reaction conditions (eg room temperature reactions) can be used to form reasonably stable ester linkages with a readily available hydroxyl-substituted spiropyran, such as N-hydroxyethylnitrobenzospirogyran **BSP-1** (Scheme 2.1). Spiropyran-substituted terthiophene monomer **BSP-2** was readily prepared from the acetic acid **TThAA** (Scheme 2.1). The precursor methyl acetate **TThMA** was synthesised as previously described<sup>24</sup> and hydrolysed to give **TThAA** in quantitative yield. Base-catalysed condensation of **BSP-1** with **TThMA** afforded **BSP-2** in 77 % yield.



**Scheme 2.1:** Synthesis and polymerisation of **BSP-2**. The inset shows a computer-generated model of a short length of the ring-opened poly-merocyanine, **p-MC2**.

The structures of the three substituted terthiophenes are fully consistent with their spectroscopic data. The <sup>1</sup>H NMR terthiophene signals are as expected unperturbed by the change in ester functionality with NMR spectral characteristics of **BSP-2** simply being a superposition of the **TTh** and **BSP** components. As expected for nitrospiropyran derivatives, the UV-*vis* absorption spectrum of **BSP-2** (Figure 2.1, blue lines) shows bands in the ultraviolet (not shown) due to the **BSP-1** substituent. In the visible, the terthiophene absorbance dominates the spectrum at 350 nm, with no absorption due to the merocyanine isomer above 500 nm. Irradiation of a dichloromethane solution of **BSP-2** with UV light leads to the formation of **MC-2** (Figure 2.1, red line), as evidenced by the peak at 563 nm.

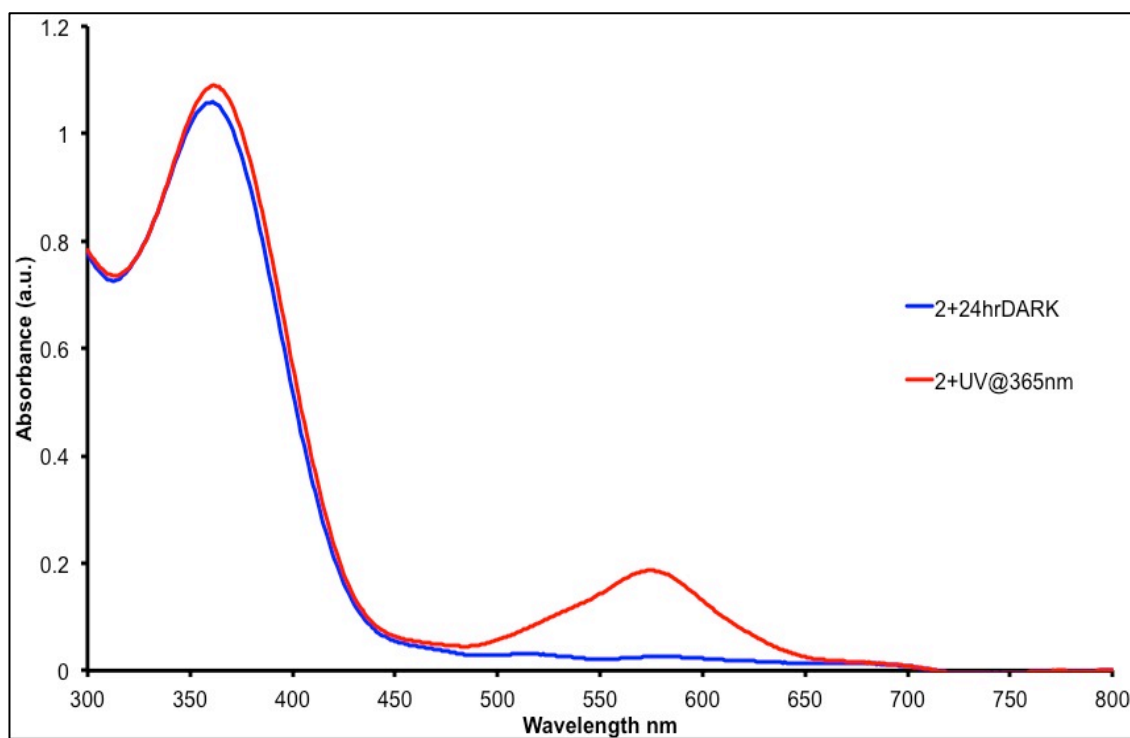


**Figure 2.1:** Photo-isomerisation in solution of **BSP-2** after irradiation with 365 nm UV light for 3 minutes.

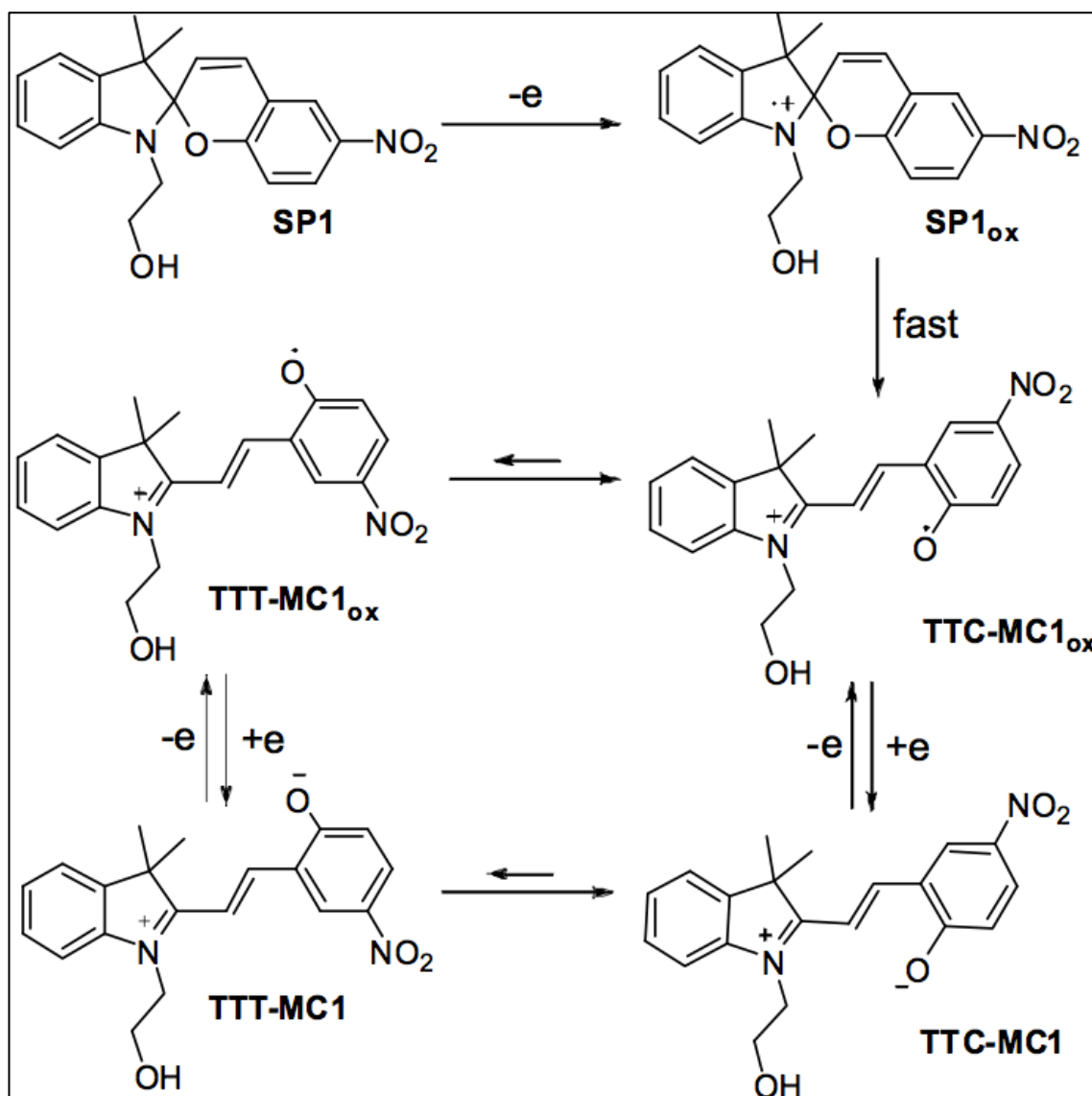
It seems, therefore, that the terthiophene moiety does not affect the photochromic properties of the spiropyran substituent but does reduce the formation of aggregates.

### 2.3.2 Electrochemistry and Spectroelectrochemistry of **BSP-1**

Initial investigations into the electrochemical polymerisation of **BSP-2** revealed that the resulting polymer had a more complex electrochemical behaviour than expected from a substituted poly-(terthiophene). This behaviour clearly arose from the presence of spiropyran, and there appeared to be a limited knowledge of the electrochemistry of spiropyrans generally. The electrochemistry of analogues of **BSP-1** has been reported previously.<sup>25-28</sup> Zhi *et al.* discuss electrochemistry and spectroelectrochemistry of N-methylnitrobenzospiropyran, specifically investigating the reduction behaviour of the molecule but providing little information about the oxidation of the spiropyran<sup>27</sup>. We do not observe the same electrooxidation characteristics as Zhi *et al.* Our results are similar to those of Campredon *et. al.*<sup>26</sup> who investigated the electrochemical behaviour of naphthalene analogues of **BSP-1**, although their report includes only a first scan of oxidation voltammograms and a brief comment regarding the instability and possible degradation of the formed radical cation. More recently, Jukes *et. al.*<sup>28</sup> reported the electrochemistry and spectroelectrochemistry of 1,3,3-trimethylindoline-6-

nitrobenzopyrylospiran, and, while they report oxidation voltammograms similar to ours, their focus is largely on the reduction influence on the oxidation.

On the first, positive scan on the **BSP-1** voltammogram (Figure 2.2 (a)), one irreversible oxidation peak at the potential 0.77 V is observed, with broad, overlapping reduction waves on the reverse scan. It has been proposed that this first oxidation of spiro compounds is a one-electron oxidation at the indoline nitrogen. Because the oxidation is irreversible, a new species must be formed from the oxidized spiropyran<sup>5</sup>. Visual inspection of the solution at the working electrode surface (Figure 2.2 (e)) during oxidation shows the presence of an orange-red colour, similar to that observed by Preigh *et al.* during electrochemical oxidation of an hydroxylspiropyran and attributed to oxidized merocyanine<sup>5</sup>. When the **BSP-1** solution is initially prepared, an equilibrium mixture of the pale yellow **BSP-1** and red **MC-1** forms is clearly present as indicated by the violet coloration (Figure 2.2 (c)). On standing in the presence of light, this initial equilibrium changes significantly in favour of the **BSP-1** form, giving the pink colour (Figure 2.2 (d)). Therefore, oxidation at the working electrode is clearly driving the **BSP-1** to the **MC-1** form (red colour). Zhi *et al.* proposed a mechanism for this type of electroisomerization.<sup>27</sup> However, they suggested that the isomerisation arises from the reduced spiropyran, which cannot be the case here. As suggested by Preigh and *et. al.*<sup>29</sup> for an hydroxyl analogue, initial oxidation of the indoline nitrogen to give the **SPox**, followed by rearrangement, affords the **MC** radical cation. During the second scan of the CV of **BSP-1** (Figure 2.2 (a)), two new broad overlapping oxidation waves appeared with potential maxima at 0.47 and 0.57 V. Because several stereoisomers of the **MC** form have been recognised,<sup>30</sup> the most dominant of which are the **TTC** (trans-trans-cis) and **TTT** (trans-trans-trans)<sup>31</sup> forms, it is likely that these peaks may represent the electrochemistry of the two **TTC-MC-1** and **TTT-MC-1** isomers (Scheme 2.2). These species themselves could undergo reversible electrochemistry as indicated by the reduction peaks at 0.44 and 0.52 V. However, there is no apparent electrochemical path back to **BSP-1** from either the oxidized or the reduced **MC-1** isomers as is indicated by a drop in height of the **BSP-1** oxidation peak at 0.77 V on the second scan of the CV (Figure 2.2 (a)).



**Scheme 2.2:** Postulated mechanism for the electrochemical redox isomerisation of **BSP-1**.

To further probe this, the absorption spectral changes of **BSP-1** oxidation processes in 0.1 M TBAP in acetonitrile were recorded at applied potentials from 0.6 to 0.9 V and are shown in Figure 2.2 (b). Significant absorbance changes were observed when the potential exceeded 0.65 V, and new absorption bands with maxima at 492 and 523 nm (corresponding to the red solution in Figure 2.2 (e)) grew rapidly. Therefore, we ascribe these two absorption bands to **MC-1<sub>ox</sub>** and **MC-1<sub>ox</sub>**. It is also interesting to note the appearance of two absorption peaks at 880 and 997 nm, which rise (0.8 V maximum) and fall as the oxidation potential is increased. Because these peaks reduce in intensity as the amount of **MC-1** increases, we propose that they arise from the formation of **MC-1** radical cation dimers. These observations provide significant insights into the electrochemistry and spectroelectrochemistry of **p-BSP2**.

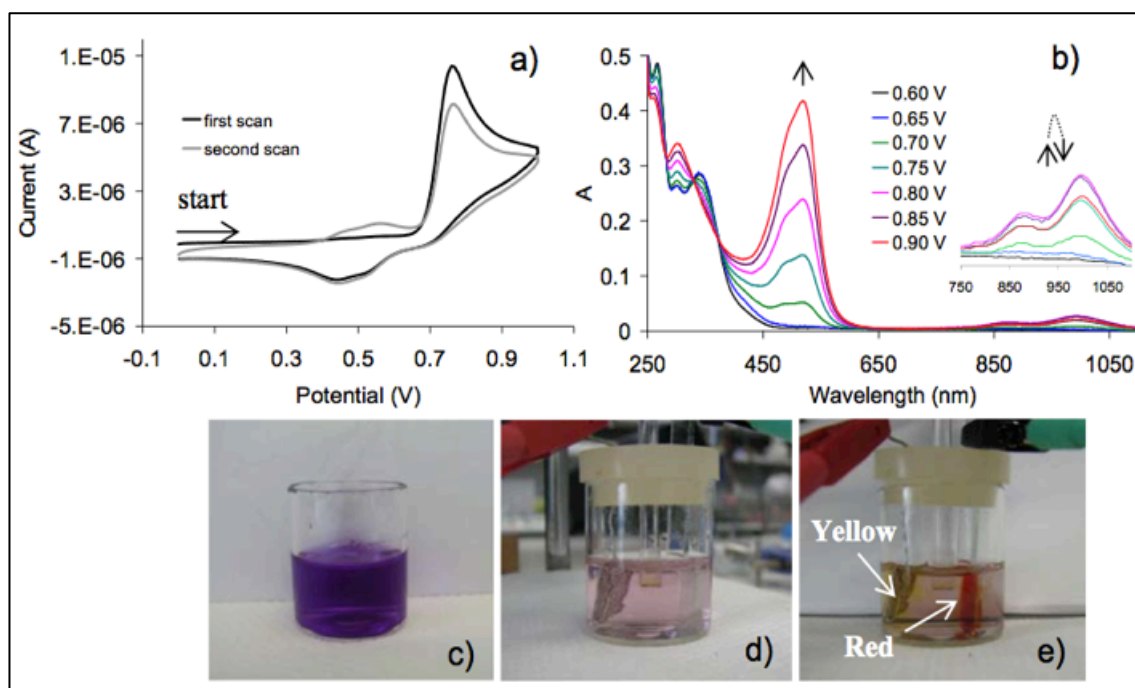


**Figure 2.2:** Cyclic voltammograms of **BSP-1**(a), spectroelectrochemistry during oxidation of  $2 \times 10^{-3}$ -M **BSP-1** in an OTTE cell (b), a solution of **BSP-1** just after preparation (c) and after 20 min exposure to visible light (d), and change in **BSP-1** solution in electrochemical cell during applied potential 1 V to the ITO electrode (e). SP1 concentrations in (a), (c), d), and (e) are  $1 \times 10^{-3}$  M in acetonitrile with 0.1 M TBAP as electrolyte.

Consequently, we propose that electrochemical oxidation of **BSP-1** irreversibly leads to isomers of oxidized **MC-1**, which themselves undergo reversible electrochemistry as depicted in Scheme 2.2. Although these are solution-based processes, we anticipated that the spiropyran substituent of **p-BSP2** would undergo similar electrochemistry given we had not observed any spectroscopic interaction between the terthiophene and spiropyran groups.

### 2.3.3 Electrochemical Polymerization of pBSP-2

The electrochemical deposition of **BSP-2** on a platinum disk electrode shows cyclic voltammograms (CVs) with an increase in current with successive cycles, indicative of successful electroactive film deposition (Scheme 2.1 and Figure 2.3 (a)). The electropolymerization process is carried out up to 0.8 V, with the onset of monomer oxidation to its radical cation at 0.62 V (inset, Figure 2.3 (a)) and the formation of bluish film, typical of oxidized poly-(terthiophene). We do not observe the characteristic red colour of merocyanine at the maximum applied potential of 0.8 V, one hypothesis is that the spiropyran ring does not open during electrodeposition. The film-coated electrode was placed in monomer-free solution for post-polymerisation CV

analysis. The post CVs show interesting, dynamic redox behaviour (Figure 2.3 (b)). During the first scan in the post CV of **p-BSP2**, three oxidation peaks are visible at 0.12, 0.34, and 0.76 V (Figure 2.3 (b)). While the origin of the peak at 0.12 V is not clear, the 0.34 V peak can be assigned to oxidation of the polymer backbone (**p-oxBSP2**, Scheme 2.3), because cycling of the **p-BSP2** film between -0.4 and 0.5 V shows consistent capacitive behaviour over more than 10 cycles (not shown). A similar oxidation peak is observed for a **p-TThMA** film (Figure 2.3 (c)), which is the analogous spiropyran free polymer, with a methyl substituent instead of the nitrobenzospiryran. In contrast, the sharp oxidation peak at 0.76 V on the first post CV scan of **p-BSP2** (Figure 2.3 (b)) is completely lost during the second scan, but appears to recover somewhat during cycling. The position of this peak is at the same potential as the first oxidation of the **BSP-1** molecule (Figure 2.2 (a)). It is likely that the oxidation peak at 0.76 V for **p-BSP2** results from loss of an electron from the indoline nitrogen of the **BSP-1** substituent, leading to the oxidized **MC** substituent on the oxidized poly-thiophene backbone (**p-TThoxMC2ox**, Scheme 2.3).

We also observed that the choice of the switching potential used during electropolymerization of **p-BSP2** (Appendix A, Figure A1 (a), (c), (e)) influences the electrochemical characteristics of the post CV voltammogram (Appendix A, Figure A1 (b), (d), (f)). When the switching potential of electropolymerization is set higher than 0.9 V (see Appendix A, Figure A1 (e)), somewhat higher than the oxidation potential of spiropyran **BSP-1** (0.77 V, Figure 2.2 (a)), the sharp oxidation peak at 0.76 V on the first post CV scan of **p-BSP2** is no longer observed. Clearly, from these post CVs, the oxidation of the appended spiropyran is not reversible, and therefore it appears likely that the substituent on **p-BSP2** remains in the **MC** form following further cycling. The CV following initial **p-BSP2** oxidation (second scan, Figure 2.3 (b)) has no peak due to **BSP** oxidation, but subsequent scans exhibit a peak at 0.65 V of increasing intensity. This could arise from the oxidation of the polymer **MC** stereoisomers, analogous to that postulated for **BSP-1** (Scheme 2.2).

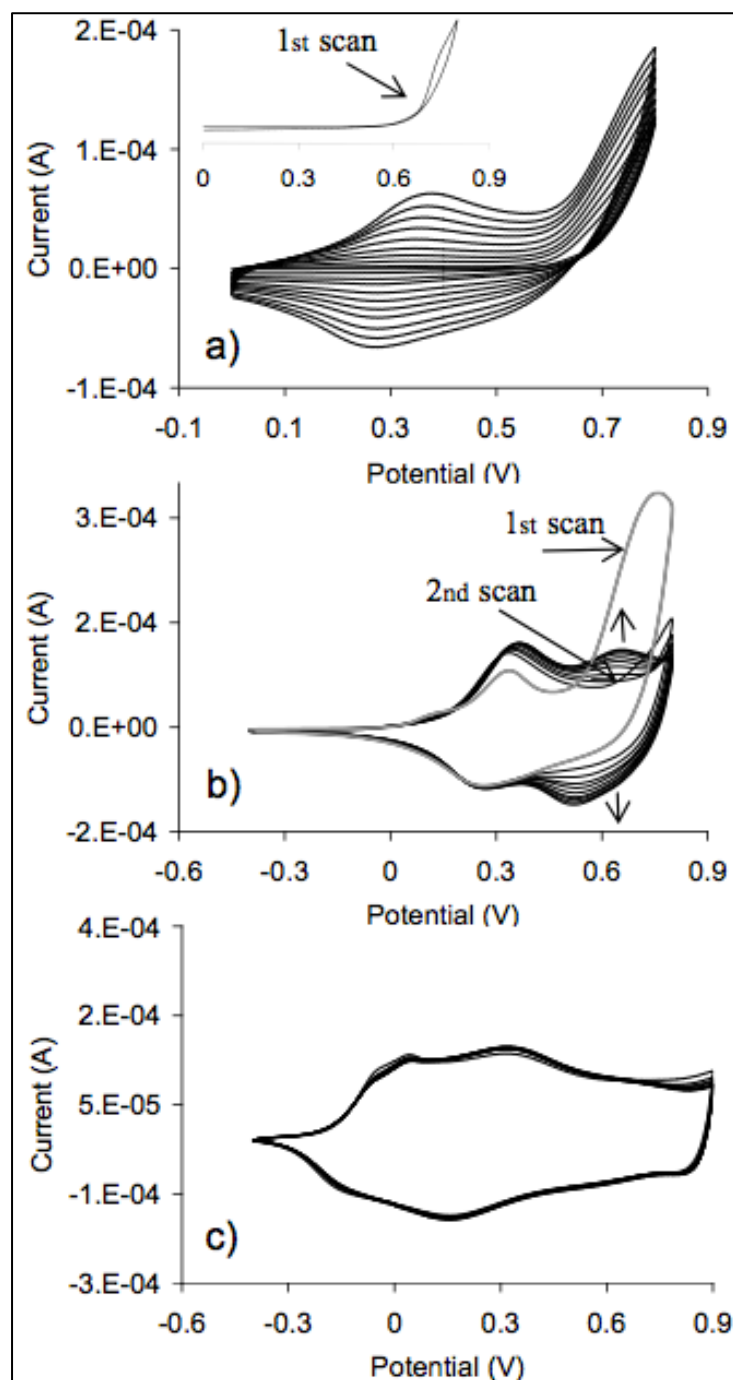
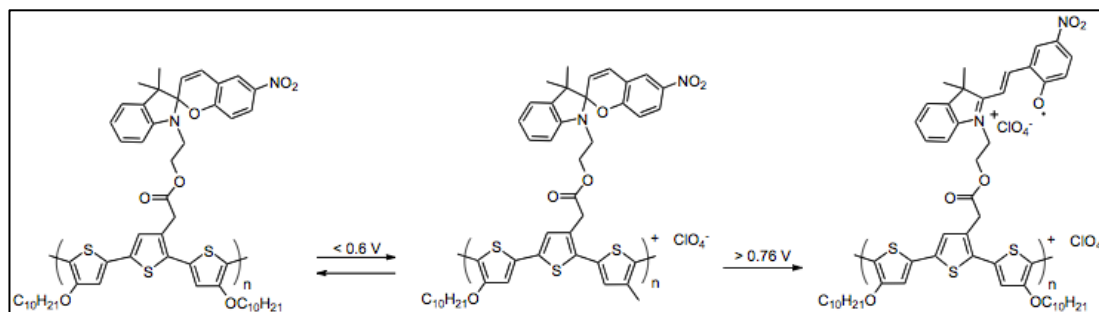


**Figure 2.3:** Electrochemical deposition of **BSP-2** with inset showing the first scan (a), post CV voltammograms of **p-BSP2** (b) and **p-TThMA** (c) on platinum disk electrodes, 10 scans at a scan rate  $100 \text{ mV s}^{-1}$ .

This oxidative electroisomerization of **p-BSP2** is also supported by the dramatic colour changes observed on oxidation of the polymer film. Polythiophene films generally exhibit two colours, depending on the doped state. For example, the colour of the parent poly-(terthiophene) in the reduced state is orange-red and brown-black-blue when the polymer is oxidized<sup>32</sup>. Reduced **p-BSP2** film is a violet-pink colour, but on oxidation to 0.5 V (polymer backbone oxidation) the colour changes to green-blue

(Scheme 2.3). Further oxidation to 0.8 V generates a more intense violet-pink film as the result of the formation of the oxidized **MC** substituent. This additional colour change at the positive potential occurs very quickly, over a narrow range of potentials. This unique photochromic behaviour in the doped state was further investigated using spectroelectrochemistry.



**Scheme 2.3:** Proposed mechanism for electro-isomerisation of **p-BSP2**.

### 2.3.4 UV-Visible Spectroelectrochemistry of poly-BSP2.

The spectral properties of **p-BSP2** were examined across the potential range used for the post-CV analyses (-0.35 to 0.9 V). **p-BSP2** exhibited typical polythiophene behaviour as the electrode potential was increased from -0.35 to 0.6 V, with initial polaron band formation (870 nm) followed by the development of a free carrier tail (Figure 2.4 (a)). As the applied potential increases from 0.6 V, the growth of a new absorbance at 540 nm is observed (Figure 2.4 (b)), which corresponds to the initial sharp oxidation shown in the post CVs (Figure 2.3 (b)). This absorbance is in a position similar to that observed for the photo-isomerized **MC-2** monomer (Figure 2.1, red line), and therefore we attribute it to the oxidized **MC** isomer of **p-TThoxMC2ox**.

To probe the reversibility of this merocyanine formation and oxidation, we monitored the 540 nm absorbance over the potential range -0.1 to 0.9 V during cyclic voltammetry (Figure 2.5). A freshly electrodeposited film was utilised to ensure that the polymer was in the **BSP** form. In addition, the same experiment was carried out with a freshly prepared **p-TThMA**. As seen in Figure 2.5 (a), the absorbance at the potential -0.1 V results from the polymer backbone, and, as the polymer becomes oxidized, the absorbance decreases (Figure 2.5 (a), black line). When the potential applied to the **p-BSP2** film is more positive than 0.6 V, the absorbance at 540 nm increases rapidly as a result of **MC** isomer formation. In contrast, **p-TThMA** film (Figure 2.5 (a), grey line) does not show any absorbance changes at the positive potential range, as is expected for a poly-(terthiophene).

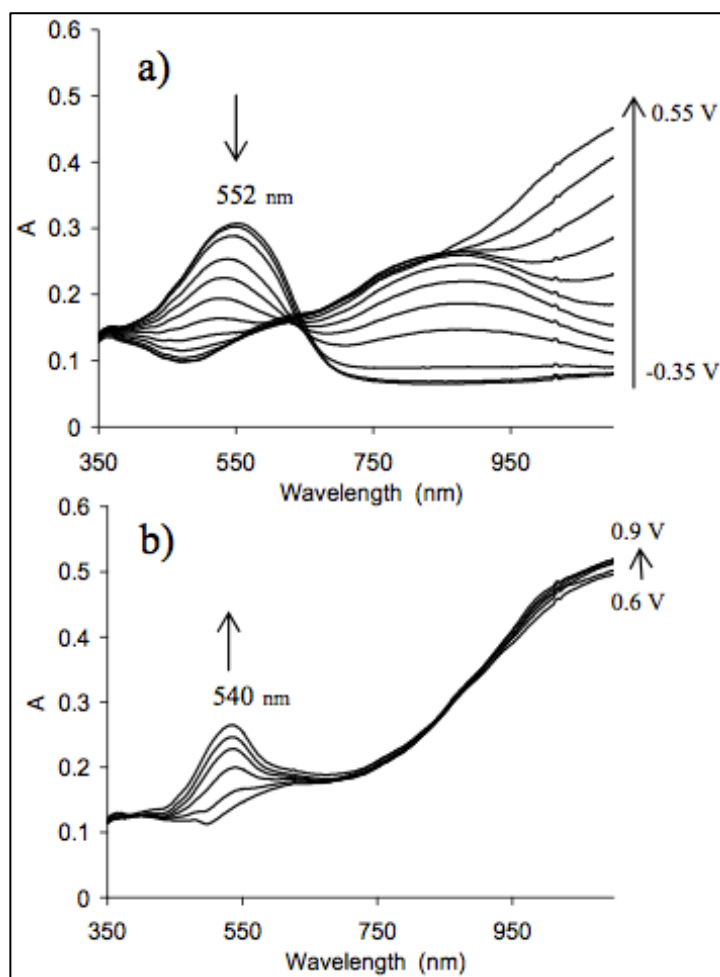


**Figure 2.4:** Spectroelectrochemistry of electrochemically polymerized film of **p-BSP2** (a and b) on ITO glass for potential ranges of -0.35 to 0.55 V (a) and from 0.6 to 0.9 V (b).

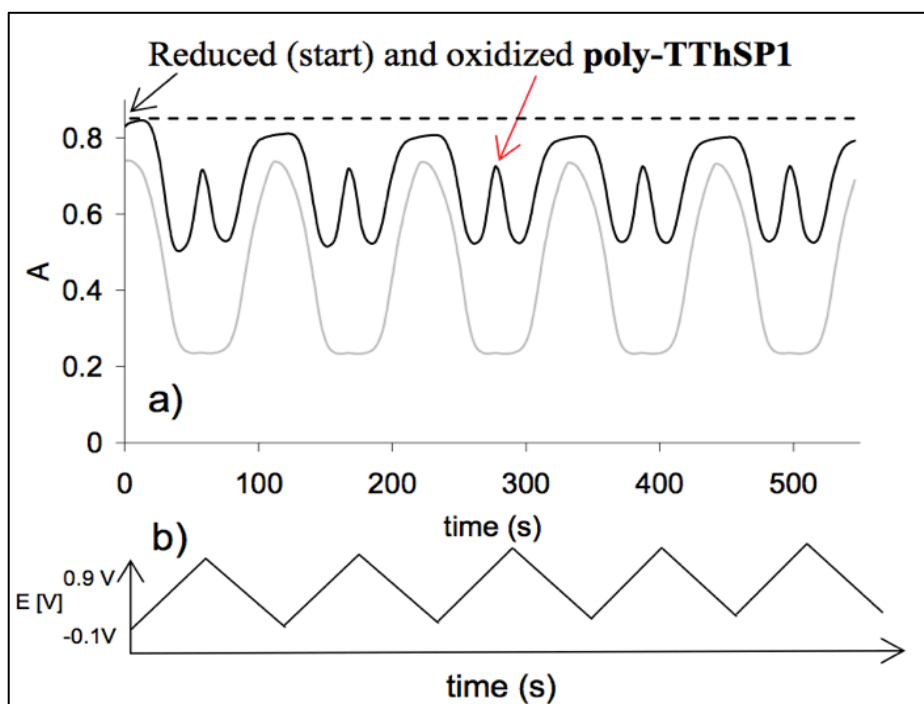


**Figure 2.5:** Absorption spectra response at 540 nm for (a) **p-BSP2** (black line) and **p-TThMA** (grey line), when the applied potential was changed from -0.1 to 0.9 V in 0.1 M TBAP in acetonitrile (b).

We also observed following **p-BSP2** oxidation for the first time ( $t = 0$ , Figure 2.6 (a)), the same level of absorbance on re-reduction (dashed line, Figure 2.5 (a)), indicative of the formation of ring-opened merocyanine isomers that do not ring close to spiropyran on reduction. This observation is consistent with the variable electrochemical response of **p-BSP2** (Figure 2.3 (b)).

To better understand these changes, a spectroelectrochemical study of fresh films of both **p-BSP2** (Figure 2.6) and control sample **p-TThMA** (see Appendix A, Figure A2) was undertaken. The aim of these measurements was to monitor the absorbance changes during a “simulation” of the film cycling. The absorbance spectra in the previous spectroelectrochemical study (Figure 2.5) only show the initial changes that occur following the oxidation of the spiropyran moiety. In this study, absorbance spectra were obtained while holding the potential at -0.1, 0.6, 0.8, and 1.0 V (Figure 2.6 (a-d)), potentials at which new peaks appeared in the post-CVs during film cycling (Figure 2.3 (b) and (c)). This was repeated six times, effectively mimicking six CV cycles.

Again, it is clear that the spectra recorded during the first “cycle” are different from all the others. Thus, the first spectrum of the reduced **p-BSP2** film (Figure 2.6 (a)) is different across the whole spectrum from the next five spectra recorded at that potential (-0.1 V), consistent with the single wavelength observation evident in Figure 2.6 (a). As expected up to 0.6 V, the poly-(terthiophene) backbone appears to be oxidized, as evidenced by the complete loss of the absorbance at 500 nm as well as the rise of the polaron band at 850 nm (Figure 2.6 (b)). However, the “second cycle” shows the rise of a new band below 500 nm, which appears to come from the opening of the spiropyran.

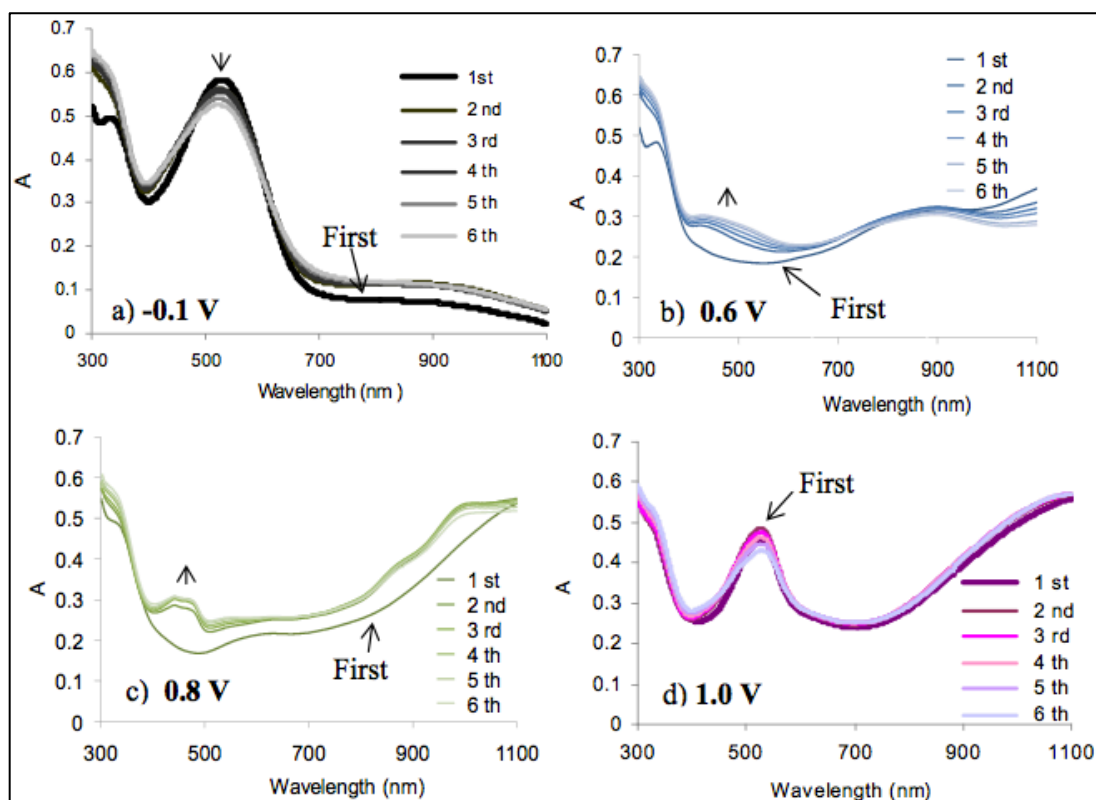


**Figure 2.6:** Spectroelectrochemistry of **p-BSP2** on ITO recorded six times at the potentials -0.1 V (a), 0.6 V (b), 0.8 V (c), and 1.0 V (d).

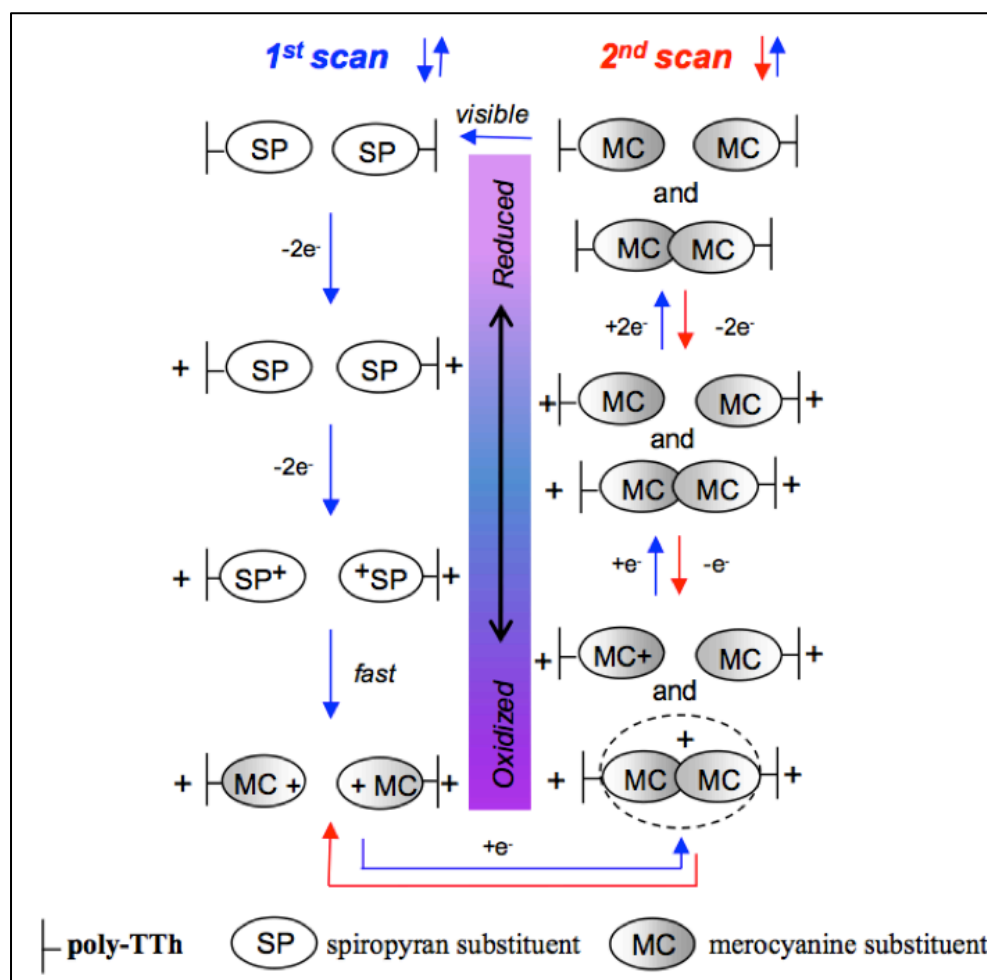
The picture becomes clearer from the absorbance spectra at 0.8 V (Figure 2.6 (c)) and 1.0 V (Figure 2.6 (d)). The first spectrum at 0.8 V is again assigned essentially to the oxidized polymer backbone, which now shows a significant free carrier tail above 700 nm. The second and later spectra exhibit much more character with two new peaks at 443 and 477 nm and broad absorbances at 870 and 995 nm. All of these bands are then either lost completely or reduced substantially at higher oxidation potential (1.0 V, Figure 2.6 (d)), with the appearance of a new band around 540 nm and the retention of the free carrier tail.

Therefore, the two bands at 443 and 477 nm are clearly not due to the fully oxidized polymer with oxidized merocyanine, which absorbs at 540 nm. A clue to the origin of these bands lies in the simultaneous appearance of the broad near-infrared absorbances that are almost identical to those observed in the spectroelectrochemistry of the oxidized parent spiropyran **BSP-1** (Figure 2.2 (b)). All of these bands appear to arise from the **BSP** substituent because an identical spectroelectrochemical experiment involving **p-TThMA** (see Appendix A, Figure A2) does not show peaks at 443 and 477 and at 870 and 995 nm following initial polymer oxidation. Because the merocyanine groups are fixed in space by the polymer backbone, the formation of large aggregates is unlikely. However, interaction of two merocyanines with antiparallel dipoles could arise from

merocyanines on neighbouring polymer chains forming  $\pi$ -dimers. The two peaks at 443 and 477 nm (Figure 2.6 (c)) could represent dimers formed from the two major merocyanine isomers **TTC** and **TTT** (see Scheme 2.2).

The removal of a single electron from this type of  $\pi$ -dimer to form a  $\pi$ -radical cation dimer might then be expected to be easier than oxidation of a single merocyanine substituent. The formation of  $\pi$ -radical cation dimers in aromatic species is well established in the literature.<sup>22,33,34</sup> Both the spectroelectrochemistry of **BSP-1** solutions (Figure 2.3 (b)) and that of the **p-BSP2** film (0.8 V, Figure 2.6 (c)) are fully consistent with the formation of merocyanine  $\pi$ -radical cation dimers. In both cases, the oxidation of the merocyanine moiety leads to low intensity, longer wavelength peaks between 800 and 1100 nm, that rise and fall as the intensity of the oxidized merocyanine band around 500 nm increases. This can be accounted for by the initial formation of  $\pi$ -radical cation dimers at a low concentration of oxidized merocyanine followed by disappearance of the dimer with complete oxidation of the merocyanine.

The presence of neutral or charged dimeric species or even larger aggregates as a result of merocyanine formation and oxidation accounts for the majority of changes seen in the spectroelectrochemical experiments. To clarify this, we have depicted the processes occurring during the first and subsequent electrochemical cycles schematically in Scheme 2.4.



**Scheme 2.4:** Schematic representation of redox cycling and aggregation of **p-BSP2**.

The left-hand side of the scheme represents the oxidation component of the first cycle with initial polymer oxidation, followed by formation of oxidized spiropyran that rapidly ring opens above 0.8 V to oxidized merocyanine. The reduction component of the first cycle (going up the right-hand side of Scheme 2.4) leads ultimately to a neutral merocyanine-substituted polythiophene that contains both single, as well as dimeric (or oligomeric), merocyanines. This accounts for the loss of peak height and the peak broadening in the second and subsequent spectra of the spectrochemical study at -0.1 V (Figure 2.6 (a)). As the polymer is oxidized and reduced, more ordering of the film occurs as a result of strong  $\pi$ -radical cation dimer coupling, leading to an overall increase in neutral dimer formation (and hence peak broadening due to increasing absorptions around 446 nm). This also may explain the apparent increased difficulty in reducing the polymer after the first cycle as evidenced by the increased polaron band at 850 nm.

On the second cycle, it is now the presence of merocyanine  $\pi$ -dimers that dominates the electrochemistry (down the right-hand side of Scheme 2.4). Oxidation of the

merocyanine polymer at 0.6 V (Figure 2.6 (b)) leads to the loss of the neutral poly-(terthiophene) absorption at 552 nm, revealing broad absorptions from 400 to 550 nm that reflect the presence in the oxidized polymer film of both free merocyanine substituents, as well as merocyanine  $\pi$ -dimers and possibly higher oligomers. Further oxidation (0.8 V, Figure 2.6 (c)) now gives the characteristic bands of both,  $\pi$ -dimers and  $\pi$ -radical cation dimers as well as both oxidized (~540 nm) and neutral merocyanines (~560 nm) on the oxidized polymer backbone. Finally, full oxidation of the merocyanine groups above 1.0 V (Figure 2.6 (d)) leads to separation of the merocyanines with only the oxidized merocyanine band at 540 nm apparent in the spectrum.

Given that the spiropyran cannot be regenerated electrochemically, we investigated the feasibility of photochemical control of this process to achieve complete reversibility of this intriguing redox system.

### 2.3.5 Light Control of BSP1 Isomerisation

The photochemical conversion of merocyanine to spiropyran is typically an easily identifiable process, as we observed in the study of **BSP-2**, because the merocyanine absorption spectrum is largely well separated from the spiropyran spectrum. However, in the case of **p-MC2**, the merocyanine absorption (assumed to be around 560 nm as for **MC-2**) is at wavelengths similar to that of the reduced polyterthiophene backbone (380-670 nm), making identification of merocyanine formation difficult. To ensure the presence of spiropyran in the polymer, a thin film (<1  $\mu\text{m}$ ) of **p-BSP2** on ITO glass was CV electrodeposited between 0 and 0.75 V (see Appendix A, Figure A1 (a)), and its UV-visible spectrum was recorded (Figure 2.7, blue line), following washing to ensure the absence of excess monomer from the polymerization. Irradiation of the dried film with ultraviolet (UV) light (254 nm, 5 min) afforded a more intense and broad UV-visible band (Figure 2.7, red line) shifted by 20 nm. This is consistent with the formation of **p-BSP2**, because the intensity of the polythiophene backbone absorption would be expected to remain constant but the growth of a new absorption centred around 560 nm would lead to a more intense broader band overall. A small broad absorption at 383 nm also appears due to the **MC** formation. Subsequent irradiation of the polymer film with visible light (40 min) gave a polymer absorption band (Figure 2.7, green line) identical to that of **p-BSP2**, albeit with a slightly higher intensity. A second UV light illumination returned the higher wavelength absorption (Figure 2.7,

violet line), again with small intensity differences. These intensity changes may well be due to conformational changes to the polymer backbone as a result of the spirocyan to merocyanine isomerisation. To ensure that these spectral changes largely resulted from spirocyan to merocyanine isomerisation, irradiation of the control polymer **p-TThMA** was investigated. No change in the absorption spectra of **p-TThMA** was observed (see Appendix A, Figure A3) following exposure of polymer film to UV light.

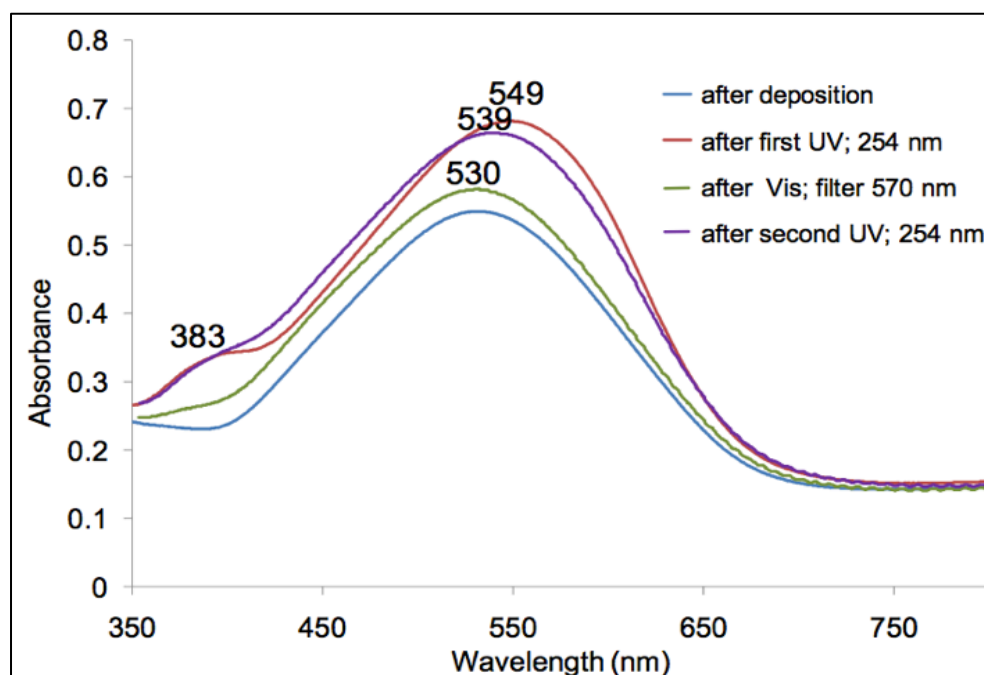


**Figure 2.7:** UV-*vis* spectra of reduced **p-BSP2** after electrochemical deposition (blue line), after first irradiation with 254 nm UV light (red line), followed by irradiation with visible light (green line), and second irradiation with 254 nm UV light (violet line).

While these experiments demonstrate that the reduced **p-BSP2** film, whose **BSP** substituent has never been electrochemically oxidized, undergoes the typical reversible **BSP** to **MC** isomerisation, further experiments were undertaken to determine whether this was the case for a **p-BSP2** film in which the isomerisation of the **BSP** moiety had occurred (through irradiation). **BSP-2** was electrochemically polymerised on optically transparent ITO-coated glass by chronoamperometric deposition at constant potential (0.8 V) in the dark. At this potential (as shown in Appendix A, Figure A1 (a)) the **SP** substituent should not be substantially oxidized to **MC**. The **p-BSP2** film was then exposed to UV light at 254 nm for 5 min, and the post-CVs (from -0.4 to 0.9 V) obtained with the UV light were still applied to the polymer film (Figure A4 (a)). As expected, no initial electrochemical response ascribed to the spirocyan moiety is

observed, suggesting that under these conditions the spiropyran is all converted to merocyanine, giving **p-MC2**.

However, in contrast to the previous experiment that only involved photoisomerisation, the **p-MC2** will have been electrochemically oxidized (both polymer backbone and **MC** substituent) during the post-CV cycling, giving  $\pi$ -cation dimers and other aggregates. The polymer film was then irradiated with visible light (390-750 nm) for 5 min, and the CVs again were recorded over the same potential range while maintaining the visible light irradiation (see Appendix A, Figure A4 (b)). Clearly, there is some photochemical regeneration of spiropyran in the film, as evidenced by the appearance of a new peak at 0.55 V in the first CV scan, and its subsequent loss in the second scan. The amplitude of the peak is low, suggesting that only a fraction of the merocyanine substituents in the film are isomerized. Given that the **p-MC2** film is likely to be composed of both free and aggregated merocyanine substituents following oxidation, spiropyran formation would be expected to be sterically limited. In addition, the isomerisation must be slow, certainly slower than the time frame of the cyclic voltammetry, because almost no spiropyran is reformed during the subsequent CV scans. This is perhaps not surprising because the reduced merocyanine film would be much more compact than that of the reduced spiropyran film, particularly with increased formation of  $\pi$ -dimers, making it sterically and energetically more difficult to reform spiropyran.

### 2.3.6 Physical Properties of **p-BSP2**

It is well-known that conducting polymers display actuation behaviour under an external redox potential, due to the movement of counter-ions and associated solvent molecules into and out of the polymer, which results in swelling and contraction<sup>35</sup>. According to the earlier spectroelectrochemical study, the initial oxidation of the spiropyran moiety provides some merocyanine dimer or oligomer aggregates within the polymer film. These processes should markedly affect the morphology of **p-BSP2**, and for this reason scanning electron micrograph (SEM) analysis of the different redox stages of the polymer was undertaken. SEM images were obtained for four **p-BSP2** samples electro-polymerised in the same way but then subjected to different redox conditions. Three of those samples were oxidized or reduced at constant potential for 2 min. The first image in Figure 2.8 (a) shows the morphology of the fresh film, obtained after 1 min constant potential deposition at 0.8 V. The second polymer sample was

oxidized at 0.5 V (Figure 2.8 (b)) from which we expect only polymer backbone oxidation, while the third one was further oxidized to 0.85 V (Figure 2.8 (c)), leading to oxidation of the spiropyran substituent on the polymer backbone. The last sample was reduced with the potential -0.4 V (Figure 2.8 (d)). The morphology of the fresh **p-BSP2** (Figure 2.8 (a)) shows a globular structure, with features approximately 1  $\mu\text{m}$  in diameter present on the polymer surface. Because the polymer backbone is oxidized with associated perchlorate anions and the bulky spiropyran is still present, this film would be expected to show the most expanded morphology. The film oxidized state at 0.5 V (Figure 2.8 (b)) showed a similar morphology with fewer of the island-particles present on the surface. This would be consistent with the loss of some of the spiropyran groups following the initial film preparation. Significantly, further oxidation of the polymer to 0.85 V (Figure 2.8 (c)) gave a film with an entirely different morphology with a distinctive webbed and close-packed structure, consistent with the formation of at least partially oxidized planar merocyanine.

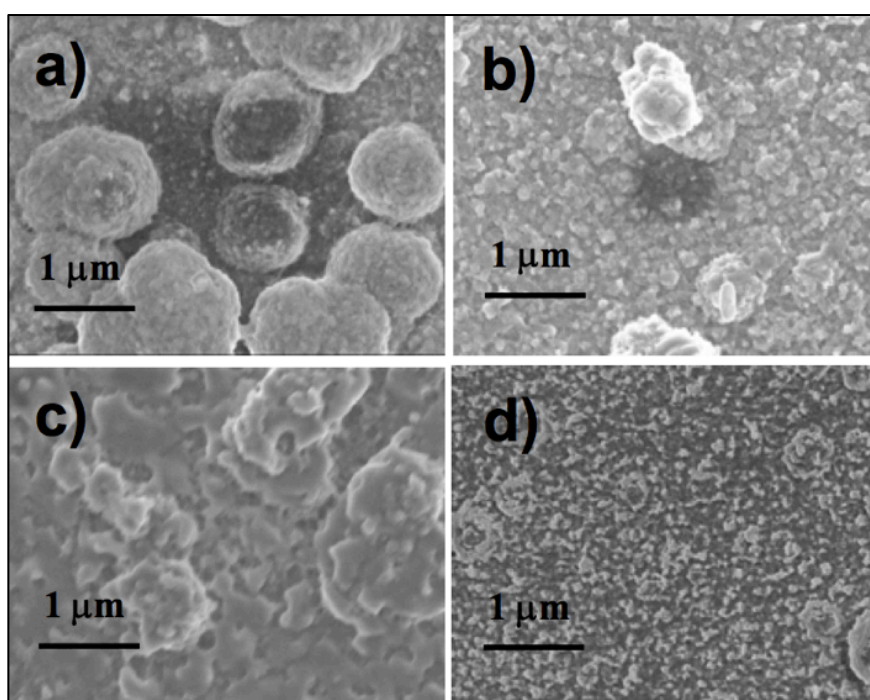


**Figure 2.8:** SEM images of **p-BSP2** after a constant potential deposition of 0.8 V (a), oxidation at 0.5 V (b), oxidation at 0.85 V (c), and reduction at -0.4 V (d).

AFM images confirm the major change in polymer structure that occurs when the **p-BSP2** film is oxidized (Appendix A, Figure A5), because the calculated surface roughness of the reduced (root mean squared, rms = 181 (8.4 nm) and oxidized (127 (5.1 nm) **p-BSP2** suggest a more porous surface for the reduced polymer, as would be expected for the more bulky **BSP** substituent.

To measure the conductivity, a freestanding film of **p-BSP2** was obtained after chronoamperometric deposition on ITO-coated glass at a constant potential of 0.8 V for 1 h and removal from the electrode. A conductivity of  $0.4 \text{ S cm}^{-1}$  was obtained, the same order of magnitude as that reported by Gallazzi *et. al.* for an analogous poly(alkoxyterthiophene) substituted with the somewhat smaller electron-withdrawing dicyanoethenyl group.<sup>36</sup>

## 2.4 Conclusion

The integration of the photochromic properties of spiropyrans with the electrical and optical properties of polythiophenes presents exciting opportunities for a variety of applications. A terthiophene monomer modified with a nitrospiropyran substituent was prepared using electropolymerization for the first time. The resulting polymer, **p-BSP2**, displayed a number of different coloured states on electrochemical redox cycling with associated complex electrochemistry. To understand this, we undertook a detailed electrochemical study of the nitrospiropyran precursor **BSP-1** because little had been reported in the extensive spiropyran literature. We have shown that **BSP-1** initially undergoes irreversible electro-oxidative ring-opening to give at least two oxidized merocyanine isomers, which can further undergo reversible redox processes. This behaviour is reflected in the electrochemical processes observed for **p-BSP2**. The polymer is initially formed with the spiropyran intact and can undergo typical polythiophene redox cycling at potentials below 0.6 V. However, oxidation of the polymer film above 0.8 V leads to spiropyran oxidation and irreversible isomerisation to the oxidized merocyanine. A detailed spectroelectrochemical study of the resulting reduction and further redox cycling revealed that the electrochemical and physical properties of the polymer are then dominated by the presence of the merocyanine and its ability to form  $\pi$ -dimers or oligomers and  $\pi$ -radical cation dimers.

The photochemical behaviour of **p-BSP2** is dramatically influenced by the electrochemistry. Typical spiropyran to merocyanine isomerization within the polymer occurs only if the polymer film has been exposed to oxidation potentials, which do not oxidise the spiropyran moiety to the merocyanine (below 0.8 V). Once the merocyanine is oxidized, the photochemical behaviour of the film is limited. Therefore, the redox properties of **p-BSP2** can be used to control its photochemical behaviour. As expected, given the large conformational differences between spiropyrans and merocyanines, there are significant morphological changes in the polymer film, although the polymer

conductivity does not appear to be dramatically affected and is similar to that of previous polythiophenes.

This unique multi-chromophoric and multiswitchable polymer system provides an exciting platform for the development of future materials that can exploit the other physical and chemical properties of spiropyrans and merocyanines such as variation in hydrophobicity, ion and molecular complexation, and conformational effect leading to polymer actuation.

### Acknowledgments

Financial support from the Australian Research Council and funding from Science Foundation Ireland under award 07/CE/I1147 "CLARITY: Centre for Sensor Web Technologies" is gratefully acknowledged.

## 2.5 References

1. W. R. Browne and B. L. Feringa, in *Annual Review of Physical Chemistry*, Editon edn., 2009, vol. 60, pp. 407-428.
2. G. Berkovic, V. Krongauz and V. Weiss, *Chemical Reviews*, 2000, **100**, 1741-1753.
3. H. Dürr, L. H. Bouas, *Photochromism-molecules and systems*, Elsevier, 2003.
4. E. Fischer and Y. Hirshberg, *Journal of the Chemical Society*, 1952, 4522-4524.
5. M. J. Preigh, M. T. Stauffer, F. T. Lin and S. G. Weber, *Journal of the Chemical Society-Faraday Transactions*, 1996, **92**, 3991-3996.
6. S. Scarmagnani, Z. Walsh, C. Slater, N. Alhashimy, B. Paull, M. Macka and D. Diamond, *Journal of Materials Chemistry*, 2008, **18**, 5063-5071.
7. I. Willner and B. Willner, *Bioelectrochemistry and Bioenergetics*, 1997, **42**, 43-57.
8. I. Willner and B. Willner, *Journal of Materials Chemistry*, 1998, **8**, 2543-2556.
9. N. Katsonis, M. Lubomska, M. M. Pollard, B. L. Feringa and P. Rudolf, *Progress in Surface Science*, 2007, **82**, 407-434.
10. T. Seki and K. Ichimura, *Macromolecules*, 1990, **23**, 31-66.
11. J. Lee, T. Kwon, E. Kim, *Tetrahedron Letters*, **2006**, 48, 249-254.
12. S. Stitzel, R. Byrne and D. Diamond, *Journal of Materials Science*, 2006, **41**, 5841-5844.
13. P. Wesenhagen, J. Areephong, T. F. Landaluce, N. Heureux, N. Katsonis, J. Hjelm, P. Rudolf, W. R. Browne and B. L. Feringa, *Langmuir*, 2008, **24**, 6334-6342.
14. T. Hugel, N. B. Holland, A. Cattani, L. Moroder, M. Seitz and H. E. Gaub, *Science*, 2002, **296**, 1103-1106.
15. B. Ustamehmetoglu, *Polymers for Advanced Technologies*, 1999, **10**, 164-168.
16. J. Roncali, *Chemical Reviews*, 1992, **92**, 711-738.
17. Y. Li and Y. Zou, *Advanced Materials*, 2008, **20**, 2952-2958.
18. S. H. Ahn, M. Z. Czae, E. R. Kim, H. Lee, S. H. Han, J. Noh and M. Hara, *Macromolecules*, 2001, **34**, 2522-2527.
19. J. Areephong, T. Kudernac, J. de Jong, G. Carroll, D. Pantorott, J. Hjelm, W. Browne and B. Feringa, *Journal of the American Chemical Society*, 2008, **130**, 12850-12851.
20. I. S. Park, Y.-S. Jung, K.-J. Lee and J.-M. Kim, *Chemical Communications*, 2010,

- 46, 2859-2861.
21. M. C. Gallazzi, L. Castellani, R. A. Marin and G. Zerbi, *Journal of Polymer Science Part a-Polymer Chemistry*, 1993, **31**, 3339-3349.
  22. D. K. Grant, K. W. Jolley, D. L. Officer, K. C. Gordon and T. M. Clarke, *Organic & Biomolecular Chemistry*, 2005, **3**, 2008-2015.
  23. K. Wagner, L. L. Crowe, P. Wagner, S. Gambhir, A. C. Partridge, J. C. Earles, T. M. Clarke, K. C. Gordon and D. L. Officer, *Macromolecules*, 2010, **43**, 3817-3827.
  24. S. Gambhir, K. Wagner and D. L. Officer, *Synthetic Metals*, 2005, **154**, 117-120.
  25. C. P. McCoy, L. Donnelly, D. S. Jones and S. P. Gorman, *Tetrahedron Letters*, 2007, **48**, 657-661.
  26. M. Campredon, G. Giusti, R. Guglielmetti, A. Samat, G. Gronchi, A. Alberti and M. Benaglia, *Journal of the Chemical Society-Perkin Transactions 2*, 1993, 2089-2094.
  27. J. F. Zhi, R. Baba, K. Hashimoto and A. Fujishima, *Journal of Photochemistry and Photobiology a-Chemistry*, 1995, **92**, 91-97.
  28. R. T. F. Jukes, B. Bozic, F. Hartl, P. Belser and L. De Cola, *Inorganic Chemistry*, 2006, **45**, 8326-8341.
  29. M. J. Preigh, M. T. Stauffer, F.-T. Lin and S. G. Weber, *Journal of the Chemical Society, Faraday Transactions*, 1996, **92**, 3991.
  30. R. Heiligmanrim, Y. Hirshberg and E. Fischer, *Journal of Physical Chemistry*, 1962, **66**, 2465-&.
  31. J. Hobley, V. Malatesta, W. Giroladini and W. Stringo, *Physical Chemistry Chemical Physics*, 2000, **2**, 53-56.
  32. J. Roncali, F. Garnier, M. Lemaire and R. Garreau, *Synthetic Metals*, 1986, **15**, 323-331.
  33. K. E. BrancatoBuentello, S. J. Kang and W. R. Scheidt, *Journal of the American Chemical Society*, 1997, **119**, 2839-2846.
  34. J. vanHaare, L. Groenendaal, E. E. Havinga, E. W. Meijer and R. A. J. Janssen, *Synthetic Metals*, 1997, **85**, 1091-1092.
  35. G. G. Wallace, P. R. Teasdale, G. M. Spinks and L. A. Kane-Maguire, *Conductive electroactive polymers: intelligent polymer systems*, CRC press, 2008.
  36. M. C. Gallazzi, F. Toscano, D. Paganuzzi, C. Bertarelli, A. Farina and G. Zotti, *Macromolecular Chemistry and Physics*, 2001, **202**, 2074-2085.



# CHAPTER 3

## Physico-Chemical Study of Spiropyran-Terthiophene Derivatives: Photochemistry and Thermodynamics



**Publication status: PUBLISHED**

**M. Zanoni**, S. Coleman, K.J. Fraser, R. Byrne, K. Wagner, S. Gambhir, D.L. Officer, G.G. Wallace and D. Diamond “Physicochemical Study of Spiropyran-Terthiophene Derivatives: Photochemistry and Thermodynamics”, *Physical Chemistry Chemical Physics*, 14, 9112-9120 (2012). DOI: 10.1039/c2cp41137g.

*For the supplementary information section see Appendix B*

## Abstract

The photochemistry and thermodynamics of two terthiophene (**TTh**) derivatives bearing benzospiropyran (**BSP**) moieties, 1-(3,3''-dimethylindoline-6'-nitrobenzospiropyranyl)-2-ethyl 4,4''-didecyloxy-2,2':5',2''-terthiophene-3'-acetate (**BSP-2**) and 1-(3,3''-dimethylindoline-6'-nitrobenzospiropyranyl)-2-ethyl 4,4''-didecyloxy-2,2':5',2''-terthiophene-3'-carboxylate (**BSP-3**), differing only by a single methylene spacer unit, have been studied. The kinetics of photogeneration of the equivalent merocyanine (**MC**) isomers (**MC-2** and **MC-3**, respectively), the isomerisation properties of **MC-2** and **MC-3**, and the thermodynamic parameters have been studied in acetonitrile, and compared to the parent, non-**TTh**-functionalised, benzospiropyran derivative, **BSP-1**. Despite the close structural similarity of **BSP-2** and **BSP-3**, their physicochemical properties were found to differ significantly; examples include activation energies ( $E_{a(\text{MC-2})} = 75.05 \text{ kJ mol}^{-1}$ ,  $E_{a(\text{MC-3})} = 100.39 \text{ kJ mol}^{-1}$ ) and entropies of activation ( $\Delta S_{(\text{MC-2})}^{\ddagger} = -43.38 \text{ J K}^{-1} \text{ mol}^{-1}$ ,  $\Delta S_{(\text{MC-3})}^{\ddagger} = 37.78 \text{ J K}^{-1} \text{ mol}^{-1}$ ) for the thermal relaxation from **MC** to **BSP**, with the **MC-3** value much closer to the unmodified **MC-1** value ( $46.48 \text{ J K}^{-1} \text{ mol}^{-1}$ ) for this latter quantity. The thermal relaxation kinetics and solvatochromic behaviour of the derivatives in a range of solvents of differing polarity (ethanol, dichloromethane, acetone, toluene and diethyl ether) are also presented. Differences in the estimated values of these thermodynamic and kinetic parameters are discussed with reference to the molecular structure of the derivatives.

### 3.1 Introduction

Benzospiropyran (**BSP**) is member of a family of photo/thermochromic molecules that have been widely studied due to their ability to be switched reversibly under various external stimuli between two molecular states that exhibit dramatically different properties.<sup>1-22</sup> This behaviour has attracted great interest in terms of possible applications such as optical memory,<sup>12</sup> biomaterials for targeted therapeutic agents,<sup>8</sup> components for ophthalmic lenses,<sup>9</sup> molecular functionalization of micro channels and as optical probes for the analysis of nano-structures in ionic liquids (**ILs**).<sup>14</sup>

Photochromism is a phenomenon that occurs when electromagnetic radiation is absorbed by a molecule that undergoes a reversible rearrangement between two forms, such as 1-(2-hydroxyethyl)-3,3-dimethylindoline-6'-nitrobenzospiropyran (**BSP-1**, Figure 3.1)<sup>1-13</sup> and its equivalent merocyanine form (**MC-1**), with dramatic accompanying changes in the absorption spectra in the visible region.<sup>13</sup>

Benzospiropyran is a molecule that exists as two heterocyclic functional units connected by a tetrahedral  $sp^3$  hybridised carbon atom. This atom co-joins two orthogonal planes (Figure 1.12) comprising an indoline subunit and a benzopyran subunit, the common component for all the spiropyran moieties.

Photo-induced isomerisation processes are well known in the literature.<sup>6,7,18-21</sup> In spiropyrans, heterocyclic ring cleavage occurs at the  $C_{\text{spiro}}\text{-O}$  bond when exposed to UV light<sup>6, 13</sup>, leading to the formation of the merocyanine (**MC**) species that can be detected via a striking colour change due to the strong absorbance of the **MC** isomer in the visible region (Figure 3.1). Upon irradiation with white light, the system reverts back to the original **BSP** form. The **MC** isomer absorbance is sensitive to its immediate molecular environment, leading to solvent dependant colour changes, and the solvent can also mediate the equilibrium between the isomers.

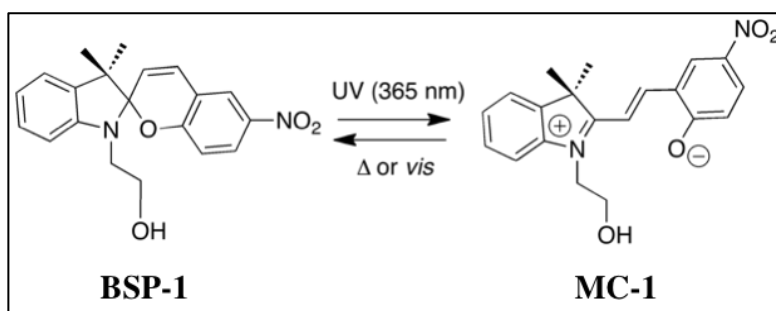


**Fig. 3.1** Molecular structure and isomerisation of 1-(2-hydroxyethyl)-3,3-dimethylindoline-6'-nitrobenzospiropyran (**BSP-1**) spiropyran.

The solvatochromism of various benzospiropyran derivatives has been reported previously including nitro- and methoxy-substituted spiro-moieties.<sup>16, 17, 22</sup> Recently, the well-known photo-, thermo- and solvatochromic properties of benzospiropyran (**BSP**) and spirooxazine derivatives have been used by our group to provide new insights into the nanostructure of ILs through in-situ mediation of their switching behaviour.<sup>16, 17</sup> Furthermore the presence of the phenolate anion in the **MC** isomer provides a weak binding capacity for certain metal ions (d- and f- elements), and the resulting complexes generate new absorbance bands in the visible region, which are directly influenced by the type of metal ion present.<sup>18-21</sup>

Polythiophenes (**PThs**) are a class of organic polymeric semiconductors with interesting conductivity, electrochromism and electroluminescence<sup>23</sup> properties, which have been explored for applications such as electrochemical sensors and energy harvesting devices.<sup>24-27</sup> From a materials chemistry perspective, they are particularly attractive due to their high chemical stability and relative ease of isolation.<sup>25</sup> Other interesting **pTh** properties previously reported in the literature include thermochromism, ionochromism, photochromism and bio-chromism.<sup>24-37</sup> Chromic variations are generated by conformational changes or folding of the polymer chains, with consequent dramatic variation in the conjugation length of the whole system, which can be monitored using spectroscopy. Substituents connected to the three-aromatic rings backbone can have a considerable effect on the overall conjugation of the system, influencing the properties and the distribution of the  $\pi$ -electrons in the structure.

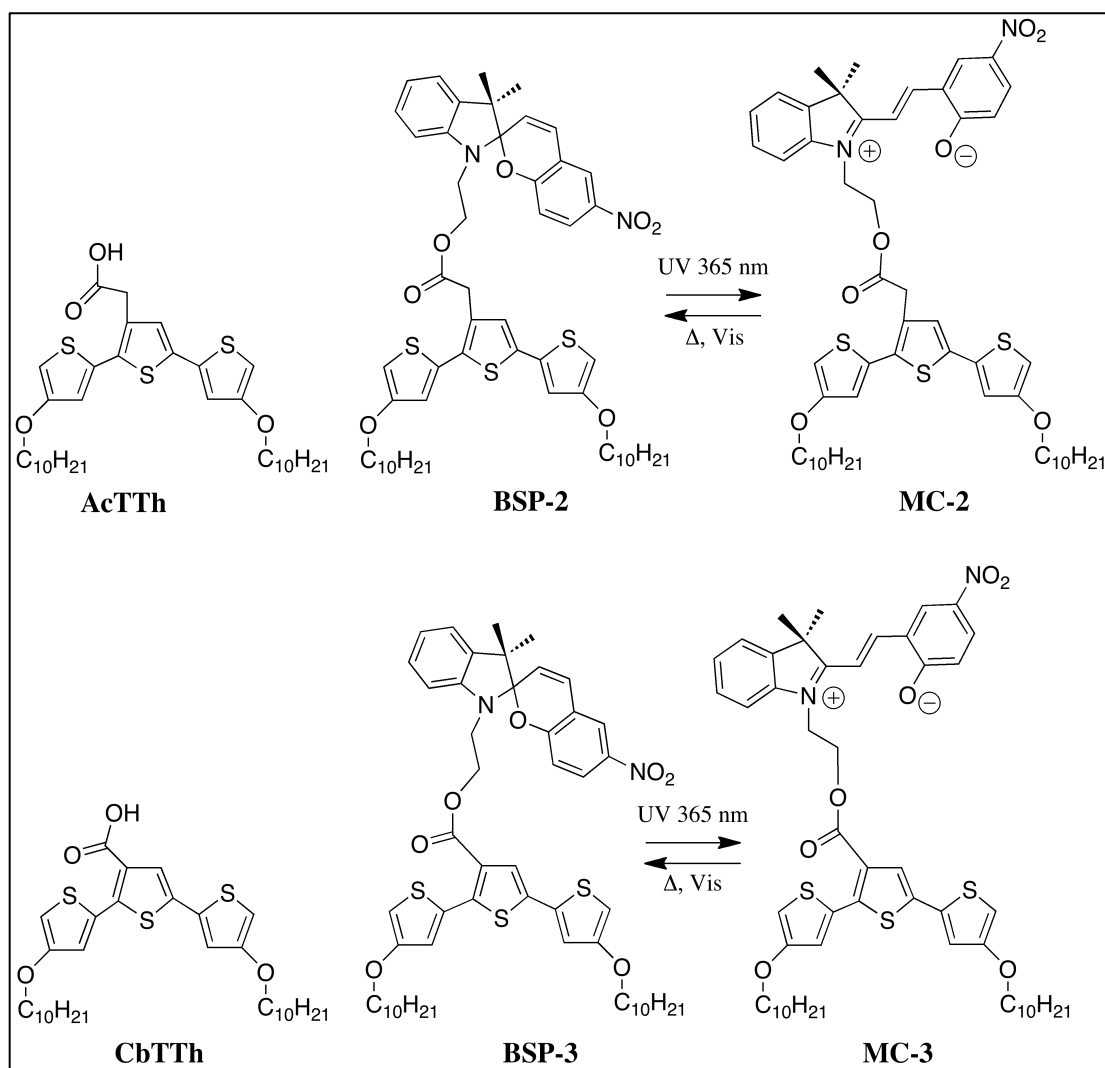


**Fig. 3.2** Structures of the **TTh** and **TTh-BSP** derivatives studied: Methyl 4,4''-didecyloxy-2,2':5',2''-terthiophene-3'-acetate (**AcTTh**); 4,4''-didecyloxy-2,2':5',2''-terthiophene-3'-carboxylic acid (**cbTTh**); 1-(3,3''-dimethylindoline-6'-nitrobenzospiropyranyl)-2-ethyl 4,4''-didecyloxy-2,2':5',2''-terthiophene-3'-acetate (**BSP-2**) and 1-(3,3''-dimethylindoline-6'-nitrobenzospiropyranyl)-2-ethyl 4,4''-didecyloxy-2,2':5',2''-terthiophene-3'-carboxylate (**BSP-3**).

As part of our ongoing interest in functionalised **PThs**, we recently reported the first synthesis of a **BSP**-functionalised poly(terthiophene) and undertook a detailed study of its complex electrochemical and photochemical properties.<sup>38</sup> The **BSP** was attached to the terthiophene monomer (**acTTh**, Figure 3.2) by an acetate linkage (**BSP-2**, Figure 3.2). Given the multiple effects of the spiropyran on the electrochemical behaviour of the poly(terthiophene), we were interested in how these might vary depending on the distance of the spiropyran from the polymer backbone. Therefore, we synthesised the **BSP**-terthiophene monomer in which the ester linkage was directly attached to the terthiophene moiety (**BSP-3**, Figure 3.2), differing from **BSP-2** only by one carbon

atom. Prior to studying its electrochemical polymerisation and resulting polymer properties, we deemed it important to determine the photochemical properties of **BSP-3** and compare them to **BSP-1** and **BSP-2**.

Therefore, in this work, the photochemical behaviour of the two **BSP**-functionalised terthiophene monomers, 1-(3,3''-dimethylindoline-6'-nitrobenzospiropyranyl)-2-ethyl 4,4''-didecyloxy-2,2':5',2''-terthiophene-3'-acetate (**BSP-2**) and 1-(3,3''-dimethylindoline-6'-nitrobenzospiropyranyl)-2-ethyl 4,4''-didecyloxy-2,2':5',2''-terthiophene-3'-carboxylate (**BSP-3**) is reported, along with a detailed study of the thermodynamics and kinetics of their photo-isomerization. Their photoswitchable behaviour is reported in comparison to the original parent **BSP-1**, as this is important for some innovative applications, such as photo-actuated valves incorporated into micro-fluidic manifolds<sup>11</sup> or light-modulated surfaces for selective cell adhesion/detachment.<sup>39</sup>

## 3.2 Experimental

### 3.2.1 Materials

1-(2-Hydroxyethyl)-3,3-dimethylindolino-6'-nitrobenzopyrlospiran (**BSP-1**) was purchased from TCI chemicals, and was used without further purification. Ethyl (3,3''-dimethylindoline-6'-nitrobenzospiropyranyl)-4,4''-didecyloxy-2,2':5',2''-terthiophene-3'-acetate (**BSP-2**) was synthesised as described previously.<sup>38</sup>

Ethyl (3,3''-dimethylindoline-6'-nitrobenzospiropyranyl)-4,4''-didecyloxy-2,2':5',2''-terthiophene-3'-carboxylate (**BSP-3**) was synthesized as follows: 4,4''-Didecyloxy-2,2':5',2''-terthiophene-3'-carboxylic acid (**cbTTh**)<sup>40</sup> (0.083 g, 0.138 mmol), dicyclohexylcarbodiimide (DCC) (0.03 g, 0.143 mmol) and 4-dimethylaminopyridine (0.0013 g, 0.011 mmol) were dissolved in DCM (12 ml) at 0 °C. 1-(2-Hydroxyethyl)-3,3-dimethylindoline-6'-nitrobenzospiropyran **BSP-1** (0.04 g, 0.11 mmol) in DCM (10 ml) was added dropwise over 30 min to the stirring solution. After **BSP-1** was completely added, the reaction mixture was allowed to reach 20 °C. After a further 90 min, 50% of the DCM was removed under reduced pressure, cold ether (10 ml) was added to precipitate the urea salt of DCC. This precipitate was removed by filtration and the filtrate was reduced to give a brown oil, which was purified on a silica column,

eluting with DCM. The resulting product was a yellowish-brown oil, which solidified on standing (0.081 g, 77%). After purification via column chromatography, the **BSP-3** was stored in the dark in a sealed glass vial under nitrogen. Characterisation data are available in Appendix B.

The solvents used for the photo- and thermo-chromic analyses (acetonitrile (ACN), ethanol (EtOH), toluene (Tol), acetone (Acet), dichloromethane (DCM) and diethyl ether (Et<sub>2</sub>O)) were Sigma Aldrich HPLC grade, and used without further purification.

### 3.2.2 Photochemical Methods

To obtain the rate constants of the ring opening process for **BSP-1**, **BSP-2** and **BSP-3** to their **MC-1**, **MC-2** and **MC-3** forms, the derivatives were continuously monitored during UV irradiation at 375 nm. The samples were kept in the dark for 24 hrs to ensure equilibrium in the solvent was reached. Diluted solutions (10<sup>-4</sup> M) of **BSP-1**, **BSP-2** and **BSP-3** were exposed to UV light and the spectrum of each was taken at intervals from t = 1 minute to t = 45 minutes.

A single exponential model (equation (3.1)) was used to determine the ring opening rate constants for **BSP-1**, **BSP-2** and **BSP-3**.

$$y = a \times (1 - e^{-kt}) + b \quad (3.1)$$

where **y** is the absorbance at  $\lambda_{\text{max}}$  (assumed to be proportional to the concentration of the merocyanine isomer), **a** is a scaling factor, **k** is the first order rate constant (s<sup>-1</sup>), **b** is the baseline offset and **t** is time (s).

Absorption spectra were recorded using a Perkin Elmer Lambda 900 UV-Vis/NIR spectrometer equipped with a thermostatted temperature control system (PTP-1 Peltier System). Photo-conversion of **BSP** to **MC** was achieved using an in-house fabricated UV light source consisting of three UV LEDs (Roithner LaserTechnik GmbH, emission  $\lambda_{\text{max}} = 375$  nm). The LEDs were powered from a 3.75 V current source, which provided an optical power output of 6 mW/cm<sup>2</sup> from each LED. The white light radiation was provided via a DDL 150 W source obtained from Polytec GmbH Waldbronn.

To determine the thermodynamic parameters of the samples and obtain an estimation of the transition state equilibrium of activation ( $K^\ddagger$ ) for the **MC**→**BSP** equilibrium, standard solutions of **BSP-1**, **BSP-2** and **BSP-3** were prepared in concentrations up to

$10^{-4}$  M in acetonitrile. The solutions were stored in volumetric flasks in the dark under nitrogen before the absorbance measurements were acquired. Thermal relaxation analysis of the thermodynamically favoured reversion of **MC** to **BSP** was measured at 5 °C increments from 283 to 308 K over a period of 1 hour. Samples were irradiated in the dark with the UV-LED system in a sealed quartz cuvette at room temperature for 3 minutes prior to acquisition of the spectra. The study of the **BSP**  $\rightleftharpoons$  **MC** equilibrium was performed using the LED system in the spectrometer chamber in order to minimise any influence of external light. The **MC**  $\rightarrow$  **BSP** thermal relaxation typically follows first order kinetics in molecular solvents and the rate is not sensitive to oxygen, but is strongly medium dependent.<sup>18-21</sup>

First-order rate constants for the thermal relaxation were determined in this work using Microsoft Excel Solver, by fitting the absorbance data to equation (3.2), where  $y$  is the absorbance value at the  $\lambda_{\max}$ ,  $a$  is the absorbance at  $t = 0$ ,  $k$  is the rate constant,  $t$  is time and  $b$  is a baseline offset, as for equation (3.1).<sup>41</sup>

$$y = ae^{-kt} + b \quad (3.2)$$

The Arrhenius equation (3.3) was used to plot the linear temperature dependence of the rate constant for **MC**  $\rightarrow$  **BSP** thermal relaxation and find the activation energy ( $E_a$ ) and the pre-exponential factor  $A$ .

$$\ln k = E_a / RT + \ln A \quad (3.3)$$

where  $k$  = rate constant ( $s^{-1}$ ),  $E_a$  = Activation energy ( $\text{kJ mol}^{-1}$ ),  $R$  = gas constant ( $\text{J mol}^{-1} \text{K}^{-1}$ ),  $T$  = temperature (K) and  $A$  = pre exponential factor ( $s^{-1}$ )

Following the generalised **BSP**  $\rightleftharpoons$  **MC** system (Figure 3.1), the Eyring equation (3.4) was used to determine the thermodynamic properties at the transition state equilibrium of activation ( $K^\ddagger$ ), entropy of activation ( $\Delta S^\ddagger$ ), and the enthalpy of activation ( $\Delta H^\ddagger$ ). A derivative of this equation, equation (3.5), can be used to derive the equilibrium of activation ( $K^\ddagger$ ).<sup>16, 17, 22</sup>

$$\ln(k / T) = -\Delta H^\ddagger / RT + \ln(k / h) + \Delta S^\ddagger / R \quad (3.4)$$

$$k = (k_B T / h) K^\ddagger \quad (3.5)$$

where  $\mathbf{k}$  = rate constant of the forward reaction,  $\mathbf{T}$  = temperature (K),  $\Delta\mathbf{H}^\ddagger$  = enthalpy of activation,  $\Delta\mathbf{S}^\ddagger$  = entropy of activation,  $\mathbf{R}$  = gas constant,  $\mathbf{k}_B$  = Boltzmann constant and  $\mathbf{h}$  = Planck's constant.

Thermodynamic activation properties such as  $\Delta\mathbf{S}^\ddagger$ ,  $\Delta\mathbf{H}^\ddagger$  and  $\mathbf{K}^\ddagger$  for each **MC** derivative were calculated using the Eyring equation. Equation (3.6) was used to calculate the Gibbs free energy of activation ( $\Delta\mathbf{G}^\ddagger$ ).

$$\Delta\mathbf{G}^\ddagger = \Delta\mathbf{H}^\ddagger - \mathbf{T}\Delta\mathbf{S}^\ddagger \quad (3.6)$$

where  $\Delta\mathbf{G}^\ddagger$  = Gibbs free energy of activation ( $\text{kJ mol}^{-1}$ ),  $\Delta\mathbf{H}^\ddagger$  = enthalpy of transition state ( $\text{kJ mol}^{-1}$ ),  $\mathbf{T}$  = temperature (K) and  $\Delta\mathbf{S}^\ddagger$  = entropy of the transition state ( $\text{J K}^{-1} \text{mol}^{-1}$ ).

The solvatochromic study was performed at room temperature in 6 different solvent systems (ethanol, toluene, acetone, acetonitrile, diethyl ether and dichloromethane). The solutions (all  $10^{-4}$  M) were sealed and stored under nitrogen overnight before the analysis was performed. Spectra were taken under controlled temperature conditions using the LED system described above to illuminate the samples.

Fluorescence (emission) spectra were recorded with a Perkin Elmer Luminescence Spectrometer LS 50B. Solutions diluted up to  $10^{-5}$  M in acetonitrile of the two freestanding **TTh** molecules, **BSP-1**, **BSP-2** and **BSP-3** were made. Excitation wavelengths were set as follows: 358 nm (**acTTh**), 362 nm (**cbTTh**), 360 nm (**BSP-2** and **BSP-3**). The solutions were stored in sealed volumetric flasks for 24 hrs under nitrogen in the dark. Photo-isomerisation to the relatives **MC-1**, **MC-2** and **MC-3** was carried out with *in situ* LED illumination ( $\lambda_{\text{max}}$  375 nm) for 180 seconds.

## 3.3 Results and Discussion

### 3.3.1 Material synthesis

The synthesis of **BSP-3** in 77% yield by a base-catalyzed substitution of **BSP-1** into **cbTTh** was straightforward and its spectral data (Appendix B) was consistent with this structure. As expected, its  $^1\text{H}$  NMR spectrum was nearly identical to that of **BSP-2** except for the absence of the methylene signal at  $\delta = 7.3$ .

### 3.3.2 Photochromic properties

It is well known that **MC** derivatives typically exhibit negative solvatochromism, meaning that the absorption maximum undergoes a hypsochromic (blue) shift as the solvent polarity increases, due to interactions between the solute and the solvent molecules that increase the energy gap between the **MC** ground and the excited states.<sup>18-21,42</sup> The focus of this study is whether the spectroscopic properties and switching behaviour of the **BSP** group is affected by attachment of the differing **TTh** sub-units.

UV-vis spectra of the two spiropyran-functionalised terthiophenes show two major absorbance bands with maxima at 352 nm and 362 nm for **BSP-2** and **BSP-3**, respectively (TTh absorbance, **BSP** contribution not shown<sup>38</sup>) and 568 nm and 572 nm for **MC-2** and **MC-3**, respectively (MC absorbance), as shown in Figure 3.3 (a) and (b). All solutions were kept in the dark for 24 hr at 293 K to establish thermodynamic equilibrium prior to UV illumination. In Figure 3.3 (a), the absorbance maximum at ca. 360 nm is greater for **MC-2** compared to **BSP-2**, whereas they are the same for **BSP-3** and **MC-3** (Figure 3.3 (b)). This suggests that there is a change in the electronic structure of **MC-2** relative to **BSP-2**, which does not occur with **BSP-3/MC-3**.

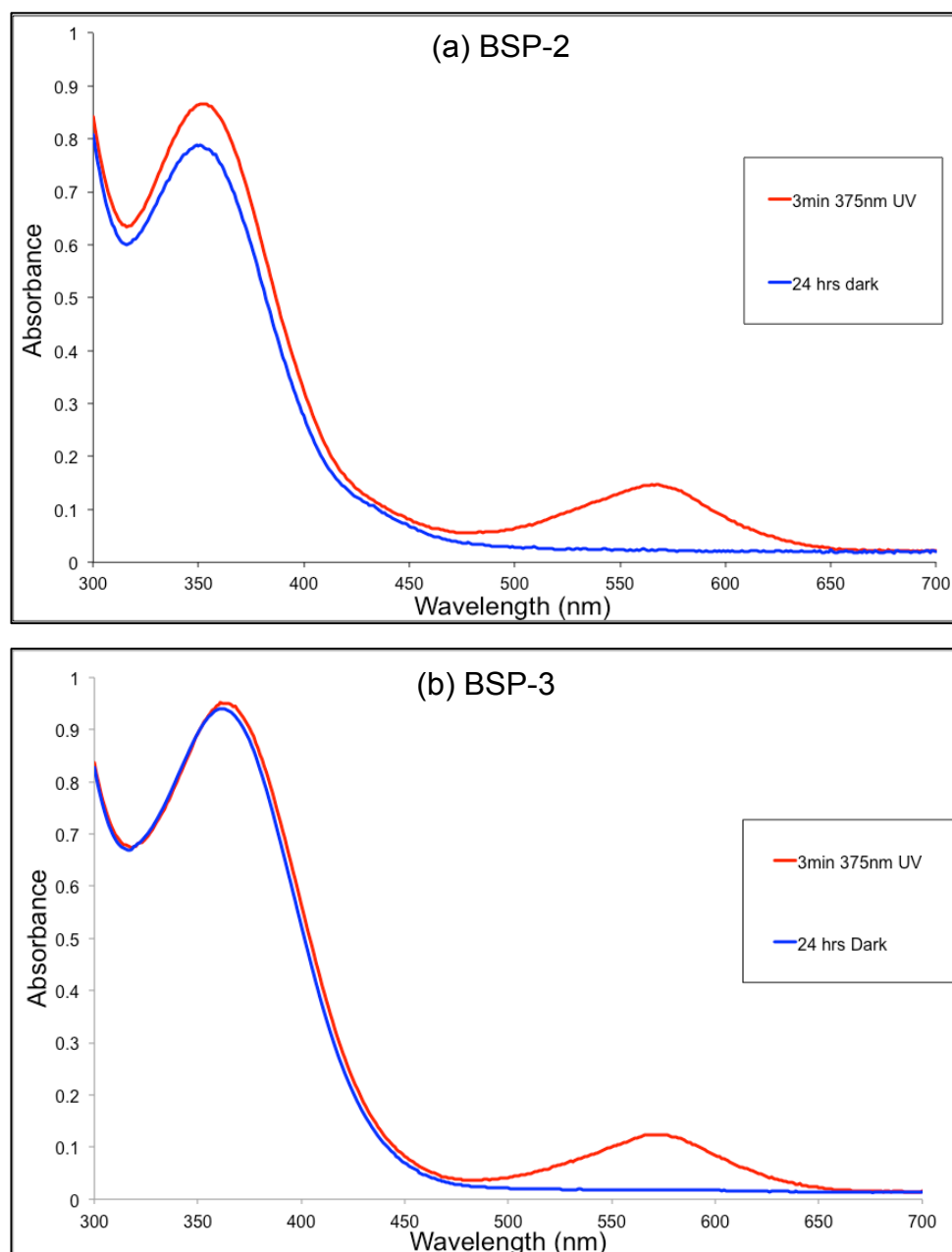


**Fig. 3.3** Baseline corrected UV-*vis* spectra before and after illumination of  $10^{-4}$  M solutions of (a) **BSP-2** with its **MC-2** absorption band at 568 nm and (b) **BSP-3** with its **MC-3** absorption band at 572 nm, using the 3 UV LED light source with  $\lambda_{\text{max}}$  emission = 375 nm; exposure time = 3 minutes.

### 3.3.3 Kinetics of photo-induced ring opening

Figures 3.4 (a) and (b) show the spectra used to obtain the  $\lambda_{\text{max}}$  values for substitution into the model (equation 3.1), while Figure 3.4 (c) gives the growth in absorbance over time (293 K) at the  $\lambda_{\text{max}}$  for **MC-1**, **MC-2** and **MC-3** (spectra for **MC-1** are given in Appendix B, Figure B1). The ring opening process analysed using equation (3.1) occurs  $\sim 1.5$  times faster for **BSP-2** compared to **BSP-3** ( $k_{\text{BSP-2}} = 4.45 \times 10^{-4} \text{ s}^{-1}$  versus  $k_{\text{BSP-3}} =$

$2.85 \times 10^{-4} \text{ s}^{-1}$ ). For **BSP-1** the equivalent rate constant was higher again ( $k_{\text{BSP-1}} = 1.09 \times 10^{-3} \text{ s}^{-1}$ ), giving an order in terms of speed of ring opening of **BSP-1** > **BSP-2** > **BSP-3**.

Extrapolation of the fitted curves using equation (3.1) allowed estimation of the steady state absorbance values for the derivatives in ACN. For the formation of **MC-2**, the model suggests the steady state (ca. 0.4 a.u.) is reached in about 150 minutes while for the formation of **MC-3** steady state absorbance is relatively constant at ca. 0.50 a.u. after about 200 min. This would be expected due to **BSP-2** having a faster ring-opening rate than **BSP-3** (Figure 3.4 (c)). Clearly, there is a significant difference in the steady state absorbance of **BSP-1** relative to **BSP-2** and **BSP-3**: the detected maximum absorbance for **BSP-1** after 45 minutes of exposure to the LED device was 1.84 a.u. at 563 nm *versus* 0.31 a.u. at 568 nm and 0.39 a.u. at 572 nm for **BSP-2** and **BSP-3**, respectively. This is most likely due to competing absorbance by the **TTh** moiety present in **BSP-2** and **BSP-3**, which reduces the availability of UV-photons for driving the ring-opening process.

Further indications supporting this statement might be found by comparing the ring opening of **BSP-2** and **BSP-3**. Extrapolation of the curves (Figure 3.4 (c)) suggests that the process reaches steady state after ca. 150 minutes for **MC-2** and ca. 200 minutes for **MC-3**. This model predicts final maximum absorbances for  $10^{-4}$  M acetonitrile solutions of ca. 0.39 a.u. for **MC-2**, and ca. 0.5 a.u. for **MC-3**, considerably smaller if compared to derivatives already reported in literature for **BSP-1** (1.8 a.u.)<sup>42</sup>. The calculated rate of ring opening in the described process, **BSP**→**MC**, is fastest for **BSP-2** compared to **BSP-3**, but both are slower than **BSP-1** by an order of magnitude.

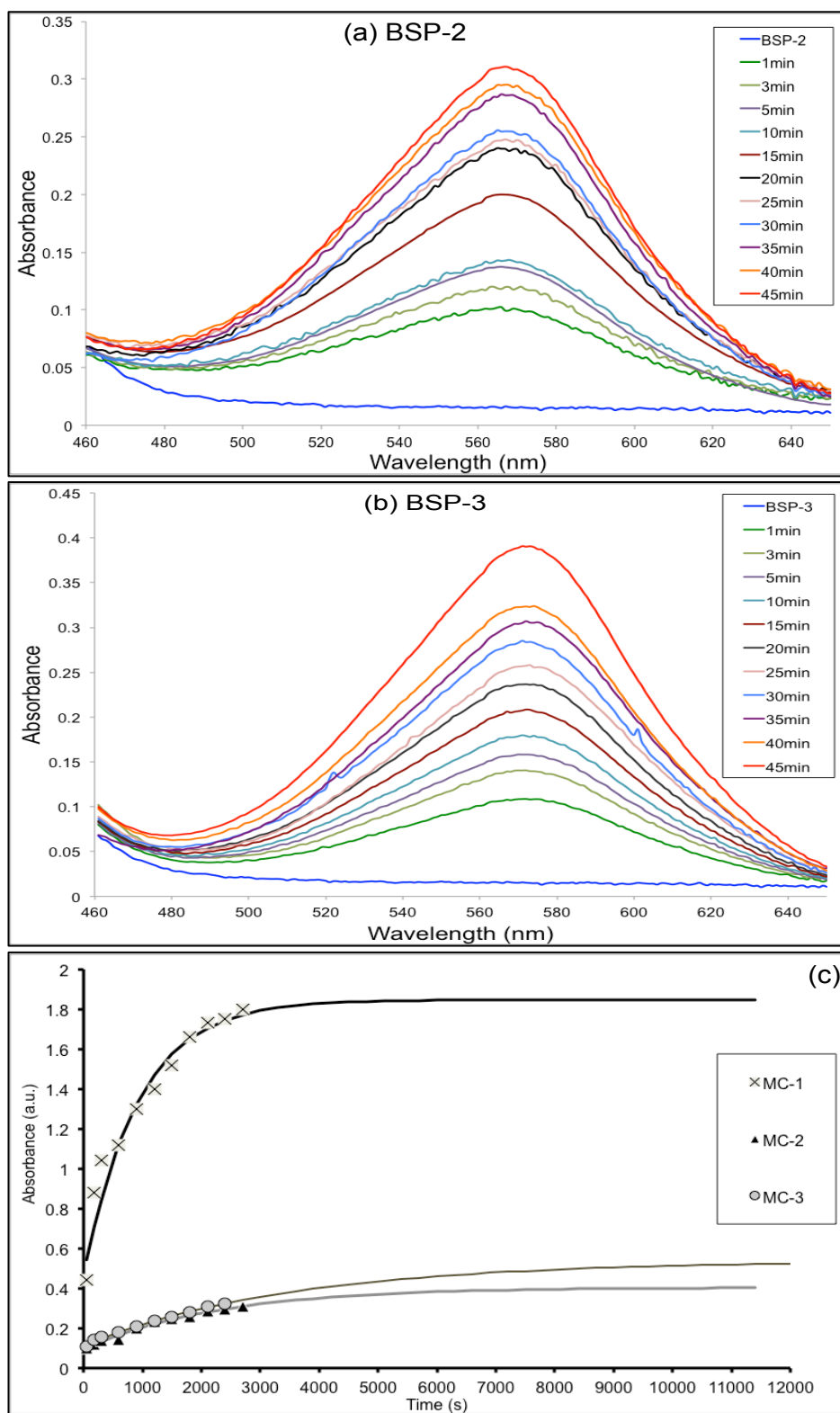


**Fig. 3.4** Exposure effects to 375 nm UV LEDs: (a) Baseline corrected conversion of **BSP-2** ( $10^{-4}$  M in ACN) to the isomer **MC-2**. (b) Baseline corrected conversion of spiropyran **BSP-3** ( $10^{-4}$  M in ACN) to the isomer **MC-3**. (c) Exponential curves extrapolated to steady state for generation of **MC** isomers versus time of UV irradiation with experimental results superimposed for **MC-2** and **MC-3**. Values were taken at  $\lambda_{\max}$  **MC-1** = 563 nm, **MC-2** = 568 nm, **MC-3** = 572 nm.

### 3.3.4 Kinetics and thermodynamics of ring closure

Table 3.1 shows the rate constants for ring closure (**MC**→**BSP**) over the temperature range 283 K – 308 K for **BSP-1**, **BSP-2** and **BSP-3**, and the ratios of the rate constants for each form. The **MC-3/MC-2** ratio steadily increases from 0.5 at 283 K to 1.4 at 308 K, meaning that at 283 K, **MC-2** relaxation is faster, whereas at 308 K, **MC-3** is faster. This pattern of behaviour is repeated for **MC-1** compared to **MC-2**, with the ratio = 0.42 at 283 K, increasing to 1.15 at 308 K. In contrast, the **MC-1/MC-3** ratio remains relatively constant over the temperature range studied, at about 0.8. These results suggest that the temperature affects ring closure kinetics in a similar manner for **BSP-3** compared to the parent **BSP-1** (increases around 3-fold), but a different type of dependency is observed with **BSP-2** (remains relatively constant). Furthermore, at 283 K **MC-2** reversion to **BSP-2** is the fastest for the three derivatives studied, whereas at 308 K, it is the slowest.

**Table 3.1** Rate constants **k** and their ratios for **MC**→**BSP** thermal relaxation for **MC-1**, **MC-2** and **MC-3** ( $10^{-4}$  M in ACN) over 283 – 308 K averaged from 3 replicates. Standard deviations reported in brackets.

	$\lambda_{\max}$ (nm)	<b>k</b> ( $10^{-3} \text{ s}^{-1}$ ) in ACN					
		283 K	288 K	293 K	298 K	303 K	308 K
<b>MC-1</b>	563	0.5 (±0.002)	1.06 (±0.001)	2.2 (±0.001)	4.5 (±0.0009)	9.04 (±0.0009)	18.3 (±0.0014)
<b>MC-2</b>	568	1.2 (±0.002)	2.6 (±0.002)	4.3 (±0.0009)	8.3 (±0.002)	11.7 (±0.008)	15.8 (±0.007)
<b>MC-3</b>	572	0.6 (±0.004)	1.5 (±0.002)	3.6 (±0.001)	5.9 (±0.001)	10.9 (±0.001)	21.6 (±0.002)
<b>Ratios MC 1/2</b>		0.42	0.40	0.50	0.52	0.77	1.15
<b>Ratios MC 1/3</b>		0.83	0.70	0.62	0.76	0.82	0.84
<b>Ratios MC 3/2</b>		0.50	0.57	0.69	0.71	0.93	1.36

Figure 3.5 shows the absorbance decrease at 568 nm for **MC-3** in ACN ( $10^{-4}$  M) at different temperatures (similar spectra for **MC-2** and **MC-1** are given Appendix B, Figures B2 and B3, respectively), from which the rate constants for ring closing (thermal relaxation) at each temperature were obtained by fitting a first order rate equation.

The resulting Arrhenius and Eyring plots are shown in Figure 3.6 (a) and (b). From the Arrhenius plots, the activation energy ( $E_a$ ) and the pre-exponential factor were derived (Table 3.2) for the thermal relaxation process. Using Eyring's transition state theory (Equation (3.4)), the activation thermodynamic parameters,  $\Delta S^\ddagger$  (entropy of activation),  $\Delta H^\ddagger$  (enthalpy of activation) and  $\Delta G^\ddagger$  (Gibbs free energy of activation), for the thermal relaxation process can be estimated, (Table 3.2, Figure 3.6 (b)).

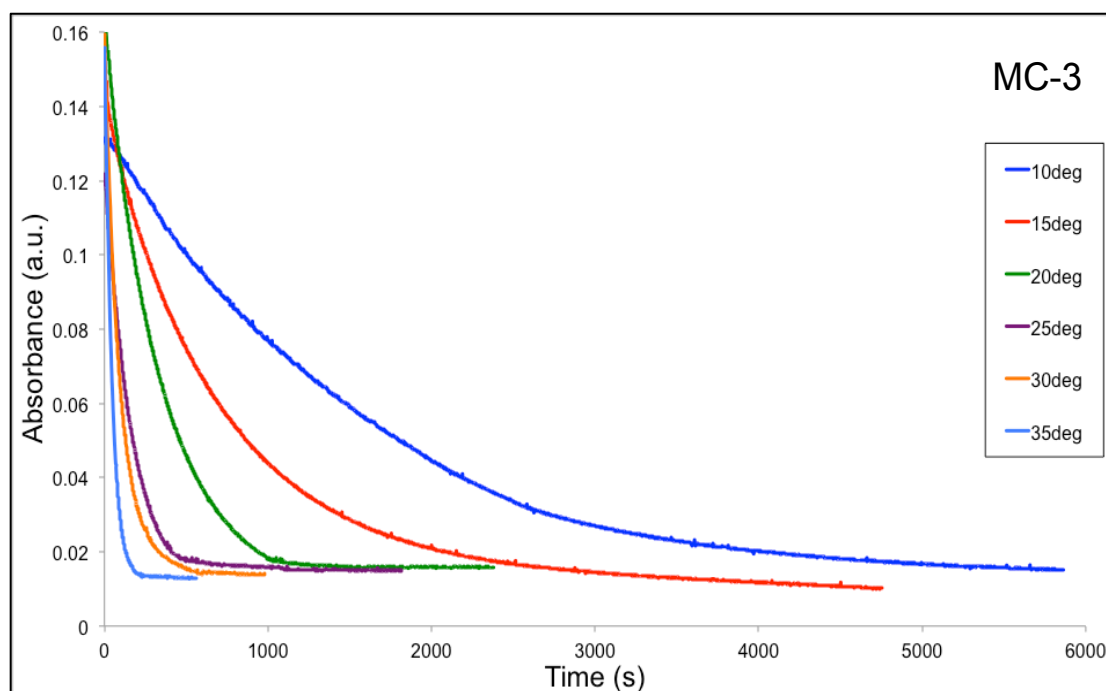


**Fig. 3.5** Thermal relaxation profiles for **MC-3** ( $10^{-4}$  M in ACN) over the temperature range 283-308 K. Prior to acquisition of the spectra, the solutions were irradiated with the 3 UV-LED device ( $\lambda_{\max} = 375$  nm) for 180 s.

The Arrhenius and Eyring plots both show that **MC-1** and **MC-3** exhibit strikingly similar behaviour, with almost identical slopes, and a slight offset, whereas **MC-2** has a lower slope in both cases, with a higher rate constant at lower temperatures that gradually converges and eventually crosses the other plots. This pattern of behaviour is reflected in the values of the rate constants (Table 3.1) discussed above, and in the thermodynamic and kinetic parameters extracted from the Arrhenius and Eyring Plots (Table 3.2). Taking each in turn, analysis by Arrhenius theory returns an activation energy for **MC-2** that is ca. 25% lower ( $75.05 \text{ kJ mol}^{-1}$  for **BSP-2** compared to  $100.39 \text{ kJ mol}^{-1}$  for **BSP-3**, and  $101.49 \text{ kJ mol}^{-1}$  for **BSP-1**), and a pre-exponential factor that is smaller by 4 orders of magnitude (ca.  $10^{11}$  vs.  $10^{15}$ ); Eyring theory returns similar Gibb's free energy of activation ( $85\text{-}87 \text{ kJ mol}^{-1}$ ) and equilibrium constants of activation

(ca.  $4\text{-}7 \times 10^{-16}$ ) in all three cases, but the entropy of activation ( $\Delta S^\ddagger$ ) is negative for **MC-2** ( $-43.38 \text{ JK}^{-1} \text{ mol}^{-1}$ ) and positive for **MC-3** ( $37.78 \text{ JK}^{-1} \text{ mol}^{-1}$ ) and **MC-1** ( $46.48 \text{ J K}^{-1} \text{ mol}^{-1}$ ). This quantity (for the process **MC**→**MC<sup>‡</sup>**) is related to the degree of order of the system as the **MC** molecules reorganise within the solvent system due to conformational changes as they pass into the transition state, **MC<sup>‡</sup>**. The negative value for **MC2**→**MC2<sup>‡</sup>** suggests that the formation of the transition state results in a more ordered system compared to the equivalent processes for **MC-1** and **MC-3**. Finally, the enthalpy of activation for **MC-2** is  $73.05 \text{ KJ mol}^{-1}$ , about 25% lower than the values for **MC-3** and **MC-1**. These data suggest that the difference in kinetics of ring closing observed for **MC-2** may arise primarily for entropic reasons, possibly due to differences in the conformation adopted by **MC-2/BSP-2** compared to the other derivatives.

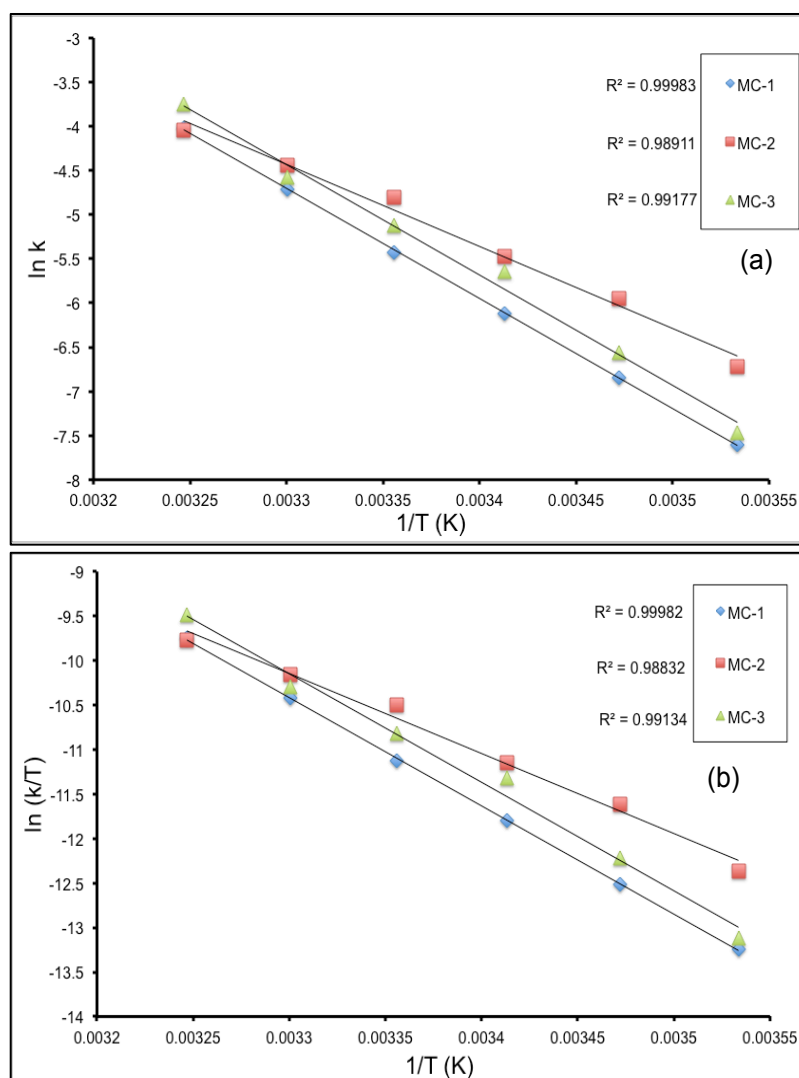


**Fig. 3.6** Comparative (a) Arrhenius plots and (b) Eyring plots for the thermal relaxation process **MC**→**BSP**. All solution concentrations were  $10^{-4}$  M in ACN. The values for **MC-2**, **MC-1** and **MC-3** were estimated from the thermal relaxation profiles in figures B2, B3 and Figure 3.5, respectively.

One explanation for these results is the additional methylene group in the **BSP-2** linker chain provides a degree of increased flexibility, and the two functional units (**BSP** and **TTh**) may be better able to align, for example, through intramolecular  $\pi$ - $\pi$  interactions. This would be particularly so when the planar merocyanine isomer is present, and this would favour the adoption of a more ordered configuration, which is consistent with the negative value of  $\Delta S^\ddagger$  for **BSP-2**.

This explanation is also supported by the difference in  $\Delta H^\ddagger$  between the three spiropyrans;  $\Delta H^\ddagger$  for **BSP-2** is  $\sim 20$  kJ mol<sup>-1</sup> lower than **BSP-1** and **BSP-3**. This suggests that the **MC-2** adopts a ground state conformation somewhat closer to the transition state leading to the spiropyran (**BSP-2**) than **MC-3** does on isomerising to **BSP-3**. Given that the formation of spiropyran from merocyanine typically requires rotation about the three bonds linking the indoline and phenolate components of the merocyanine, as discussed extensively by Wojtyk *et al.*<sup>43</sup>, a  $\pi$ - $\pi$  interaction between the terthiophene and the phenolate component of **MC-2** that brought the phenolate oxygen (in polar solvents) or quinone oxygen (in non-polar solvents) closer to the indoline nitrogen should lower  $\Delta H^\ddagger$ . Such an **MC** conformation could be determined by  $\pi$ - $\pi$  interactions during the ring opening of the spiropyran to form the merocyanine initially.

**Table 3.2** Thermodynamic parameters expressed as a mean of 3 replicates and standard deviation (standard deviations values are reported in brackets) for **MC-2**  $\rightleftharpoons$  **BSP-2** and **MC-3**  $\rightleftharpoons$  **BSP-3** thermal relaxation compared to the results obtained from a reference solution of **BSP-1** 10<sup>-4</sup> M in ACN.

MC	$\lambda_{\text{max}}$ (nm)	$k_{293}$ (10 <sup>-3</sup> s <sup>-1</sup> )	Arrhenius		Eyring			
			Ea (kJ mol <sup>-1</sup> )	A (s <sup>-1</sup> )	$\Delta S^\ddagger$ (JK <sup>-1</sup> mol <sup>-1</sup> )	$\Delta G^\ddagger_{293}$ (kJ mol <sup>-1</sup> )	$\Delta H^\ddagger$ (kJ mol <sup>-1</sup> )	$K^\ddagger_{293}$ (10 <sup>-16</sup> )
<b>MC-1</b>	563	2.2	101.49 ( $\pm 2.06$ )	$3.51 \times 10^{15}$ ( $\pm 2.83$ )	46.48 ( $\pm 2.92$ )	86.59 ( $\pm 0.082$ )	99.04 ( $\pm 2.06$ )	3.56 ( $\pm 0.108$ )
<b>MC-2</b>	568	4.3	75.05 ( $\pm 1.5$ )	$1.35 \times 10^{11}$ ( $\pm 0.9$ )	-43.38 ( $\pm 2.07$ )	85.17 ( $\pm 0.18$ )	73.05 ( $\pm 1.5$ )	6.57 ( $\pm 0.73$ )
<b>MC-3</b>	572	3.6	100.39 ( $\pm 3.06$ )	$8.62 \times 10^{15}$ ( $\pm 0.24$ )	37.78 ( $\pm 2.81$ )	85.94 ( $\pm 0.23$ )	96.74 ( $\pm 1.42$ )	5.93 ( $\pm 0.74$ )

### 3.3.5 Solvatochromic effects

Samples of **BSP-2** and **BSP-3** were dissolved in selected solvents and kept in the dark for 24 hr before solvatochromic studies were carried out. For this study, a polar protic solvent (ethanol) and polar aprotic solvents (acetone, acetonitrile) were used and their effect compared to non-polar solvents (toluene, dichloromethane and diethyl ether). Figure 3.7 shows spectra obtained for **MC-3** in a number of solvents after irradiation for 180 seconds with UV light (375 nm), along with inset photographs of the resulting

solutions. In addition, the thermal relaxation rate constants were estimated at 293 K (Figures 3.8 (a) and (b), extrapolated from Figure B4 (a) and (b), Appendix B) in each solvent. The formation of J-aggregates (Figure 3.7) in non-polar solvents typical of many **BSP** derivatives is evident from the appearance of new absorbance bands at 605 nm and 599 nm for **MC-3**, and at 605 nm and 597 nm for **MC-2** (Figure B3, Appendix B), in toluene and diethyl ether, respectively.

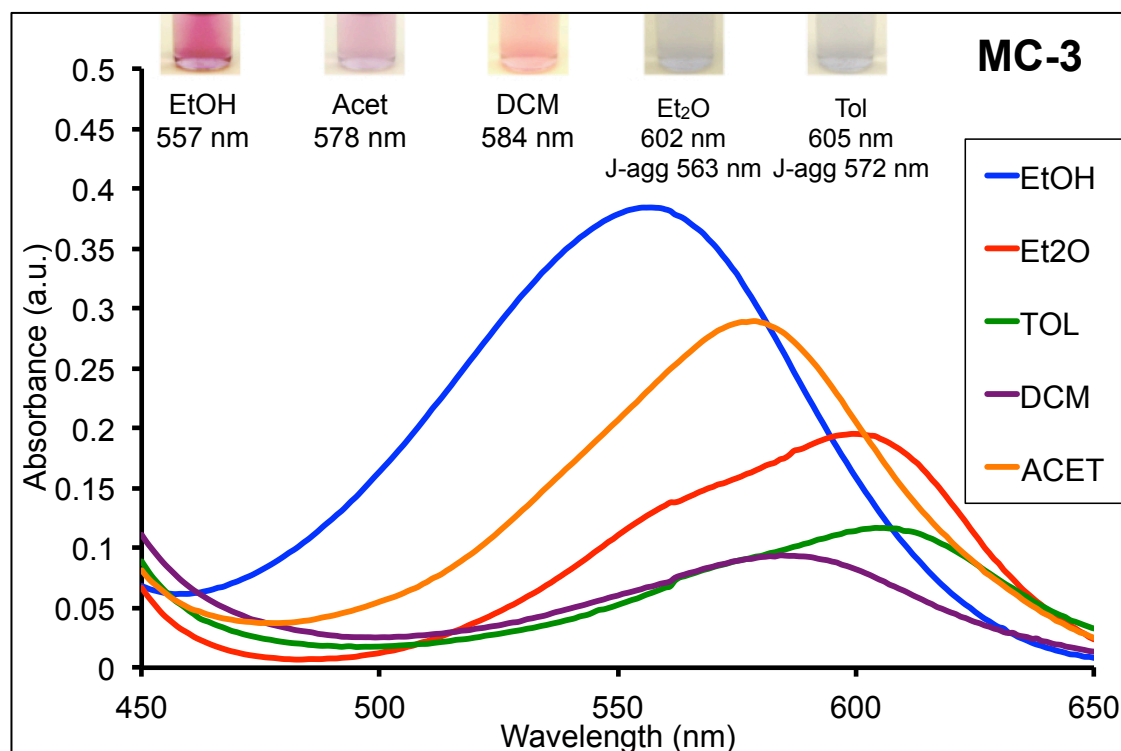


**Fig. 3.7** Solvatochromic effects of **MC-3** in the following solvents: EtOH, Acet, DCM, Et<sub>2</sub>O and Tol, listed and inset in terms of decreasing polarity. Prior to acquisition of the spectra, the solutions were irradiated with UV-LED device ( $\lambda_{\text{max}} = 375$  nm) for 180 s at 293 K. [**BSP-3**] =  $10^{-4}$  M in all cases.

Table 3.3 shows clearly that for both **MC-2** and **MC-3**, the  $\lambda_{\text{max}}$  is blue-shifted as the solvent polarity increases (negative solvatochromism) from toluene through to ethanol (605 nm to 552 nm for **MC-2**, 552 nm to 557 nm for **MC-3**). As is well established in the literature, merocyanines exhibit negative solvatochromism as a result of both a decrease in the dipole moment on electronic excitation and an increase in the dipolar nature of the ground state.<sup>43</sup> It has also been shown that this tends to be independent of the nature of the N-substituent, and this is indeed the case for **MC-2** and **MC-3**, which show near identical solvatochromic behaviour.

In contrast, the rate constant for ring closure ( $k$ ) decreases by an order of magnitude from  $24.3 \times 10^{-3} \text{ s}^{-1}$  to  $2.4 \times 10^{-3} \text{ s}^{-1}$  for **MC-2** for increasing solvent polarity, while for

**MC-3** an even greater rate decrease occurs ( $25.7 \times 10^{-3} \text{ s}^{-1}$  to  $0.7 \times 10^{-3} \text{ s}^{-1}$ ). The values for the rate constants for ring closure are similar in acetonitrile, acetone, diethyl ether and toluene, implying that solvation of the **MC** isomers must be quite similar. However, in ethanol this is not the case, as ring closure is four times faster for **MC-2**.

**Table 3.3** Photo and thermal properties of **MC-2** and **MC-3** derivatives ( $10^{-4} \text{ M}$ ) in a selection of solvents.  $\lambda_{\text{max}}$  measured after 15 hrs in the dark. The thermal relaxation rate constants were calculated by plotting  $\ln k$  vs. time, where  $k = \text{slope}$ .

<i><b>SOLVENT</b></i>	<b>MC-2</b>			<b>MC-3</b>		
	$\lambda_{\text{max}}$ nm	Abs	$k (10^{-3} \text{ s}^{-1})$	$\lambda_{\text{max}}$ nm	Abs	$k (10^{-3} \text{ s}^{-1})$
<i>Ethanol</i>	552	0.42	2.4	557	0.3	0.7
<i>Acetonitrile</i>	568	0.12	4.3	572	0.1	3.6
<i>Acetone</i>	570	0.44	6.3	578	0.4	6.3
<i>Dichloromethane</i>	587	0.13	9.2	584	0.4	17.3
<i>Diethyl ether</i>	597	0.29	21.9	602	0.2	19.3
<i>Toluene</i>	605	0.42	24.3	605	0.5	25.7

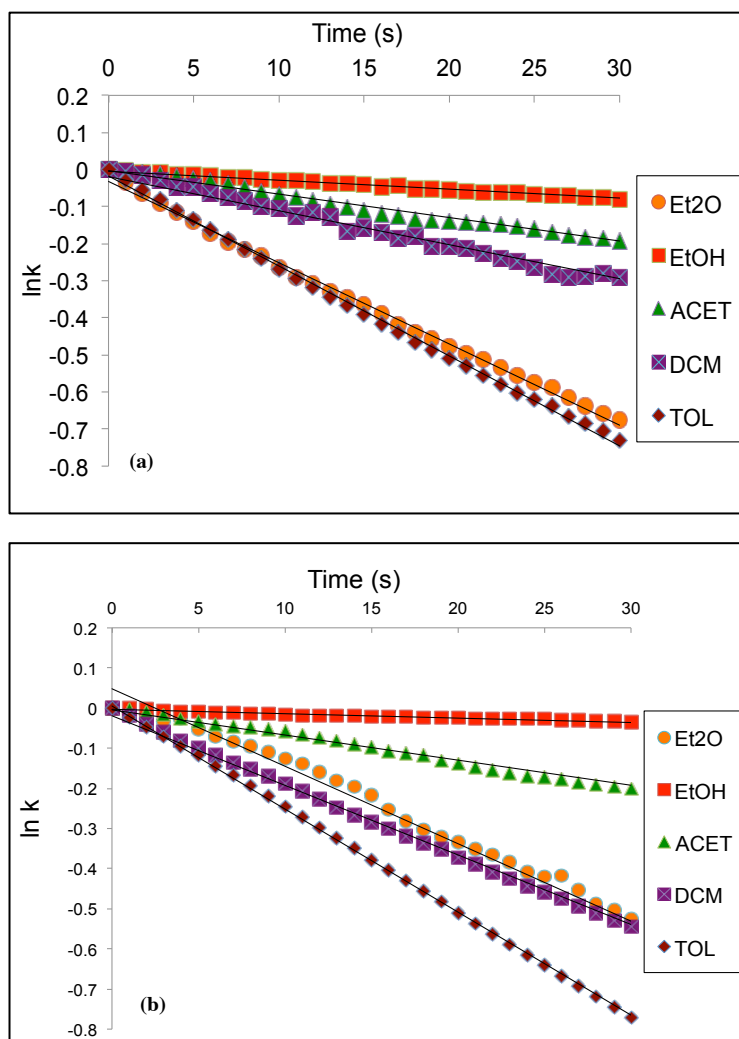


**Fig. 3.8** The  $\ln k$  vs. time plots used to calculate the rate of thermal relaxation of  $10^{-4} \text{ M}$  solutions of **BSP-2** (a) and **BSP-3** (b) in common organic solvents at 293 K.

This implies that, even though the dipolar nature of the **MC-2** ground state is similar to that of **MC-3** (similar  $\lambda_{\text{max}}$  values), the ethanol is acting like a less polar solvent with regard to ring closure rate. If intramolecular  $\pi$ - $\pi$  interactions do indeed control the ground state conformation of **MC-2**, then **MC-2** is in effect partly solvated by the  $\pi$  bonds of terthiophene, a less polar “solvent”, diminishing the full effect of the polar ethanol solvent. Somewhat more surprising is the contrary effect of dichloromethane for which ring closure is almost twice as fast for **MC-3** relative to **MC-2**, even though they appear to be electronically similar in this solvent. A more detailed study needs to be undertaken to probe the reasons for this behaviour.

### 3.3.6 Fluorescence spectroscopy

The presence of intramolecular  $\pi$ - $\pi$  interactions in **MC-2** would be expected to have a significant impact on the emissive properties of the molecule. The emissions of the terthiophene components of both **BSP-2** and **BSP-3** and their corresponding merocyanines were investigated since excitation of the molecules at 360 nm would lead to typical terthiophene emissions<sup>26</sup> around 450 nm that overlapped with the edge of the merocyanine absorptions (Figure 3.3). The corresponding emission spectra, as well as those of **BSP-1/MC-1** and the terthiophene acids are presented in Figure 3.9 (a) and (b), and the relevant data given in Table 3.4. A comparison of the emission spectra of the two terthiophenes shows, as expected, that **acTTh** is blue shifted by 28 nm (Figure 3.9 (a),  $\lambda_{\text{max,em}} = 439$  nm) compared to **cbTTh** (Figure 3.9 (b),  $\lambda_{\text{max,em}} = 467$  nm) as a result of the effect of the loss of conjugation of the carboxylic acid. However, both **BSP-2** ( $\lambda_{\text{max,em}} = 464$  nm) and **MC-2** have notably red-shifted ( $\sim 25$  nm) terthiophene emissions (Figure 3.9 (a) and Table 3.4) whilst those of **BSP-3** and **MC-3** are largely unchanged (Figure 3.9 (b) and Table 3.4).

Clearly, there is a much larger structural effect on the emission properties of **BSP-2** and **MC-2** than can be accounted for by a single carbon atom, and this is fully consistent with the influence of intramolecular  $\pi$ - $\pi$  interactions. However, it should be noted that since the emission shift is similar for both **BSP-2** and **MC-2**, similar interactions must be present in both isomers.

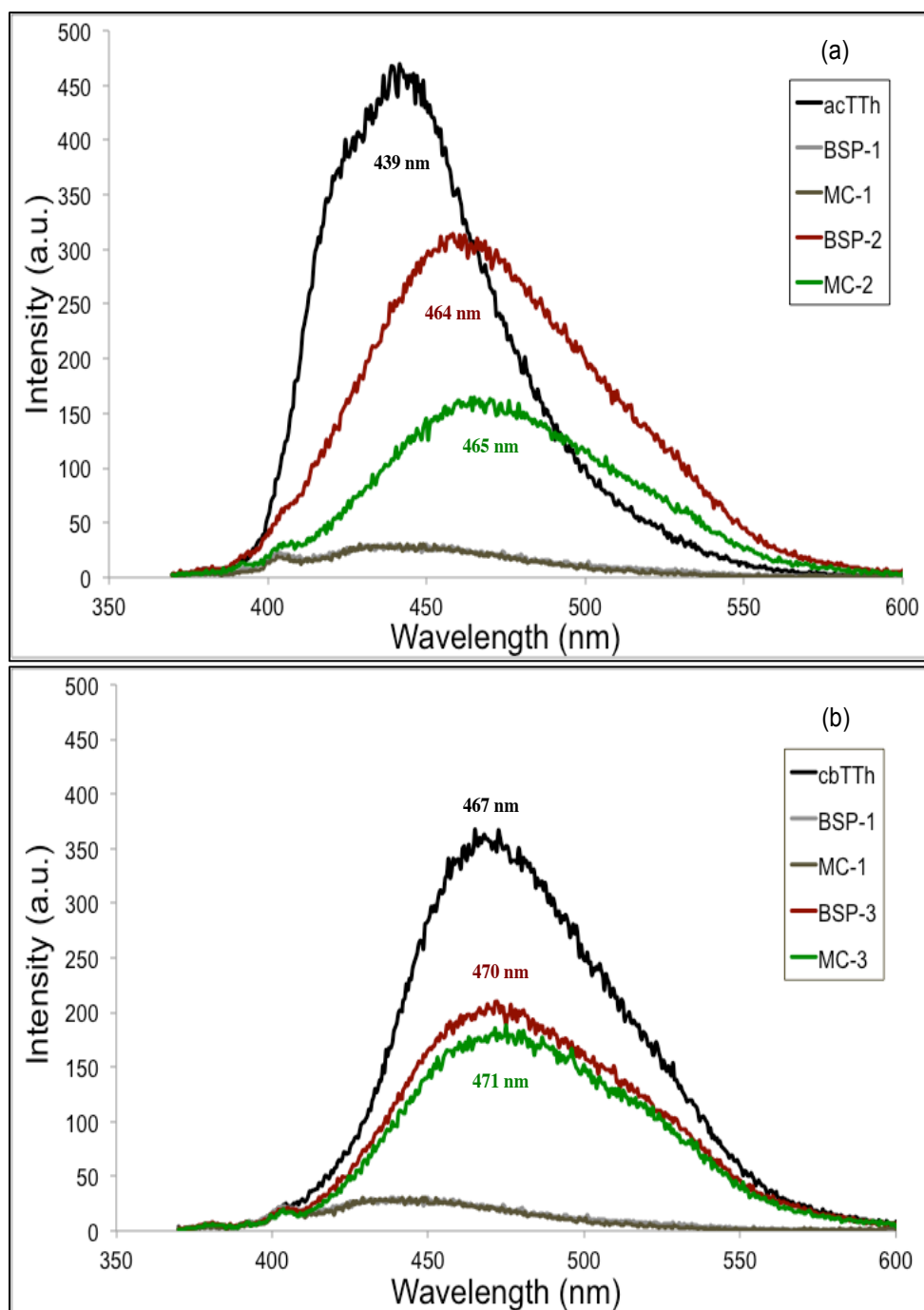


**Fig. 3.9** (a) Emission spectra of **acTTh**, **BSP-1**, **BSP-2** and their related **MC** isomers. (b) Emission spectra of **cbTTh**, **BSP-1**, **BSP-3** and their related **MC** isomers. All the solutions were  $10^{-5}$  M in ACN and all excitation wavelengths were 360 nm.

**Table 3.4** Parameters derived from the analysis of the emission spectra of **acTTh**, **cbTTh**, **BSP-2** and **BSP-3**. Stokes shifts are also indicated.

<i>Molecules</i>	$\lambda_{\text{max UV-vis}} \text{ cm}^{-1} (\text{nm})$	$\lambda \text{ Excitation (nm)}$	$\lambda_{\text{max Emission}} \text{ cm}^{-1} (\text{nm})$	Stokes Shift $\text{cm}^{-1}$
<b>acTTh</b>	28,090 (356)	358	22,727 (440)	5363
<b>cbTTh</b>	27,472 (364)	362	21,413 (467)	5874
<b>BSP-2</b>	28,090 (356)	360	21,598 (463)	6492
<b>BSP-3</b>	27,472 (364)	360	21,276 (470)	6196

Equally significant in this regard is the change in emission intensity for the **BSP-2/MC-2** isomers, which is absent for **BSP-3/MC-3**. While the quantum yields of the molecules were not measured and therefore, it is difficult to draw any conclusions from the relative intensities of the two sets of molecules, the apparent quenching of the **MC-2** terthiophene emission is again consistent with a intramolecular  $\pi$ - $\pi$  interaction between the planar merocyanine moiety and the terthiophene. This may also explain the increase in the merocyanine absorbance at 355 nm (Figure 3.3 (a)) when **BSP-2** is exposed to UV light, which does not manifest when the same experiment is performed with **BSP-3**, suggesting that a new interaction occurs when **BSP-2** is switched to **MC-2**.

Therefore, these results suggest that the extra methylene group present in the **BSP-2** linker chain provides a degree of additional flexibility that leads to enhanced intramolecular interaction between the **MC** and **TTh** units, most likely through alignment of  $\pi$ -electrons, as the molecule folds around the linker chain. A 3-D representation of this intramolecular alignment of the **MC** and **TTh**  $\pi$ -electrons is shown in Figure 3.10 (a) and (b)). This was produced by generating the energy minimised **MC** and **TTh** sub units in Chem-3D Ultra using standard molecular mechanics and arranging these with the appropriate linker chain, while applying typical constraints for the various bond lengths and angles. This tentatively suggests that is possible for the sub-units to align, with a separation as close as 3-5-3.7Å, which is well within the range for  $\pi$ -stacking. As indicated by the shift in the emission spectra, such an interaction is also likely between the **BSP** and **TTh** moieties in **BSP-2**, although perhaps not as strongly given the non-planar nature of the **BSP** unit. In the case of **BSP-3/MC-3**, the shorter linker group, coupled with the extended conjugation of the **TTh**- $\pi$  electrons into the carbonyl group prevents this interaction from occurring and the fluorescence and absorbance spectra are not affected in the same manner. A more rigorous *ab initio* study using molecular orbital theory calculations is currently underway and will be the subject of a separate publication.

This explanation is also consistent with the observed differences in the kinetic and thermodynamic behaviour of the **BSP-2** and **BSP-3**. For example, **BSP-3** is similar to **BSP-1** in terms of thermal relaxation behaviour. Table 3.1 shows that the ratio of the rate constants remains virtually constant over the temperature range studied (283 K-308 K), whereas for **BSP-2**, the ratio increases markedly towards the higher end of the range. This could be explained in terms of disruption of the **MC** and **TTh**  $\pi$ -electron

alignment as the system energy increases. Similar explanations have been advanced for observed patterns in the kinetics the thermal relaxation of the merocyanine form of spironaphthooxazine derivatives.<sup>44</sup>

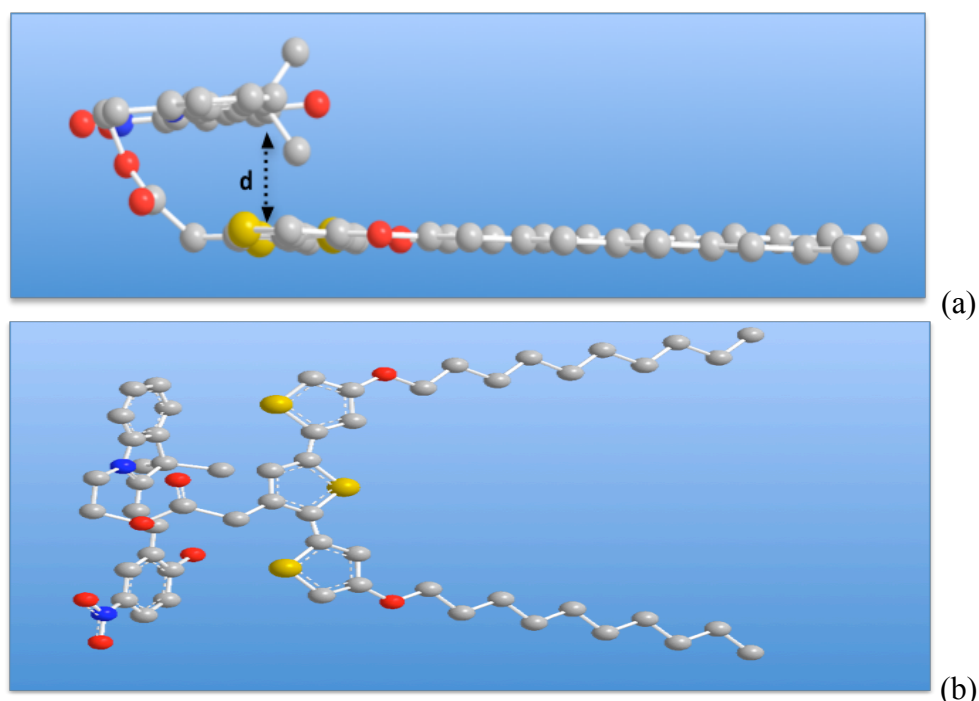


**Fig. 3.10** (a) Side view of **MC-2** in a ‘U’ arrangement showing the distance ‘d’ (3-5-3.7Å) between the aligned **MC** and **TTh** moieties and (b) alternative view of the same arrangement of the **MC** and **TTh** moieties. Images generated using Chem-3d Ultra V10.0. Atom types carbon (grey), oxygen (red), nitrogen (blue), sulphur (yellow); hydrogen atoms not displayed for clarity.

### 3.4 Conclusions

The photochemical and thermodynamic properties of two derivatives, **BSP-2** and **BSP-3**, incorporating terthiophene units attached to spiropyrans via the indoline nitrogen atom and ester linkers that differ by one methylene unit have been investigated. In **BSP-2**, the pyran is separated from the ester group by a methylene group, whereas in **BSP-3**, the ester group is directly linked to the terthiophene group. This apparently rather small structural difference results in quite striking differences in the characteristics of the derivatives, such as the fluorescence emission spectra (dominated by the terthiophene unit) and the thermal relaxation kinetics of the spiropyran unit. We believe these differences arise from the ability of the  $\pi$ -electron clouds of the thiophene and spiropyran units to align and form intramolecular p-p interactions in **BSP-2** due to the flexibility of the longer linker chain. In **BSP-3**, the terthiophene conjugation extends

into the ester group of the linker, and this additional rigidity, coupled with the shorter linker length, prevents a similar type of interaction from occurring. We are now developing a new generation of polymers based on these derivatives that could exploit such effects.

### 3.5 Acknowledgements

MZ, RB and DD acknowledge funding from Science Foundation Ireland (SFI) under the CLARITY CSET award (Grant 07/CE/I1147). KJF acknowledges the European Commission for financial support through a Marie Curie Actions International Re-integration Grant (IRG) (PIRG07-GA-2010-268365) and Irish Research Council for Science, Engineering and Technology. We also acknowledge support from the European Commission for funding under grant PIRSES-GA-2010-269302. Financial support from the Australian Research Council and access to the Australian National Fabrication Facility are also gratefully acknowledged.

### 3.6 References

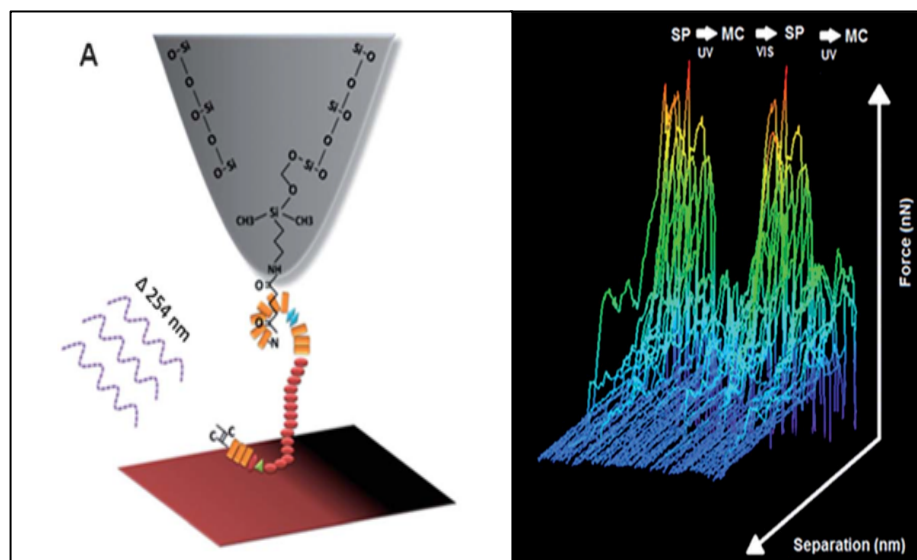
1. Y. Hirshberg, *Journal of the American Chemical Society*, 1956, **78**, 2304-2312.
2. E. Berman, R. E. Fox and F. D. Thomson, *Journal of the American Chemical Society*, 1959, **81**, 5605-5608.
3. C. A. Heller, D. A. Fine and R. A. Henry, *The Journal of Physical Chemistry*, 1961, **65**, 1908-1909.
4. J. G. Calvert and J. N. J. Pitts, *Photochemistry*, John Wiley and Sons, Inc., New York, N.Y., 1966.
5. R. Guglielmetti, *Studies in Organic Chemistry*, 1990, **40**, 855-879.
6. V. I. Minkin, *Chemical Reviews*, 2004, **104**, 2751-2776.
7. T. Yoshida and A. Morinaka, *Journal of Photochemistry and Photobiology a-Chemistry*, 1994, **78**, 179-183.
8. I. Willner, S. Rubin and Y. Cohen, *Journal of the American Chemical Society*, 1993, **115**, 4937-4938.
9. J. C. Crano, T. Flood, D. Knowles, A. Kumar and B. VanGemert, *Pure and Applied Chemistry*, 1996, **68**, 1395-1398.
10. S. Stitzel, R. Byrne and D. Diamond, *Journal of Materials Science*, 2006, **41**, 5841-5844.
11. F. Benito-Lopez, R. Byrne, A. M. Răduță, N. E. Vrana, G. McGuinness and D. Diamond, *Lab on a Chip*, 2010, **10**, 195-201.
12. A. S. Dvornikov, J. Malkin and P. M. Rentzepis, *Journal of Physical Chemistry*, 1994, **98**, 6746-6752.
13. H. Bouas-Laurent and H. Dvorr, in *Photochromism*, eds. D. r. Heinz and B.-L. Henri, Elsevier Science, Amsterdam, 2003, pp. XXVII-LIII.
14. R. Byrne, K. J. Fraser, E. Izgorodina, D. R. MacFarlane, M. Forsyth and D. Diamond, *Physical Chemistry Chemical Physics*, 2008, **10**, 5919-5924.
15. S. Coleman, R. Byrne, S. Minkovska and D. Diamond, *Journal of Physical Chemistry B*, 2009, **113**, 15589-15596.

16. R. Byrne, S. Coleman, K. J. Fraser, A. Raduta, D. R. MacFarlane and D. Diamond, *Physical Chemistry Chemical Physics*, 2009, **11**, 7286-7291.
17. R. Byrne, S. Coleman, S. Gallagher and D. Diamond, *Physical Chemistry Chemical Physics*, 2010, **12**, 1895-1904.
18. A. K. Chibisov and H. Gorner, *Chemical Physics*, 1998, **237**, 425-442.
19. H. Gorner, *Chemical Physics Letters*, 1998, **288**, 589-589.
20. H. Gorner, *Physical Chemistry Chemical Physics*, 2001, **3**, 416-423.
21. H. Gorner and A. K. Chibisov, *Journal of the Chemical Society-Faraday Transactions*, 1998, **94**, 2557-2564.
22. K. J. Laidler and J. H. Meiser, *Physical Chemistry* Houghton Mifflin, Boston, MA, 1999.
23. J. Roncali, *Chemical Reviews*, 1992, **92**, 711-738.
24. J. Roncali, *Chemical Reviews*, 1997, **97**, 173-205.
25. S. Gambhir, K. Wagner and D. L. Officer, *Synthetic Metals*, 2005, **154**, 117-120.
26. P. Wagner and D. L. Officer, *Synthetic Metals*, 2005, **154**, 325-328.
27. M. C. Gallazzi, L. Castellani, R. A. Marin and G. Zerbi, *Journal of Polymer Science Part a-Polymer Chemistry*, 1993, **31**, 3339-3349.
28. C. H. E. Zhou, Z. Tan, C. Yang, Y. Li, *Journal of Polymer Science Part B*, 2006, **44**, 4916-4922.
29. S. H. Hosseini and A. A. Entezami, *Polymers for Advanced Technologies*, 2001, **12**, 524-534.
30. L. Kumpumbu-Kalemba and M. Leclerc, *Chemical Communications*, 2000, 1847-1848.
31. I. Levesque, P. Bazinet and J. Roovers, *Macromolecules*, 2000, **33**, 2952-2957.
32. I. Levesque and M. Leclerc, *Chemistry of Materials*, 1996, **8**, 2843-2849.
33. I. Levesque and M. Leclerc, *Macromolecules*, 1997, **30**, 4347-4352.
34. F. Raymond, N. Di Cesare, M. Belletete, G. Durocher and M. Leclerc, *Advanced Materials*, 1998, **10**, 599-602.
35. A. Yassar, C. Moustrou, H. K. Yousoufi, A. Samat, R. Guglielmetti and F. Garnier, *Macromolecules*, 1995, **28**, 4548-4553.
36. K. Yoshino, S. Nakajima, M. Onoda and R. Sugimoto, *Synthetic Metals*, 1989, **28**, 349-357.
37. G. Zotti, R. A. Marin and M. C. Gallazzi, *Chemistry of Materials*, 1997, **9**, 2945-2950.
38. K. Wagner, R. Byrne, M. Zanoni, S. Gambhir, L. Dennany, R. Breukers, M. Higgins, P. Wagner, D. Diamond, G. G. Wallace and D. L. Officer, *Journal of the American Chemical Society*, 2011, **133**, 5453-5462.
39. A. Higuchi, A. Hamamura, Y. Shindo, H. Kitamura, B. O. Yoon, T. Mori, T. Uyama and A. Umezawa, *Biomacromolecules*, 2004, **5**, 1770-1774.
40. J. M. Locke, S. Gambhir, R. D. Breukers, K. Wagner, K. W. Jolley, G. G. Wallace and D. L. Officer, *Manuscript in preparation.*, 2012.
41. D. Diamond and V. C. A. Hanratty, *Spreadsheet Applications for Chemistry Using Microsoft Excel*, John Wiley and Sons, New York, 1997.
42. J. B. Flannery, *Journal of the American Chemical Society*, 1968, **90**, 5660-5671.
43. J. T. C. Wojtyk, A. Wasey, P. M. Kazmaier, S. Hoz and E. Buncel, *The Journal of Physical Chemistry A*, 2000, **104**, 9046-9055.
44. T. W. Shin, Y. S. Cho, Y. D. Huh, K. D. Lee, W. K. Yang, J. Park and I. J. Lee, *Journal of Photochemistry and Photobiology a-Chemistry*, 2000, **137**, 163-168.



# CHAPTER 4

## Optical Switching of Protein Interactions on Photosensitive–Electroactive Polymers Measured by Atomic Force Microscopy



**Publication Status: PUBLISHED**

A. Gelmi, **M. Zandoni**, M. J. Higgins, S. Gambhir, D. L. Officer, D. Diamond, G. G. Wallace, “Optical Switching of Protein Interactions on Photosensitive-Electroactive Polymers Measured by Atomic Force Microscopy”, *Journal of Materials Chemistry B*, 1, 2162-2168 (2013). DOI: 10.1039/c3tb00463e

## Abstract

The ability to switch the physico-chemical properties of conducting polymers opens up new possibilities for a range of applications. Appropriately functionalized materials can provide routes to multi-modal switching, for example, in response to light and/or electrochemical stimuli. This capability is important in the field of bionics wherein remote and temporal control of the properties of materials is becoming attractive. The ability to actuate a film via photonic stimuli is particularly interesting as it facilitates the modulation of interactions between host binding sites and potential guest molecules. In this work, we studied two different poly-terthiophenes: one was functionalized with a spiropyran photoswitch (**pTTh-SP**) and the second with a non-photoswitchable methyl acetate moiety (**pTTh-MA**). These substrates were exposed to several cycles of illumination with light of different wavelengths and the resulting effect studied with UV-vis spectroscopy, contact angle and atomic force microscopy (AFM). The AFM tips were chemically activated with fibronectin (FN) and the adhesion force of the protein to the polymeric surface was measured. The **pTTh-MA** (no SP incorporated) showed a slightly higher average maximum adhesion ( $0.96 \pm 0.14$  nN) than the modified **pTTh-SP** surface ( $0.77 \pm 0.08$  nN), but after exposure of the **pTTh-SP** polymer to UV, the average maximum adhesion of the **pTTh-MC** (merocyanine form) was significantly smaller ( $0.49 \pm 0.06$  nN) than both the **pTTh-MA** and **pTTh-SP**. In addition, the tip-sample separation distances of the adhesive interactions are indicative of the FN interaction occurring over a distance more closely related to the average dimensions of its compact conformation. The results suggest that surface energy and hydrophobic forces are predominant in determining the protein adhesion to the films studied and that this effect can be photonicallly tuned. By extension, this further implies that it should be possible to obtain a degree of spatial and temporal control of the surface binding behaviour of certain proteins with these functionalized surfaces through photo-activation/ deactivation, which, in principle, should facilitate patterned growth behaviour (e.g. using masks or directional illumination) or photocontrol of protein uptake and release.

## 4.1 Introduction

Switchable surfaces offer control over the material interface via an external stimulus, including light, temperature, pH and electrical field, which can be applied either as a 'once-off' or a reversible change.<sup>1</sup> For cell-based applications, switchable materials offer the ability to control interactions at the cell-material interface. In particular, the switching of protein adsorption and conformation can be used to modulate cellular proliferation and differentiation.<sup>1-3</sup> Light switching in 'once-off' switching materials can promote specific biomolecular adhesion to the surface,<sup>4</sup> while electrical switching is particularly applicable to organic conductors (e.g. CNT, conducting polymers) and shown to enhance cell growth and differentiation.<sup>5-10</sup> In biosensing applications, however, the surface adsorption of proteins is undesirable and decreases the efficacy of the device.<sup>11-13</sup> A dynamic material that controls both the adsorption and desorption of proteins and living cells opens up several possibilities in patterned cell growth, tissue engineering, and biosensing applications.<sup>14-16</sup>

Polymer-based materials have been designed to take advantage of switchable properties for the above applications.<sup>17-20</sup> Polymers can be switched through a variety of external stimuli that typically provide a single pathway to control the interfacial response. A developing area in the field of switchable materials is the implementation of multiple stimuli via copolymers as this provides increased flexibility in the manner by which the interfacial behavior is controlled. This in turn is important for applications wherein both spatial and temporal control over surface interactions is desired. For example, a material comprising both thermoresponsive poly(N-isopropylacrylamide) (pNIPAM) and photoresponsive spirobenzopyran (SP) enables both control over the spatial direction of cellular growth with UV light and the removal of cells via low temperature washing.<sup>14</sup> This strategy has been taken a step further by combining light, temperature, and pH to control tunable microgels comprising a temperature/pH sensitive pNIPAM-allylamine copolymer microgel functionalized with the SP photosensitive molecule.<sup>21</sup> In this case, the optical properties of the copolymer changed the thermal threshold for volume changes of the microgel, as well as a photochromic change when switched. The amine groups in the microgel were pH sensitive and reduced swelling capability with an increase in pH.

When designing a material with bi-modal switching capabilities, the incorporation of photoswitchability is often attractive as it enables fast, non-invasive, and highly

controllable switching with spatial resolution. Photocleavable groups that are actively switched via specific wavelengths of light have previously been used to inhibit or facilitate cell adhesion.<sup>4</sup> This type of switching induces an irreversible change but despite this, it is useful for surface patterning or release of molecules (e.g. drug delivery).<sup>22</sup> The second common optical switching mechanism is photoisomerisation wherein the molecule undergoes heterolytic bond cleavage producing an isomer that will have a different polarity to the original molecule. SP is a commonly used in this regard as it undergoes a heterolytic cleavage of the spiro carbon-oxygen bond to create an open ringed structure that has two resonance merocyanine-like and quinoidal-like MC forms. SP has been studied in combination with temperature responsive pNIPAM polymers to produce photosensitive copolymer materials.<sup>22-24</sup> They have also been incorporated as a copolymer with methyl methacrylate to produce a photosensitive poly(spiropyran-co-methyl methacrylate) material that upon switching from the SP to MC form can induce the detachment of platelets and mesenchymal stem cell.<sup>25</sup> The SP molecule has also been incorporated into materials such as self-assembled monolayers,<sup>26</sup> bilayers,<sup>27</sup> polymers,<sup>28</sup> and more recently organic conducting polymers.<sup>29-</sup>

31

A novel organic conducting polymer, a polyterthiophene with SP attached to the polymer backbone, has recently been synthesized to produce a photosensitive conductive polymer.<sup>30</sup> The SP was covalently bound to the alkoxyterthiophene monomer units to produce the polymer poly(2-(3,3"-dimethylindoline-6'-nitrobenzospiropyranyl)ethyl-4,4"-didecyloxy-2,2':5',2"-terthiophene-3-acetate). Electrical switching of the polythiophene backbone showed good reversibility and stability and additional photoswitching of the SP moiety was possible using optical stimulus. Figure 4.1A shows the chemical structure of the polymer and reversible transition between the SP and MC forms as a function of UV/visible light switching. While the effect of both light and electrical switching on the redox properties and SP-to-MC conversion was investigated, the material was not exploited to demonstrate control over the physical interactions of proteins or living cells.

In this study, we focused on the effect of optical stimulation on the poly(2-(3,3"-dimethylindoline-6'-nitrobenzospiropyranyl)-ethyl-4,4"-didecyloxy-2,2':5',2"-terthiophene-3-acetate) (termed **pTTh-SP**) polymer described in our above study<sup>30</sup> to investigate the ability to control fibronectin (FN) protein adhesion, which is an important interaction within extracellular matrix for mediating cell adhesion. In order to

support cell adhesion and signalling via  $\alpha 5 \beta 1$  integrin binding receptors to RGD sites within FN, the protein must be in the appropriate conformation whilst possessing adhesion to the substrate. FN binding to cell integrin receptors triggers the formation of actin stress fibres that promotes cell adhesion and proliferation. Subsequent cell signalling is modulated through a continuum of mechanical forces (i.e. mechanotransduction) and thus is dependent on the strength of FN adhesion to a surface.

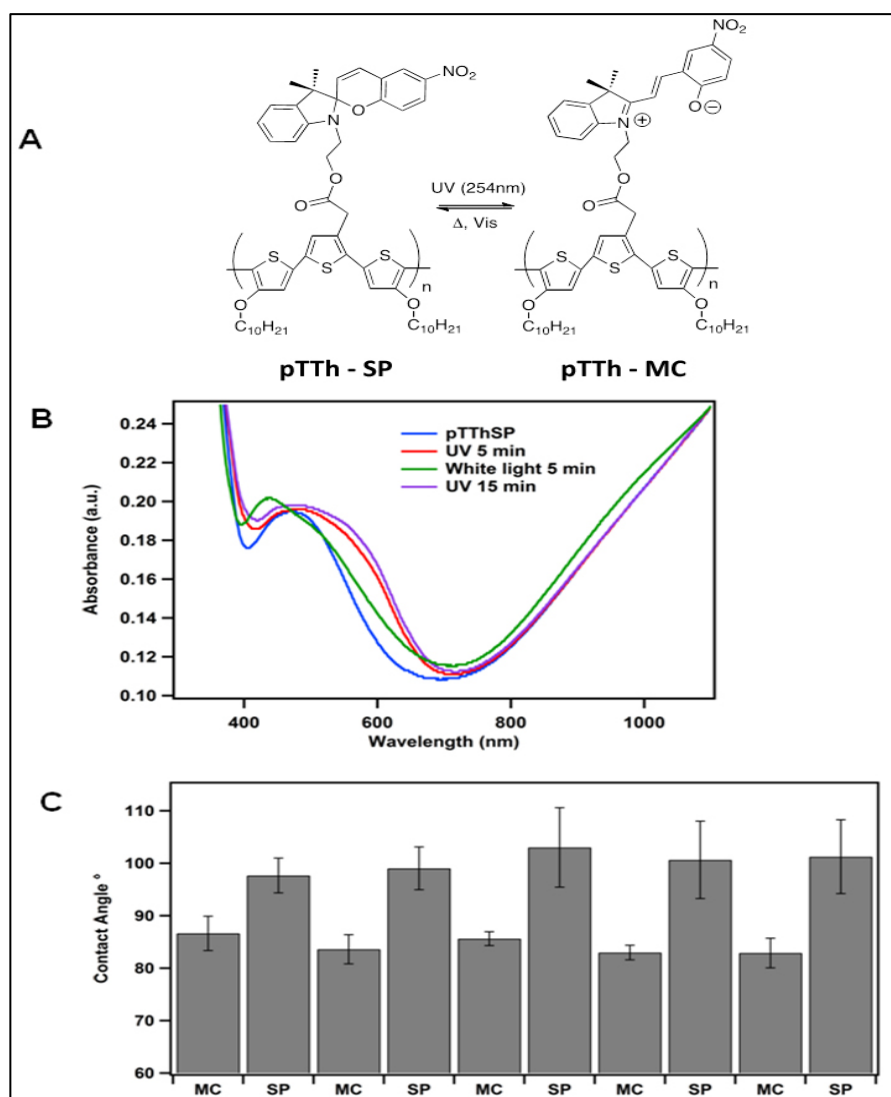


**Figure 4.1:** (A) (left structure) Spiropyran covalently bound to alkoxyterthiophene monomer units to produce the polymer poly(2-(3,3"-dimethylindoline-6'-nitrobenzospiropyran)ethyl 4,4"-didecyloxy-2,2':5',2"-terthiophene-3-acetate) (termed **pTTh-SP**) and (right structure) after light switching to the zwitter-ionic isomer in open form (termed **pTTh-MC**). (B) UV-vis spectra of initial **pTTh-SP** (blue), UV stimulated 5 min (red), white light stimulated 5 min (green) and UV stimulated 15 min (purple). (C) Contact angle measurements on polymer as it is optically switched, measured on 4 individual films, cycled 5 times. Error bars are standard deviation.

## 4.2 Materials and Methods

The molecules used for this study (**pTTh-MA** and **pTTh-SP**) were synthesized and then electro-polymerized according to the procedure previously reported.<sup>30</sup> The electrodes selected were the optically transparent ITO (Indium Tin Oxide) coated glass (Delta Technologies, Limited, resistivity  $R_s = 4-8 \Omega$ ). Absorbance spectra were recorded using a Shimadzu UV-1800 spectrophotometer. The polymers were washed in acetonitrile after the polymerization in order to remove the excess of electrolyte and the absorbance spectra measured. The absorbance spectra was then measured for the **pTTh-SP** exposed to UV (254 nm) light for 5 min, and then once exposed to visible light (full spectrum) for 5 min. The **pTTh-SP** was then exposed to UV light for 15 min and the absorbance spectra measured. All light switching was performed at room temperature. Four different freshly polymerized films (stored at -0.4 V) were subjected to 5 cycles of exposure to UV light (254 nm, 15 min) and 5 cycles of exposure to visible light (full spectrum, 15 min). After each exposure, contact angles were obtained for each film in triplicate.

The functionalization precursors 3-ethoxydimethylsilylamine propyl (3-EDSPA) and gluteraldehyde (GAH) were obtained from Sigma Aldrich. Human plasma fibronectin (FN) was obtained from Sigma Aldrich. Phosphate buffer saline (PBS) was prepared at pH 7 in Milli-Q water (18.2 M $\Omega$ ). The tip is functionalized using an aminosilanization method to covalently bind the protein to the tip. Silicon nitride tips are used for this method due to the availability of silicon oxide groups on the surface. The tips were initially prepared with a plasma cleaner to remove any impurities or functionalized groups on the surface. Once cleaned the tips were immediately functionalized to minimize contaminants on the surface. The tips were placed into the 3-EDSPA solution at room temperature for 1 h. The tips were then removed, washed consecutively with toluene and then in PBS solution. The tips were then immersed in the GAH solution for 1 h and then rinsed with PBS solution. The tips were finally immersed in the FN solution for 1 h, then rinsed and refrigerated in PBS solution until use. The AFM parameters for the force measurements were set to 500 nm for the z-distance, 0.5 Hz scan rate, 1 s dwell toward the surface, and 1 nN trigger force. Single point force spectroscopy measurements were performed with 5 consecutive measurements at one point, with a rest of 3 s, across 5 different points on the sample surface. 25 force curves were performed by 3 individual tips on 3 samples for measurements on **pTTh-MA** and

**pTTh-SP** (total number of force curves 228 and 200 on **pTTh-MA** and **pTTh-SP**, respectively).

The modified polymers were switched using optical stimulation to measure protein adhesion on the SP and MC form. The polymer was irradiated with UV light (wavelength 254 nm) for 10 min in order to switch it from **pTTh-SP** to **pTTh-MC** in PBS solution. The polymer was then exposed to room light for 10 min to switch from **pTTh-MC** to **pTTh-SP**. Force spectroscopy measurements were performed with 5 consecutive measurements at one point, with a rest of 3 s, across 5 different points on the sample surface. 25 force curves were performed on the polymer after the light stimulation was applied and 4 samples with 4 individual tips were used (total number of force curves 200 and 150 for SP and MC form respectively). Contact angle experiments on the polymer surfaces were obtained with a First Ten Ångströms FTA200 analyser at room temperature and environment humidity, using water as the probe liquid. The **pTTh-SP** polymer was initially electrically stimulated at a constant -0.4 V after polymerization in 0.1 M TBAP electrolyte (acetonitrile solvent) in order to guarantee the higher concentration possible of the SP isomer, subjected to the illumination cycles as previously described and then analysed with the contact angle. Six freshly synthesized samples of **pTTh-MA** were washed in acetonitrile to remove the excess of electrolyte. Three of them were electrically stimulated at -0.4 V and the other three were kept at 0.9V and then tested with the contact angle analyser.

## 4.3 Results and Discussion

### 4.3.1 UV-Vis Spectra

The UV-vis absorbance spectra for the switching **pTTh-SP** is shown in Figure 4.1B. The fully switched, oxidized **pTTh-SP** polymer was initially measured (blue). The polymer was then switched to the MC form by exposure to UV light (red) and then switched back to the SP form again (green). The polymer was switched to MC a final time (purple). The absorbance spectra show a shift with the optical stimulation, indicating that the polymer is undergoing photoisomerisation.

### 4.3.2 Contact Angle Measurements

The optical stimulation was shown to induce a change in the wettability of the **pTTh-SP** functionalized polymer, as demonstrated by the contact angle measurements. As a control, optical stimulation did not produce any effect on the SP-free **pTTh-MA** polymer. Figure 4.1C displays the average contact angle measurement as the polymer is optically switched from SP to MC form five times. The measurements show a stable, reversible change of the contact angle of the polymer. The SP form is the more hydrophobic form (an average contact angle of  $100.0 \pm 5.6^\circ$ ), and the MC form is more hydrophilic (an average contact angle of  $84.3 \pm 2.5^\circ$ ). The hydrophobic nature of SP has previously been related to its chemical structure<sup>24, 32</sup> and similarly confirmed using contact angle measurements.<sup>25</sup> The weaker hydrophobicity of the MC form is attributed to its zwitterionic structure that forms due to cleavage of the spiro carbon-oxygen bond and results in the heterolysis of the nitrogen and oxygen (Figure 4.1A).<sup>32</sup> Furthermore, the contact angle measurements demonstrated that the change in wettability was reversible upon cycling of the optical switching and agrees with a previous study on the reversible optical switching properties of the SP.<sup>33</sup>

### 4.3.3 Protein Adhesion

The interaction of FN with the polymer was measured using AFM force spectroscopy, as depicted in Figure 4.2A. In these measurements, a chemically functionalized FN tip is brought into contact, and then withdrawn from, the polymer surface whilst measuring the tip-sample adhesive forces as a function of optical stimulation. A typical force curve on the **pTTh-MA** polymer with no SP incorporated and without optical stimulation shows a large peak upon retraction of the tip, indicating the presence of an adhesive interaction between the FN and polymer (Figure 4.2B). The strength of protein adhesion is given as the peak maximum (Figure 4.2B, vertical arrow), which is on the order of nanonewtons ( $\sim 1$  nN). This type of adhesion is typically due to the interaction of several proteins on the tip, involving both intra and inter- protein interactions, and their subsequent detachment from the surface. Inter-protein interactions may include electrostatic, hydrophobic and hydrogen bonding, while inter-protein interactions include unfolding of the protein or adhesion between proteins, all of which may contribute to the strength or energy (integral of area under peak) of protein adhesion. The **pTTh-MA** showed a slightly higher average maximum adhesion ( $0.96 \pm 0.14$  nN)

than the modified **pTTh-SP** surface ( $0.77 \pm 0.08$  nN), as displayed in Figure 4.2C. After exposure of the **pTTh-SP** polymer to UV, the average maximum adhesion of the **pTTh-MC** was significantly smaller ( $0.49 \pm 0.06$  nN) than both the **pTTh-MA** and **pTTh-SP**. When comparing the change in surface energy (contact angle) and adhesion, both parameters show a decrease in the order of **pTTh-MA** > **SP** > **MC**, suggesting that an increase in hydrophilicity (or conversely a decrease in hydrophobicity) correlates with a decrease in protein adhesion. Based on this correlation, it appears that hydrophobic interactions may be the dominant forces involved in protein adhesion. The increased hydrophobicity of the **pTTh-MA** is due to its neutral backbone, in addition to the presence of polar decyloxy and acetate groups. This is in contrast to the **pTTh-SP** where the nitro groups will contribute to hydrophilicity. The reduction in hydrophobicity of the MC form is attributed to the zwitterionic nature of the MC molecule, which has previously been shown to also reduce protein adhesion.<sup>34, 35</sup> Zwitterionic surfaces are believed to be resistant to non-specific protein adhesion due to hydration layer(s) bound through solvation of charged terminal groups, as well as hydrogen bonding around molecular chains.<sup>36</sup> This switch to the more hydrophilic MC form with zwitterionic species may either diminish the extent of hydrophobic interactions and/or play a role in actually deterring protein adhesion.

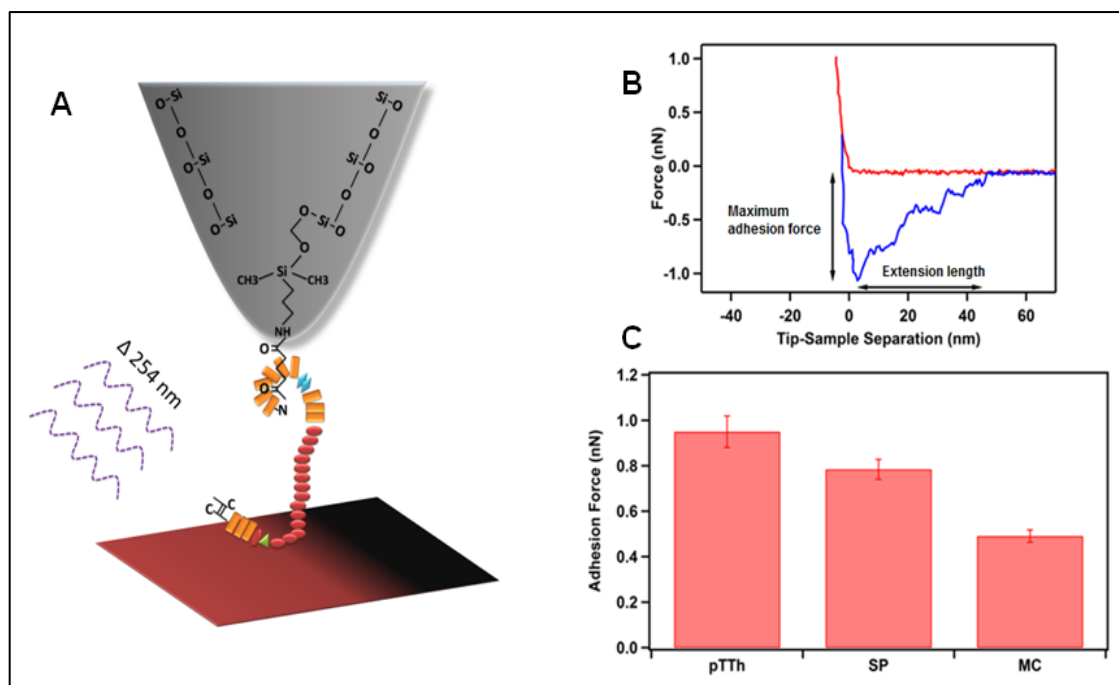


**Figure 4.2:** (A) Schematic diagram of AFM tip functionalized with FN interacting with a chromophoric surface stimulated with UV light (wavelength 254 nm). (B) Example force curve analysis, extension (red) and retraction (blue) curves. (C) Average adhesion forces for as-grown **pTTh-MA** ( $n=228$ ), **SP** ( $n=200$ ) and **MC** form ( $n=150$ ). Error bars are standard error.

Figure 4.3A displays the reversibility in protein adhesion as the polymer is switched between the SP and MC forms. Representative force curves on **pTTh-SP** demonstrate a much higher adhesion force (larger peaks) compared to **pTTh-MC**, clearly indicating a reversible effect of the optical stimulus on protein adhesion. Figure 4.3B shows the average maximum adhesion force of the SP and MC forms as they are reversibly switched over 2 cycles. The initial SP form (electrically stimulated to ensure complete conversion to the SP form) was measured to have a mean of  $0.91 \pm 0.04$  nN (mean  $\pm$  s.d., n=50). The first switch to **pTTh-MC** with UV light reduced the mean maximum adhesion to  $0.31 \pm 0.01$  nN (mean  $\pm$  s.d., n=75). The first switch back to **pTTh-SP** with visible light measured an increase in the mean maximum adhesion to  $0.67 \pm 0.03$  (mean  $\pm$  s.d., n=150) and the second switch to **pTTh-MC** with UV light decreased the mean again to  $0.46 \pm 0.01$  (mean  $\pm$  s.d., n=75). The reversibility of the protein adhesion exhibits a small amount of hysteresis as the switching is performed over multiple cycles. In particular, the average adhesion force of the SP does not return to its initial value (27% reduction in the average adhesion force) after switching back from the MC form, suggesting that not all of the MC isomers undergo switching back to the SP form. As the force measurements are not performed simultaneously during the optical switching (i.e. only before or after switching is performed), the measurements may be susceptible to time-dependent (e.g. 'lag' time) changes in the **SP-to-MC** conversion.

A previous study using a copolymer of nitrobenzospiropyran and methyl methacrylate has shown that the amount of adsorbed fibrinogen protein on SP surfaces and those surfaces already in the MC form is almost comparable, even though the MC form results in a significant decrease in contact angle (increased hydrophilicity).<sup>25</sup> In the same study, however, it was shown that the amount of adsorbed fibrinogen on SP surfaces significantly decreases when those same surfaces are exposed to UV irradiation, suggesting that the physical movement associated with the molecular switching, rather than a change in surface energy, is primarily responsible for inducing protein detachment. This detachment of the fibrinogen was also related to the ability to induce detachment of platelet cells.<sup>25</sup> The AFM force spectroscopy measurements in our study are analogous to the situation where the direct measurement of protein adhesion is made on surfaces already in the SP and MC form, thus limiting any effects to only the static properties of the surfaces. Therefore, contrary to the above study, we observe a significant difference in protein adhesion between the **pTTh-MA**, SP and MC forms

that correlates with a change in their hydrophobicity. Specifically, the protein adhesion decreases with an increase in hydrophilicity. In a different study, UV irradiation of a spiropyran–poly(N-isopropylacrylamide) copolymer prior to low temperature washing was shown to promote the adhesion of CHO-K1 cells, suggesting an attractive interaction between the zwitterionic isomer and cell membrane that also has zwitterionic groups. However, the surface energies, switching mechanisms of the copolymer, or influence on protein adhesion were not addressed in the study.<sup>14</sup> The findings from the above different studies highlight the potential complexities and differences in underlying mechanisms for controlling protein and cell interactions using optical stimulation, particularly in dual stimuli systems where the photosensitive SP is combined with another polymer constituent that may be electroactive, temperature sensitive or simply of different surface chemistry.

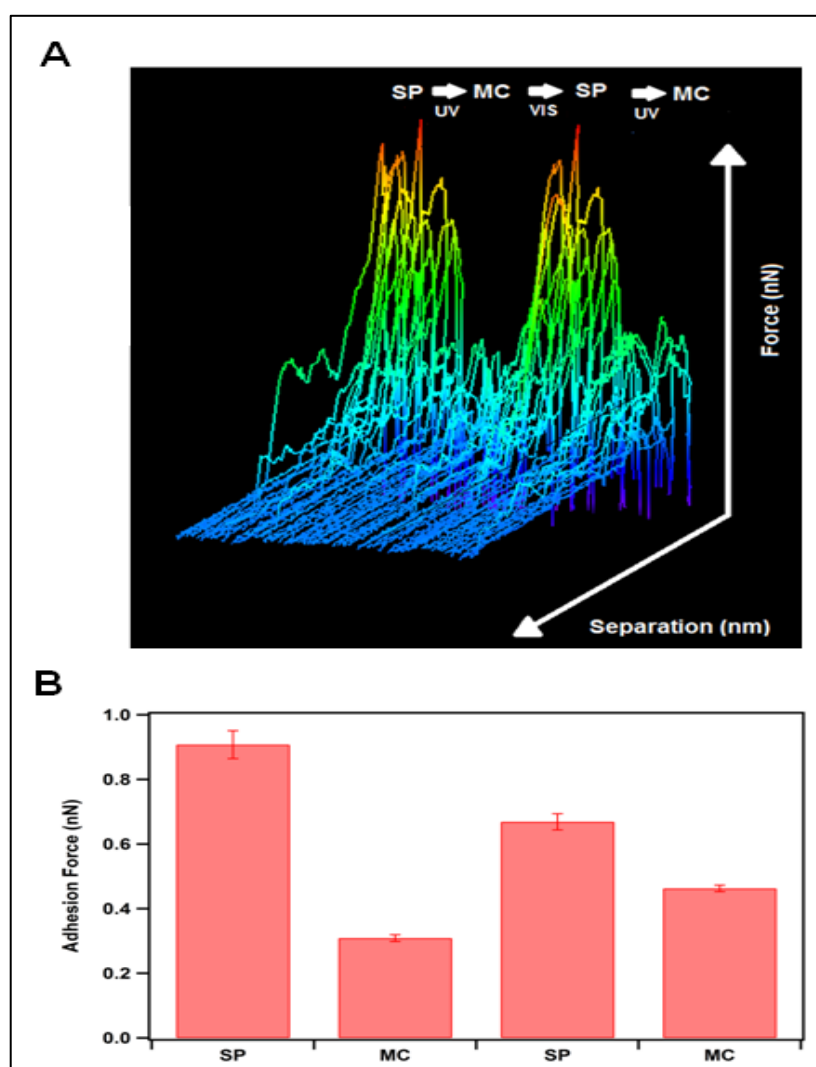


**Figure 4.3:** (A) Representative force curves during optical switching. Maximum force 2.4 nN, maximum tip-sample separation 100 nm. (B) Average adhesion forces during optical switching ( $n = 50, 75, 150, 75$ ). Error bars are standard error.

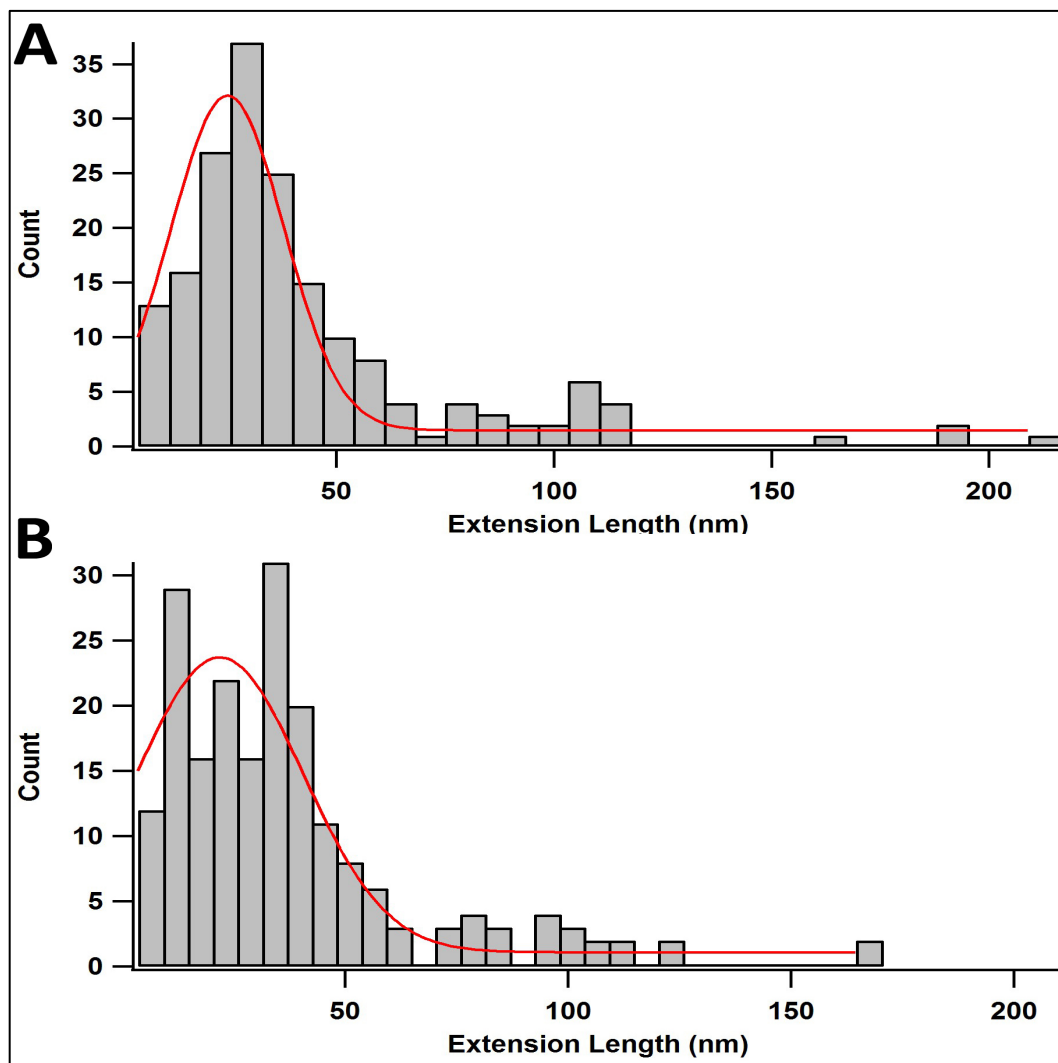


**Figure 4.4.** Distribution of extension length for SP (A) and MC (B), N=180 and N=198 respectively. Red curves are individual Gaussian fits.

During the adhesive interaction of the FN, the maximum extension length, or elongation, of the protein(s) is given as the distance on the x-axis (i.e. tip-sample separation distance) where the protein eventually detaches from the surface and the force returns to zero (Figure 4.2B, horizontal arrow). Histograms showing the distribution of the protein extension lengths did not show any significant difference between the SP and MC forms of the polymer (Figure 4.4). Mean peak distribution values for the **pTTh-SP** (Figure 4.4A) and **pTTh-MC** (Figure 4.4B) were  $24.9 \pm 0.8$  nm and  $21.9 \pm 2.3$  nm, respectively. These extension lengths, which are significantly smaller than the theoretical and experimentally observed 160-180 nm contour length of

FN in its extended conformation,<sup>37-40</sup> indicate that the protein interaction is occurring over a distance more closely related to the average dimensions of FN in its compact conformation (i.e.  $\approx 20$  nm x 15 nm).<sup>40</sup> These extension lengths of  $\approx 25$  nm for the **pTTh-SP** and **pTTh-MC** are also much shorter than the distribution of extension lengths, 60 nm, 120 nm and 160-175 nm, observed in our recent AFM study on FN interactions with the conducting polymer, polypyrrole, doped with glycosaminoglycan's (GAGs) such as chondroitin sulfate, hyaluronic acid and dextran sulfate.<sup>41</sup> In this case, the presence of the GAGs, which are large, highly negatively charged polyelectrolytes, dramatically increases the surface hydrophilicity (contact angles of  $<22^\circ$ )<sup>42</sup> and causes the FN to adopt a more extended conformation during its interaction with the polymer.<sup>41</sup> It is well known that the wettability of a surface is important for controlling the conformation of FN. On hydrophobic surfaces, FN adopts a compact, 'pretzel' conformation that is stabilized by intermolecular bonds but can be disrupted by interacting surface groups of hydrophilic and negatively charged surfaces, causing the protein to adopt an extended conformation.<sup>43</sup> Furthermore, the redox-dependent conformation of FN on conducting polymers is thought to influence the ability to control cell adhesion<sup>44</sup> and migration.<sup>45</sup> By looking at the ensemble conformation of FN protein using fluorescence techniques, it was proposed that the proteins electrically 'switch' between a folded and unfold state to control the cell interaction.<sup>46</sup> Hence, for the hydrophobic **pTTh-SP** and **pTTh-SP** polymers (CA = 85-100°), the observed extension lengths suggest that the FN protein retains its compact conformation during adhesive interactions with the surface.

## 4.4 Conclusion

The switchable nature of the copolymer in this study and its effect on protein adhesion as well as conformation suggest a potential use in priority-driven cellular adhesion to control cell growth, spatially and directionally. This has been demonstrated previously for controlling cell detachment<sup>14</sup> but the ability to resolve reversible, protein interactions with resolution comparable to the nanoscale, as done in this study and others,<sup>41</sup> provides significant insight into the possibilities of exerting fine, molecular level control over cellular interactions.

## 4.5 Acknowledgements

This work has been supported by the Australian Research Council under the Australian Research Fellowship and DP110104359 (Dr Michael Higgins) and ARC Federation Fellowship of Prof. Gordon Wallace. We also greatly acknowledge the Australian National Fabrication Facility (ANFF) for providing Atomic Force Microscopy instrumentation. MZ and DD acknowledge funding from Science Foundation Ireland (SFI) under the CLARITY CSET award (Grant 07/CE/I1147). We also acknowledge support from the European Commission for funding under grant PIRSES-GA-2010-269302.

## 4.6 References

1. M. A. Cole, N. H. Voelcker, H. Thissen and H. J. Griesser, *Biomaterials*, 2009, **30**, 1827-1850.
2. A. J. Garcia, M. D. Vega and D. Boettiger, *Molecular Biology of the Cell*, 1999, **10**, 785-798.
3. B. G. Keselowsky, D. M. Collard and A. J. Garcia, *Journal of Biomedical Materials Research Part A*, 2003, **66A**, 247-259.
4. J. Nakanishi, Y. Kikuchi, T. Takarada, H. Nakayama, K. Yamaguchi and M. Maeda, *Journal of the American Chemical Society*, 2004, **126**, 16314-16315.
5. B. C. Thompson, R. T. Richardson, S. E. Moulton, A. J. Evans, S. O'Leary, G. M. Clark and G. G. Wallace, *Journal of Controlled Release*, 2010, **141**, 161-167.
6. A. Kotwal and C. E. Schmidt, *Biomaterials*, 2001, **22**, 1055-1064.
7. X. Liu, K. J. Gilmore, S. E. Moulton and G. G. Wallace, *Journal of Neural Engineering*, 2009, **6**.
8. A. S. Rowlands and J. J. Cooper-White, *Biomaterials*, 2008, **29**, 4510-4520.
9. C. E. Schmidt, V. R. Shastri, J. P. Vacanti and R. Langer, *Proceedings of the National Academy of Sciences of the United States of America*, 1997, **94**, 8948-8953.
10. J. Y. Wong, R. Langer and D. E. Ingber, *Proceedings of the National Academy of Sciences of the United States of America*, 1994, **91**, 3201-3204.
11. B. Haimovich, L. Difazio, D. Katz, L. Zhang, R. S. Greco, Y. Dror and A. Freeman, *Journal of Applied Polymer Science*, 1997, **63**, 1393-1400.
12. M. Morra and C. Cassineli, *Journal of Biomaterials Science-Polymer Edition*, 1999, **10**, 1107-1124.
13. W. J. Sung and Y. H. Bae, *Biosensors & Bioelectronics*, 2003, **18**, 1231-1239.
14. J.-I. Edahiro, K. Sumaru, Y. Tada, K. Ohi, T. Takagi, M. Kameda, T. Shinbo, T. Kanamori and Y. Yoshimi, *Biomacromolecules*, 2005, **6**, 970-974.
15. J. Jagur-Grodzinski, *Polymers for Advanced Technologies*, 2006, **17**, 395-418.
16. A. Yasuda, K. Kojima, K. W. Tinsley, H. Yoshioka, Y. Mori and C. A. Vacanti, *Tissue Engineering*, 2006, **12**, 1237-1245.
17. J. Auernheimer, C. Dahmen, U. Hersel, A. Bausch and H. Kessler, *Journal*

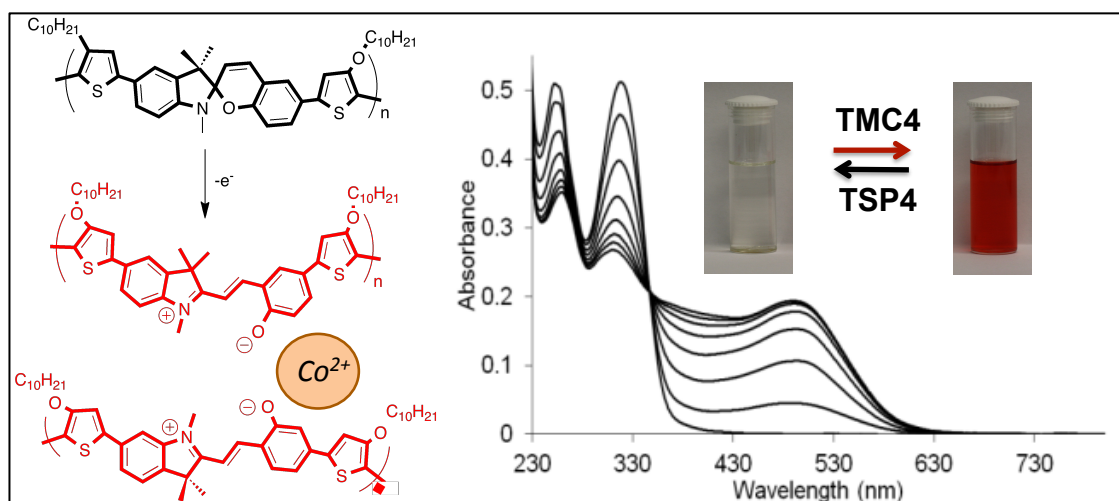
- of the American Chemical Society*, 2005, **127**, 16107-16110.
18. O. H. Kwon, A. Kikuchi, M. Yamato and T. Okano, *Biomaterials*, 2003, **24**, 1223-1232.
  19. O. H. Kwon, A. Kikuchi, M. Yamato, Y. Sakurai and T. Okano, *Journal of Biomedical Materials Research*, 2000, **50**, 82-89.
  20. P. Uhlmann, N. Houbenov, N. Brenner, K. Grundke, S. Burkert and M. Stamm, *Langmuir*, 2006, **23**, 57-64.
  21. A. Garcia, M. Marquez, T. Cai, R. Rosario, Z. Hu, D. Gust, M. Hayes, S. A. Vail and C.-D. Park, *Langmuir*, 2007, **23**, 224-229.
  22. T. Shimboji, E. Larenas, T. Fowler, S. Kulkarni, A. S. Hoffman and P. S. Stayton, *Proceedings of the National Academy of Sciences of the United States of America*, 2002, **99**, 16592-16596.
  23. A. E. Ivanov, N. L. Eremeev, P. O. Wahlund, I. Y. Galaev and B. Mattiasson, *Polymer*, 2002, **43**, 3819-3823.
  24. K. Sumaru, M. Kameda, T. Kanamori and T. Shinbo, *Macromolecules*, 2004, **37**, 4949-4955.
  25. A. Higuchi, A. Hamamura, Y. Shindo, H. Kitamura, B. O. Yoon, T. Mori, T. Uyama and A. Umezawa, *Biomacromolecules*, 2004, **5**, 1770-1774.
  26. N. Katsonis, M. Lubomska, M. M. Pollard, B. L. Feringa and P. Rudolf, *Progress in Surface Science*, 2007, **82**, 407-434.
  27. T. Seki and K. Ichimura, *Macromolecules*, 1990, **23**, 31-66.
  28. S. Stitzel, R. Byrne and D. Diamond, *Journal of Materials Science*, 2006, **41**, 5841-5844.
  29. Y. Bardavid, I. Goykhman, D. Nozaki, G. Cuniberti and S. Yitzchaik, *Journal of Physical Chemistry C*, 2011, **115**, 3123-3128.
  30. K. Wagner, R. Byrne, M. Zanoni, S. Gambhir, L. Dennany, R. Breukers, M. Higgins, P. Wagner, D. Diamond, G. G. Wallace and D. L. Officer, *Journal of the American Chemical Society*, 2011, **133**, 5453-5462.
  31. M. Zanoni, S. Coleman, K. J. Fraser, R. Byrne, K. Wagner, S. Gambhir, D. L. Officer, G. G. Wallace and D. Diamond, *Physical Chemistry Chemical Physics*, 2012, **14**, 9112-9120.
  32. M. Irie, K. Hayashi and A. Menju, *Polymer Photochemistry*, 1981, **1**, 233-242.
  33. G. Joseph, J. Pichardo and G. Chen, *Analyst*, 2010, **135**, 2303-2308.
  34. S. F. Chen, J. Zheng, L. Y. Li and S. Y. Jiang, *Journal of the American Chemical Society*, 2005, **127**, 14473-14478.
  35. S. G. Olenych, M. D. Moussallem, D. S. Salloum, J. B. Schlenoff and T. C. S. Keller, *Biomacromolecules*, 2005, **6**, 3252-3258.
  36. J. Ladd, Z. Zhang, S. Chen, J. C. Hower and S. Jiang, *Biomacromolecules*, 2008, **9**, 1357-1361.
  37. H. P. Erickson, *Proceedings of the National Academy of Sciences of the United States of America*, 1994, **91**, 10114-10118.
  38. H. P. Erickson, N. Carrell and J. McDonagh, *Journal of Cell Biology*, 1981, **91**, 673-678.
  39. Y. Mao and J. E. Schwarzbauer, *Matrix Biology*, 2005, **24**, 389-399.
  40. M. L. Smith, D. Gourdon, W. C. Little, K. E. Kubow, R. A. Eguiluz, S. Luna-Morris and V. Vogel, *Plos Biology*, 2007, **5**, 2243-2254.
  41. A. Gelmi, M. J. Higgins and G. G. Wallace, *Small*, 2013, **9**, 393-401.
  42. K. Gilmore, M. Kita, Y. Han, A. Gelmi, M. Higgins, S. Moulton, G. Clark, R. Kapsa and G. Wallace, *Biomaterials*, 2009, **30**, 5292-5596.

- 
43. M. Bergkvist, J. Carlsson and S. Oscarsson, *Journal of Biomedical Materials Research Part A*, 2003, **64A**, 349-356.
  44. K. Svennersten, M. H. Bolin, E. W. H. Jager, M. Berggren and A. Richter-Dahlfors, *Biomaterials*, 2009, **30**, 6257-6264.
  45. A. Gumus, J. P. Califano, A. M. D. Wan, J. Huynh, C. A. Reinhart-King and G. G. Malliaras, *Soft Matter*, 2010, **6**, 5138-5142.
  46. A. M. D. Wan, R. M. Schur, C. K. Ober, C. Fischbach, D. Gourdon and G. G. Malliaras, *Advanced Materials*, 2012, **24**, 2501-2505.



# CHAPTER 5

## A Merocyanine–Based Conductive Polymer



### Publication Status: PUBLISHED

K. Wagner, M. Zanoni, A. B. S. Elliott, P. Wagner, R. Byrne, L. E. Florea, D. Diamond, K. C. Gordon, G. G. Wallace, D. L. Officer, *Journal of Materials Chemistry C*, **2013**, DOI: 10.1039/c3tc30479e.

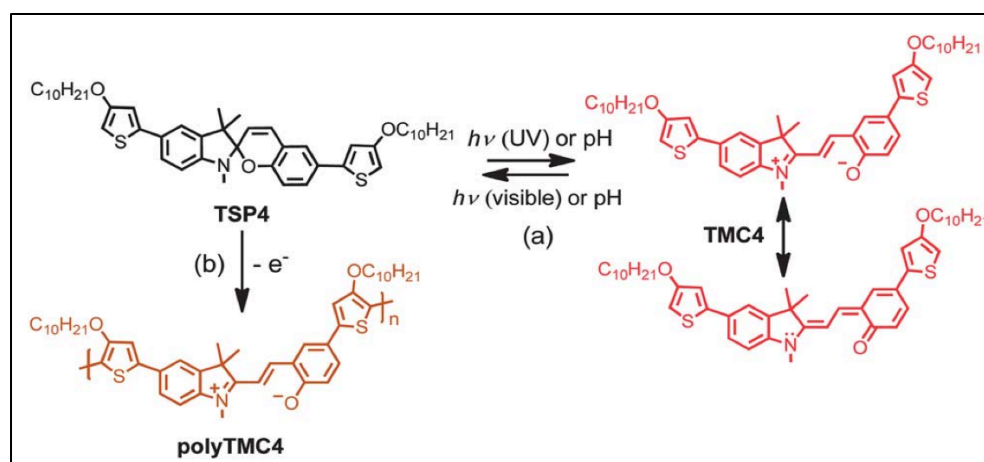
*For the supplementary information section see Appendix C*

**Abstract**

We report the first example of a conducting polymer with a merocyanine incorporated into the polymer backbone by electropolymerisation of a spiropyran moiety covalently linked between two alkoxythiophene units. Utilizing the known metal coordination capabilities of merocyanines, introduction of cobalt ions into the electropolymerisation led to an enhancement of the conductivity, morphology and optical properties of the polymer films.

## 5.1 Introduction

Spiropyrans (**SPs**) are one of the most widely studied classes of photoswitchable compounds, whose molecular structure can be altered after exposure to light, temperature, pH or electrochemistry. Under these conditions, heterolytic cleavage of the spiro carbon-oxygen bond of **SPs** typically occurs, producing a merocyanine (**MC**).<sup>1</sup> Incorporation of **SPs** into other materials such as polymers<sup>2</sup> provides a way to attenuate the inherent properties of the polymer such as fluorescence,<sup>3, 4</sup> self assembly,<sup>5</sup> and surface properties.<sup>6</sup> In this regard, we have demonstrated the potential of combining the photoswitchability of **SPs** with the electroactivity of conducting polymers.<sup>7</sup> This was achieved for monomers with covalently linked **SPs** pendant on the polymer backbone. Here, we describe a new **MC**-based conducting polymer, **polyTMC4**, in which a dithiophenespiropyran monomer leads to the incorporation of the **MC** moiety into the polymer backbone (Scheme 5.1). The dithiophenespiropyran monomer **TSP4** was readily prepared from the dibromospiropyran with thiopheneboronic acid via a double Suzuki coupling reaction. The synthesis details are given in Appendix C, as is the characterization data, which is typical of a substituted **SP**.



**Scheme 5.1:** (a) **TSP4** and its stimuli induced zwitterionic and quinoidal isomers that contribute to the open form **TMC4** and (b) **TSP4** electrochemical polymerization.

## 5.2 Results and Discussion

The synthesis details and the analytical characterization of **TSP4** are reported in Appendix C. Irradiation of a near colourless solution of **TSP4** with UV light leads to the formation of the violet **TMC4** (Figure 5.1 (a)), as evidenced by the peak at 490 nm. The same coloration (490 nm) is obtained through an acid-induced ring opening reaction

(Figure 5.1 (b) and details in Appendix C). After adding base to the acidified solution, it becomes colourless, and the spectra exhibit the original 215 nm and 315 nm peaks. It seems, therefore, that the ability of the **SP** unit in **TSP4** to respond to light and to acid in the solution state in a manner typical of **SPs**<sup>1</sup> is still preserved when it is substituted with thiophene moieties.

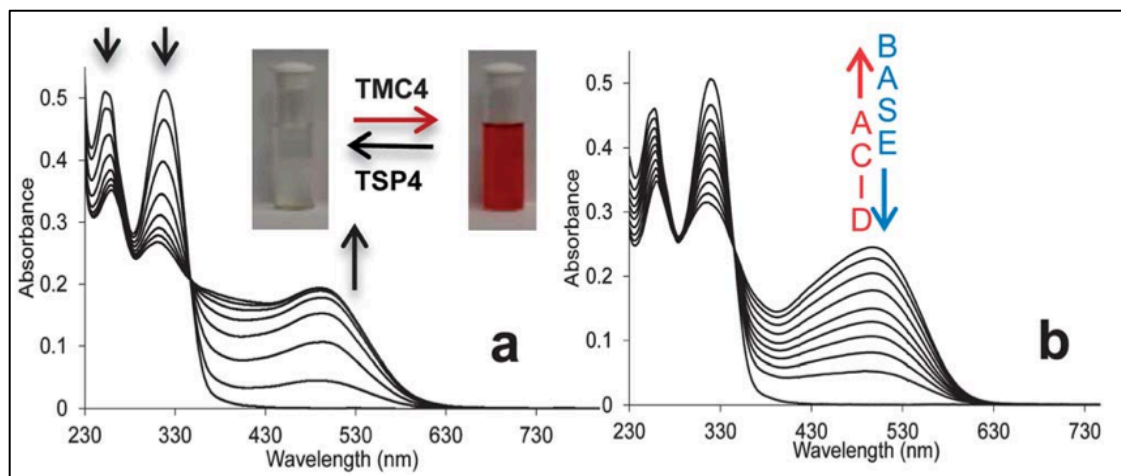


**Figure 5.1:** UV-*vis* spectra of **TSP4** monomer after (a) irradiation with 254 nm UV light; (b) after adding an excess of acid and then base in a 1:1 DCM-MeOH mixture.

The electro response of **TSP4** upon cycling the solution between 0 and 0.8 V is very similar to that reported previously.<sup>7,8</sup> The irreversible oxidation peak (I) at 0.64 V (Appendix C, Figures C1 and C2) is described in the literature<sup>7,9</sup> as the one-electron oxidation of the spiro compound at the indoline nitrogen, which leads to isomers of oxidized merocyanines. This is, as expected, a diffusion-controlled process, concluded from the linear relationship between the current of the peak (I) and the square root of the scan rate (Appendix C, inset Figure C1). When the electropolymerisation of **TSP4** is carried out up to 1.2 V (Figure 5.2), a second peak (II) at 1.1 V is visible and polymer film forms on the surface of the electrode. This second oxidation is related to the electron removal from the thiophene unit. The lower potential (0.64 V) for the spiropyran oxidation leads to electroisomerization of the spiropyran **TSP4** into merocyanine **polyTMC4** during film deposition. Post-polymerization CV analysis (Figure 5.2, inset) revealed three oxidation peaks at 0.25, 0.41 and 0.60 V and three reductions at 0.22, 0.39 and 0.70 V. These types of voltammetric responses are typical for polythiophenes and are associated with the complex mechanisms of the charging-discharging processes taking place upon reverse cycling.<sup>10</sup> The colour of the oxidized film is bluish and orange when the film is reduced, typical of a conducting polymer (see inset, Figure 5.3).

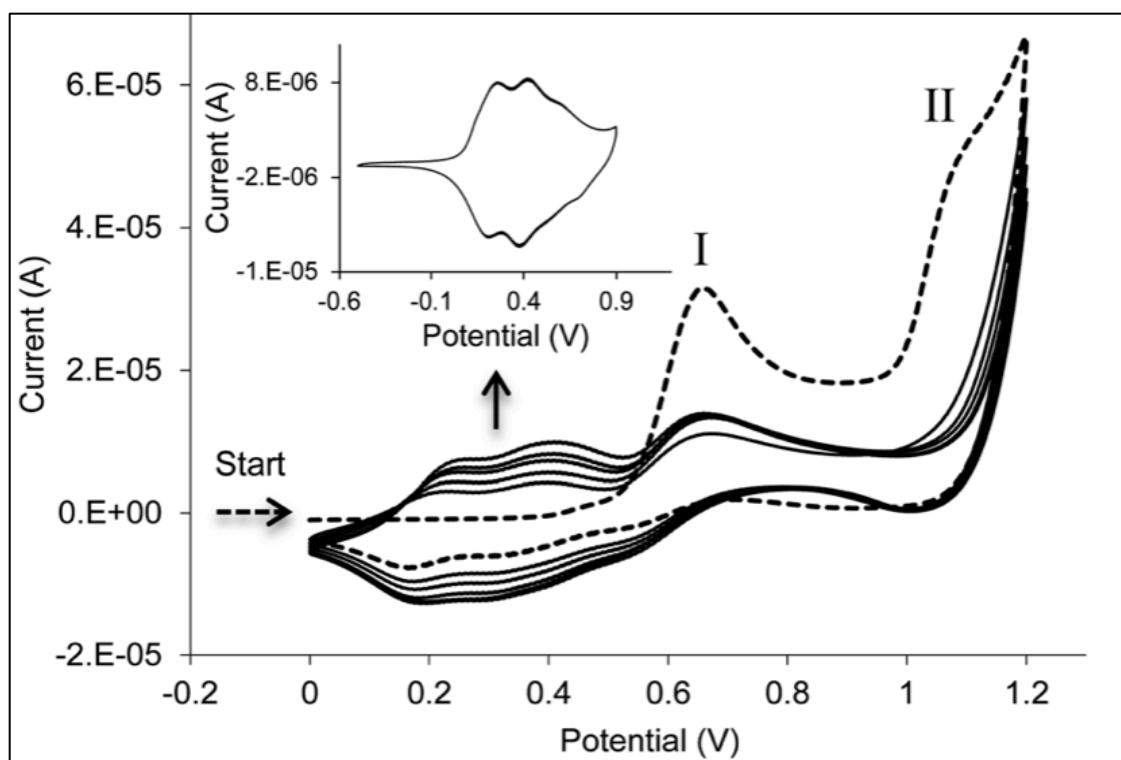


**Figure 5.2:** Electrochemical deposition of  $8 \times 10^{-3}$  M TSP4 between 0 and +1.2 V with the first scan marked as a dotted line. The inset shows the post CV voltammogram of **polyTMC4** on a platinum disc electrode. All scan rates are  $100 \text{ mV s}^{-1}$ .

To further investigate the absorption behavior of **polyTMC4**,<sup>45</sup> the spectral properties of the film were examined across the potential range used for the post-CV analysis ( $-0.5 \rightarrow 0.9 \text{ V}$ ) (Figure 5.3). **PolyTMC4** exhibited quite a complex spectral pattern, atypical of the common polythiophene.

The reduced spectrum exhibited two peaks at 425 nm and 510 nm. As the applied potential is increased from  $-0.5$  to  $0.3 \text{ V}$ , both peaks are decrease and new absorbances at 680, 820 and 930 nm are observed. The absorbance at 510 nm, which we attribute to the oxidized **MC** in the **polyTMC4**,<sup>7</sup> start to rise again when the potential exceeds  $0.4\text{V}$ . Since the peak at 510 nm is present in the reduced and oxidized spectra, we conclude that the **MC** form is trapped in the polymer backbone. To the best of our knowledge, this is the first example of a backbone incorporated merocyanine-based conducting polymer.

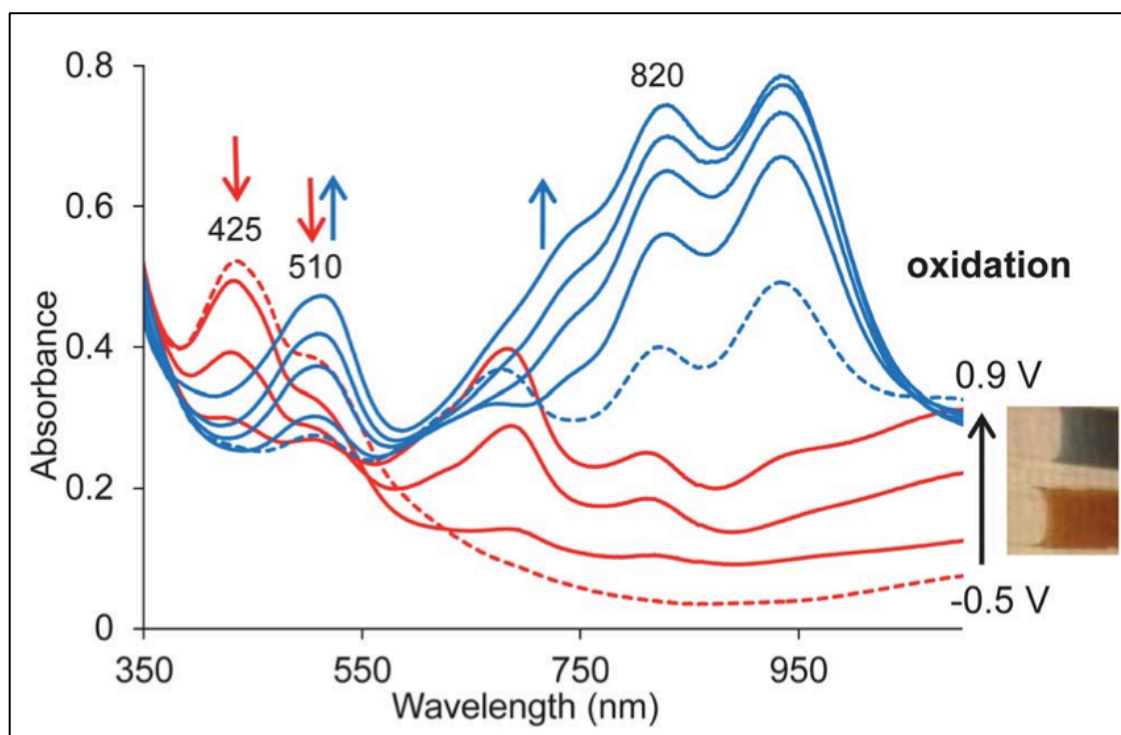


**Figure 5.3:** Spectroelectrochemistry of electrodeposited **polyTMC4** on ITO glass for potential ranges of -0.5V (red dotted line) to 0.9 V, with photograph showing colours of reduced (orange) and oxidized (blue) films. The blue dotted line (0.4 V) indicates the beginning of growth of the 510 nm peak.

Support for the assignment of an **MC** structure and the nature of the electronic spectra was obtained from computational chemistry and Raman spectroscopy. DFT calculations on the neutral and oxidized forms of models of **polySP4** and **polyTMC4**, bis(dithiophene)-substituted spiropyran **BDSP** and merocyanine **BDMC** (Figure 5.4 (a)) respectively, were carried out in order to obtain simulated Raman spectra and probe the electronic structure of the neutral and oxidized polymers.

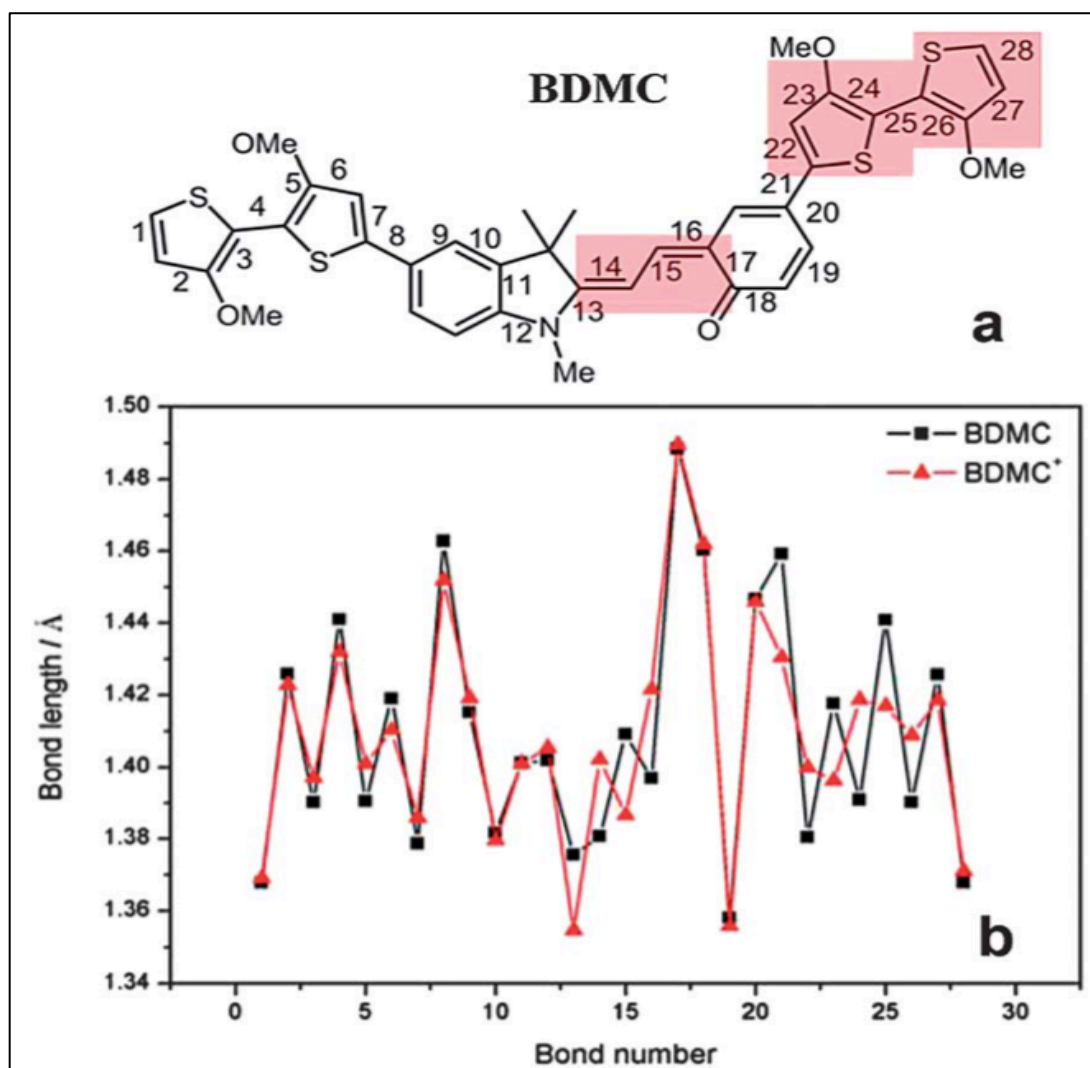


**Figure 5.4:** (a) Bis(dithiophene)-substituted **BDMC** with bond numbering and shaded boxes indicating where the radical cation is localized; (b) bond length alternation diagram of the calculated neutral and oxidized **BDMC**.

The experimental Raman spectra of the oxidized and neutral films of **polyTMC4** both show features more closely matching the simulated Raman spectra of the monomer unit in the **MC** over **SP** form (Appendix C, Figures C5 and C6). This is fully consistent with the electronic absorption spectra (Figures 5.3) and supports the proposal that both the neutral and oxidized polymers are in the **MC** form. Given the similarities of the neutral and oxidized **polyTMC4** Raman spectra, we were interested in determining the extent to which the **MC** moiety was involved in the polymer oxidation. A bond length alternation diagram<sup>11</sup> (Figure 5.4 (b)) was constructed from the calculated geometries of the neutral and oxidized **BDMC** in order to visualize the structure of the radical cation. The major bond length changes occur on bonds 13-16, the **MC** component, and 21-28, one of the dithiophenes. This extra conjugation effect on only one of the two dithiophenes is consistent with the planarity of that segment; with respect to the **MC**

portion, the calculated dihedral angles of the dithiophene moieties for the neutral **BDMC** are  $-22^\circ$  and  $-26^\circ$  (around bond 8 and around bond 21 respectively), while for the oxidized **BDMC** they are  $13^\circ$  and  $0^\circ$  respectively. In the experimental Raman spectra, the neutral polymer shows an enhancement of the band at  $1410\text{ cm}^{-1}$ ; a single strong band is predicted. Upon oxidation, three strong bands in the  $1400\text{--}1470\text{ cm}^{-1}$  are predicted and these are observed at  $1407$ ,  $1439$  and  $1474\text{ cm}^{-1}$ .

TD-DFT calculations were also undertaken in order to predict electronic properties such as the nature of the electronic transitions for the neutral and oxidized **BDMC** calculations (Appendix C, Figure C7). In good agreement with the experimental electronic absorption data (Figure 5.3), the neutral calculation is dominated mainly by higher energy bands while the oxidized one includes the lower energy transitions. These transitions can be described as charge-transfer in nature. The calculated electron density changes for the transitions show, for the neutral species, a decrease at the indole dithiophene (bonds 1-8, Figure 5.4a) and an increase at the phenol and indole rings (bonds 9-20). In contrast, for the cationic species, the electron transfer is from the quinone dithiophene (bonds 22-28) to dithiophene bonds 9-20.

One of the exciting features of this type of conducting polymer is the potential to control its conductivity with light by way of spiropyran formation. However, both oxidized and reduced polymer films of this merocyanine-based polymer proved unresponsive to either ultraviolet or visible light. This may not be surprising given that, as we observed previously for a spiropyran- substituted poly(terthiophene),<sup>7</sup> the planar merocyanine-containing polymer would likely form a highly compact solvent- excluded film as a result of interchain stacking and merocyanine aggregation making it sterically and energetically difficult to form the spiropyran.

The presence of the conjugated **MC** in the polymer presented the opportunity to influence the polymer properties by metal ion coordination. It is well established that **MCs** interact with a variety of divalent metal ions such as  $\text{Co}^{2+}$ .<sup>2, 12</sup> Conductive metallo-polymers have been prepared for different polymer architectures,<sup>13</sup> include polythiophenes.<sup>14, 15</sup> To achieve maximum interaction between the polymer and the metal, the metal ligands were incorporated directly into the polymer backbone (inner sphere), which allows strong coupling between the orbitals of the metal and those involved in the electronic conduction.<sup>16</sup> Therefore, we investigated the interaction of **polyTMC4** with cobalt.

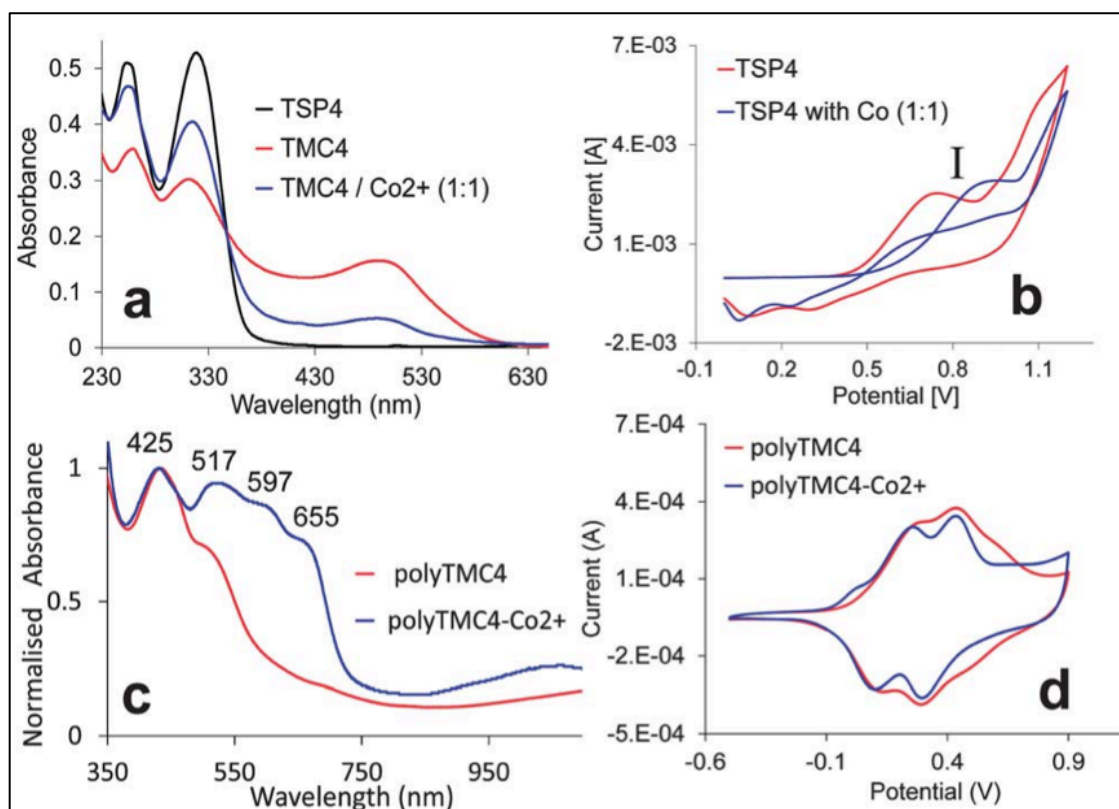


**Figure 5.5:** (a) absorbance spectra of  $2 \times 10^{-5}$  M **TSP4** (black line), **TMC4** (red line) and **TMC4** with  $\text{Co}^{2+}$  (1 : 1) (blue line); (b) cyclic voltammetry of  $8 \times 10^{-3}$  M **TSP4** (red line) and **TSP4** with  $\text{Co}^{2+}$  (1 : 1) (blue line) on ITO glass; (c) reduced spectrum of **polyTMC4** (red line) and **polyTMC4-Co<sup>2+</sup>** (blue line); (d) post CV voltammogram of **polyTMC4** (red line) and **polyTMC4-Co<sup>2+</sup>** (blue line) on ITO electrode at the scan rate  $100 \text{ mV s}^{-1}$ .

To probe the interaction between **TMC4** and  $\text{Co}^{2+}$  in solution, a UV-Vis spectroscopic study was undertaken. **TSP4** exhibits a spectrum with two peaks 215 nm and 315 nm (Fig. 5.5 (a) and expanded in Appendix C, Figure C2 for clarity) and as expected, exposure of the solution to 254 nm UV light, generated merocyanine **TMC4** (Fig. 5.5 (a), dashed line,  $\lambda_{\text{max}} = 490 \text{ nm}$ ). The addition of  $\text{Co}^{2+}$  to the merocyanine solution changes the spectrum with a decrease of the 490 nm peak and the appearance of a low intensity peak at 415 nm (see Appendix C, Figure C2 inset, dotted line). As a similar spectrum has been previously reported,<sup>12, 17</sup> we propose the formation of a merocyanine-cobalt complex, presumably as a result of the interaction of two neighboring **MC** phenolate groups with  $\text{Co}^{2+}$ . However, it should be noted that the intensity of the 215 nm and 315 nm peaks, ascribed to the spiropyran, increased upon  $\text{Co}^{2+}$  addition, suggesting that  $\text{Co}^{2+}$  not only complexed to **TMC4** but also augmented spiropyran formation. Therefore, it is likely that the **TMC4-Co<sup>2+</sup>** complex is not particularly strong and the resulting solution is an equilibrium mixture of **TSP4/TMC4/TMC4-Co<sup>2+</sup>**.

When electrochemical cycling of **TSP4** is performed on ITO 95 glass, (Figure 5.5 (b),

red line) the potential of **SP** oxidation (I) is 0.72 V. After the addition of cobalt ions (1:1), the position of the peak (I) shifted 170 mV more positive (EI = 0.89 V, Fig. 5.5 (b), blue line), indicative of a higher activation barrier for the oxidation of the species present in solution and consistent with the increase in 100 spiropyran formation on  $\text{Co}^{2+}$  addition to **TSP4** as observed in the UV-visible spectrum (Fig. 5.5 (a)). The second difference between **TSP4** electrochemistry with  $\text{Co}^{2+}$  ions is the presence of the “nucleation loop” (Figure 5.5 (b), blue line), which involves a crossover effect in the voltammogram on the reverse sweep of the first cycle.

This phenomenon was first described by Pletcher and coworkers<sup>18</sup> and, in the case of conductive polymers, is interpreted as the start of the nucleation process, resulting from an autocatalytic reaction between charged oligomers and the starting monomer.<sup>19</sup> This suggests that a different nucleation and growth occurs for **polyTMC4** in the presence of  $\text{Co}^{2+}$ , which should significantly affect the resulting film morphology. However, the post CV of **polyTMC4-Co<sup>2+</sup>** (Figure 5.5 (d) blue line) on ITO retained a similar shape voltammogram to **polyTMC4** (Figure 5.5 (d) red line) on the same electrode. Scanning electron micrographs of the **polyTMC4** films were obtained and are shown in Appendix C, Fig. C4. It can be clearly seen that **polyTMC4** itself initially grows as a flat film firmly adhered to the electrode surface, with subsequent growth of coral-like structures off this layer (Appendix C, Figure C4 (a)). This kind of dual growth mechanism, proposed by Schrebler *et al.*<sup>20</sup> and described as formation of the dense film by 2D nucleation and growth followed by oxidative swelling (3D growth), may account for this film morphology. In contrast, the growth of **polyTMC4-Co<sup>2+</sup>** film (Appendix C, Figure C4 (b)) is more uniform, distinguished by a “grainy” looking morphology, and a better quality film, demonstrating that the  $\text{Co}^{2+}$  does indeed have a significant influence on polymer growth and film morphology.

A comparison of the spectroelectrochemistry of a **polyTMC4-Co<sup>2+</sup>** film (Appendix C, Figure C3) with that of **polyTMC4** (Figure 5.3) showed a much broader band for the reduced Co-containing polymer, with two additional peaks present at 597 nm and 655 nm (clearly visible only in the case of thin films) (Figure 5.5 (c) blue line and Appendix C, Figure C3 red dotted line). This is consistent with an increased effective conjugation length for the **polyTMC4-Co<sup>2+</sup>** film. In contrast, there is little difference between the oxidized forms of the two polymers.

Supporting these observations of increased effective conjugation length is the conductivity of **polyTMC4-Co<sup>2+</sup>**, which was found to be 11.1 S/cm, two orders of magnitude higher than that for **polyTMC4** (0.1 S/cm). While this may simply be due to

the  $\text{Co}^{2+}$  ion affecting the polymer chain conformations or interchain interactions, the participation of the  $\text{Co}^{2+}$  ion in the conduction pathway cannot be ruled out.

In order to probe the character of the polymer film as well as the effect of the  $\text{Co}^{2+}$  ion treatment, the experimental Raman spectra of both oxidized and reduced **polyTMC4** and **polyTMC4-Co<sup>2+</sup>** were compared (Appendix C, Figures C5 and C6). There are negligible differences between the polymer and the  $\text{Co}^{2+}$  infused polymer for both the oxidized and reduced forms. This implies minimal structural differences with incorporation of the  $\text{Co}^{2+}$ .

This is consistent with the elemental analysis of the **polyTMC4-Co<sup>2+</sup>** film, which shows that the film contains only 0.23 wt% cobalt. This corresponds to around one cobalt ion every thirty **TMC4** units, thus implying that the  $\text{Co}^{2+}$  ion influences the polymer structure and morphology without being strongly complexed to the **MC**.

### 5.3 Conclusions

In summary, electropolymerisation of a spiropyran moiety covalently linked between two alkoxythiophene units leads to incorporation of merocyanine into the polymer backbone. The electrochemical and spectroscopic (UV-Vis, FT-Raman supported with TD-DFT calculations) data, demonstrate that the merocyanine form is trapped in the polymer backbone. While the resulting polymer is indeed electroactive, incorporation of a small amount of cobalt ions into the polymer film modifies the film properties and significantly enhances its conductivity.

### 5.4 Acknowledgements

Financial support from the Australian Research Council, the EU IRSES Program, the University of Otago and MacDiarmid Institute for Advanced Materials and Nanotechnology in New Zealand, and Science Foundation Ireland (SFI) under the CLARITY CSET award (Grant 07/CE/I1147) with the support from the European Commission (Grant PIRSES-GA-2010- 269302) are gratefully acknowledged for funding this research. The assistance of Tony Romeo and Fargol Bijarbooneh at the UoW Electron Microscopy Centre is also acknowledged.

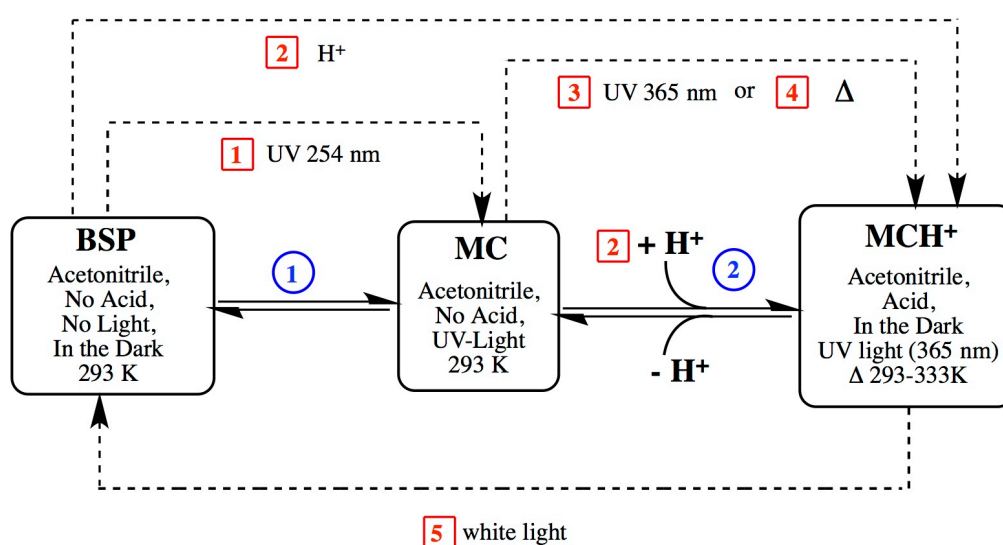
## 5.5 References

1. V. I. Minkin, *Chemical Reviews*, 2004, **104**, 2751-2776.
2. L. Florea, D. Diamond and F. Benito-Lopez, *Macromolecular Materials and Engineering*, 2012, **297**, 1148-1159.
3. Y.-H. Chan, M. E. Gallina, X. Zhang, I. C. Wu, Y. Jin, W. Sun and D. T. Chiu, *Analytical Chemistry*, 2012, **84**, 9431-9438.
4. J. Chen, D. Wang, A. Turshatov, R. Munoz-Espi, U. Ziener, K. Koynov and K. Landfester, *Polymer Chemistry*, 2013, **4**, 773-781.
5. L. Ma, J. Li, D. Han, H. Geng, G. Chen and Q. Li, *Macromolecular Chemistry and Physics*, 2013, **214**, 716-725.
6. H. Schenderlein, A. Voss, R. W. Stark and M. Biesalski, *Langmuir*, 2013, **29**, 4525-4534.
7. K. Wagner, R. Byrne, M. Zanoni, S. Gambhir, L. Dennany, R. Breukers, M. Higgins, P. Wagner, D. Diamond, G. G. Wallace and D. L. Officer, *Journal of the American Chemical Society*, 2011, **133**, 5453-5462.
8. M. N. Campredon, G. Giusti, R. Guglielmetti, A. Samat, G. R. Gronchi, A. Alberti and M. Benaglia, *Journal of the Chemical Society, Perkin Transactions 2*, 1993, 2089.
9. M. J. Preigh, M. T. Stauffer, F.-T. Lin and S. G. Weber, *Journal of the Chemical Society, Faraday Transactions*, 1996, **92**, 3991.
10. J. Roncali, *Chemical Reviews*, 1992, **92**, 711-738.
11. T. M. Clarke, K. C. Gordon, D. L. Officer and D. K. Grant, *Journal of Chemical Physics*, 2006, **124**.
12. R. J. Byrne, S. E. Stitzel and D. Diamond, *Journal of Materials Chemistry*, 2006, **16**, 1332-1337.
13. B. J. Holliday and T. M. Swager, *Chemical Communications*, 2005, 23-36.
14. M. O. Wolf, *Advanced Materials*, 2001, **13**, 545-553.
15. S. S. Zhu and T. M. Swager, *Advanced Materials*, 1996, **8**, 497-&.
16. T. L. Stott and M. O. Wolf, *Coordination chemistry reviews*, 2003, **246**, 89-101.
17. A. Radu, S. Scarmagnani, R. Byrne, C. Slater, K. Tong Lau and D. Diamond, *Journal of Physics D: Applied Physics*, 2007, **40**, 7238-7244.
18. S. Asavapiriyant, G. K. Chandler, G. A. Gunawardena and D. Pletcher, *Journal of Electroanalytical Chemistry*, 1984, **177**, 229-244.
19. J. Heinze, A. Rasche, M. Pagels and B. Geschke, *Journal of Physical Chemistry B*, 2007, **111**, 989-997.
20. R. Schrebler, P. Grez, P. Cury, C. Veas, M. Merino, H. Gomez, R. Cordova and M. A. del Valle, *Journal of Electroanalytical Chemistry*, 1997, **430**, 77-90.



# CHAPTER 6

## Spiropyran-Terthiophene multi-modal molecular switches: photochromic, acidochromic and electrochromic properties



**Publication status: In preparation.**

M. Zanoni, K. Wagner, R. Byrne, S. Gambhir, K.J. Fraser, P. Wagner, G. G. Wallace, D. L. Officer and D. Diamond, "Spiropyran-Terthiophene multi-modal molecular switches: photochromic, acidochromic and electrochromic properties", In preparation (June, 2013).

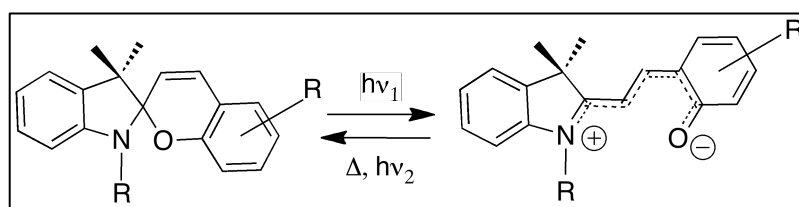
*For supplementary information section see Appendix D*

## Abstract

This work describes the synthesis, photochromic, acidochromic and electrochromic properties of three new spiropyran moieties, 1',3',3'-trimethylspiro(chromene-2,2'-indolin)-6-yl acetate (**BSPe**) two of which are Photo-electroactive spiropyran terthiophene derivatives; 1',3',3'-trimethylspiro(chromene-2,2'-indolin)-6-yl-4,4''-bis(decyloxy)-(2,2':5',2''-terthiophene))-3'-acetate (**BSP6**) and 1',3',3'-trimethylspiro[chromene-2,2'-indolin]-6-yl-4,4''-bis(decyloxy)-(2,2':5',2''-terthiophene)-3'-carboxylate (**BSP7**). The difference between **BSP6** and **BSP7** is a single methylene group in the linking functionality, but this singularity was found to be responsible for differing behaviour of the two molecules, an example being the different rates of protonation found ( $3.38 \times 10^{-4} \text{ s}^{-1}$  for **BSP6** and  $0.90 \times 10^{-4} \text{ s}^{-1}$  for **BSP7**). A study of the photochromic properties of **MCe**, **BSP6** and **BSP7** was carried out in diluted solutions (up to  $10^{-4} \text{ M}$ ). The photoinduced formation of **MCe** from **BSPe** follows a similar process to that of **BSP6** and **BSP7**, however the reverse reaction leads to irreversible molecular aggregates, which were also studied through SEM analysis. The analysis of the acidochromic behaviour was supported by a detailed thermodynamic analysis of the protonation reaction. This showed that **MCe** was the strongest base among the merocyanine isomers, suggesting that the chemical reactivity of **BSP6** and **BSP7** is influenced by the presence of the terthiophene. The spectral properties of the electrochemically generated **pBSP6** and **pBSP7** showed some unique features for **pBSP7**: the polymer was not completely reduced at -0.4 V and when the voltage applied was 0.85 V a new peak appeared at 460 nm. For both polymers the electro-generated **MC** reached the steady state at 1.2 V. Both polymers were found to be photoresponsive upon illumination with 254 nm UV light through generation of the **MC** isomer. Interestingly, the photo-induced **pMC7** presented a hypsochromic shift to 541 nm (from 556 nm), the peak at 383 nm was lost and a higher absorbance (0.49 units compared to 0.3 units) occurs. Prolonged illumination with white light induced the re-formation of the band at 383 nm, which was assigned to **BSP**. **pMC6** displayed similar behaviour, and furthermore, after illumination with white light, a shoulder at 476 nm appeared, indicating the formation of aggregates. SEM and AFM confirmed different structural conformations for **pBSP6** and **pBSP7**, at different potentials (oxidized or reduced) that further demonstrated the influence of the electrochemically switched spiropyran functionality on the polymer morphology. The conductivity of the freestanding polymers was found to be  $19.1 \text{ S/cm}^{-1}$  (**pBSP6**) and  $18.3 \text{ S/cm}^{-1}$  (**pBSP7**).

## 6.1 Introduction

The properties of a novel family of photo- and electro-active polymers based on benzospiropyran and terthiophene attached to a common molecular backbone have been investigated. Spiropyran (**BSP**) is member of a widely studied family of molecules that quickly isomerizes between two states under photochemical stimulation (one colourless, **BSP** and one highly coloured, **MC**, Scheme 6.1).<sup>1</sup> Initially described by Hirschberg and Fischer in the early 1950's,<sup>2, 3</sup> **BSP**'s still attract a high level of interest and attention due to their broad range of potential applications such as memory devices and photoresponsive molecular sensors.<sup>1, 4</sup> The rapid inter-conversion between **BSP** and its thermodynamically stable isomer, **MC**, can be controlled by external stimuli, such as UV light and illumination with wavelengths in the visible region (photochromism),<sup>2, 5-7</sup> thermal modulation of the local environment (thermochromism)<sup>8, 9</sup> or electrochemical variation of the electronic state (electrochromism).<sup>10</sup> The zwitterionic merocyanine isomer (**MC**) is susceptible to binding with certain metal ions (most favourable are the d- and f-element) due to the phenolate anionic site<sup>11, 12</sup>. Furthermore the phenolate anion of the **MC** isomer is readily protonated under acidic conditions to the **MCH**<sup>+</sup> form (pKa 4 - 8).<sup>13-16</sup> Similar photo-switchable binding activity has been shown also with DNA, amino acids, metal ions and organic ions to form a range of **MC**-Guest species.<sup>17-19</sup> The ability to make spiropyrans derivatives with enhanced binding activity that can be modulated using external stimulation via accessible synthetic steps is a key factor driving a significant proportion of the research into these molecules.<sup>1, 12</sup> These groups can significantly influence spiropyrans photochemistry when substituted at positions 6 and 8 (i.e., the pyran portion of the molecule) and, together with solvent polarity and viscosity, they can improve the quantum yield of **MC** coloration and also influence the kinetics of ring-opening and ring closure.<sup>8, 20, 21</sup>



**Scheme 6.1:** Reversible photo and thermochromism of a generic **BSP** (left) to the **MC** isomer (right).

Electroactive molecules have attracted considerable attention since their first description in 1978 by Chiang *et al.*, due in part to their ability to electrochemically switch between two (or more) isomers that in some cases exhibit dramatically differing

properties.<sup>22-25</sup> Poly-terthiophene (**pTTh**) based conducting polymers have been the focus of particular attention in this regard and to date, a wide number of procedures have been reported for the substitution of functional groups and chromophores on to polythiophenes, in order to broaden their original characteristics.<sup>26-34</sup> However, the incorporation of large functionalities onto a terthiophene monomer can introduce a significant steric effect that can considerably affect the optical and electronic properties of the monomer and the related polymer processability.<sup>7,35</sup> To avoid this issue, 4, 4''-dialkoxy-3-substituted terthiophenes are typically used as precursors for developing novel derivatives with reduced steric interactions between the polymer backbone and the substituents, and thus allowing improved control of the polymer regiochemistry.<sup>26,30,36</sup> Alkoxy side chains are also able to activate the monomer for polymerization and ensure better polymer processability.<sup>26,37,38</sup> Other interesting properties previously reported in the literature include thermochromism, ionochromism, photochromism and biochromism.<sup>30,36</sup> Chromic variations are generated by conformational changes or folding of the polymer chains, with consequent dramatic variation in the conjugation length of the whole system, which can be followed using spectroscopy.

The combination of conjugated  $\pi$ -systems with photoactive molecular switches has opened the way of the development of a completely new class of materials that is only beginning to be reported in the literature.<sup>7, 35, 39, 40</sup> As the spirocyanine substituent is connected orthogonal to the polymer backbone (Scheme 6.2), it can have an effect on the overall extent of conjugation of the system, influencing the properties and the distribution of the  $\pi$ -electrons in the structure.<sup>7</sup> Therefore, combining polythiophene scaffolds with photochromic moieties could lead to new materials with switchable optical and electronic characteristics. Recent publications have reported the successful substitution of thiophene with chromophores, such as azobenzene, on side chains, in order to achieve a double photochromism (one contribution from the side functional group and the other from the polymer backbone) together with improved conductivity and resistance to fatigue.<sup>41, 42</sup>

An important quality previously described for BSP is its chromo-reversibility when exposed to an external source of energy (photonic, thermal or electrochemical). A significant challenge during the synthesis process is the direct substitution of the chromophore on the monomer constituting the building unit: the pathway chosen is monomer functionalization first and polymerization of the modified monomer second,

and this strategy must not affect the structure and the functionality of both the switching units.

In this study two different TTh-based monomers were functionalized and characterized with a hydroxyl-benzospiropyran moiety covalently bound to the central thiol unit. The new derivatives (and their respective polymers) have been given the identifiers **BSP6 (pBSP6)** and **BSP7 (pBSP7)**. The electrochromism and conductivity of these new hybrid materials have been investigated from the spectrochemical, electrochemical and spectroelectrochemical perspective. Furthermore the effect of the spacer linking the chromophore to the monomer unit must be considered as this can affect the overall characteristics of the derivative. For this purpose, a new spiropyran derivative (**BSPe**) bearing methyl-ester functionality in position 6 has been prepared in order to understand the influence of the linker group.

## 6.2 Experimental

Experimental details (synthesis & analytical techniques) are given in Appendix D.

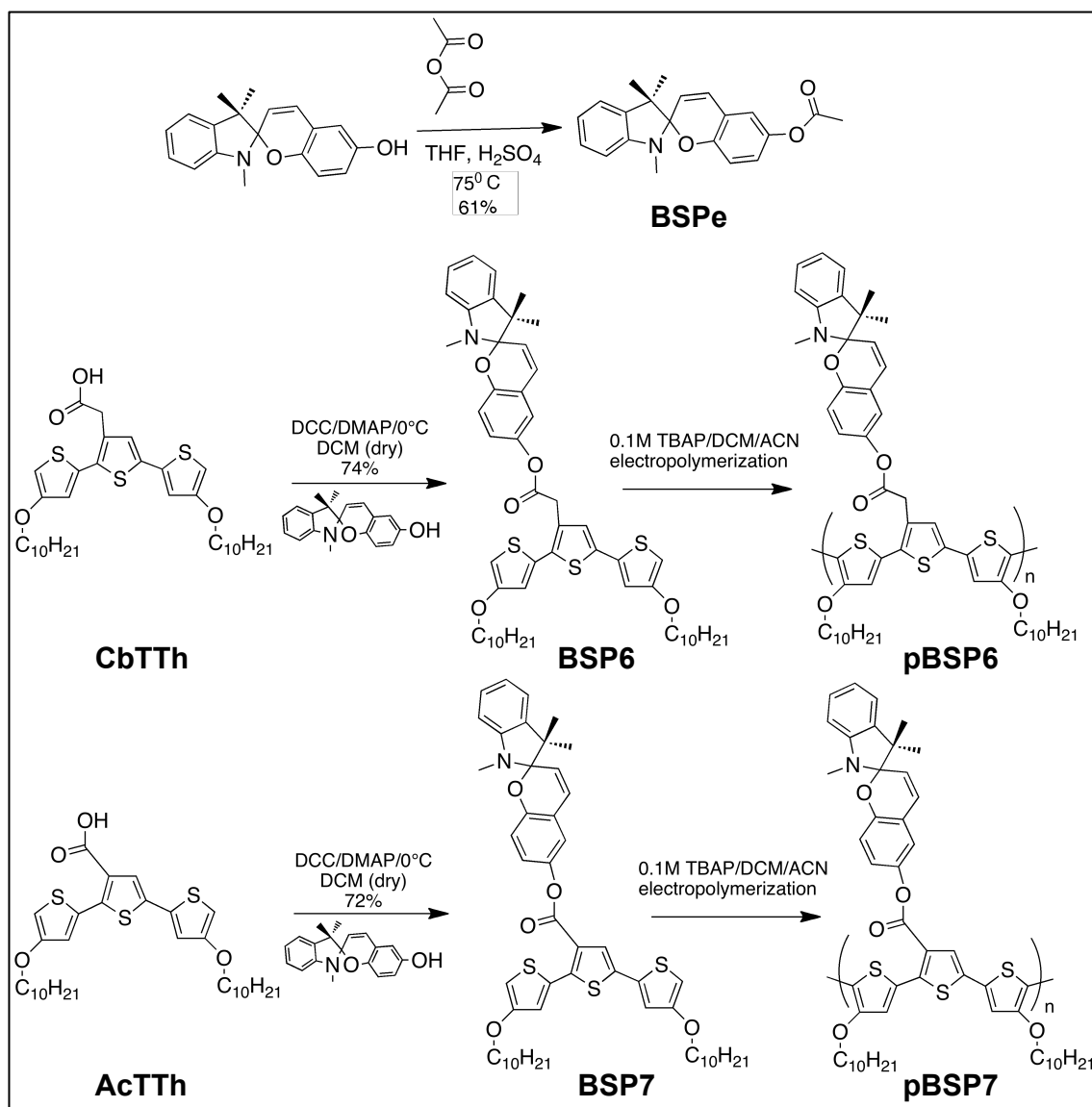
## 6.3 Results and Discussion

### 6.3.1 Synthesis of BSPe, BSP 6 & BSP7

**BSPe** was synthesised in order to understand the role of the methyl-ester functionality substituted at position 6 on the spiropyran moiety using the same experimental conditions as for the other monomers. For the preparation of **BSPe**, particular attention was paid to the control of the humidity of the glassware. All flasks used were carefully washed with 1M solutions of NaOH in ethanol and dried overnight in a drying cabinet. Purification of the crude product was achieved by a step gradient change of the eluent composition. This was due to the progressive opening of the spiropyran induced by interactions with the silica inside the column.  $^1\text{H}$  NMR was used to confirm the product, where the singlet at  $\delta$  2.65 and the simultaneous lack of the signal at  $\delta$  5.69 (**BSP5** phenolic hydroxyl group) indicated the formation of the desired ester.

In the past, we have employed successful strategies when covalently immobilising BSP onto polymers, silica and micro-beads.<sup>19,43</sup> In this case, we decided to prepare the photochromic monomer first; this was made possible by utilizing terthiophene chemistry developed by Officer *et. al.*<sup>26</sup> **BSP6** and **BSP7** were synthesized by base

catalysed condensation of **BSP5** with terthiophene acetic acid (**AcTTh**) and terthiophene carboxylic acid (**CbTTh**), Scheme 6.2. It can be seen from the structures that the two monomers have a small but significant structural difference arising from the single methylene group in the ester functionality, i.e., the linker between the two main units of these monomers.  $^1\text{H}$  NMR confirmed this important difference: the two spectra are comparable except for an additional signal at  $\delta$  3.77 (extra-methylene in the tether).



**Scheme 6.2:** synthesis and molecular structures of **BSPe**, **BSP6** and **BSP7** and electrochemical polymerization of **pBSP6** and **pBSP7**.

## 6.3.2 Photochemistry study

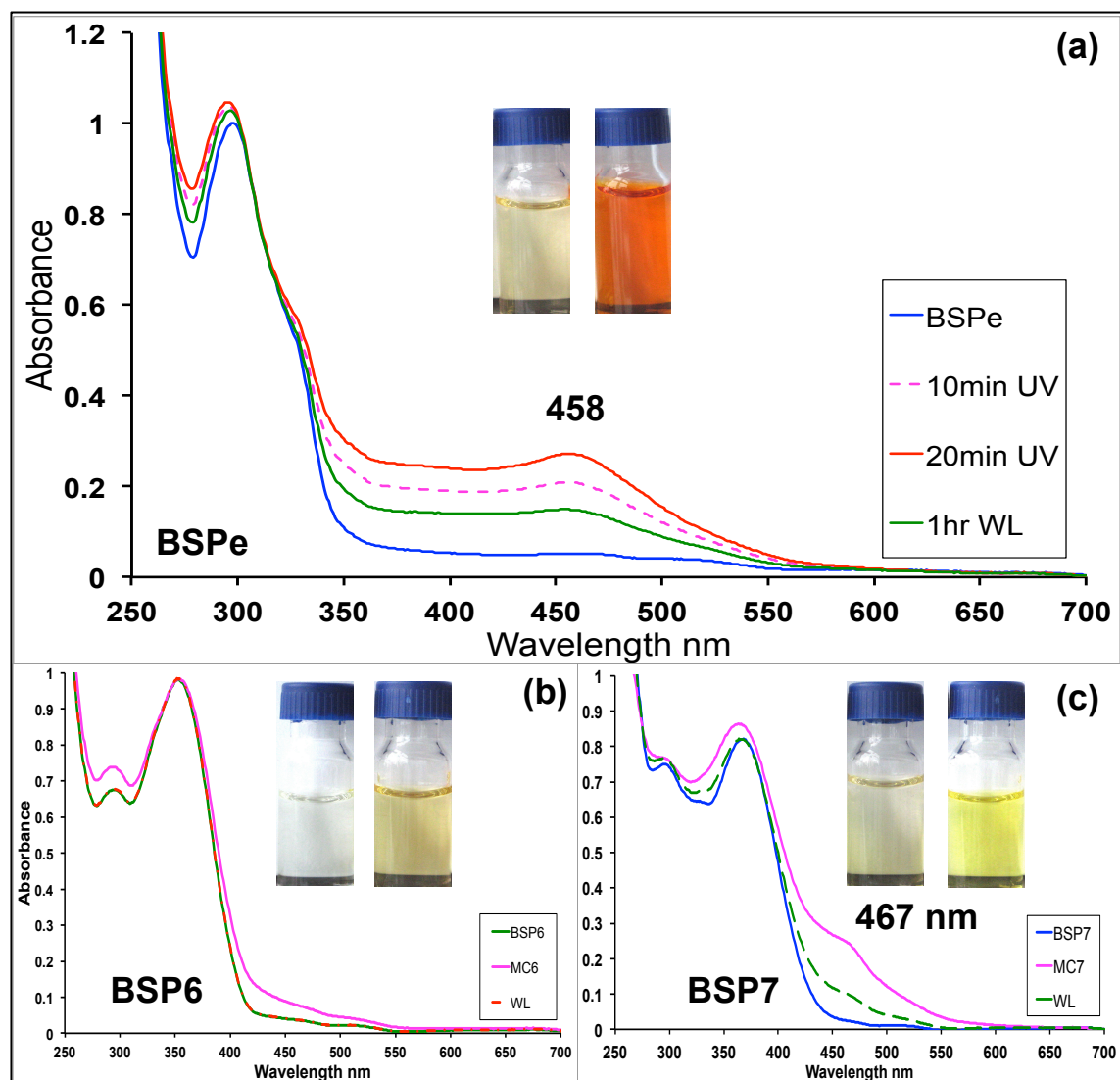
### 6.3.2.1 Photochemical generation of MC isomers

Figure 6.1 (a) shows changes in the UV-*vis* spectrum that accompany the photo-induced isomerization of **BSPe** (blue line, maximum at 294 nm) to **MCE** (red line,  $\lambda_{\max}$  = 458 nm) after illumination with a 254 nm UV light for 20 minutes. Upon standing in the dark, the stock solution of **BSPe** turned from colourless to pale pink. This unusual behaviour was studied by UV-*vis*, NMR and High Resolution Mass Spectroscopy (Figures D1-3). Figure D4 (a) shows effects that are consistent with spontaneous aggregation in a polar solvent (Acetonitrile) for **BSPe**, with the formation of the two new absorbance bands at 510 nm and 544 nm over time. In these experiments, a stock solution of **BSPe** was diluted up to  $10^{-4}$  M in acetonitrile and kept sealed under inert atmosphere. This solution was monitored every day for 120 days with the UV-*vis* in the dark and under N<sub>2</sub>. The bands at 510 and 544 nm are normally associated with merocyanine aggregation species, but in this case only a minimal increase in intensity was observed (0.1 to 0.2 for the band at 544 nm) when illuminated with a 254 nm UV light source (Figure D4 (b)). The most striking feature is the formation of a new broad signal with a maximum at 420 nm, and the solution changes from colourless to orange (Figure 6.1 (a) and Figure D4 (b)). Complete spectra are given in the inset. When the **MC** isomer is then exposed to white light, the band at 420 nm did not revert back to the **BSP** isomer, instead a new absorbance band appears at 471 nm (a 51 nm bathochromic shift). However, when the **BSP** isomer solution is illuminated for 5 minutes at 254 nm, the **MC** peak is completely recovered. These illumination cycles were repeated 30 times using the same solution at room temperature, (see Appendix D, Figure D4 (c)). This behaviour can be ascribed to the irreversible formation of J-aggregates during the isomerization process.<sup>45</sup> Furthermore, in Figure D4 (c) the photo-induced formation of new aggregation species is suggested by the appearance of a band at 377 nm.

NMR and High Resolution Mass Spectroscopy analysis suggests that the **BSPe** isomer does not dimerize in the conditions observed, and that these aggregation phenomena are electrostatic in nature (see Appendix D, Figures D1, D2 and D3).

To further support this SEM was used to observe the surface morphology. A  $10^{-4}$  M solution of **BSPe** was prepared and 100  $\mu$ l added to a glass slide. The solution was then dried under a N<sub>2</sub> flow for 30 min under white light illumination until the solvent was evaporated and the sample was prepared for SEM analysis. The surface morphology of

**BSPe** show globular structures with an average size of 20  $\mu\text{m}$  alternated with platelet structures of approximately the same size, (see Appendix D, Figure D5 (a)-(f)). Upon closer inspection of the platelets, the presence of a high density of globules on their surface, with a sub-micrometre diameter (Figure D5 (f)) can be seen. Uznanski has previously reported similar structures in his work,<sup>46</sup> but in that case, the aggregates were formed in a non-polar environment.



**Figure 6.1:** UV-vis spectra of: (a)  $10^{-5}$  M solutions in acetonitrile of **BSPe** (blue line) and the photonic generated **MCe** (irradiated 5 minutes at 254 nm red line) and the resulting new aggregates of **BSPe** after 5 minutes irradiation with white light (green line). (b)  $10^{-4}$  M solutions in acetonitrile of **BSP6** (green line), the photonic generated **MC6** (irradiated 5 minutes at 254 nm, pink line) and the white light induced **BSP6** (5 minutes, dashed-red line). (c)  $10^{-4}$  M solutions in acetonitrile of **BSP7** and the photonic generated **MC7** (5 minutes at 254 nm, pink line) and the resulting **BSP7** after 5 minutes irradiation with white light (dashed-green line).

Normally, the photochemical isomerization of spiropyran to the intensively coloured merocyanine species occurs rapidly when a diluted solution is irradiated with a 365 nm light source.<sup>7</sup> For the derivatives reported, this process is inhibited by the electron donor effect of the ester linker in position 6 and by the presence of the terthiophene functionality, with  $\pi$ - $\pi$  interactions between the two aromatic units of the spiro and the 3-ring system of the terthiophene. Therefore the stacked configuration between the two units (additionally favoured in **BSP6** by the flexibility provided by the extra methylene carbon) and the intramolecular  $\pi$ - $\pi$  interactions require higher energy to allow formation of the **MC** isomers.<sup>7</sup> **MC6** and **MC7** spectra obtained from diluted solutions in acetonitrile after 5 minutes illumination with a 254 nm light source can be seen in Figure 6.1 (b) and (c). All solutions were kept in the dark for 24 hrs at 293 K to establish thermodynamic equilibrium prior to UV illumination. In Figure 6.1 (b), the absorbance at ca. 296 nm is greater for **MC6** compared to **BSP6**, whereas this band is comparable for **BSP7** and **MC7** (Figure 6.1 (c)). This suggests that there is a change in the electronic structure of **MC6** relative to **BSP6**, which does not occur with **BSP7/MC7**.<sup>7</sup> It has been previously found that the introduction of an electron-withdrawing group (-NO<sub>2</sub> or -OCH<sub>3</sub>) at the 6, 8 position of the benzopyran moiety,<sup>21</sup> together with an increase in the polarity of the solvent, will stabilize the more highly coloured trans form of the zwitterionic **MC** isomer.<sup>47, 48</sup> For these derivatives, the presence of the **MC isomer** cannot be identified via a new peak arising between 550 and 600 nm in the spectrum. In this case, **MC6** and **MC7** are characterised (after, 5 min illumination at 254 nm) by broad bands between 500 nm and 430 nm for **MC6** and between 550 nm and 440 nm for **MC7**. The formation of the **MC7** is apparent from the increase in absorbance centred on 467 nm (Figure 6.1 (b) and (c)). It was observed that after 5 minutes of white light illumination, **BSP6** was fully re-generated, whilst **MC7** had a slower back-isomerization rate.

### 6.3.2.2 Protonation of BSPe, BSP6 and BSP7

Figures 6.2 (a) and (b) show the impact of addition of dilute HCl on solutions of **MC6** and **MC7** in acetonitrile over a period of 3000 s at 293 K.

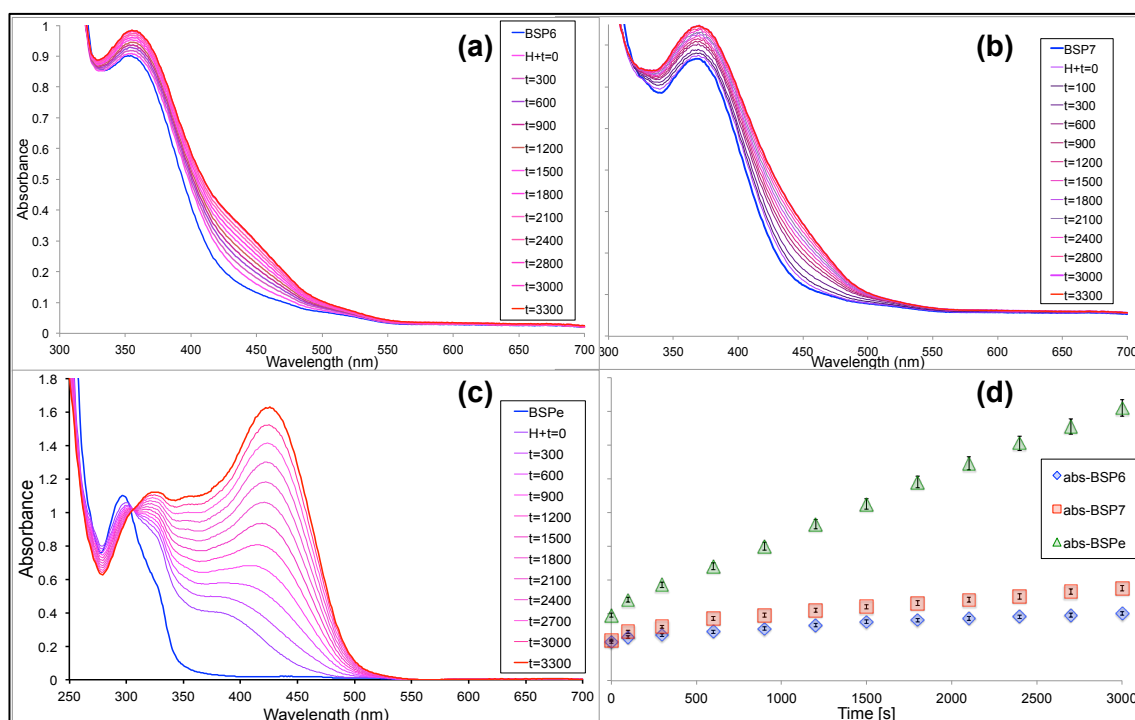


**Figure 6.2:** UV-vis spectra of showing the effect of protonation in acetonitrile of 3 ml of  $10^{-4}$  M solutions of (a) **BSP6** (b) **BSP7**, (c) **BSPe** due to the formation of their respective  $\text{MCH}^+$  species. Spectra collected every 300 s after addition of 100  $\mu\text{l}$  HCl ( $3.2 \times 10^{-3}$  M). (d) Increasing absorbance at the  $\lambda_{\text{max}}$  for each of the  $\text{MCH}^+$  isomers. Error bars are the standard deviation of 3 replicate experiments. The y scale of (b) and (d) are the same as (a) and (c). Omitted for clarity.

When **BSP6** and **BSP7** (3 ml,  $10^{-4}$  M in acetonitrile) are acidified with 100  $\mu\text{l}$  HCl ( $3.2 \times 10^{-3}$  M), changes in the spectra arising from the formation of protonated merocyanine ( $\text{MCH}^+$ ) occur (Figure 6.2 (a) and (b)). From the plots (Figure 6.2 (d)), it can be seen that in all cases the reaction was not complete (less than 100% **BSP** converted into the  $\text{MCH}^+$ ) in the time scale of the experiment (3300 s). For both monomers, the intensity of the signal at  $\sim 350$  nm increased during the protonation process. We ascribe this to the presence of the  $\text{MCH}^+$  isomer, a hypothesis that is supported by the observed reversibility during the de-protonation process of this band. The acid-induced formation of  $\text{MCeH}^+$  occurs according to a similar process, but with a higher yield of formation of the protonated merocyanine ((Figure 6.2 (c)). This is most likely due to either the difference in pKa or the ease of access to the **BSPe**, which, in contrast to **BSP6** and **BSP7**, does not possess a terthiophene group. Furthermore, the shape of the  $\text{MCeH}^+$

band is markedly different, appearing more defined, and more importantly it appears that the ester functional group associated with the peak at 544 nm is not involved in the process of protonation (its intensity does not change and therefore it is not affected).

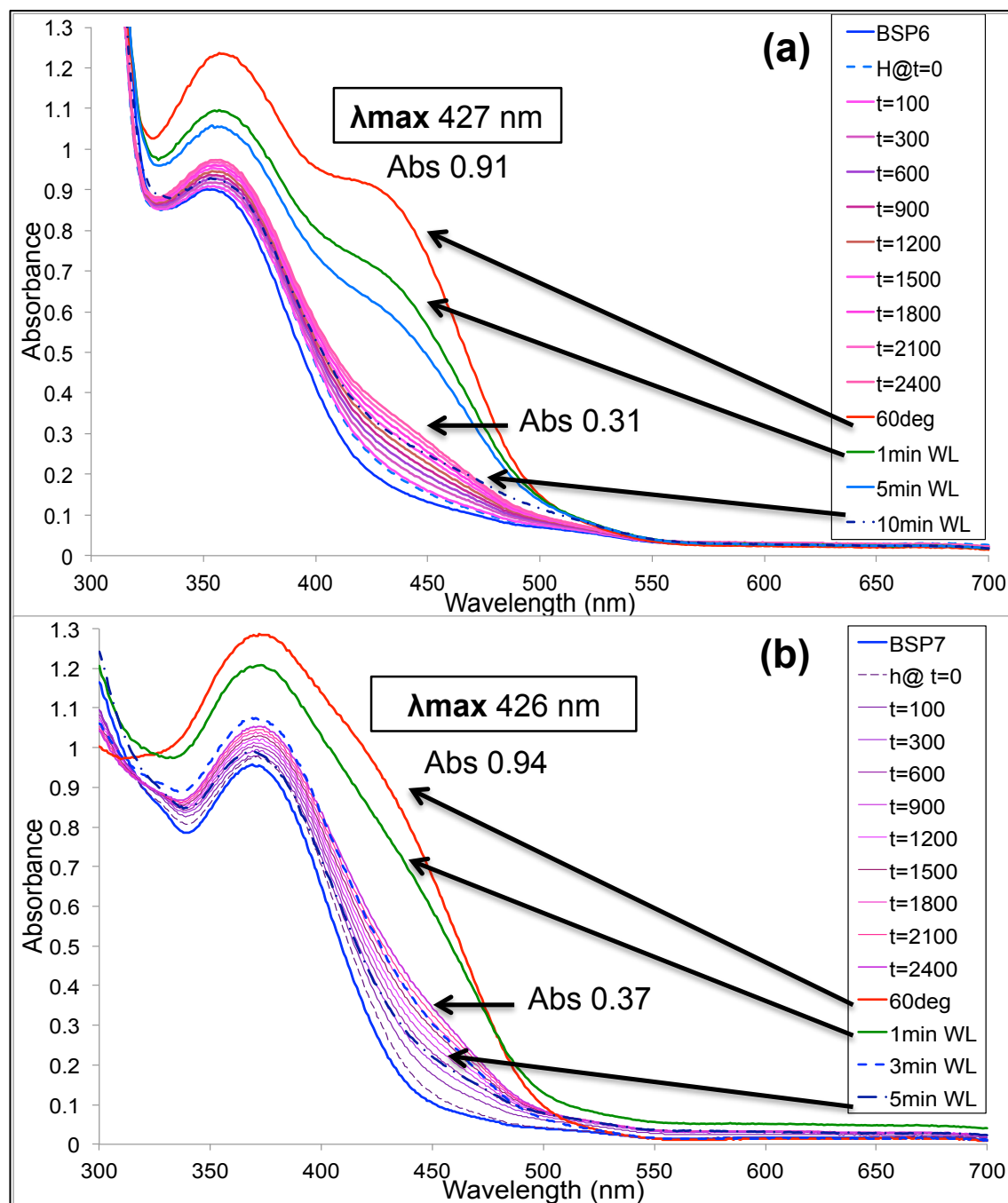


**Figure 6.3:** Thermally induced protonation for the processes (a)  $\text{BSP6} + \text{H}^+ \rightarrow \text{MC6H}^+$  and (b)  $\text{BSP7} + \text{H}^+ \rightarrow \text{MC7H}^+$ .

At room temperature and in absence of light, the protonation process is relatively slow for both **BSP6** and **BSP7**. Figure 6.3 (a) and (b) shows a gradual increase around 440 and 460 nm, occurring over a period up to 40 minutes and reaching a maximum absorbance of 0.31 (**MC6H<sup>+</sup>**, Figure 6.3 (a)) and 0.37 (**MC7H<sup>+</sup>**, Figure 6.3 (b)). Upon heating to 343 K, the absorbance increases ca. 3 fold, 0.91 for **MC6H<sup>+</sup>** (Figure 6.3 (a)) and 0.94 for **MC7H<sup>+</sup>** (Figure 6.3 (b)) in a much shorter time frame (75 seconds). Further heating of the solutions to higher temperatures (348 K, 353 K and 358 K) did not affect these absorbances, and this observation allows us to conclude that a thermodynamic steady state has been reached in acetonitrile at 343 K for both **MC6H<sup>+</sup>** and **MC7H<sup>+</sup>**. When the samples at 343 K are exposed to white light, the absorbance in both cases are reduced from 0.91 to 0.28 at 447 nm and 0.94 to 0.23 at 454 nm, respectively, as the protonated merocyanine reverts to the spiropyran (**MC6H<sup>+</sup>** → **BSP6+H<sup>+</sup>** and **MC7H<sup>+</sup>** → **BSP7+H<sup>+</sup>**). One interesting observation is that if both **BSP6** and **BSP7** are left in the dark overnight at 293 K in acidified acetonitrile, the same steady state spectra are reached, similar to the those observed at 343 K (0.90 for **MC6H<sup>+</sup>** and 0.92 for **MC7H<sup>+</sup>**, see Figure D6, Appendix D). This suggests that the spectral changes occurring in both cases are primarily due to a kinetic effect rather than a shift in the equilibrium in favour of **MCH<sup>+</sup>**.

### 6.3.2.3 Photo reversibility of protonation for **BSP6** and **BSP7**.

In Figure 6.4 (a) and (b) the UV-vis spectra (100  $\mu$ L of  $3.2 \times 10^{-3}$  M HCl in acetonitrile) shows the effect of LED induced protonation (UV) and de-protonation (white light) tests performed on the processes **MC6H<sup>+</sup>** → **BSP6+H<sup>+</sup>** and **MC7H<sup>+</sup>** → **BSP7+H<sup>+</sup>**. The absorbance after UV illumination in each case (ca. 0.55) is comparable; suggesting that the degree of formation of **MCH<sup>+</sup>** is similar in both cases observed. The absorbance after illumination with visible light is much lower for **MC6H<sup>+</sup>** than **MC7H<sup>+</sup>**, (0.3 vs. 0.45). Clearly, the kinetics of the forward and reverse processes are faster for **BSP6+H<sup>+</sup>** ⇌ **MC6H<sup>+</sup>** than **BSP7+H<sup>+</sup>** ⇌ **MC7H<sup>+</sup>**. It is found that **BSP6** and **BSP7** exhibit little tendency to switch to **MC6** and **MC7** when exposed to 254 nm light,<sup>1</sup> most likely due to the electron donor nature of the group in position 6. However this process was achievable when the **BSP6** and **BSP7** solutions in acetonitrile were acidified.

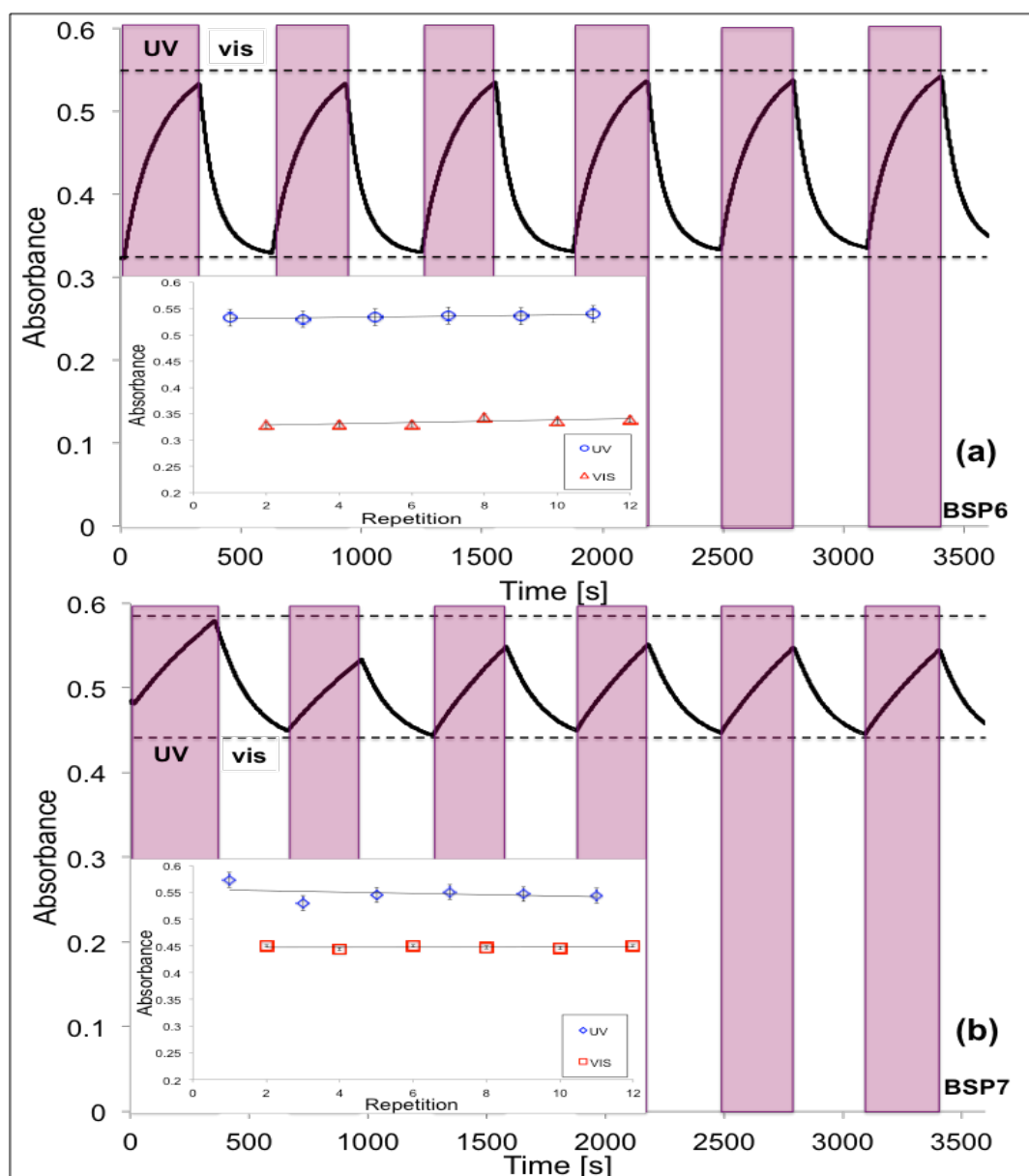


**Figure 6.4:** UV-vis absorbance “on-off” spectra of LED induced (a)  $\text{MC6H}^+ \rightarrow \text{BSP6} + \text{H}^+$  monitored at 447 nm and (b)  $\text{MC7H}^+ \rightarrow \text{BSP7} + \text{H}^+$  monitored at 453 nm after addition of 100  $\mu\text{l}$  HCl ( $3.2 \times 10^{-3}$  M).

#### 6.3.2.4: Photochromic and acidochromic effect on BSP/MC equilibria.

Figure 6.5 shows the two linked equilibria that describe the  $\text{BSP/MC/MCH}^+$  system. Normally (at room temperature, no acid present) equilibrium process 1 is primarily on the left hand side, favouring **BSP**. Illumination with UV light increases the amount of **MC** present, shifting the equilibrium process 1 to a limited extent towards the right hand side. Acidification leads to rapid protonation of **MC** to  $\text{MCH}^+$  (equilibrium process 2), and equilibrium process 1 shifts to generate more **MC**. This continues until the  $\text{MCH}^+$  form predominates.

With UV light (254 nm) we affect the equilibrium process 1 (Figure 6.5) by favouring the formation of **MC**; however, not all the **BSP** is converted into the **MC** (Figure 6.1 (b), (c)). Upon the addition of acid this small amount of **MC** rapidly becomes protonated (pka value, 4-7)<sup>49-51</sup> to **MCH<sup>+</sup>**, which lowers the concentration of **MC** and shifts the equilibrium to favour the right hand side (Figure 6.5). In doing so, this disturbs equilibrium process 1, which shifts to maintain the **MC** concentration; this process continues leading to the conversion of **MC** to **MCH<sup>+</sup>** (equilibrium process 2).

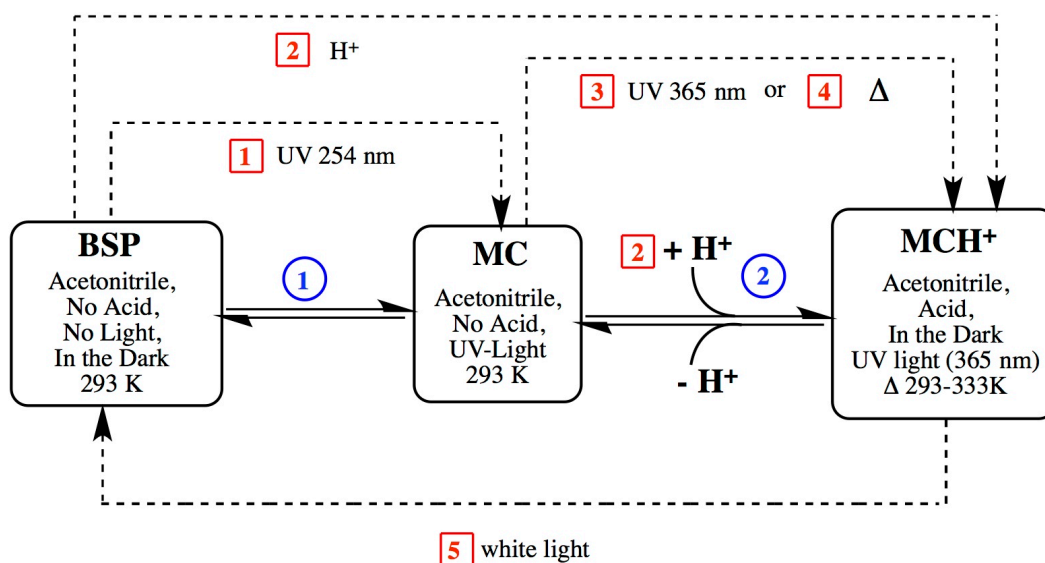


**Figure 6.5:** The blue circles indicate the main equilibria states between **BSP**, **MC** and **MCH<sup>+</sup>**. The red squares indicate the stimulus applied that influence the equilibria of **BSP**, **MC** and **MCH<sup>+</sup>** where 1: UV light 254 nm, 2: Acidichromism ( $3.2 \times 10^{-3}$  M HCl), 3: UV light (365 nm), 4: Heat and 5: White light (> 470 nm)

### 6.3.3 Kinetics of protonation

In Figure 6.6 (a), (b) and (c) the time vs. absorbance plots of **BSPe**, **BSP6** and **BSP7** are shown under three different conditions; (1) rate of protonation in presence of 100  $\mu$ l of HCl  $10^{-3}$  M, (2) rate of de-protonation in the presence of white light and (3) the rate of de-protonation under UV light. In all cases the temperature was kept constant at 293 K.

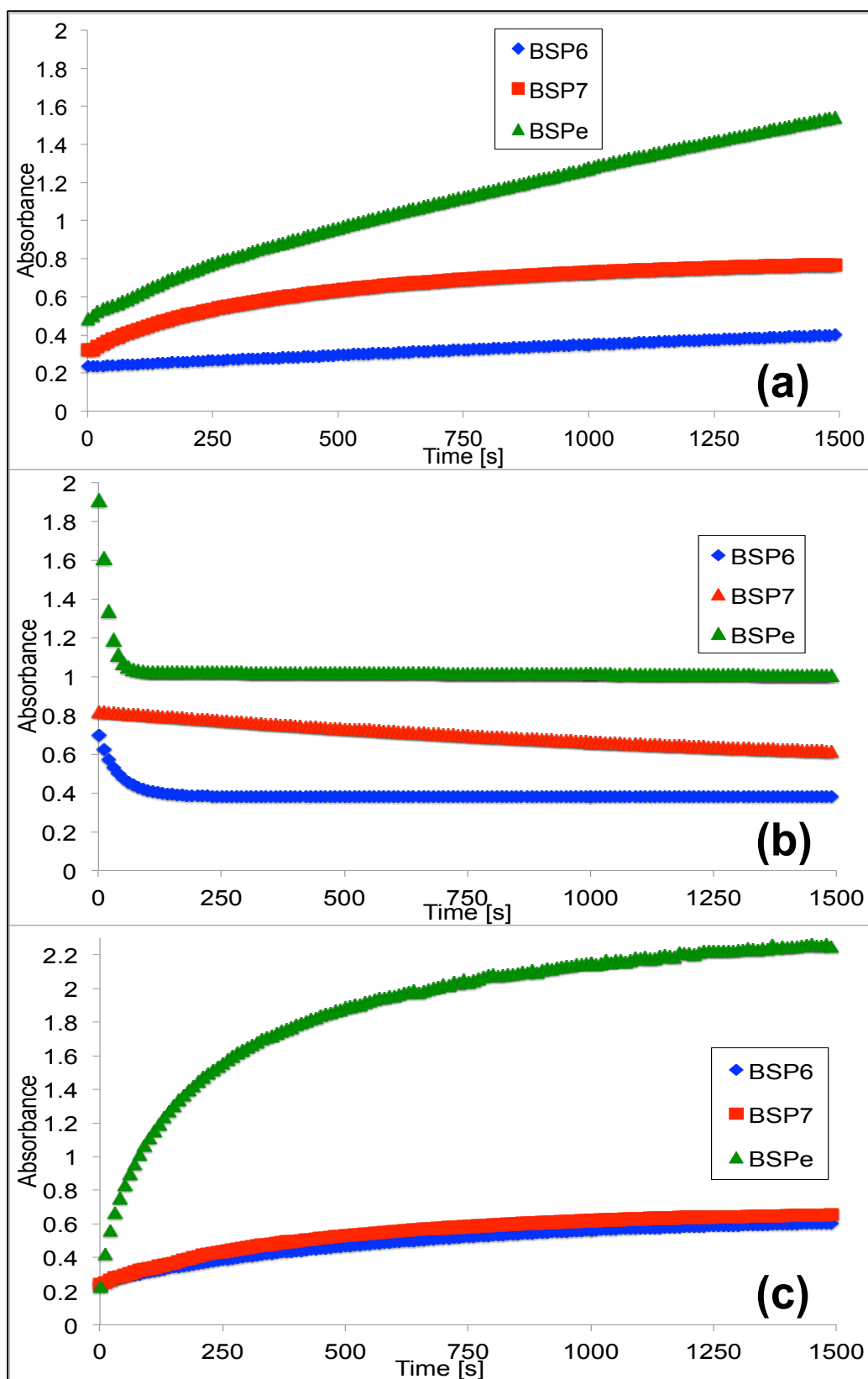


**Figure 6.6:** (a) Kinetics of protonation for **BSPe**, **BSP6** and **BSP7** over time, (b) kinetics of white light-assisted de-protonation for **MCeH<sup>+</sup>** ( $\lambda_{\text{max}} = 424$  nm), **MC6H<sup>+</sup>** ( $\lambda_{\text{max}} = 447$  nm) and **MC7H<sup>+</sup>** ( $\lambda_{\text{max}} = 453$  nm) and (c) kinetics of UV light (365 nm) assisted protonation after addition of 100  $\mu$ l HCl ( $3.2 \times 10^{-3}$  M). Each measurement was repeated for  $n = 3$  times.

**Table 6.1:** rate constants  $k$  for the processes of protonation (from Figure 6.5(a)), light-assisted deprotonation (from Figure 6.5(b)) and UV-assisted protonation (from Figure 6.5(c)) for **MCeH<sup>+</sup>**, **MCH<sup>+</sup>6** and **MCH<sup>+</sup>7**. Results averaged from 3 replicates. Standard deviations values are reported in brackets.

Molecule	$\lambda_{\max}$ for MC-H <sup>+</sup> /nm	Abs (after 5 min under illumination)	protonation $k$ (s <sup>-1</sup> )	de-protonation $k$ (s <sup>-1</sup> )	UV-protonation $k$ (s <sup>-1</sup> )
<b>BSPe</b>	424	2.33	$1.29 \times 10^{-3}$ ( $\pm 0.03$ )	$5.71 \times 10^{-2}$ ( $\pm 0.1$ )	$1.17 \times 10^{-2}$ ( $\pm 0.09$ )
<b>BSP6</b>	447	0.47	$3.38 \times 10^{-4}$ ( $\pm 0.09$ )	$1.48 \times 10^{-3}$ ( $\pm 0.07$ )	$2.15 \times 10^{-3}$ ( $\pm 0.04$ )
<b>BSP7</b>	453	0.59	$9.00 \times 10^{-4}$ ( $\pm 0.05$ )	$5.57 \times 10^{-4}$ ( $\pm 0.08$ )	$2.54 \times 10^{-3}$ ( $\pm 0.06$ )

Table 6.1 presents the rates of protonation for the three different processes studied for **BSP6**, **BSP7** and **BSPe** and the wavelength of protonation of each moiety at 293 K.

From the spectra shown in Figure 6.6 (a) formation of **MCH<sup>+</sup>** is much more pronounced for **BSPe** than for **BSP6** and **BSP7**; **BSP7** seems to achieve a steady state relatively quickly compared to **BSP6**, and the absorbance is higher suggesting that a higher concentration of **MC7H<sup>+</sup>** is formed. In Figure 6.6 (b) it can be seen deprotonation is very rapid for **MCeH<sup>+</sup>** and **MC6H<sup>+</sup>** compared to **MC7H<sup>+</sup>** although the steady state for **BSPe** does not return to the expected absorbance due to the proton inhibiting the return to the initial former **BSP** isomer, remaining around 1.0. Reversion of **MC7H<sup>+</sup>** to **BSP7** is slower suggesting the protonation is more difficult to reverse. In Figure 6.6 (c) repeating these experiments in presence of UV light has a big effect on **BSPe**; leading to more rapid conversion to **MCe**, and establishment of steady state absorbance  $> 2.0$  during the experiment; **BSP6** and **BSP7** are again much more sluggish and the % conversion seems much lower (assuming the molar extinction coefficients are similar); **BSP6** becomes more or less equivalent to **BSP7** in kinetics and % conversion (see Table 6.1).

This assumption can be explained with the chemical composition of **BSP7**: the shorter tether allows the ester functionality to be directly conjugated with one of the aromatic rings of the terthiophene, therefore a slightly higher resonance donation could arise, which competes with the stabilization of the ester enolate and makes **BSP7** less stable and less acidic than **BSP6**.<sup>52</sup> A concomitant contribution can come from the relative  $pK_a$  of **MC7** (from the available literature the  $pK_a$  value of a general spiro derivative is in the range 4.5 to 7):<sup>13, 44, 49</sup> the absence of the extra methylene group in the ester-linker with the terthiophene will extend the extent of conjugation over the three building blocks, and therefore the overall  $pK_a$  of this molecule is increased (stronger base) and the de-protonation process is therefore inhibited.<sup>53</sup> Therefore, from the results obtained,

it is evident that **BSPe** > **BSP7** > **BSP6** in terms of basicity. Protonation and de-protonation control experiments were performed on freestanding terthiophene, **AcTTh** and **CbTTh** (Figure D7 (a) and (b), Appendix D), under the same conditions. It was found that in each case there was no evidence of acid-base behaviour.

### 6.3.4 Thermodynamics of protonation

Table 6.2 shows the thermodynamic parameters of the de-protonation processes (**MCH<sup>+</sup> → BSP+H**) over the temperature range 283-303 K for **BSP6**, **BSP7** and **BSPe**. Figure 6.7 shows the absorbance increase at 447 nm for the reaction **BSP6+H<sup>+</sup> → MC6H<sup>+</sup>** in ACN ( $10^{-4}$  M) at different temperatures (similar spectra for **MC7H<sup>+</sup>** and **MCeH<sup>+</sup>** are given in Appendix D, Figure D8, (a) and (b) respectively), from which the rate constants for protonation-induced ring opening (thermal formation) at each temperature were obtained by fitting a first order rate equation. The resulting Arrhenius and Eyring plots are shown in Figure 6.7(b) and (c). From the Arrhenius plots and from equation (D2), the activation energy ( $E_a$ ) and the pre-exponential factor  $A$  were derived (Table 6.2) for the thermal relaxation process. Using Eyring's transition state theory (equation (D3)), the activation thermodynamic parameters,  $\Delta S^\ddagger$  (entropy of activation) and  $\Delta H^\ddagger$  (enthalpy of activation) were derived. A derivation of Eyring's equation (eqn (D4)) was used to determine the equilibrium of activation ( $K^\ddagger$ ) and equation (D5) was used to obtain  $\Delta G^\ddagger$  (Gibbs free energy of activation).

**Table 6.2:** Thermodynamic parameters expressed as mean of three replicates and standard deviation values (standard deviation values are reported in brackets) for the general process **BSP+H<sup>+</sup> → MCH<sup>+</sup>** for **BSPe**, **BSP6** and **BSP7**.

MCH	$\lambda_{\max}$ (nm)	$k_{293}$ ( $10^{-3} \text{ s}^{-1}$ )	Arrhenius		Eyring			
			$E_a$ (kJ mol <sup>-1</sup> )	$A$ (s <sup>-1</sup> )	$\Delta S^\ddagger$ (JK <sup>-1</sup> mol <sup>-1</sup> )	$\Delta G^\ddagger_{293}$ (kJ mol <sup>-1</sup> )	$\Delta H^\ddagger$ (kJ mol <sup>-1</sup> )	$K^\ddagger_{293}$ ( $10^{-16}$ )
<b>MCHe</b>	424	1.29	92.05 (±1.94)	$1.99 \times 10^{13}$ (±0.54)	1.54 (±0.97)	89.16 (±2.45)	89.62 (±0.95)	1.31 (±0.09)
<b>MCH6</b>	447	0.33	103.64 (±1.12)	$6.66 \times 10^{15}$ (±0.92)	-24.67 (±0.97)	93.68 (±1.39)	86.45 (±1.26)	0.164 (±0.14)
<b>MCH7</b>	453	0.9	75.07 (±2.04)	$7.65 \times 10^9$ (±0.35)	-63.86 (±0.41)	91.35 (±2.51)	72.64 (±1.42)	0.491 (±0.23)

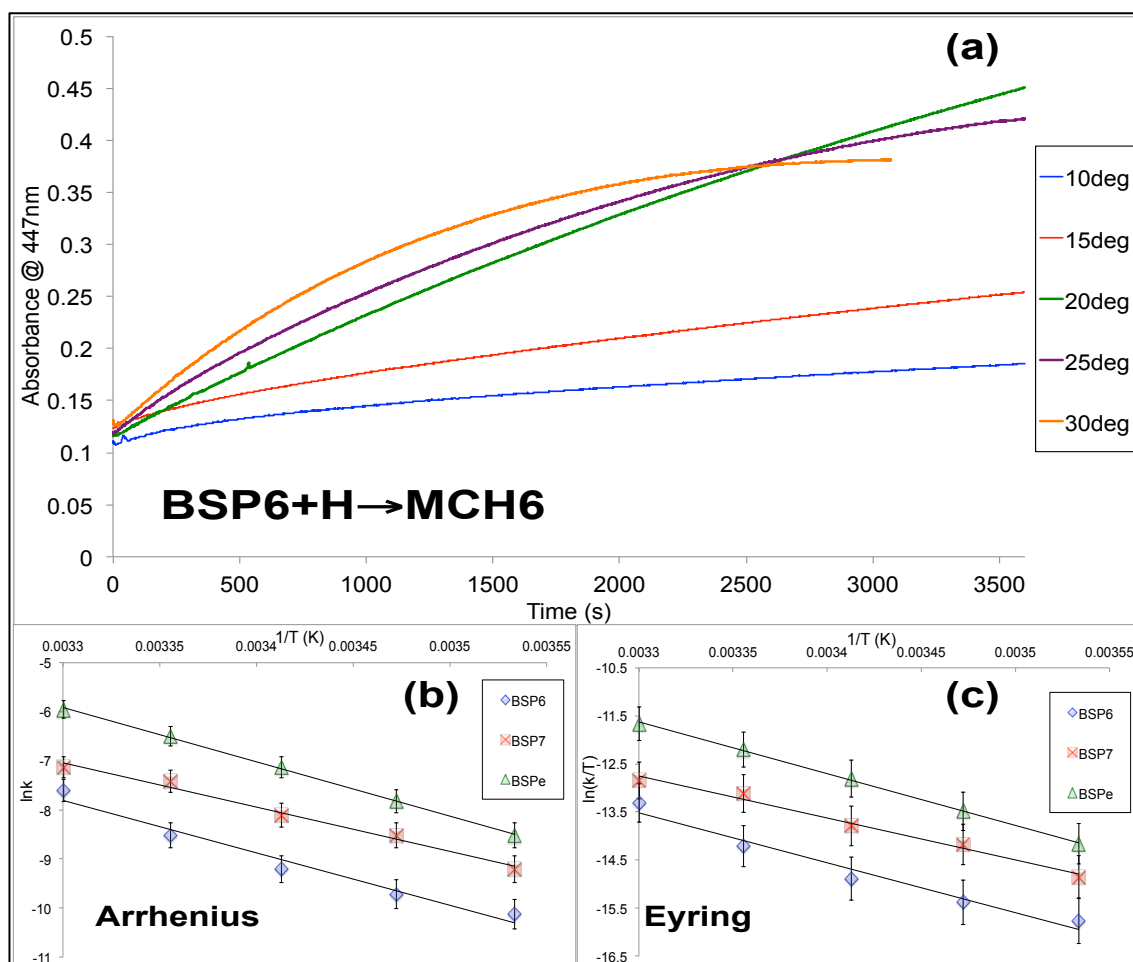


**Figure 6.7:** (a) thermally assisted protonation curves for the process  $\text{BSP6} + \text{H}^+ \rightarrow \text{MCH6}^+$  in the temperature range 283-303 K. **BSP6** concentration was  $10^{-4}$  M in acetonitrile and HCl final concentration was  $3.2 \times 10^{-3}$  M. (b) Arrhenius and (c) Eyring plots of the thermally driven process  $\text{BSP} + \text{H}^+ \rightarrow \text{MCH}^+$ . Error bars derived from 3 replicates

The Arrhenius and Eyring plots both show that both molecules exhibit similar behaviour, with very similar slopes, and **BSP7** showing a lesser slope in both cases. This pattern of behaviour is reflected in the values of the rate constants of deprotonation (Table 6.1) presented above and in the thermodynamic and kinetic parameters extracted from the Arrhenius and Eyring Plots (Table 6.2), with the exception of the  $\Delta G^\ddagger$  value, which is higher than  $\text{MCeH}^+$ . The activation energy of  $\text{MC6H}^+$  thermal protonation is quite high compared to the other derivatives studied. This suggests that the  $\text{MC6H}^+$  spontaneous protonation process is enhanced at higher temperature. It was observed that  $\text{MC7H}^+$  had the smallest thermal formation  $E_a$  and  $\Delta H^\ddagger$  values; i.e.,  $75.07 \text{ kJ mol}^{-1}$  and  $72.64 \text{ kJ mol}^{-1}$  ( $103.64 \text{ kJ mol}^{-1}$  and  $86.45 \text{ kJ mol}^{-1}$  for  $\text{MC7H}^+$  and  $92.05 \text{ kJ mol}^{-1}$  and  $89.62 \text{ kJ mol}^{-1}$  for  $\text{MCeH}^+$ ), respectively. For some applications, a photochrome such as **MC** with low activation energy  $E_a$  would be

desirable in order to not have a large temperature dependence on the formation of the protonated merocyanine. Small frequency factors ( $10^9$ – $10^{10}$  s<sup>-1</sup>) are associated with negative activation energies with respect to photochromic dyes.<sup>54</sup>

It has been suggested that the **BSP**–**MC** equilibrium is almost isentropic, reflecting a balance between two opposite contributions to  $\Delta S_0$ : a positive contribution, which is related to the increased torsional freedom in the **MC** isomer, and a negative contribution, which is due to solvent reorientation around the more polar **MC** form.<sup>55</sup> In this case an extra component participated to the reaction: the proton, which can increase the level of solvation of the **MC** isomer when in the protonated form. In this case,  $\Delta S^\ddagger$  values for **MC7H**<sup>+</sup> show a strong linear correlation with  $E_a$ : the experimental activation entropies ( $\Delta S^\ddagger$ ) found for **MC** was significantly negative ( $-63.86$  JK<sup>-1</sup> mol<sup>-1</sup>), indicating a more strongly solvated species, possibly due to the charged phenolate group interacting with the proton. For **MC6H**<sup>+</sup> a less negative value of  $\Delta S^\ddagger$  ( $-24.67$  JK<sup>-1</sup> mol<sup>-1</sup>) combined with a surprisingly higher  $E_a$  ( $103.64$  kJ mol<sup>-1</sup>) and  $\Delta H^\ddagger$  ( $86.45$  kJ mol<sup>-1</sup>) suggest a reduced solvation effect (possibly due to higher intramolecular  $\pi$ - $\pi$  interactions which increase the overall molecular rigidity).<sup>7</sup>

## 6.3.5 Electrochemistry

### 6.3.5.1 Electrochemistry and spectroelectrochemistry of **BSPe**

A detailed electrochemical and spectroelectrochemical investigation of the new spiropyran derivative **BSPe** was carried out using previously published methodologies.<sup>35</sup> New features are observed which arise from both terthiophene and spiropyran units, (Scheme 6.2).

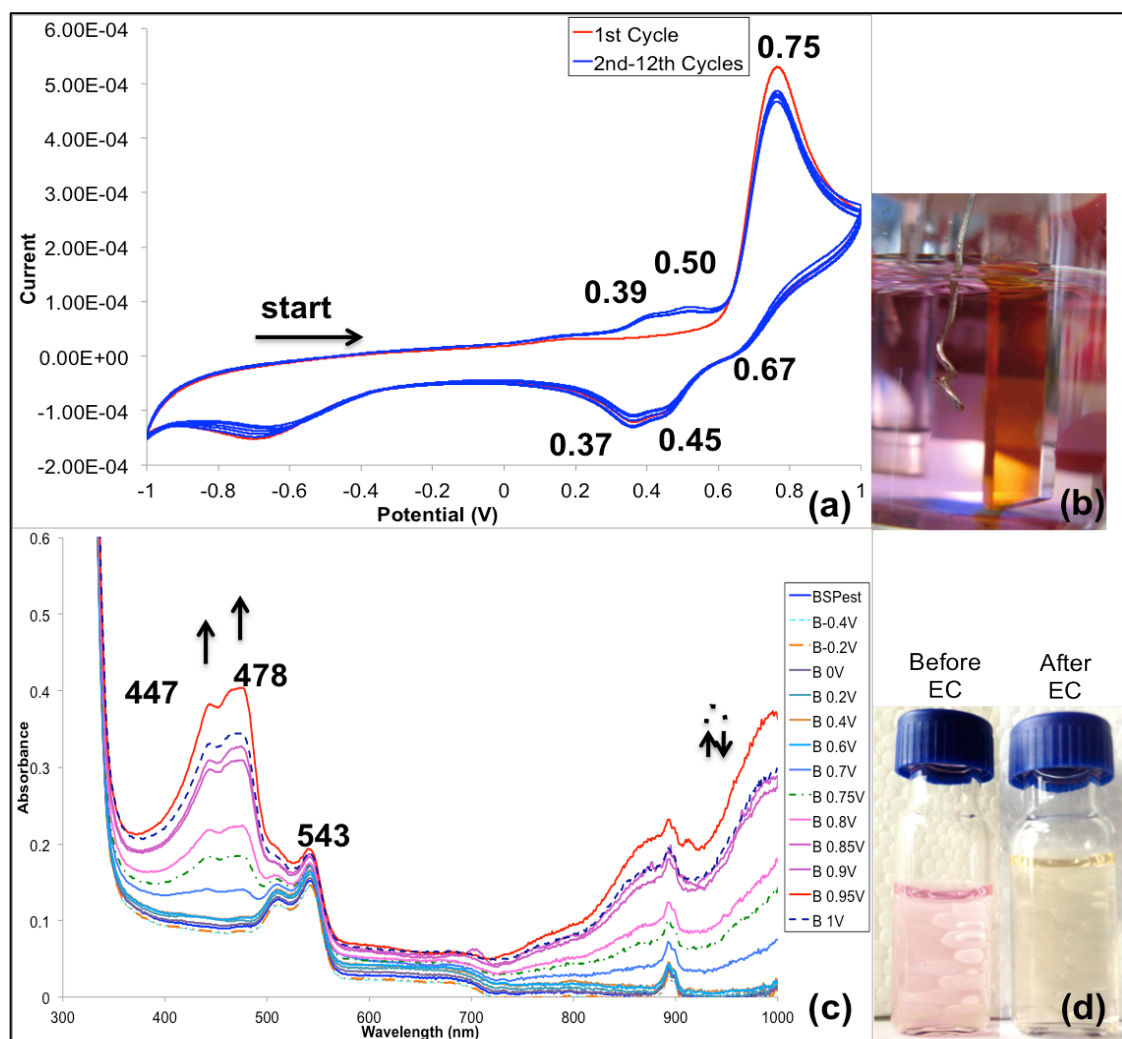


**Figure 6.8:** (a) Cyclic voltammograms of **BSPe**. (b) Formation of a deposit, which dissolved at the end of the electrochemical stimulation of **BSPe** on the working electrode at 1.0 V applied potential. (c) Spectroelectrochemistry of **BSPe**. (d) Coloration of **BSPe** before and after electrochemistry treatment. All solutions were  $10^{-4}$  M in acetonitrile with 0.1 M TBAP as electrolyte.

In Figure 6.8 (a) the cyclic voltammogram of **BSPe** is shown: after the first positive scan, one irreversible oxidation peak at 0.75 V is obtained, followed by broad and overlapping reduction bands during the return scan. As previously noted by Preigh *et al.* and Wagner *et al.*,<sup>10, 35</sup> during the oxidative phase of the analysis, an orange deposit appears on the working electrode (Figure 6.8 (b)) which is assigned to oxidized merocyanine.

Similarities with previous reports also occur during the second cycle through the appearance of two new broad oxidation bands at 0.39 V and 0.50 V.<sup>35</sup> These peaks are completely reversible in the return scans, as shown by the two bands at 0.37 V and 0.45 V. This indicates that the electrochemical processes involving **BSPe** also induce the formation of merocyanine isomers previously identified (in our case **TTC-MC<sub>eox</sub>** and

**TTT-MCe<sub>ox</sub>**)<sup>35</sup>, which are reversible under the experimental conditions studied.<sup>56</sup> To further support these conclusions, the spectroelectrochemistry of **BSPe** was obtained (Figure 6.8 (c)) and the spectral changes upon consecutive increases in the oxidative potential (from -0.4 V up to 1.0 V in acetonitrile with 0.1 M TBAP) were acquired. In this case new bands with maxima at 478 nm and 447 nm appear only after the potential was increased to 0.7 V, reaching their maximum absorbance at 0.95 V. When the potential was reduced to 1 V, the overall intensity also decreased. It is also interesting to note that between 700 nm and 1000 nm, the absorbance bands increased up to 0.95 V, and then fell as the potential was switched to 1.0 V, possibly indicating the reversible formation of **MCe<sub>ox</sub>** aggregates.

### 6.3.5.2 Electropolymerization of **BSP6** and **BSP7**.

The monomers were electrochemically polymerised on ITO electrodes as shown by the cyclic voltammograms in Figures 6.9 (a) and (b). The increase in current with successive cycles indicates effective deposition of the electroactive films. The process is carried out up to 0.9 V with the onset of monomer oxidation occurring at 0.58 V for **BSP6** and at 0.67 V for **BSP7**, resulting in the formation of a dark blue film, characteristic of the oxidized polythiophene. The rapid colour conversion of the electrodeposited film during the growth masked the typical reddish colouration of the merocyanine at the maximum applied potential and therefore it is difficult to determine whether the spiropyran is in its open or closed form during the deposition. Nevertheless both polymers produced irreversible and unique signals arising in the post-synthesis cyclic voltammograms (from -0.4 V to 0.9 V in an acetonitrile monomer free solution, 0.1 M TBAP) thus indicating that most of the spiropyran units isomerize quantitatively to the corresponding merocyanine only after the synthesis (Figure 6.9 (c) and (d)). These features cannot be recovered during the analysis and this is markedly different from what has been previously reported for a similar derivative under the same conditions.<sup>35</sup> In spite of the similarities between **pBSP6** and **pBSP7**, some differences can be observed in the voltammograms. For example, **pBSP6** has 3 oxidation peaks at 0.25 V, 0.58 V and 0.91 V, while **pBSP7** shows only 2 peaks at 0.61 V (which shifts to 0.64 V after the first cycle) and 0.86 V. The peak at 0.25 V in **pBSP6** is difficult to assign to a specific electrochemical process, but signals at 0.58 V (**pBSP6**) and 0.61 V (**pBSP7**) both originate from the oxidation of the poly-terthiophene chains.<sup>35</sup> Interestingly the oxidation band of the spiropyran of both polymers appears at potentials

shifted relative to **BSPe** CV (i.e. 0.9 V for **pBSP6** and 0.85 V for **pBSP7** compared to 0.75 V of **BSPe**). This could arise from conjugation between the two functional units that would require a higher potential to obtain the oxidized **MC6/MC7** substituent on the oxidized polymer backbone. To measure the conductivity, freestanding films of **pBSP6** and **pBSP7** were obtained after chronoamperometric deposition on ITO-coated glass at a constant potential of 0.8 V for 1 h and removal from the electrode. Similar conductivity values were found for these two polymers: 19.1 S/cm<sup>-1</sup> for **pBSP6** and 18.3 S/cm<sup>-1</sup> for **pBSP7**. These values are higher if compared with a similar derivative reported previously in our work,<sup>35</sup> but they are in the same range of magnitude reported by Visy *et. al.* in their work for analogous 3-substituted terthiophenes.<sup>57</sup>

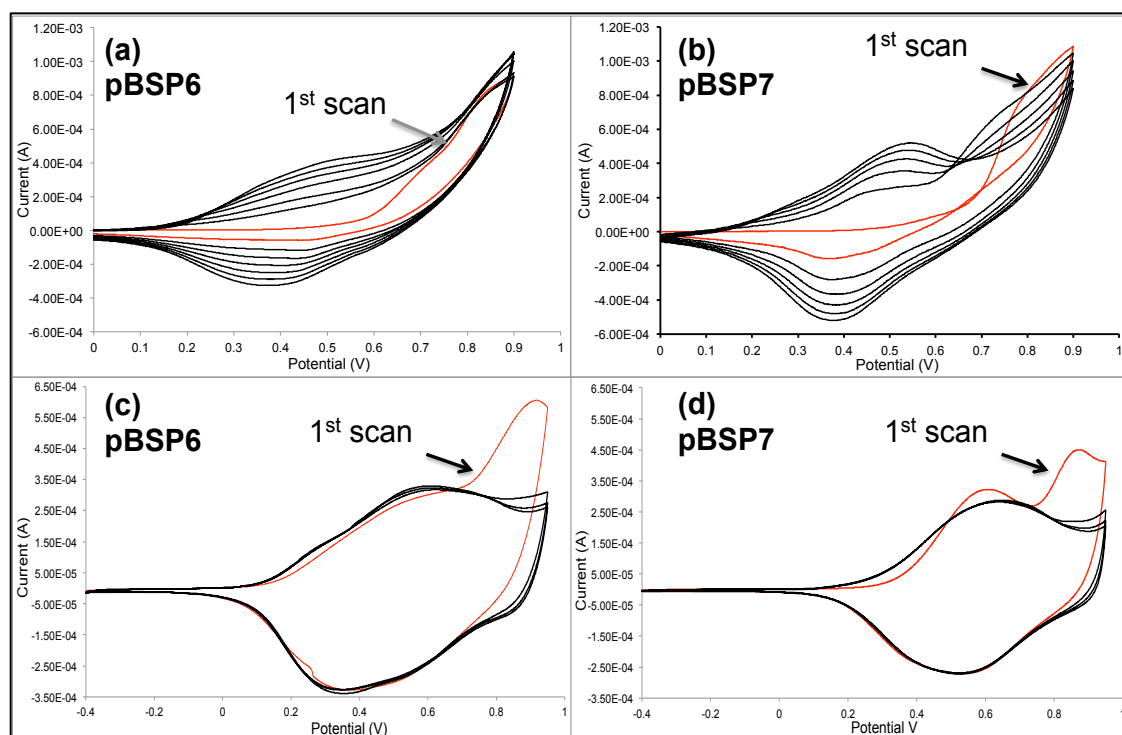


**Figure 6.9:** (a) and (b) electrochemical deposition on ITO and their post-synthesis cyclic voltammograms (c) and (d) of **pBSP6** and **pBSP7**, respectively.

### 6.3.5.3 UV-vis Spectroelectrochemistry of **pBSP6** and **pBSP7**

The spectral features of both **pBSP6** and **pBSP7** were studied in an in situ built electrochemical cell in the same potential range as used for cyclic voltammetry (-0.4 up to 1 V). Results are shown in Figure 6.10 (a) and (b) for freshly polymerized films of **pBSP6** and **pBSP7**. In both cases, they show characteristics of the free-carrier absorption of the metallic state in typical poly-terthiophene (between 800 and 1000 nm) as the electrode potential is increased from -0.4 V to 0.6 V, (Figure 6.10 (a) and (b), between 800 and 1050 nm). Even if **pBSP7** was kept at -0.4 V for the same amount of

time as **pBSP6**, an extent of the polymer seems to be not fully reduced (signals between 1000 and 750 nm). **pBSP6** looks completely reduced, instead. As the applied electrode potential increases above 0.6 V (up to 1 V), the maximum peak assigned to the **TTh** contribution (539 nm for **pBSP6** and 544 nm for **pBSP7**), loses gradually intensity in both cases. From 0.65 V up to 1 V, broad signals indicating the formation of TTC and TTT dimers of oxidized merocyanine were formed; particularly, for **pBSP6** the assigned absorbance at 0.65 V was 462 nm. At 1 V this signal up-shifted to 478 nm. For **pBSP7** the formation of the dimers occurs at 0.85 V at 481 nm, which is 0.2 V higher than the potential required for **pBSP6**. The signals relative to the formation of the **MC** isomers were observed at 508 nm for **pBSP6** and at 510 nm for **pBSP7**. From the results obtained, the formation of the **MC** begins at lower potential for **pBSP7** (0.85 V) than for **pBSP6** (0.95 V), contrarily from what observed for the formation of the dimers, (0.65 V for **pBSP6** and 0.85 V for **pBSP7**).

The process in both cases is completed at 1.2 V. The broad shoulder appearing for **pBSP6** at 478 nm at 1.05 V has not been found in the spectroelectrochemical analysis of the free standing p-terthiophene, but has been assigned to H-aggregation of **MC** isomers for other derivatives in literature.<sup>58</sup> This supports the assignment of these signals to the spiro-functionality. When **pBSP7** is stimulated at 0.85 V, a new signal appears at 460 nm and it can be related to the formation of **MC** aggregates. A similar feature was observed during the spectroelectrochemistry of **BSPe** at 0.7 V (Figure 6.8 (c)), with the formation of a signal at 447 nm. This feature, together with the difficulties encountered in the reduction process of **pBSP7**, constitute the biggest differences between the two polymers. The ability to open the **BSP** isomer to the **MC** isomer electrochemically offers another approach for controlling the isomerisation process. The possibility to control specific aggregation types of monomer units within a polymer by altering the geometry of the **BSP** molecule on the polymer backbone may facilitate some advanced functions, controllable at the molecular level. In order to probe the reversibility of this merocyanine formation and oxidation, we monitored the absorbances at 508 nm (for **pBSP6**) and at 510 nm (for **pBSP7**) over the potential range -0.4 V to 1 V during cyclic voltammetry (Figure D9, Appendix D). A freshly electrodeposited film was used in order to ensure that the spiropyran unit was in its closed form. Once again, both polymers showed similar features, with a sharp peak arising at potentials greater than 0.75 V. What is surprising is that the intensity of this signal is much higher for **pBSP7** (sometimes even higher than the poly-terthiophene contribution) than for **pBSP6**, a trend that can be reproduced over the time frame of the

experiment. The main difference between these two experiments is that the spectroelectrochemistry is a static experiment, while the kinetics during cyclic voltammetry is a dynamic experiment. Therefore, the differences in the amount of MC generated can be related to kinetics issues of formation. From this we can conclude that for both derivatives, the cycling capability of the polymer backbone decreases after several cycles, as the intensity of their bands decays over time.

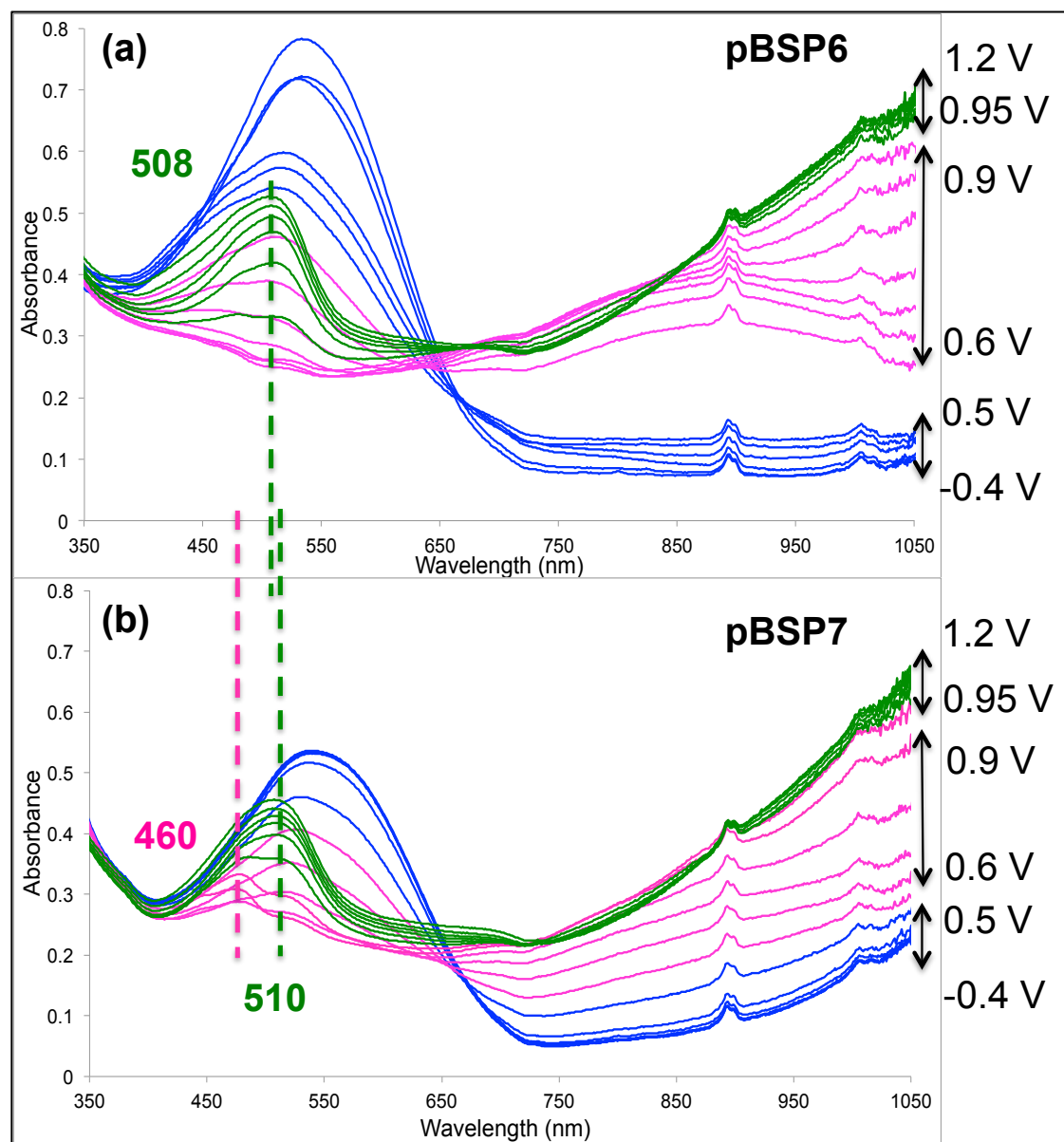


**Figure 6.10:** Spectroelectrochemistry of the electrochemically grown polymers, (a) **pBSP6** and (b) **pBSP7** on ITO glass, in 0.1 M TBAP in acetonitrile and in the potential window -0.4 – 1 V. In both (a) and (b) the blue signals are referred to the potential range between -0.4 and 0.5 V; the pink lines indicate the spectra obtained in the potential range of 0.6 and 0.9 V; the green lines indicate the potential range between 0.95 and 1.2 V.

### 6.3.6 Photonic response of the polymers

As described thus far, the combination of the spiropyran functionality with the well known conducting polymer poly-terthiophene modifies the spectrochemical features of the monomers and the electrochemically dependent optical properties of the polymers themselves. In solution the **BSP**→**MC** process is identifiable due to the different spectral areas of absorption of the three species involved (~290 for **BSP**, ~340 nm for **TTh** and for a general **MC** ~560 nm)<sup>47</sup>, but for **pBSP6** and (b) **pBSP7** the spectral region usually associated with **MC** is coincidental with the absorbance of the reduced poly-terthiophene backbone (Figure 6.10 (a) and (b) between 360 and 700 nm). In order to detect the presence of the photochemically generated merocyanine, fresh films of **pBSP6** and **pBSP7** were prepared, kept at -0.4 V in a monomer free electrolyte solution for 3 minutes and then washed in acetonitrile in order to remove the excess of electrolyte. The spectrum of the sample obtained in a quartz cuvette (Figure 6.11 and Figure D10, Appendix D) showed two maxima at 556 and 383 nm. **pBSP7** was then illuminated for 60 minutes with UV light and the resulting spectrum showed a hypsochromic shift of the maximum at 541 nm, and the overall absorbance was almost twice as big (from ~0.3 to ~0.5). Furthermore, the signal at 383 nm disappeared. Subsequent sequences of illumination (15, 30 and 45 minutes) with the white light source reduced the overall intensity of the main band at 541 nm. The band at 383 nm could not be regenerated immediately, however after 45 minutes of irradiation with white light it began to re-appear (Figure 6.11).

Although the original absorbance maximum of **pBSP7** could not be reached in subsequent experiments, a proportional amount of spiropyran was re-generated using white light illumination. A similar hypsochromic shift was observed also after UV illumination of **pBSP6** (from the original 529 nm to the new maximum at 521 nm) but the increased intensity was not as striking as seen with **pBSP7**. When the polymer was exposed to white light, a surprising decrease in the overall absorbance was observed, down to levels lower than obtained with **pBSP6** before illumination. This result suggests that for this polymer there is a higher concentration of **MC<sub>ox</sub>** formed during the electrochemical polymerization process, which can then be photonicly switched to the **BSP** isomer. Moreover a new shoulder at 476 nm that can be seen after white light stimulation may indicate the formation of inter-chain aggregates throughout the polymeric structure.

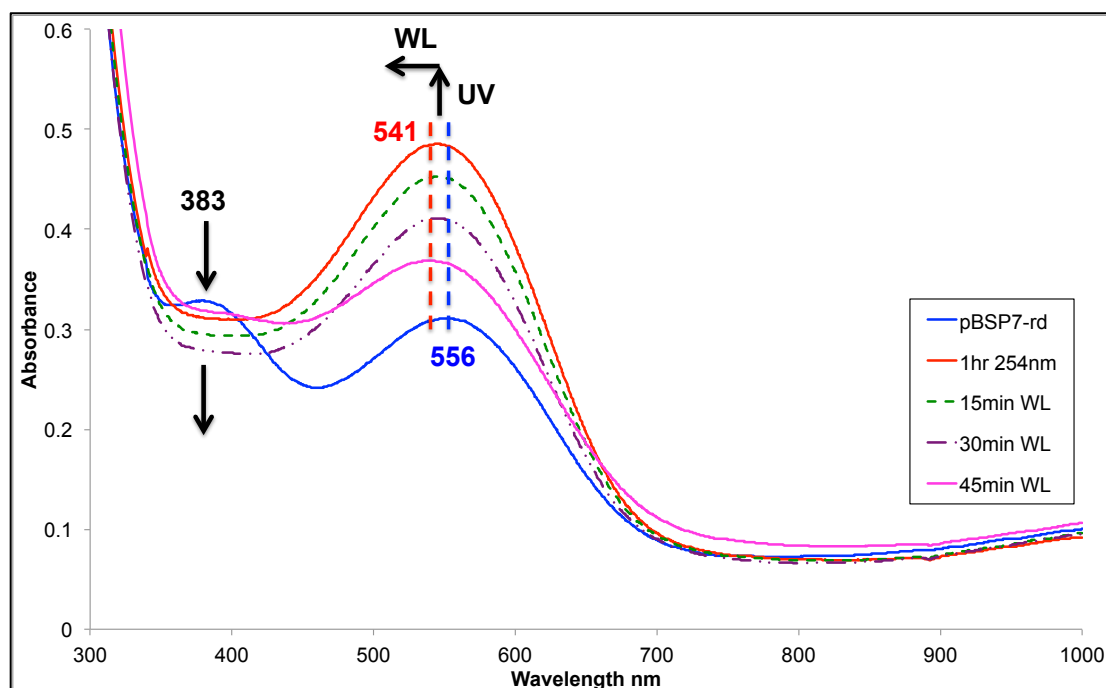


**Figure 6.11:** UV-vis of reduced **pBSP7** before (blue line) and after UV light (254 nm) illumination (red line). The dashed-green and purple lines together with the pink line represent three sequences of illumination with white light.

### 6.3.7 Surface properties

#### 6.3.7.1 SEM analysis

SEM images of the reduced **pBSP6** at -0.4V, Figure 6.12 (a) and (b) showed webbed structures on the polymer surface. When the polymer is oxidised to +1.0 V, significant changes can be seen in the polymer structure, Figure 6.12 (c) and (d), which look like a swollen structure of the original conformation. The same webbed porous structure and similar morphology is observed in **pBSP7**, see Figure D11 (a)-(d), Appendix D, with approximately 100 nm ‘pores’ formed when the polymer is oxidised. As this morphology is not common in similar terthiophene polymers, it is believed that this process is due to the formation of MC aggregates, most likely H-aggregates in both cases, as suggested by the spectroelectrochemical results. More importantly, these morphological changes were also observed to be electrochemically reversible.

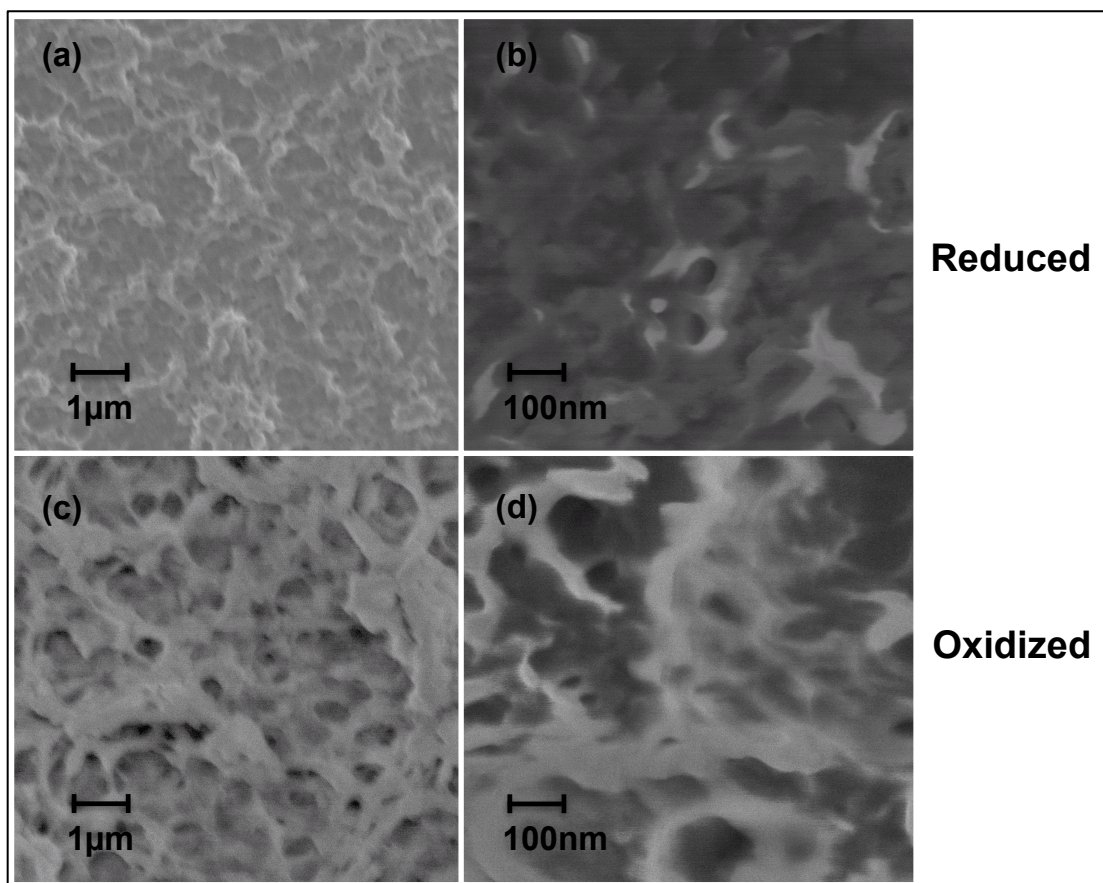


**Figure 6.12:** SEM pictures of **pBSP6** after stimulation at constant potential, at -0.4 V (a) and (b) for 3 min and +1.0 V (c) and (d) for 3 min.

### 6.3.7.2 AFM analysis

Figure 6.13 (a) and (b) illustrates the **pBSP6** surface morphology when reduced at -0.4 V. These images show a rough nodular structure for the reduced polymer, the rms roughness values were estimated to be 261.4 nm (root mean squared, rms =  $\pm 1.52$  nm) and 13.29 nm (root mean squared, rms =  $\pm 2.65$  nm) for Figure 6.13 (a) and (b), respectively. When the polymer is oxidised 1.0 V, the surface morphology changes, as can be seen from Figure 6.13 (c) and (d). In this case, rms roughness values were estimated to be 102.1 nm and 16.85 nm for Figure 6.13 (c) and (d), respectively. Pore size for the oxidised **pBSP6** was calculated to be approximately 156 nm (root mean squared, rms =  $\pm 3.98$  nm) wide and 68 nm (root mean squared, rms = 2.31 nm) deep. Changes between the two-oxidation states were also observed for **pBSP7** as can be seen in Figure D12, Appendix D.

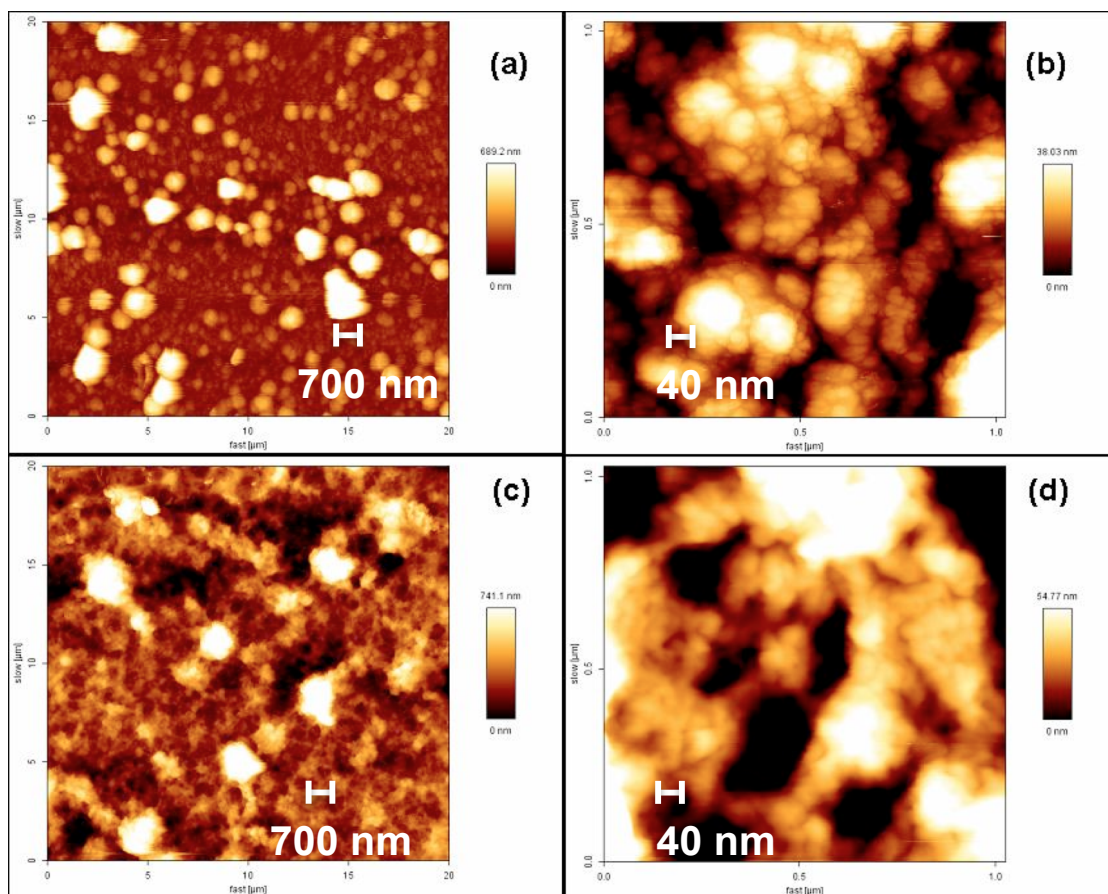


**Figure 6.13:** AFM pictures of **pBSP6** after stimulation at constant potential, at  $-0.4$  V (a) and (b) and at  $1$  V (c) and (d).

For the reduced state the roughness values were found to be  $241.34$  (root mean squared,  $\text{rms} = \pm 4.23$  nm) nm and  $63.89$  nm (root mean squared,  $\text{rms} = \pm 1.76$  nm) for Figure D12 (a) and (b), respectively, whilst for the oxidized states the rms roughness values were estimated as  $32.1$  nm (root mean squared,  $\text{rms} = \pm 0.8$  nm) and  $26.35$  nm (root mean squared,  $\text{rms} = \pm 1.04$  nm) for Figure D12 (c) and (d). From the images some important differences can be deduced between the two polymers. The surface of **pBSP7** shows a smaller number of cavitations and it appears smoother when oxidized, in agreement with the rms roughness values given. This is surprising since they differ from each other only through a single extra methylene group in the linker **pBSP6** (Scheme 6.2). It can be speculated that the formation of merocyanine-dependent aggregates during the polymerization process is more favoured for **pBSP6**, possibly because of the extra level of freedom and flexibility provided by the additional methylene group in the **pBSP6** linker chain.

## 6.4 Conclusions

The synthesis and characterization of two new spiropyran-terthiophene molecules, along with a novel spiropyran molecule functionalised with an ester-group in position 6 for comparative reasons has been described in detail. The spectrochemical study showed interesting photochemical profiles for all three molecules studied. While the conversion of **BSP6** and **BSP7** into their respective **MC** isomers is relatively difficult and slow due to their molecular configuration, it was found that **BSP7** is slightly easier to switch than **BSP6** (higher absorbance in the same illumination time frame). The photoinduced formation of **MCE** is somewhat faster, but the reverse reaction occurs via a different path and leads to irreversible molecular aggregates. A study of their behaviour in protonated solutions showed that **MCE** was the strongest base among the merocyanine isomers, suggesting that the chemical reactivity of **BSP6** and **BSP7** is influenced by the presence of the terthiophene.

**BSPe** was also used as a reference molecule for the electrochemical analysis. The results obtained with **pBSP6** and **pBSP7** were found to be consistent with a previous study<sup>35</sup> on other spiro-derivatives. These polymer films were electrochemically grown from dilute monomer solutions on optically transparent ITO glass, and the detailed spectroelectrochemical study undertaken suggested strong contributions were arising from both of the functional units present in the polymers. When the redox processes of the poly-terthiophenes was repeated over a number of cycles, the redox activity of the spiropyran units became limited, as shown by cyclic voltammetry, possibly due to the formation of aggregates, ( $\pi$ -dimers). Both polymers presented interesting photochemical reactivity, strongly influenced by the redox state of the polymer. If the polymer is reduced at -0.4 V for 3 minutes the photo-induced conversion between **BSP** and **MC** is achievable and can be consistently repeated over time. This suggests that electrochemical control can modify the polymer's photochemical behaviour. These polymers require a UV illumination over a long period of time (up to 1hr) to generate significant amounts of the **MC** form. **pBSP6** and **pBSP7** exhibit improved switching efficiency and repeatability compared to the previous derivative reported.<sup>35</sup> Furthermore the surface study showed a surface roughness differing between the two polymers, with **pBSP6** presenting more cavitations a globular conformation (resulting from intra chain aggregation) and a higher roughness than **pBSP7**.

## 6.5 Acknowledgments

M.Z acknowledges support under the Marie Curie IRSES- MASK project (PIRSSES-GA-2010-269302). M.Z and D.D acknowledge funding from Science Foundation Ireland under award 07/CE/ I1147 “CLARITY: Centre for Sensor Web Technologies”. M.Z. also acknowledges Giusy Matzeu for the SEM pictures. K.J.F. acknowledges the European Commission for financial support through a Marie Curie Actions International Re-integration Grant (IRG) (PIRG07-GA-2010-268365). Financial support from the Australian Research Council is also acknowledged.

## 6.6 References

1. V. I. Minkin, *Chemical Reviews*, 2004, **104**, 2751-2776.
2. Y. Hirshberg and E. Fischer, *Journal of Chemical Physics*, 1953, **21**, 1619-1620.
3. E. Berman, R. E. Fox and F. D. Thomson, *Journal of the American Chemical Society*, 1959, **81**, 5605-5608.
4. R. Byrne and D. Diamond, *Nature Materials*, 2006, **5**, 421-424.
5. R. Heiligmanrim, Y. Hirshberg and E. Fischer, *Journal of Physical Chemistry*, 1962, **66**, 2470-2477.
6. B. Seefeldt, R. Kasper, M. Beining, J. Mattay, J. Arden-Jacob, N. Kemnitzer, K. H. Drexhage, M. Heilemann and M. Sauer, *Photochemical & Photobiological Sciences*, 2010, **9**, 213-220.
7. M. Zanoni, S. Coleman, K. J. Fraser, R. Byrne, K. Wagner, S. Gambhir, D. L. Officer, G. G. Wallace and D. Diamond, *Physical Chemistry Chemical Physics*, 2012, **14**, 9112-9120.
8. H. Gorner, *Physical Chemistry Chemical Physics*, 2001, **3**, 416-423.
9. H. Gorner and A. K. Chibisov, *Journal of the Chemical Society-Faraday Transactions*, 1998, **94**, 2557-2564.
10. M. J. Preigh, M. T. Stauffer, F.-T. Lin and S. G. Weber, *Journal of the Chemical Society, Faraday Transactions*, 1996, **92**, 3991-3996.
11. M. Natali and S. Giordani, *Organic & Biomolecular Chemistry*, 2012, **10**, 1162-1171.
12. M. Natali and S. Giordani, *Chemical Society Reviews*, 2012, **41**, 4010-4029.
13. G. Mistlberger, G. A. Crespo, X. Xie and E. Bakker, *Chemical Communications*, 2012, **48**, 5662-5664.
14. S. T. Abdel-Halim and M. K. Awad, *The Journal of Physical Chemistry*, 1993, **97**, 3160-3165.
15. M. Dekhtyar and W. Rettig, *Journal of Photochemistry and Photobiology A: Chemistry*, 1999, **125**, 57-62.
16. B.-H. Tan, M. Yoshio, T. Ichikawa, T. Mukai, H. Ohno and T. Kato, *Chemical Communications*, 2006, 4703-4705.
17. J. Andersson, S. Li, P. Lincoln and J. Andréasson, *Journal of the American Chemical Society*, 2008, **130**, 11836-11837.

18. X. Li, J. Li, Y. Wang, T. Matsuura and J. Meng, *Journal of Photochemistry and Photobiology A: Chemistry*, 2004, **161**, 201-213.
19. S. Scarmagnani, Z. Walsh, C. Slater, N. Alhashimy, B. Paull, M. Macka and D. Diamond, *Journal of Materials Chemistry*, 2008, **18**, 5063-5071.
20. Y. Sheng, J. Leszczynski, A. A. Garcia, R. Rosario, D. Gust and J. Springer, *The Journal of Physical Chemistry B*, 2004, **108**, 16233-16243.
21. S.-R. Keum, M.-S. Hur, P. M. Kazmaier and E. Buncel, *Canadian Journal of Chemistry*, 1991, **69**, 1940-1947.
22. M. Akhtar, J. Kleppinger, A. G. MacDiarmid, J. Milliken, M. J. Moran, C. K. Chiang, M. J. Cohen, A. J. Heeger and D. L. Peebles, *Journal of the Chemical Society, Chemical Communications*, 1977, **22**, 473-474.
23. C. K. Chiang, M. A. Druy, S. C. Gau, A. J. Heeger, E. J. Louis, A. G. MacDiarmid, Y. W. Park and H. Shirakawa, *Journal of the American Chemical Society*, 1978, **100**, 1013-1015.
24. H. Shirakawa, E. J. Louis, A. G. MacDiarmid, C. K. Chiang and A. J. Heeger, *Journal of the Chemical Society, Chemical Communications*, 1977, **16**, 578-580.
25. R. H. Baughman, P. A. Apgar, R. R. Chance, A. G. MacDiarmid and A. F. Garito, *Journal of the Chemical Society, Chemical Communications*, 1977, **2**, 49-50.
26. S. Gambhir, K. Wagner and D. L. Officer, *Synthetic Metals*, 2005, **154**, 117-120.
27. K. Wagner, L. L. Crowe, P. Wagner, S. Gambhir, A. C. Partridge, J. C. Earles, T. M. Clarke, K. C. Gordon and D. L. Officer, *Macromolecules*, 2010, **43**, 3817-3827.
28. P. Wagner and D. L. Officer, *Synthetic Metals*, 2005, **154**, 325-328.
29. P. Wagner, A. C. Partridge, K. W. Jolley and D. L. Officer, *Tetrahedron Letters*, 2007, **48**, 6245-6248.
30. J. Roncali, *Chemical Reviews*, 1992, **92**, 711-738.
31. D. Li, H. Wang, J. Fu and W. Wang, *Journal of Physical Chemistry B*, 2008, **112**, 16290-16299.
32. D. Officer, G. Swiegers, C. Too and G. Wallace, *Electrochimica Acta*, 2002.
33. J. B. Spires, H. Peng, D. E. Williams, B. E. Wright, C. Soeller and J. Travas-Sejdic, *Biosensors and Bioelectronics*, 2008, **24**, 928-933.
34. D. L. Wakeham, S. W. Donne, W. J. Belcher and P. C. Dastoor, *Synthetic Metals*, 2008, **158**, 661-669.
35. K. Wagner, R. Byrne, M. Zanoni, S. Gambhir, L. Dennany, R. Breukers, M. Higgins, P. Wagner, D. Diamond, G. G. Wallace and D. L. Officer, *Journal of the American Chemical Society*, 2011, **133**, 5453-5462.
36. J. Roncali, *Chemical Reviews*, 1997, **97**, 173-205.
37. M. C. Gallazzi, L. Castellani, R. A. Marin and G. Zerbi, *Journal of Polymer Science Part a-Polymer Chemistry*, 1993, **31**, 3339-3349.
38. D. K. Grant, K. W. Jolley, D. L. Officer, K. C. Gordon and T. M. Clarke, *Organic & Biomolecular Chemistry*, 2005, **3**, 2008-2015.
39. A. Gelmi, M. Zanoni, M. J. Higgins, S. Gambhir, D. L. Officer, D. Diamond and G. G. Wallace, *Journal of Materials Chemistry B*, 2013, **1**, 2162-2168.
40. I. S. Park, Y.-S. Jung, K.-J. Lee and J.-M. Kim, *Chemical Communications*, 2010, **46**, 2859.
41. V. C. Gonçalves and D. T. Balogh, *European Polymer Journal*, 2006, **42**, 3303-3310.
42. X. Y. Zhao, *eXPRESS Polymer Letters*, 2007, **1**, 450-455.
43. S. Stitzel, R. Byrne and D. Diamond, *Journal of Materials Science*, 2006, **41**, 5841-5844.
44. D. S. Achilleos and M. Vamvakaki, *Macromolecules*, 2010, **43**, 7073-7081.
45. H. Tomioka and T. Itoh, *Journal of the Chemical Society, Chemical Communications*, 1991, **7**, 532-533.

46. P. Uznanski, *Langmuir*, 2003, **19**, 1919-1922.
47. J. B. Flannery, *Journal of the American Chemical Society*, 1968, **90**, 5660-5671.
48. X. Q. Song, J. W. Zhou, Y. T. Li and Y. W. Tang, *Journal of Photochemistry and Photobiology a-Chemistry*, 1995, **92**, 99-103.
49. A. V. Chernyshev, M. S. Chernov'yants, E. N. Voloshina and N. A. Voloshin, *Russian Journal of General Chemistry*, 2002, **72**, 1468-1472.
50. J. P. Guthrie, *Canadian Journal of Chemistry*, 1978, **56**, 2342-2354.
51. P. Michorczyk and J. Ogonowski, *Chemical Communications*, 2012, **48**, 7283-7285.
52. F. A. Carey and R. M. Giuliano, *Organic Chemistry, 9th Edition*, McGraw Hill Education, 2013.
53. C. J. Drummond, D. N. Furlong and G. Georgaklis, *Journal of the Chemical Society, Faraday Transactions*, 1990, **86**, 3913.
54. M. R. di Nunzio, P. L. Gentili, A. Romani and G. Favaro, *ChemPhysChem*, 2008, **9**, 768-775.
55. D. E. Wetzler, P. F. Aramendia, M. L. Japas and R. Fernandez-Prini, *Physical Chemistry Chemical Physics*, 1999, **1**, 4955-4959.
56. J. Hobley and V. Malatesta, *Physical Chemistry Chemical Physics*, 2000, **2**, 57-59.
57. C. Visy, J. Lukkari and J. Kankare, *Macromolecules*, 1994, **27**, 3322-3329.
58. C. P. McCoy, L. Donnelly, D. S. Jones and S. P. Gorman, *Tetrahedron Letters*, 2007, **48**, 657-661.



# CHAPTER 7

## Thesis Conclusions and Future Work

## 7.1 Thesis Conclusions

The work presented in this thesis describes six new spiroopyran derivatives and their photo-, electro- and solvatochromic behaviour in different solvents, characterised using various spectroscopic methods. Four of these new moieties featured a spiroopyran unit covalently substituted onto a terthiophene scaffold. One of these spiroopyrans (**BSPe**) was isolated for comparison reasons. Another spiro-moiety (**TSP4**) was intercalated between two thiophene units. It was found that the presence of the chromophore over the terthiophene backbone modified the properties of the molecules, yielding a new dual-control stimuli responsive family. The **BSP-MC** conversion was observed, both in solution and on the solid phase from the ITO-coated films. Different molecular environments were used to study this equilibrium along with the influence of the terthiophene unit on the photochemical response. Also investigated was the specific interactions with protonated solutions, and the photo-modulated surface relations with a protein of the integrins family (fibronectin).

Chapter 1 gives a general overview of the physico-chemical details of the two main molecules studied in this Thesis, the synthetic metal terthiophene and the photoswitchable spiroopyran. Their synthesis and functionalization, the effect of the substituents on their thermo, electro and photochemical response's were introduced.

The first derivative of the spiroopyran-terthiophene family (**pBSP2**) is introduced and studied in Chapter 2: this molecule was a combination of a nitrospiroopyran covalently substituted onto a terthiophene moiety. The electrochemically-polymerized material was then characterized through UV-*vis* spectroelectrochemistry and with electrochemical techniques. Surface characterization was investigated through SEM and AFM techniques. **pBSP2** was shown to photochemically actuate and the features of the photoactive **BSP** $\rightleftharpoons$ **MC** system were observed from an electroactive polymer for the first time. Furthermore, the spiroopyran photochemistry influenced the electrochemical behavior of the polymer: upon illumination with UV light, the features of the spiroopyran were recovered and observed during the cyclic voltammograms.

In Chapter 3 a new **BSP-TTh** derivative (**BSP3**) was prepared and differentiated from **BSP3** by a shorter ester-tether between the two active units (**BSP** and **TTh**). The spectro-physical properties of both the monomers were reported by UV-*vis* and fluorescence spectroscopy. The kinetics of photogeneration of their equivalent

merocyanine (**MC**) isomers, their isomerisation properties, and the thermodynamic parameters have been studied in acetonitrile, and compared to the parent, non-**TTh**-functionalised, benzospiropyran derivative. It was found that the parameters derived from the transition state theory differed significantly, with the short-tethered molecule showing a similar behavior to the **TTh**-free spiropyran. The thermal relaxation kinetics and solvatochromic behaviour of the derivatives in a range of solvents of differing polarity (ethanol, dichloromethane, acetone, toluene and diethyl ether) were also reported.

In Chapter 4 the ability to actuate the **BSP** $\rightleftharpoons$ **MC** conversion via photonic stimuli on the polymeric matrix is used to modulate the interactions between host binding sites and guest molecules. In this chapter, two different poly-terthiophenes were studied: one was functionalized with a spiropyran photoswitch (**pTTh-SP**) and the second with a non-photoswitchable methyl acetate moiety (**pTTh-MA**). These substrates were exposed to several cycles of illumination with light of different wavelengths and the resulting effect studied with UV-vis spectroscopy, contact angle and atomic force microscopy (AFM). The AFM tips were chemically activated with the cellular matrix protein fibronectin (FN), and the adhesion force of the protein to the polymeric surface was measured. The results suggest that surface energy and hydrophobic forces are predominant in determining the protein adhesion to the films studied and that this effect can be photonically tuned. This further implies that it should be possible to obtain a degree of spatial and temporal control of the surface binding behavior of certain proteins with these functionalized surfaces through photo-activation / deactivation and more generally through the **BSP** $\rightleftharpoons$ **MC** equilibrium. The ability to resolve reversible, protein interactions with resolution comparable to the nanoscale, as done in this study, provides significant insight into the possibilities of exerting fine, molecular level control over cellular interactions.

The synthesis of a new derivative bearing a spiropyran functionality intercalated between two thiophenes units is presented in Chapter 5. The electropolymerisation of a spiropyran moiety covalently linked between two alkoxythiophene units leads to incorporation of merocyanine onto a poly-dithiophene backbone. The electrochemical and spectroscopic (UV-Vis, FT-Raman, supported with TD-DFT calculations) data, demonstrate that the merocyanine form is trapped in the polymer backbone. The metal coordination capabilities of merocyanines were exploited and the introduction of cobalt

ions into the electropolymerisation led to an enhancement of the conductivity and of the morphology and optical properties of the polymer films.

In Chapter 6 three new spiropyran moieties were isolated and studied. Two of them, **BSP6** and **BSP7**, were synthesised with a spiropyran chromophore esterified on their position 6 on two different terthiophenes. Their difference was a single methylene group in the linking functionality, but this singularity was found to be responsible for the differing behaviour of the two molecules. The third spiropyran (**BSPe**) was synthesized for comparative reasons, and is synthesized with a methyl-ester on position 6. The electrochemical analysis in combination with the spectroscopic techniques, were used to understand the behaviour of these molecules: the architecture of these spiropyrans presented a different **BSP**⇌**MC** switching mechanism, which required a 254 nm UV light to be activated. The response in presence of protons was studied and it was found that, once they are protonated, they could be switched with 365 nm light. Transition state theory was applied to obtain the physical parameters of the protonation of spiropyran derivatives and to understand the reaction mechanism. When electropolymerized, the two **pBSP6** and **pBSP7** displayed dual control stimuli responsiveness, and showed a better response to the optical stimulation than previous polymer (**pBSP2**, Chapter 2), including high reversibility and low photo bleaching in all conditions studied.

## 7.2 Future Work

Stimuli responsive materials have been a focus of many researchers over the past decades and still attract considerable attention for their high number of applications and adaptability in various systems and devices. Having described and studied the molecular properties and the background behaviour of this new class of derivatives there is now scope for the study of their applications in various fields, biomaterials (the interactions with fibronectin described in Chapter 4) and analytical science (the ability to chelate ions, as reported in Chapter 5). However, the photochromic properties of these materials can still be improved and evolved, e.g. by using a different synthetic approach that will allow ease of photo actuation and slower photo bleach of the chromophore.<sup>1,2</sup>

Of particular interest is the development of devices incorporating materials that can improve analytical performances such as the limit of detection and the lifetime of the systems. This is especially true for lab-on-a-chip technologies.<sup>3</sup> The **BSP-TTh** hybrid

materials synthesized can provide a new, low cost, means for actuation (photo-electro), transduction (spectrochemical and electrochemical) of the analytical signal and is regenerable. Within the group, much effort is focused on the combination of all these properties into one simple portable platform, which can be easily analysed through electrochemical and / or spectroscopic techniques.

More recently, the class of conducting polymers has found to be a versatile scaffold for the regeneration of living tissues that are sensitive to electrochemical stimulation and a good platform for bioanalytical devices.<sup>4-6</sup> In the human body, biological control is achieved at all scales, from the differentiated tissues (e.g. temperature and pH) down to the single cell (e.g. membrane potential) by organic receptors and efficient chemical mechanisms. Using biological systems as an inspiration, leads one to explore different types of preparation and functionalization of new materials, with the aim to incorporate them into innovative designs than those typical in the traditional engineering sense.<sup>4, 5</sup>

### **7.2.1 Poly-Spiropyran-Terthiophenes Incorporated into Micro Total Analytical Systems ( $\mu$ TAS)**

The introduction of a new class of materials with dual control properties will improve the range of applications for these molecules and could greatly reduce system complexity. The first potential use of these photo-electro actuating materials shall be their incorporation into a fluid-handling system, where they can act as actuators and control the flow-rate and direction of the analytes through micro-channels and towards the reaction site. Our preliminary results suggested also that the spiropyran-terthiophene based materials could be the transducing molecules themselves. With an on-going collaboration with the University of Wollongong, Australia, we have designed a new chip based on an optically transparent electrode ITO. This chip was fabricated by selectively laser ablating patterns and electrochemically coated with pBSP7 (following the procedure presented in Chapter 6) and then assembled to cell wells, created by laser cutting a laminate of pressure-sensitive-adhesive and biocompatible acrylic parts (Figure 7.1). The reasons of this particular design lay into two simple concepts: (1) the flow control is not needed, as the analyte solution will be directly placed in the reaction site; (2) the polymer grown onto the electrode surface is also a sensing molecule, which is able to transduce two types of information once in contact with the analytes. The information transduced are as follows; (i) electrochemical (thanks to the interdigitated

electrode design) and (ii) photochemical (allowed by the photoresponsive nature of the spiro-functionality). One drawback of the system however, is the **pBSP7** poor solubility in aqueous environments with the electropolymerization technique used. The preparation of similar polymers indicates the need for need organic solvents, limiting the material used for device fabrication. Materials such as polymethylmethacrylate (PMMA) and polydimethylsiloxane (PDMS) cannot be used, only glass-based devices and solvent resistant electrodes. This would constitute a limitation for these derivatives, in the field of wearable electrochemical devices for example.

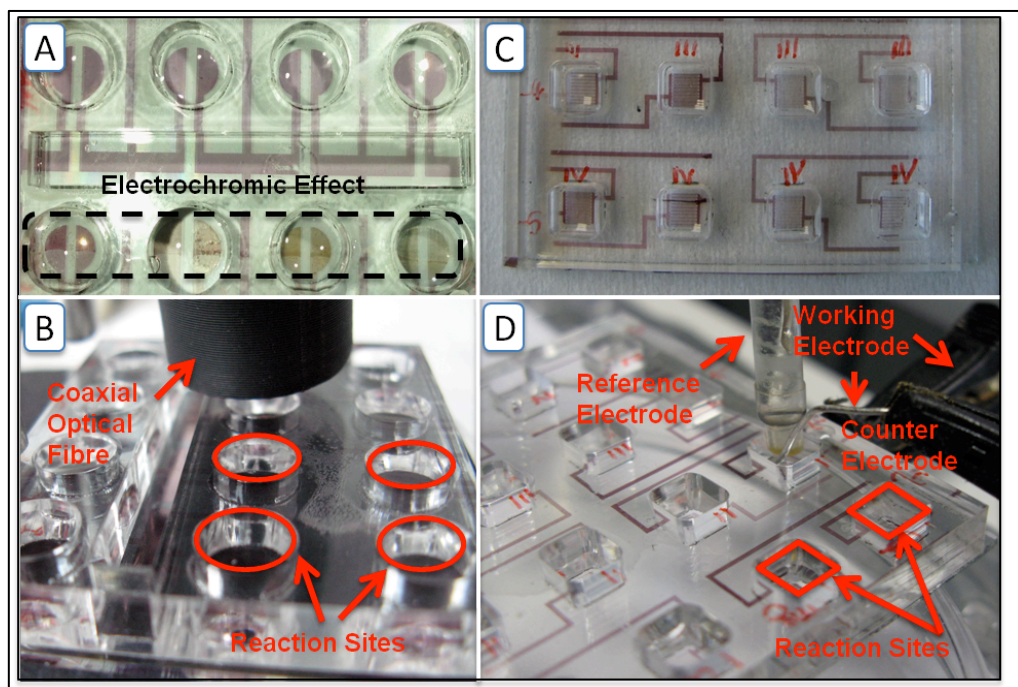


**Figure 7.1:** A) Rounded electrode design and B) Setup for spectro-photochemistry experiments. C) Interdigitated electrode design and D) setup for electrochemical experiments. Notice in A) Varying the concentrations of ions showed an electrochromic effect as well.

## 7.2.2 Living Cell Adhesion on Photo-Switchable Conducting Polymers

Cell adhesion is an essential event for cell proliferation and differentiation.<sup>7</sup> In this part of the project, the idea is to exploit the photo-switching properties of the polymers presented in order to favour the adhesion of living cells on the surface and to allow their initial proliferation.<sup>8-10</sup> To investigate the impact of UV exposure on cell adhesion on the photo-switchable polymer, primary human skeletal muscle myoblast cells (HSMM) have been seeded on **pBSP7** film (prepared as described in Chapter 6), which was previously exposed to UV light (254 nm) for 20 min. From the same batch of polymer films, another fresh sample of **pBSP7** was illuminated with visible light for 20 min and

this has been used as a control. The first preliminary results are reported in Figure 7.2.

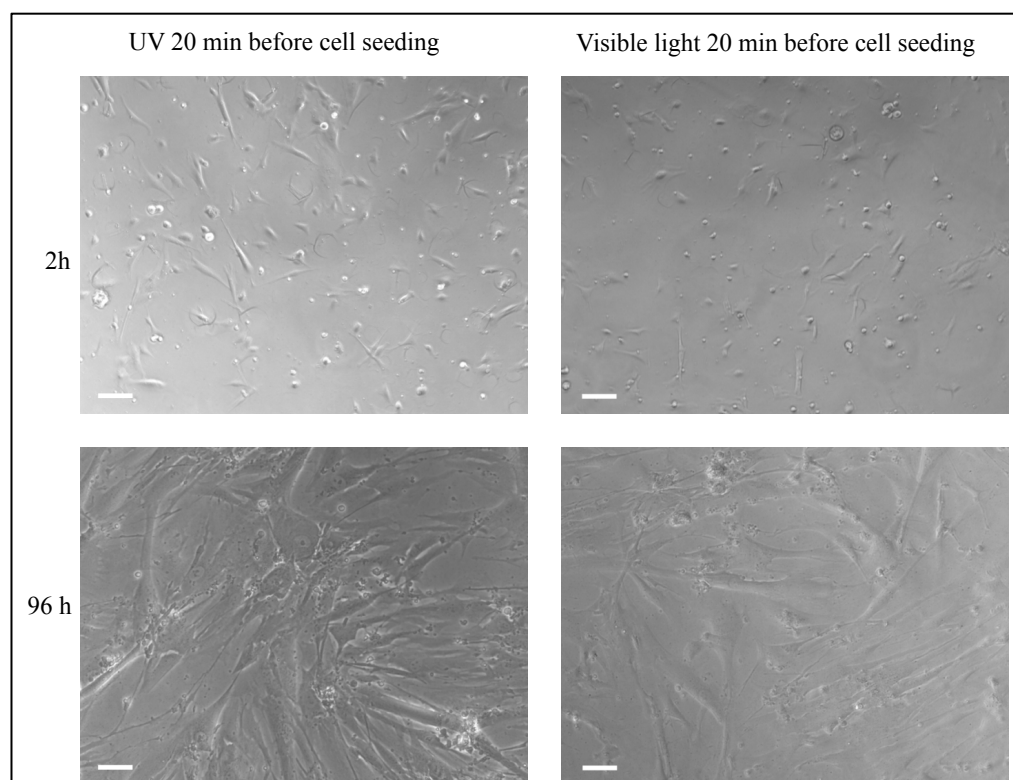


**Figure 7.2.** HSMM cell adhesion and proliferation obtained on photo-switchable polymer. The scale bars represent 100  $\mu\text{m}$ . The rounded cells indicated poor cell adhesion, however, these cells are still alive, they will eventually settle down when the environment becomes more suitable.

From initial results we can conclude that the impact of UV exposure on muscle cell adhesion is short term. Considering the cell migration and secretion of cell adhesion molecules by themselves, patterning of this type of cells via UV exposure is difficult to achieve. However, it still has potential application for certain cells such as neural stem cell, which has been shown to be sensitive to initial cell density.<sup>11</sup> High cell density will favour the adoption of glial fate while low densities will favour neuronal phenotypes. Furthermore, a quick washing off of poor adhered cells in first 2 h of seeding may reinforce the difference of final cell density between UV treated sample and control. New experiments will be addressed in this direction and they are currently being undertaken. The length of the illumination will be increased and the cell types will be chosen accordingly to the results generated.

### 7.2.3 Bi-Modal Uptake and Release of Metal Ions from Diluted Solutions of Photo-Switchable Conducting Polymers

A more thorough spectroscopic investigation has been initiated into the photo-induced metal-ion chelation behavior of **pBSP6** and **pBSP7**. In particular, **pBSP7** was found to be selective to the calcium ion (Figure 7.3). The binding and release mechanisms of this ion, from the polymeric matrix, was directly controlled by the photochemical and electrochemical induced conversion of the **BSP**  $\rightleftharpoons$  **MC** equilibrium. This reaction will be studied by means of spectroscopy, electrochemistry, microscopy and complexometry, exploiting the Calcium-selective fluorophore Calcein (Figure 7.4) to quantify the amount of ions photonically up taken from one site and electrochemically released in a different cell.

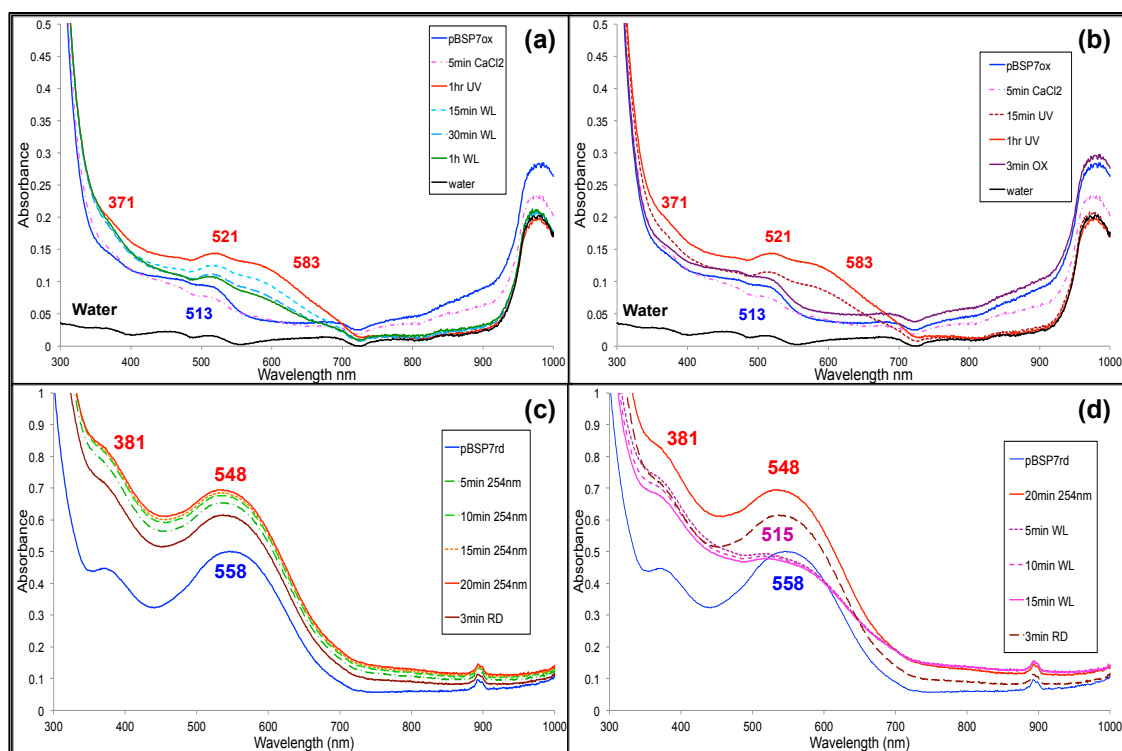


**Figure 7.3:** (a) Oxidized pBSP7 (blue line) thin film, photochemical response to a  $10^{-3}$  M solution of  $\text{Ca}^{2+}$  and (b) white light reversibility in deionised water. (c) Reduced pBSP7 (blue line) thin film, photochemical response to a  $10^{-3}$  M solution of  $\text{Ca}^{2+}$  and (d) white light reversibility in acetonitrile.

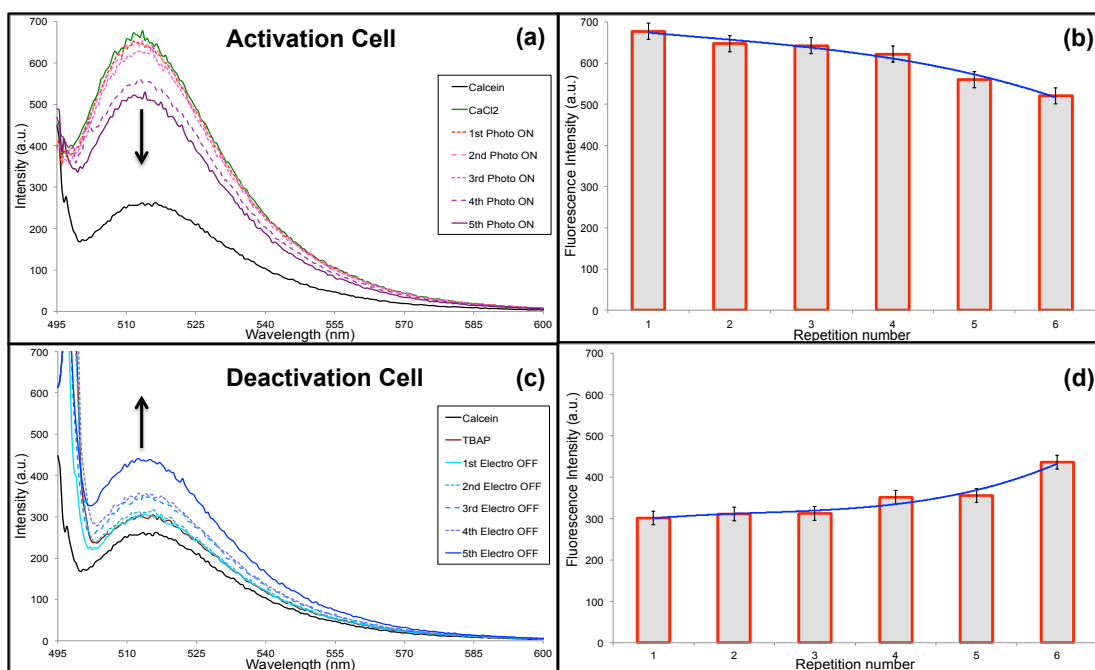


**Figure 7.4:** (a) Luminescence spectra indicating the decrease of the intensity of the complex Calcein-Ca<sup>2+</sup> deriving from an aqueous solution containing 10<sup>-3</sup> M CaCl<sub>2</sub> after the photo activation of the complex pBSP7+Ca<sup>2+</sup>. (b) Columns plot resuming the progressive decrease of the Ca<sup>2+</sup> concentration after the cycles of complexation with pBSP7. (c) Luminescence spectra indicating the increase of the concentration of Ca<sup>2+</sup> indicated by Calcein, in a 0.1 M TBAP.

The author believes that this project has contributed to an increase in the knowledge of the field of stimuli responsive materials and particularly within the family of photo-electro responsive substrates and also hopes that this work will be inspirational for future research in interdisciplinary science and materials chemistry.

### 7.3 References

1. G. E. Collis, W. M. Campbell, D. L. Officer and A. K. Burrell, *Organic & Biomolecular Chemistry*, 2005, **3**, 2075-2084.
2. B. S. Lukyanov and M. B. Lukyanova, *Chemistry of Heterocyclic Compounds*, 2005, **41**, 281-311.
3. M. Madou and J. Florkey, *Chemical Reviews*, 2000, **100**, 2679-2692.
4. M. J. Higgins, P. J. Molino, Z. Yue and G. G. Wallace, *Chemistry of Materials*, 2012, **24**, 828-839.
5. S. E. Moulton, M. J. Higgins, R. M. I. Kapsa and G. G. Wallace, *Advanced Functional Materials*, 2012, **22**, 2003-2014.
6. K. Gilmore, M. Kita, Y. Han, A. Gelmi, M. Higgins, S. Moulton, G. Clark, R. Kapsa and G. Wallace, *Biomaterials*, 2009, **30**, 5292-5596.

7. L. J. del Valle, F. Estrany, E. Armelin, R. Oliver and C. Alemán, *Macromolecular Bioscience*, 2008, **8**, 1144-1151.
8. J. Auernheimer, C. Dahmen, U. Hersel, A. Bausch and H. Kessler, *Journal of the American Chemical Society*, 2005, **127**, 16107-16110.
9. J.-i. Edahiro, K. Sumaru, Y. Tada, K. Ohi, T. Takagi, M. Kameda, T. Shinbo, T. Kanamori and Y. Yoshimi, *Biomacromolecules*, 2005, **6**, 970-974.
10. A. Higuchi, A. Hamamura, Y. Shindo, H. Kitamura, B. O. Yoon, T. Mori, T. Uyama and A. Umezawa, *Biomacromolecules*, 2004, **5**, 1770-1774.
11. R. A. Green, N. H. Lovell, G. G. Wallace and L. A. Poole-Warren, *Biomaterials*, 2008, **29**, 3393-3399.

# APPENDIX A

## Multiswitchable Poly-(Terthiophene) Bearing a Spiropyran Functionality: Understanding Photo- and Electrochemical Control

**Publication status: PUBLISHED**

K. Wagner, R. Byrne, **M. Zanoni**, S. Gambhir, L. Dennany, R. Breukers, M. Higgins, P. Wagner, D. Diamond, G. G. Wallace and D. L. Officer, "A Multiswitchable Poly-(terthiophene) Bearing a Spiropyran Functionality: Understanding Photo- and Electrochemical Control" *Journal of the American Chemical Society*, 133, 5453-5462 (2011). DOI: 10.1021/ja1114634.

## A-1 Electrochemical Deposition of p-BSP2

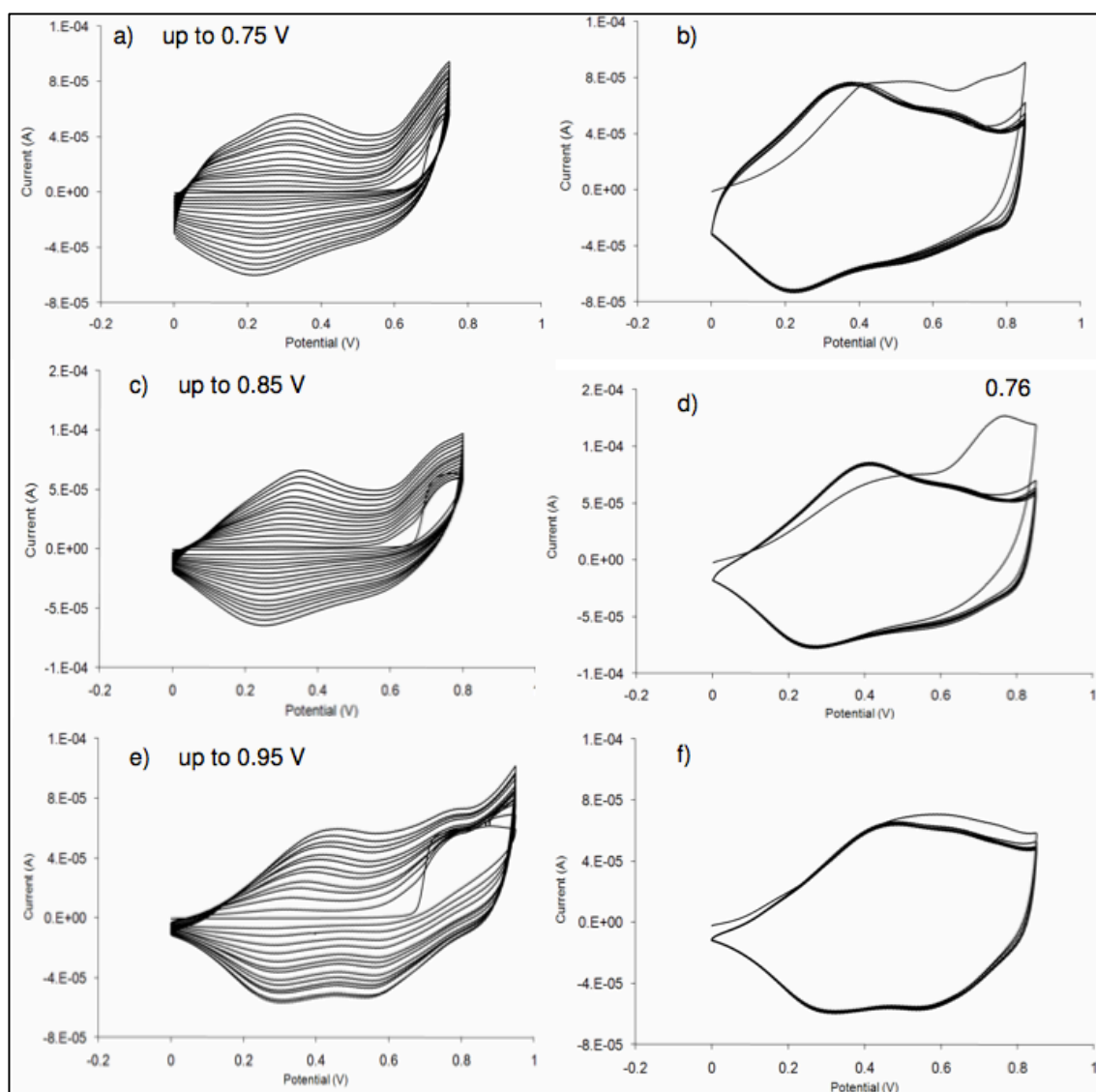


**Figure A1:** Electrochemical deposition of **p-BSP2** at the switching potentials of 0.75 V (a), 0.85 V (c) 0.95 V (e) and the equivalent post CV voltammograms of those films (b), (d), (f).

## A-2 Spectroelectrochemistry of p-TThMA

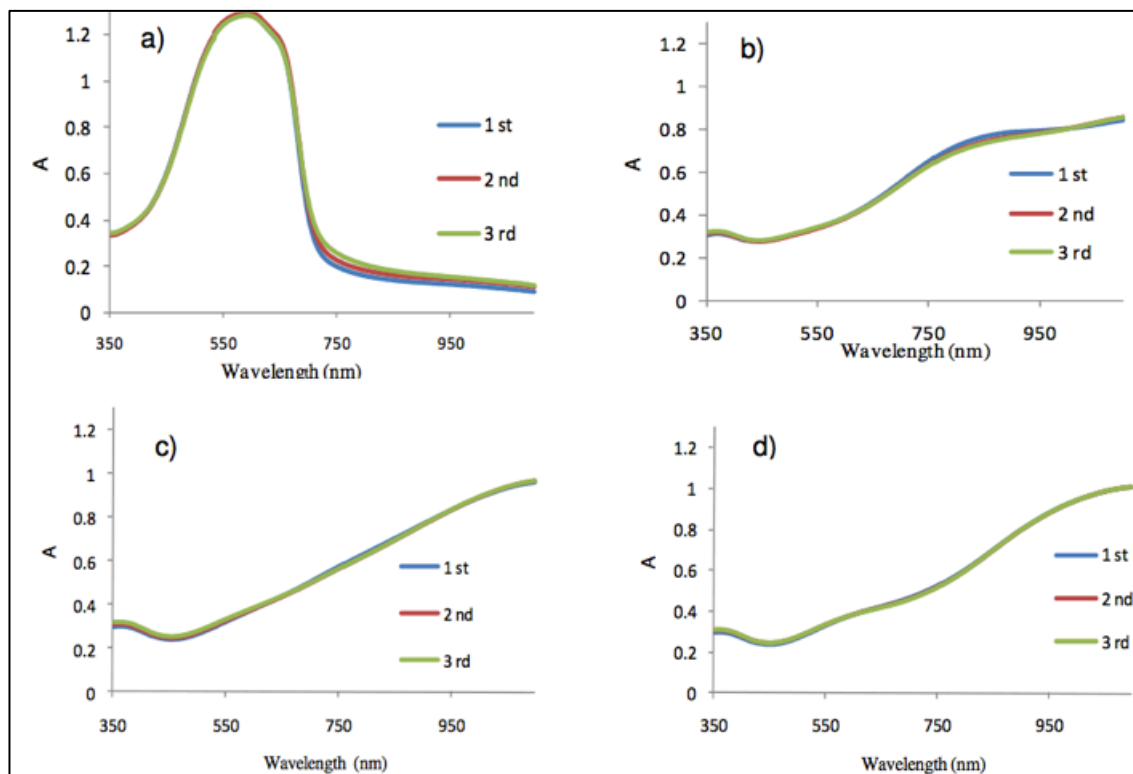


Figure A2: Spectroelectrochemistry of **poly-TThMA** on ITO electrode, recorded three times at the potentials: -0.1 V (a), 0.6 V (b), 0.8 V (c), 1.0 V (d).

## A-3 Spectroelectrochemistry of p-TThMA

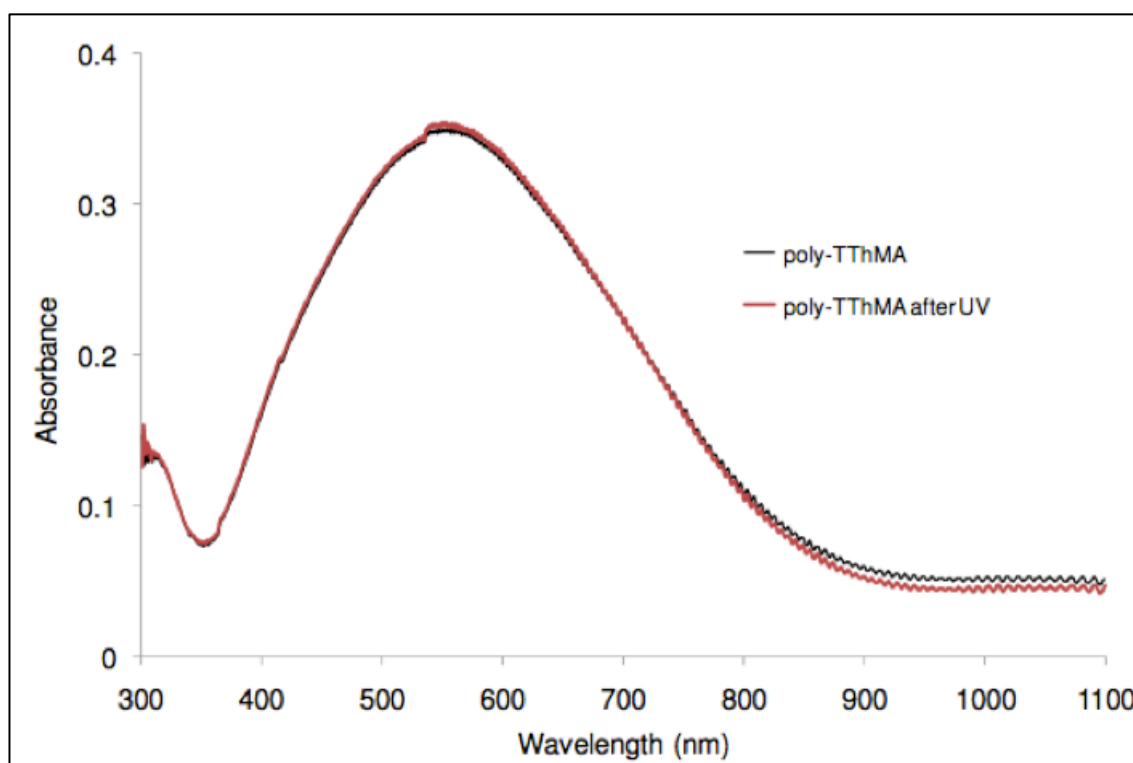
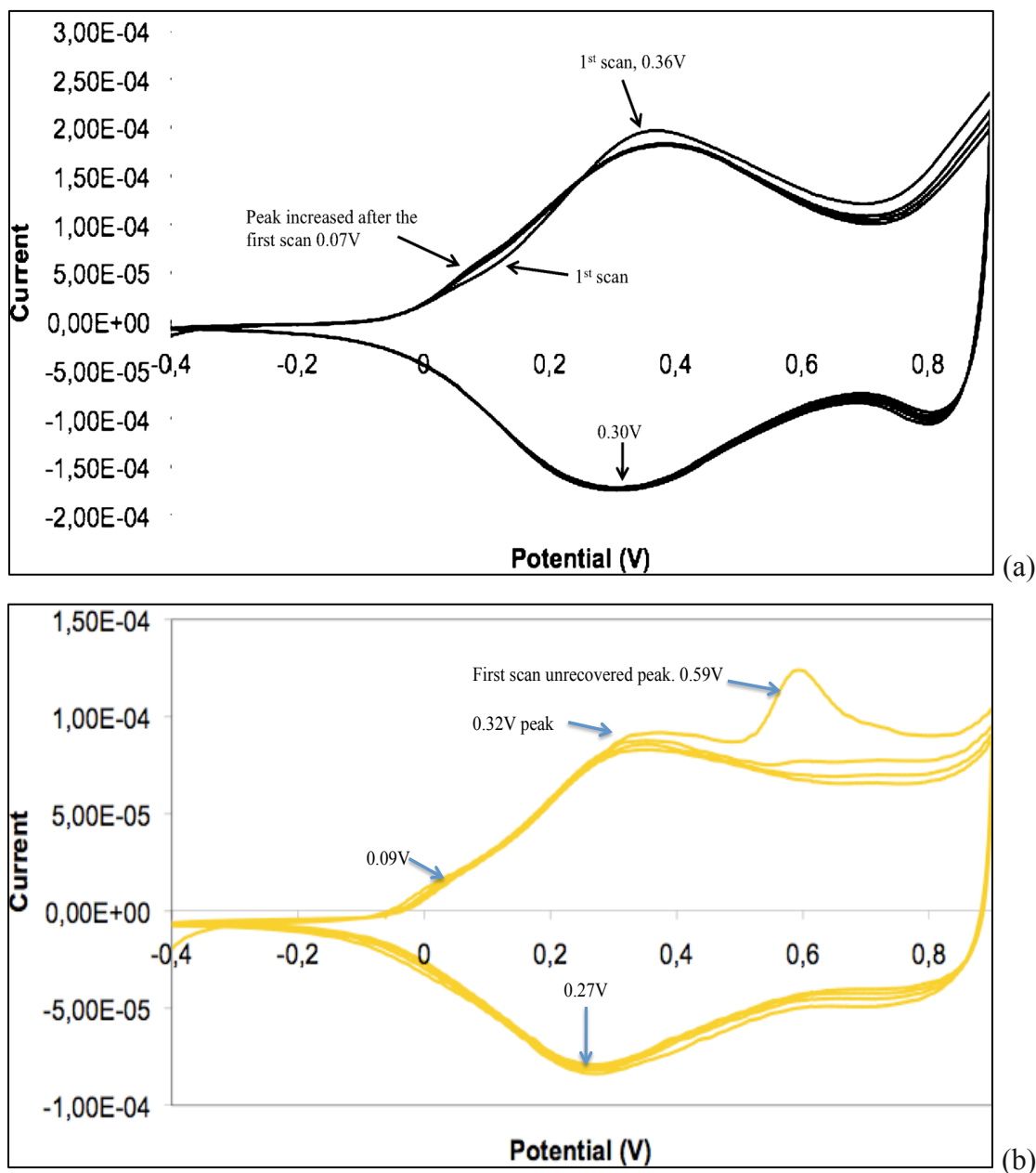


Figure A3: Spectroelectrochemistry of **p-TThMA**.

## A-4 Photo-regeneration of p-BSP2



**Figure A4:** Cyclic Voltammetry with irradiation of UV-light of **p-BSP2**. Evidences of Photochemical regeneration of **BSP1** on the film. (a) first CV. (b) CV under UV-light.

## A-5 AFM analysis of the polymer

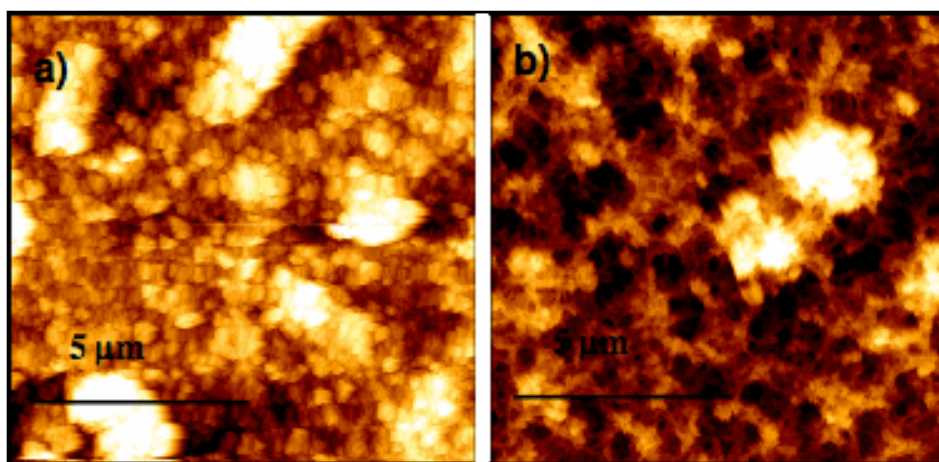


Figure A5: AFM images of p-BSP2.

# APPENDIX B

## Physico-Chemical Study of Spiropyran-Terthiophene Derivatives: Photochemistry and Thermodynamics

**Publication status: PUBLISHED**

**M. Zanoni**, S. Coleman, K.J. Fraser, R. Byrne, K. Wagner, S. Gambhir, D.L. Officer, G.G. Wallace and D. Diamond “Physicochemical Study of Spiropyran-Terthiophene Derivatives: Photochemistry and Thermodynamics”, *Physical Chemistry Chemical Physics*, 14, 9112-9120 (2012). DOI: 10.1039/c2cp41137g.

## B-1 Analytical characterization of BSP-3

$^1\text{H}$  NMR (400 MHz,  $\text{CDCl}_3$ )  $\delta$  7.98 (dd, 1H,  $J = 8.9$  and  $2.8$  Hz, 7-H of benzopyran); 7.90 (d, 1H,  $J = 2.8$  Hz, 5-H of benzopyran); 7.17 (m, 1H, 6'-H of indoline); 7.06 (dd, 1H,  $J = 1.3$  and  $7.3$  Hz, 4-H of indoline) 6.93 (s, 1H, H4'); 6.88 (dt, 1H,  $J = 7.3$  and  $0.8$  Hz, 5'-H of indoline); 6.83 (d, 1H,  $J = 1.7$  Hz, H3); 6.81 (d, 1H,  $J = 1.7$  Hz, H3''); 6.75 (d, 1H,  $J = 10$  Hz, 4-H of benzopyran); 6.71 (d, 1H,  $J = 8.9$  Hz, 8-H of benzopyran); 6.61 (d, 1H,  $J = 7.7$  Hz, 7'-H of indoline); 6.21 (d, 1H,  $J = 1.7$  Hz, H5); 6.14 (d, 1H,  $J = 1.7$  Hz, H5''); 5.67 (d, 1H,  $J = 10$  Hz, 3-H of benzopyran); 4.29 (m, 2H,  $\text{NCH}_2$ ); 3.94 (m, 4H,  $2\text{OCH}_2$ ); 3.71 (2H,  $\text{CH}_2\text{COO}$ ); 1.81-0.86 ( $16\text{CH}_2$ ,  $4\text{CH}_3$ ).  $^{13}\text{C}$  NMR (100.6 MHz)  $\delta$  170.5, 159.5, 157.6, 146.6, 141.0, 136.3, 135.8, 134.7, 133.1, 132.6, 130.3, 128.8, 128.2, 127.8, 126.2, 125.8, 122.7, 121.8, 121.7, 119.9, 118.9, 118.5, 116.3, 115.4, 106.5, 98.0, 96.6, 70.2, 68.1, 63.1, 52.7, 34.8, 31.9, 30.3, 29.7, 29.5, 29.4, 29.3, 29.2, 28.9, 26.0, 25.7, 22.7, 19.7, 14.1, 14.0. HRMS calcd. for  $\text{C}_{53}\text{H}_{66}\text{N}_2\text{O}_7\text{S}_3$ ,  $m/z$ : 938.4257. Found  $m/z$ : 938.3226. Spectrum ( $\text{CH}_3\text{CN}$ )  $\lambda_{\text{max}}$  nm: 362, 252, 572.

## B-2 Thermal Relaxation Profile of MC-2 in Acetonitrile

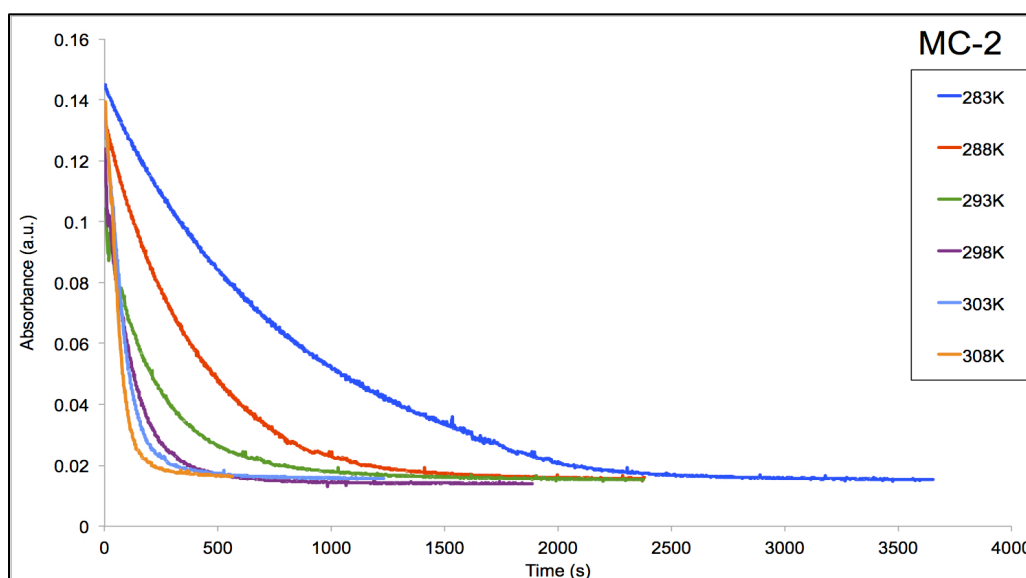


**Figure B1:** Thermal relaxation rate of **MC-2** at  $10^{-4}$  M concentration in the range of temperatures comprised between 283 and 308 K. Arrhenius and Eyring parameters derived from this analysis are reported in Table 3.2. Prior to acquisition of the spectra, the solutions were irradiated with UV-LED device ( $\lambda_{\text{max}} = 375$  nm) for 180 s in the spectrophotometer chamber.  $[\text{BSP-3}] = 10^{-4}$  M in all cases.

### B-3 Thermal Relaxation Profile of MC-1

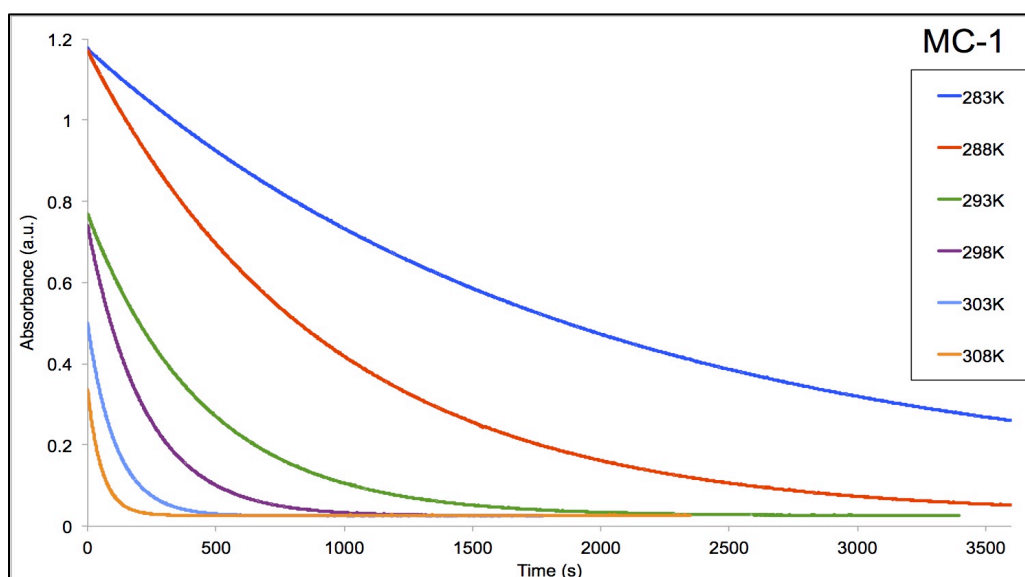


**Figure B2:** Thermal relaxation profiles for **MC-1**  $10^{-4}$  M in acetonitrile over the temperature range 278-308 K. Prior to acquisition of the spectra, the solutions were irradiated with UV-LED device ( $\lambda_{\text{max}} = 375$  nm) for 180 s in the spectrophotometer chamber.  $[\text{BSP-1}] = 10^{-4}$  M in all cases.

### B-4 Solvatochromic effect on MC-2

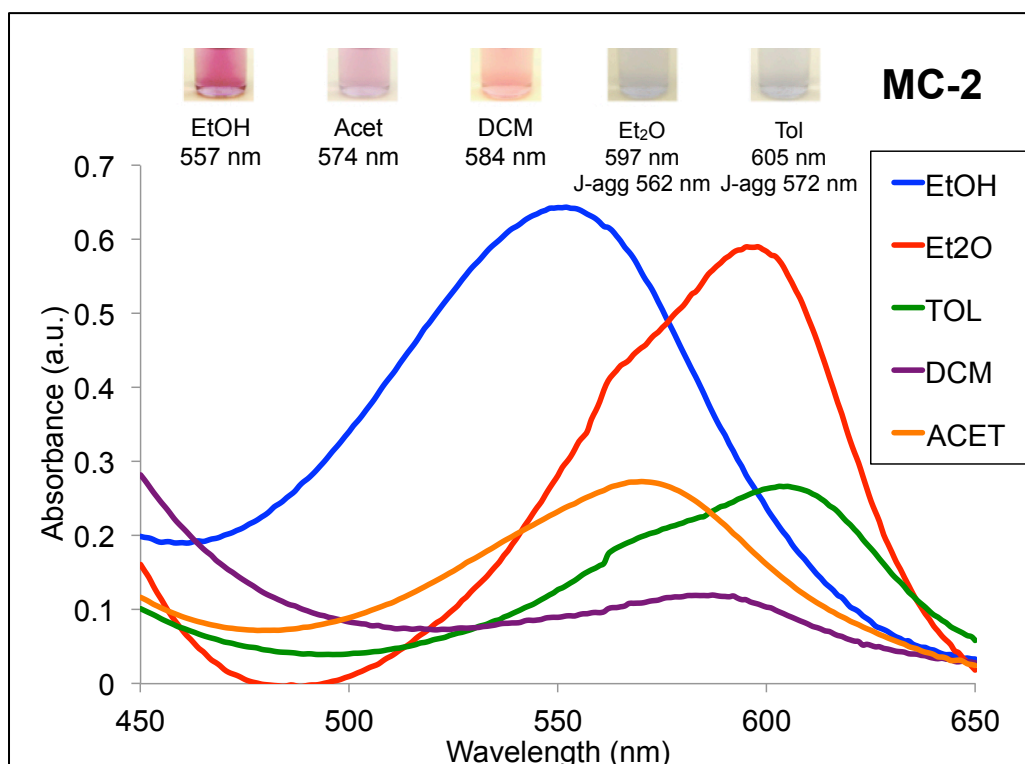


**Figure B3:** Solvatochromic effect of **MC-2** in 5 different solvents. All the solutions were  $10^{-4}$  M. Spectra were measured after exposure to 375 nm UV LED light source for 180 seconds. Results are reported in Table 3.3.

## B-5 Thermal Relaxation Profiles of MC-2 and MC-3 in The Molecular Solvents Studied

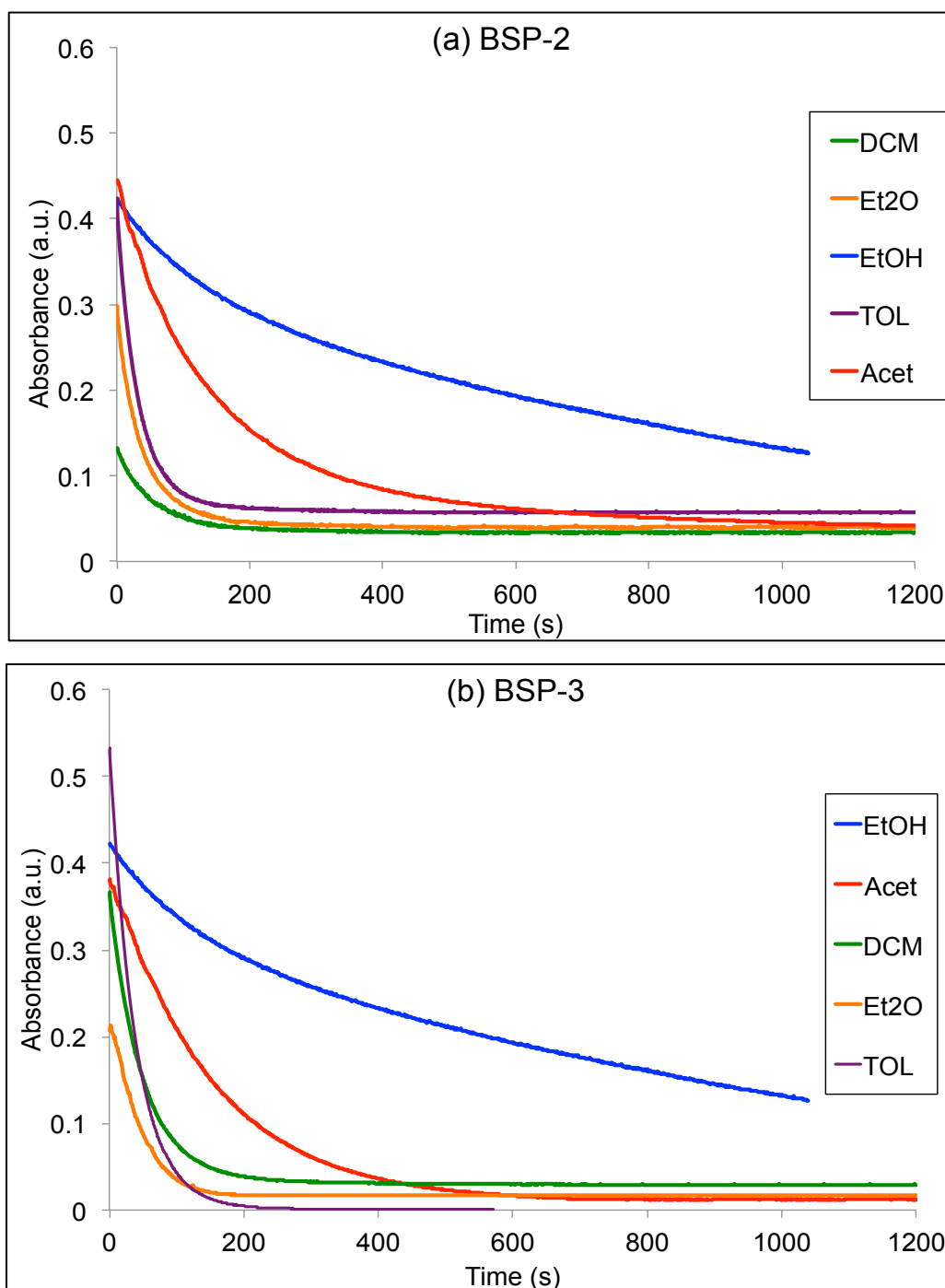


**Figure B4:** (a) Thermal relaxation profiles for **MC-2** in six organic solvents; (b) thermal relaxation profile for **MC-3** in the same solvents. Prior to acquisition of the spectra, the solutions were irradiated with UV-LED device ( $\lambda_{\max} = 375$  nm) for 180 s at 293 K. [**BSP-2**] and [**BSP-3**] =  $10^{-4}$  M in all cases.

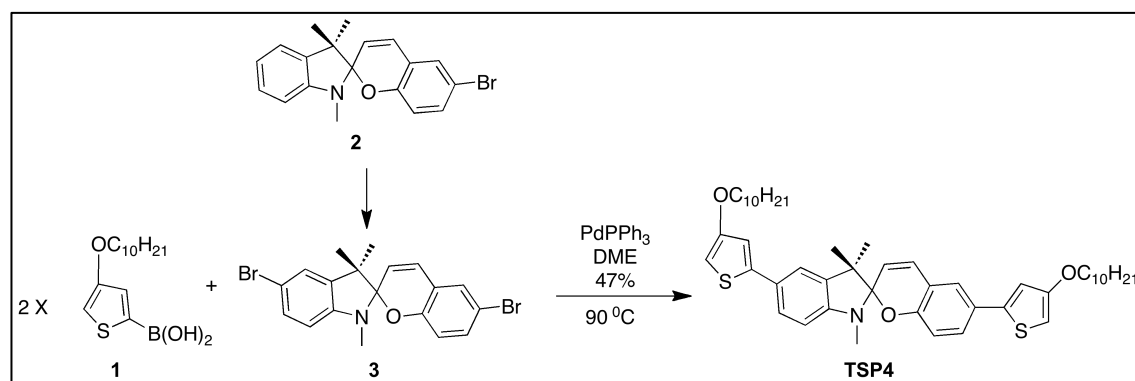
# APPENDIX C

## A Merocyanine–Based Conductive Polymer

**Publication Status: PUBLISHED**

K. Wagner, **M. Zanoni**, A. B. S. Elliott, P. Wagner, R. Byrne, L. E. Florea, D. Diamond, K. C. Gordon, G. G. Wallace, D. L. Officer, *Journal of Materials Chemistry C*, **2013**, DOI: 10.1039/c3tc30479e.

## C-1 Synthesis of 5',6-Bis(4-decyloxythien-2-yl)-1',3'-dihydro-1',3',3'-Trimethyl-Spiro[2H-1-Benzopyran- 2,2'-[2H]Indole] (TSP4)



Scheme C1: Synthesis of TSP4.

The detailed synthesis of **1** will be described elsewhere [1]. Spiropyran **2** was prepared according to the procedure of Silvia et al. [2]. The other compounds were commercially available and used without further purification.

5',6-Dibromo-1',3'-dihydro-1',3',3'-trimethyl-spiro[2H-1-benzopyran-2,2'-[2H]indole] (**3**): We modified the method described previously [3]: **2** (5.27 g, 14.8 mmol) was dissolved in chloroform (40 mL), brought to reflux and NBS (2.63 g, 14.8 mmol, 1 eq) in chloroform (150 mL) was added dropwise in time of 60 min. The resulting mixture was refluxed for additional 30 min then cooled to room temperature. The solid was filtered off and washed with chloroform. The filtrate was washed twice with water, dried over magnesium sulphate evaporated to dryness at 50 °C under vacuum. The amorphous mass was recrystallised from ethanol to give fine yellow-green crystals of **3**. Yield: 5.60 g, 87%, The spectroscopic data was identical with that reported previously [3].

5',6-Bis(4-decyloxythien-2-yl)-1',3'-dihydro-1',3',3'-trimethyl-spiro[2H-1-benzopyran-2,2'-[2H]indole] (**TSP4**): **1** (1.03 g, 6 mmol) and **3** (0.87 g, 2 mmol) were dissolved in dimethoxyethane (35 mL) and degassed. The 1M solution of potassium carbonate (10 mL) was added followed by tetrakis(triphenylphosphine) palladium(0) (0.34 g, 4 mol%). The resulting mixture was stirred at 90 °C overnight then cooled to room temp.

The mixture was diluted with dichloromethane, washed with brine, dried over magnesium sulphate and evaporated to dryness at 50<sup>0</sup> C under vacuum. In order to remove the dithiophene impurity, the resulting dark oil was dissolved in a minimal amount of dichloromethane and treated with warm methanol (~50 mL). The warm milky solution was decanted from the resulting yellow oil. The procedure was repeated twice to give the product **TSP4** as a yellow oil, which solidified with time. Yield: 0.71 g, 47%. <sup>1</sup>H NMR (CDCl<sub>3</sub>, ppm) δ: 7.39 (dd, 1H, J = 8.1 and 1.9 Hz, Ar-H), 7.30 (dd, 1H, J = 8.5 and 2.3 Hz, Ar-H), 7.25-7.23 (m, 2H, Ar-H), 6.90-6.81 (m, 3H, 2 x Th-H + CH), 6.72 (d, 1H, J = 8.5 Hz, Ar-H), 6.50 (d, 1H, J = 8.1 Hz, Ar-H), 6.11 (d, 1H, J = 1.8 Hz, Th-H), 6.08 (d, 1H, J = 1.8 Hz, Th-H), 5.72 (d, 1H, J = 10.0 Hz, CH), 3.98-3.90 (m, 4H, OCH<sub>2</sub>), 2.75 (s, 3H, NCH<sub>3</sub>), 1.82-1.72 (m, 4H, CH<sub>2</sub>), 1.50-1.41 (m, 4H, CH<sub>2</sub>), 1.39-1.23 (m, 30 H, Alk-CH<sub>2</sub> + 2 x CH<sub>3</sub>), 0.92-0.85 (m, 6H, Alk-CH<sub>3</sub>); HRMS (ESI, M<sup>+</sup>+1) found: 754.4333, for C<sub>47</sub>H<sub>64</sub>NO<sub>3</sub>S<sub>2</sub> requires: 754.4328. <sup>13</sup>C NMR (CDCl<sub>3</sub>, 100 MHz, ppm) δ: 157.90, 157.84, 154.22, 148.09, 143.87, 142.41, 137.40, 136.02, 129.34, 127.07, 126.94, 126.13, 125.34, 123.77, 119.76, 119.27, 118.88, 115.89, 115.42, 114.67, 113.95, 106.86, 104.58, 96.40, 95.61, 94.83, 70.17, 70.05, 69.97, 51.79, 31.92, 29.60, 29.59, 29.43, 29.41, 29.39, 29.33, 29.27, 29.24, 28.95, 26.10, 26.08, 25.92, 22.69, 20.13, 14.12.

## C-2 Electrochemical Polymerization of TSP4

**PolyTMC4** films were electrochemically grown on either a platinum disc working electrode, with a 0.02 cm<sup>2</sup> surface area (Bioanalytical System) or on an optically transparent ITO (Indium Tin Oxide) coated glass (Delta Technologies, Limited, resistivity R<sub>s</sub> = 4-8 Ω by cyclic voltammetry (0 – 1.2 V, scan rate 100 mV s<sup>-1</sup>) or chronoamperometric deposition at constant potential (1.2 V for up to 30 mins) from an anhydrous dichloromethane : acetonitrile (1:2) solution containing 0.1 M tetrabutylammonium perchlorate (TBAP) and the monomer at a concentration of 8 mM. **PolyTMC4-Co<sup>2+</sup>** films were electrodeposited from the same solution containing additionally 8 mM cobalt acetate tetrahydrate (1:1, **TSP4:Co<sup>2+</sup>**) obtained by adding the appropriate amount of a 0.238 M methanol solution of cobalt acetate tetrahydrate. Pt mesh and Ag/Ag<sup>+</sup> electrodes were used as counter electrode and quasi- reference electrode, respectively. For calibration of the Ag/Ag<sup>+</sup> electrode, half-wave potentials were measured for 1 mM ferrocene, i.e. E<sub>1/2</sub> = 0.165 V vs. Ag/ Ag<sup>+</sup> reference electrode. Solutions were degassed prior to the measurements.

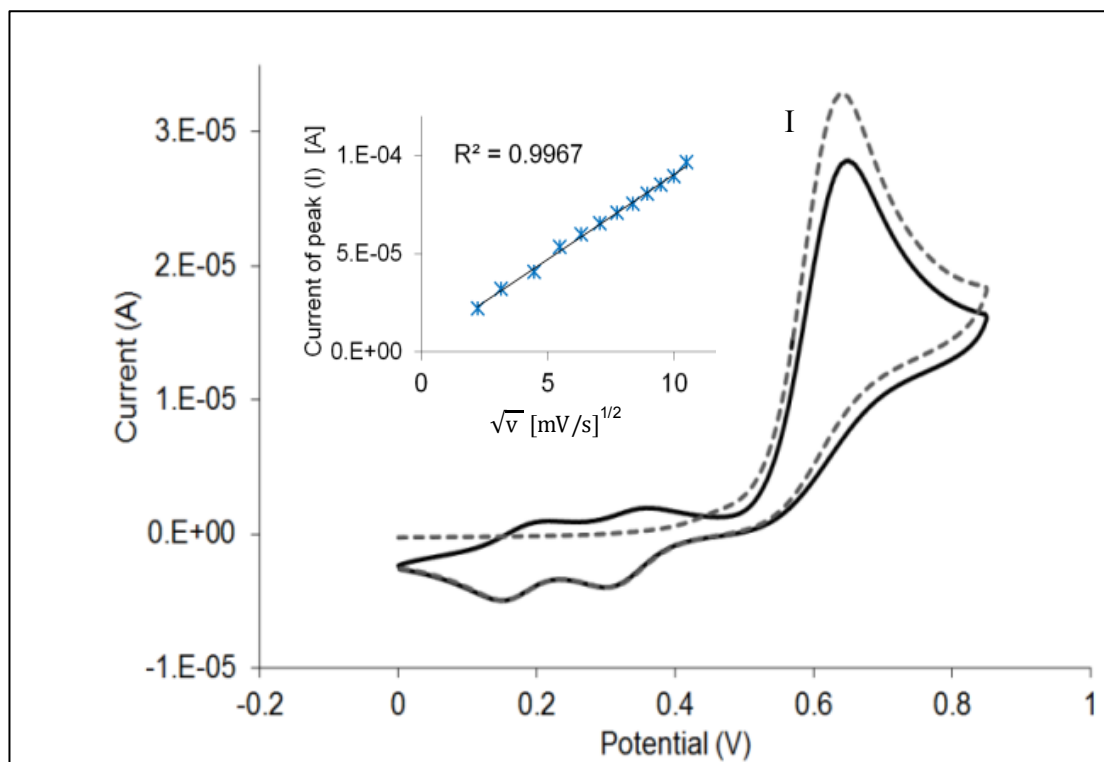


**Figure C1:** Cyclic voltammograms of  $8 \times 10^{-3}$  M TSP4 between 0 V and 0.8 V, inset current of peak (I) versus square root of scan rate.

### C-3 UV-vis Spectroscopy

- a) **Acidic/base isomerisation of TSP4.** Solution of  $2 \cdot 10^{-5}$  M TSP4 monomer in dichloromethane :methanol (1:1) was illuminated with 254 nm UV light and the spectra were collected every 1 min (total exposure time to the UV was 7 min) Results are showed on the Figure 5.2a. 100  $\mu$ L of 1 M HCl has been introduced into 50 mL of  $2 \cdot 10^{-5}$  M TSP4 monomer in dichloromethane : methanol (1:1) giving an excess of the acid (100:1,  $2 \cdot 10^{-3}$ : $2 \cdot 10^{-5}$ M). The spectra of this solution were collected every 1 min. The same amount of 1 M NaOH was introduced into acidified solution and the spectra were collected immediately (Fig. 5.2b).
- b) **UV-Vis of TSP4 with  $\text{Co}^{2+}$ .** Absorbance spectra of  $2 \cdot 10^{-5}$  M TSP4 in dichloromethane: methanol (1:1) solution were collected first, then the solution has been exposed to 254 nm UV light for 7 min. Then cobalt acetate tetra hydrate (0.238 M) dissolved in methanol was adjusted with micropipette into solution to get molar ratio with monomer (1:1).
- c) **Spectroelectrochemistry of polymer films.** The spectroelectrochemistry of the polymer films deposited on ITO electrode was investigated in solutions of 0.1 M TBAP in acetonitrile vs. Ag wire for the reference electrode. These applied voltages for the Ag wire were rescaled vs.  $\text{Ag}/\text{Ag}^+$  by using ferrocene. The

controlled-potentials measurements were carried out with eDAQ system controlled by EChem software. All absorbance spectra were recorded using a Shimadzu UV-1800 spectrophotometer.

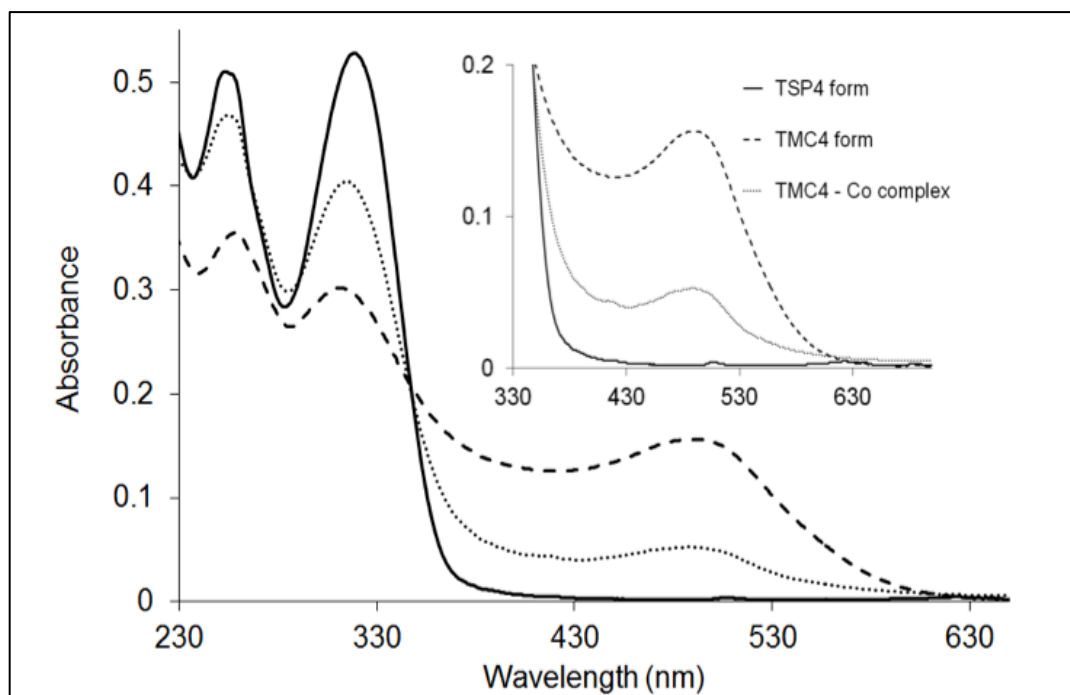


**Figure C2:** Absorbance spectra of  $2 \cdot 10^{-5}$  M TSP4 (black line), TMC4 (dashed line) and TMC4 with  $\text{Co}^{2+}$  (1:1) (dotted line).

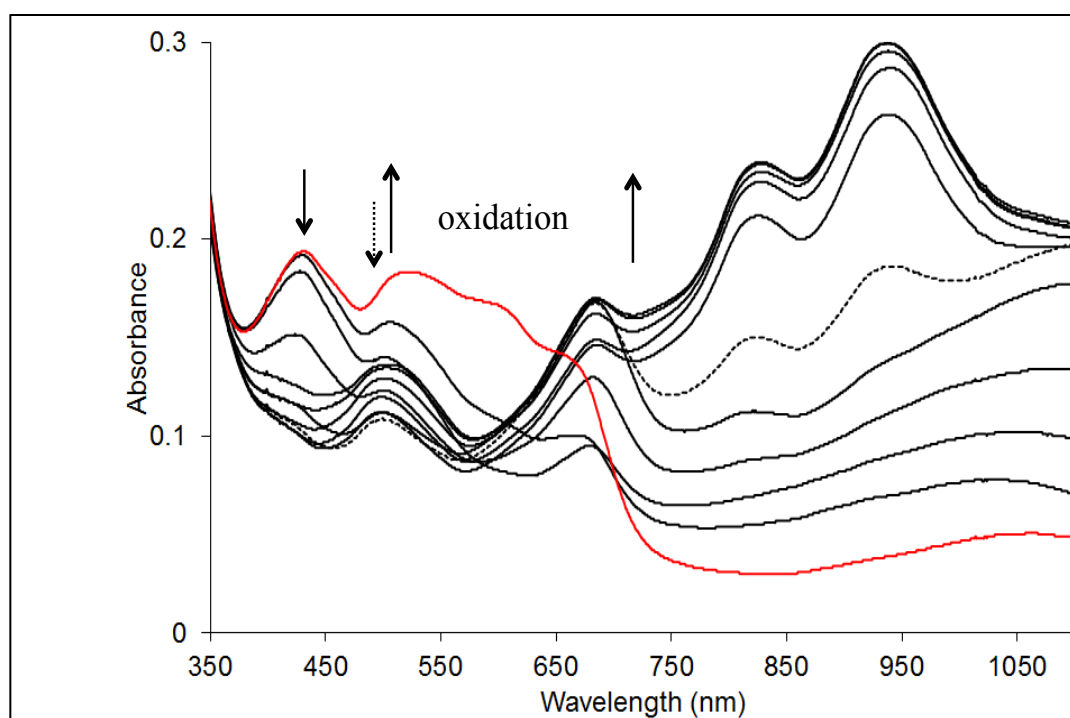


**Figure C3:** Spectroelectrochemistry of polyTMC4- $\text{Co}^{2+}$  electrodeposited on ITO glass for potential ranges of -0.5 V (red line) – 0.9 V.

## C-4 Conductivity Measurement.

4 point resistivity meter (JANDEL Model RM2), with spacing in square array 0.635 mm, was used in conductivity measurements. **PolyTMC4** and **polyTMC4-Co<sup>2+</sup>** was electrochemically grown on optically transparent ITO-coated glass by chronoamperometric deposition at constant potential 1.2 V during 30 min. The polymer was then peeled off the electrode and the conductivity measurement was performed on the freestanding film.

## C-5 Elementary Analysis.

**PolyTMC4-Co<sup>2+</sup>** was electrochemically grown at the conditions described in (2) by chronoamperometric deposition at constant potential 1.2 V during 30 min, multiple times to archived 2.2 mg samples. The analyses were done in Research School of Chemistry, Australian National University in Canberra.

Results			ICP-OES Results	
Element	Found %	Method	Element	Found %
N	1.81	EA 3000		
C	62.83	EA 3000		
H	7.47	EA 3000		
S	7.79	Dionex (Sulphur only)	Co	0.23

**Table C1:** Elementary analysis of **pTMC4**

Assuming that there is one perchlorate counter ion per monomer unit, the calculated analytical data is a reasonable match to the experimental data. Therefore, this was assumed in calculating the likely ratio of 1 Co<sup>2+</sup> to 30 monomer units (Calc. for C<sub>1410</sub>H<sub>1890</sub>Cl<sub>30</sub>N<sub>30</sub>O<sub>210</sub>S<sub>60</sub>Co: 65.98% C, 7.42% H, 4.14% Cl, 1.64% N, 13.09% O, 7.50% S, 0.23% Co).

## C-6 SEM Imaging.

**PolyTMC4** and **PolyTMC4-Co<sup>2+</sup>** films for SEM analyses were electrodeposited on ITO during applied a potential 1.2 V during 10 s. Jeol7500 field emission scanning electron microscope (FESEM) was use for SEM analysis.

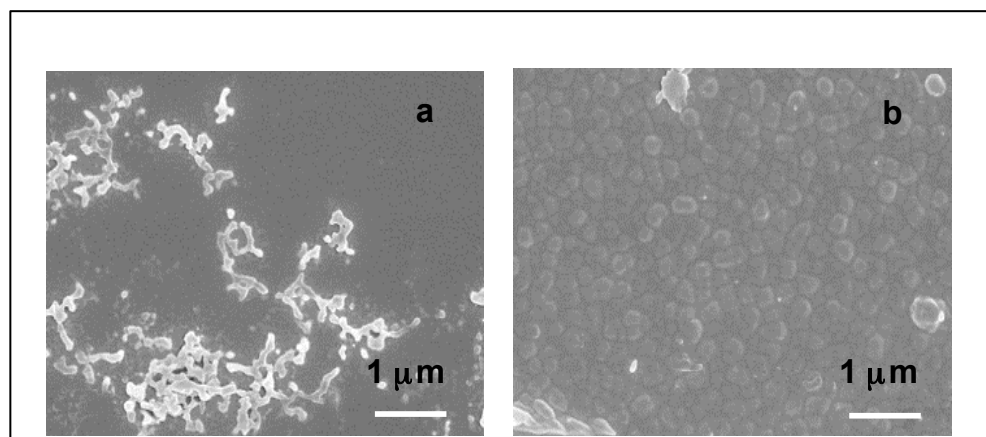


**Figure C4:** SEM images of **polyTMC4 (a)** and **polyTMC4-Co<sup>2+</sup>** on ITO glass after a constant potential deposition 1.2 V for 10 s.

## C-7 Fourier-Transform Raman

(**FT-Raman**) spectra were obtained from solid samples utilising a Bruker Equinox-55 FT-interferometer with an FRA106/5 Raman accessory and D418T liquid-nitrogen-cooled Germanium detector. 1064 nm excitation was provided by a ND:YAG laser operating at 120 mW, while the software used was the Bruker OPUS v5.5 package.

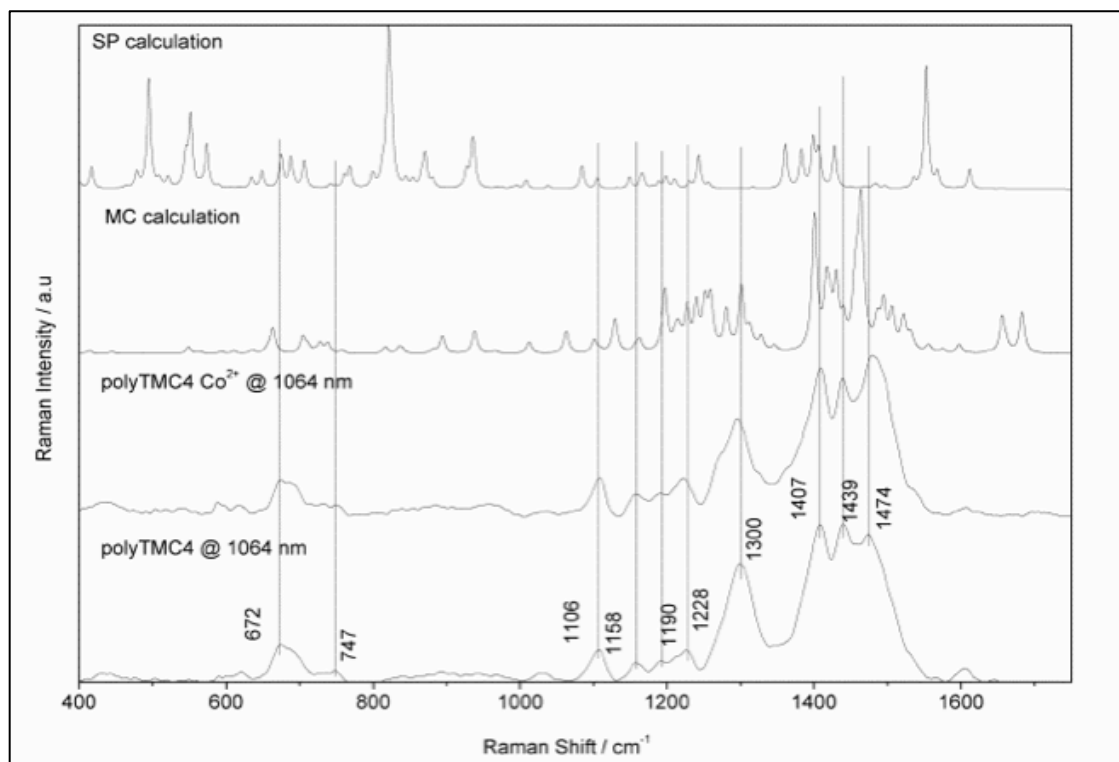


**Figure C5:** Calculated Raman spectra of the **SP** form (top) and **MC** form (2<sup>nd</sup> from top) compared to experimental FT-Raman spectra of **polyTMC4** (bottom) and **polyTMC4-Co<sup>2+</sup>** (2<sup>nd</sup> from bottom) in their oxidised forms.

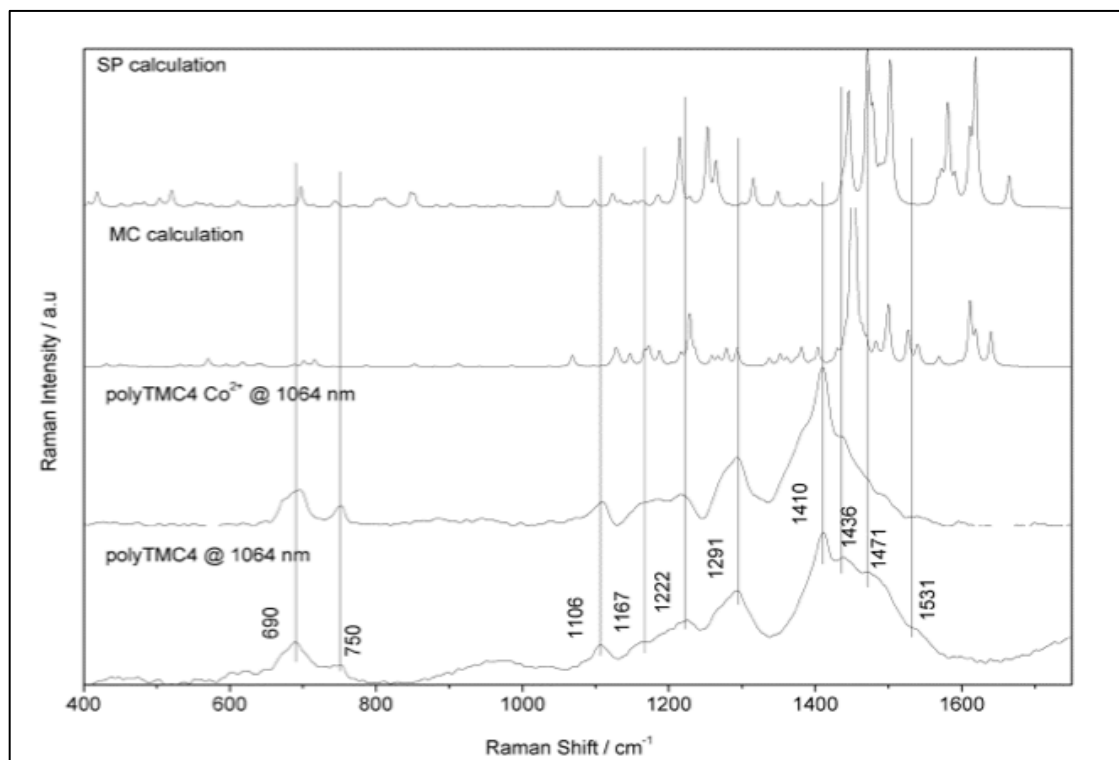


**Figure C6:** Calculated Raman spectra of the **SP** form (top) and **MC** form (2<sup>nd</sup> from top) compared to experimental FT-Raman spectra of **polyTMC4** (bottom) and **polyTMC4-Co<sup>2+</sup>** (2<sup>nd</sup> from bottom) in their reduced forms.

## C-8 Computational Modelling

Computational modelling was performed using Gaussian 09 software.<sup>3</sup> Density functional theory (DFT) calculations of the molecular geometries and vibrational modes were accomplished with the B3LYP functional and 6-31G(d) basis. Time-dependent (TD-)DFT calculations were performed using the B3LYP method and 6-31G(d) basis functions. A scale factor of 0.974 was used when generating theoretical spectra using Gausssum v2.26 software. Molecular orbital visualisation was accomplished with Gaussview v5.0.84 and vibrational modes with Molden [7]. Bond length alternation diagrams were obtained from density functional theory calculations by uniquely numbering the bonds (as shown in Fig. 5.5a) and plotting this versus the bond length (in Å) calculated by Gaussian (Fig. 5.5b).

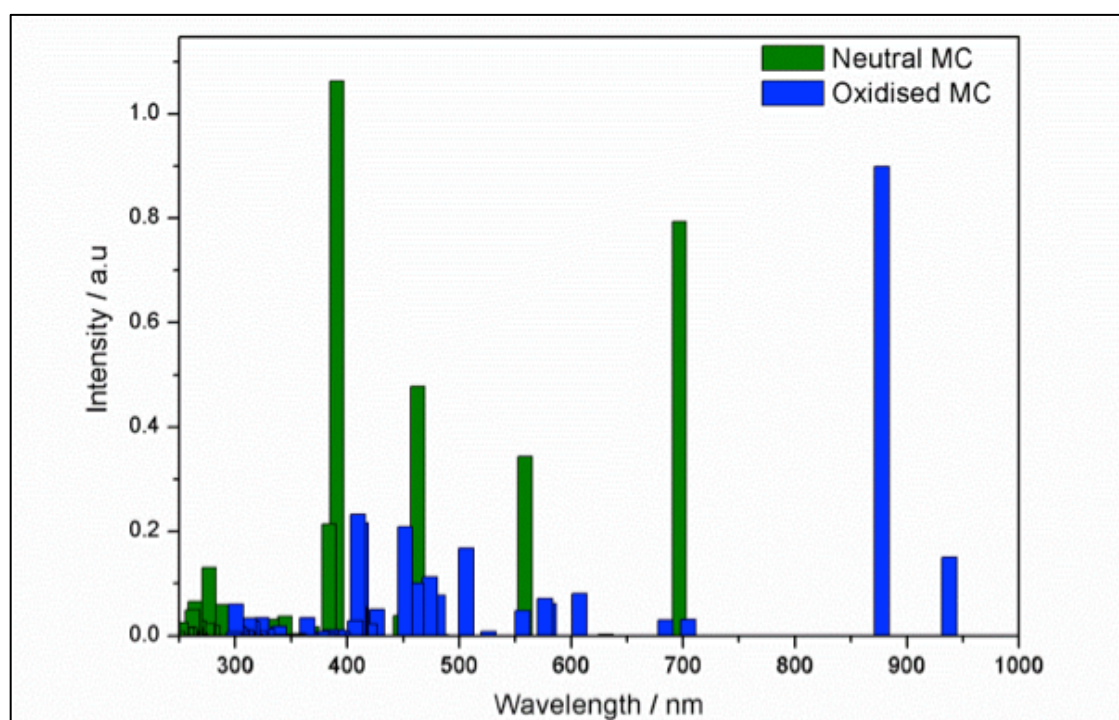


Figure C7: TD-DFT results comparing the neutral and oxidised MC form.

## C-9 References

- (1) Julie M. Locke, Robert Breukers, Sanjeev Gambir, Klaudia Wagner, David Officer, Development of Processable Terthiophene Co-polymers Incorporating Reactive Carboxylate Groups. - *manuscript in preparation*
- (2) T. R. Silvia, V. S. L. Ana, Eduardo A. S. Gonzalez, *Synthetic Communications* **1995**, 25, 105-110.
- (3) M. J. T. Frisch, G. W.; Schlegel, H. B.; Scuseria, G. E.; Robb, M. A.; Cheeseman, J. R.; Scalmani, G.; Barone, V.; Mennucci, B.; Petersson, G. A.; Nakatsuji, H.; Caricato, M.; Li, X.; Hratchian, H. P.; Izmaylov, A. F.; Bloino, J.; Zheng, G.; Sonnenberg, J. L.; Hada, M.; Ehara, M.; Toyota, K.; Fukuda, R.; Hasegawa, J.; Ishida, M.; Nakajima, T.; Honda, Y.; Kitao, O.; Nakai, H.; Vreven, T.; Montgomery, Jr., J. A.; Peralta, J. E.; Ogliaro, F.; Bearpark, M.; Heyd, J. J.; Brothers, E.; Kudin, K. N.; Staroverov, V. N.; Kobayashi, R.; Normand, J.; Raghavachari, K.; Rendell, A.; Burant, J. C.; Iyengar, S. S.; Tomasi, J.; Cossi, M.; Rega, N.; Millam, N. J.; Klene, M.; Knox, J. E.; Cross, J. B.; Bakken, V.; Adamo, C.; Jaramillo, J.; Gomperts, R.; Stratmann, R. E.; Yazyev, O.; Austin, A. J.; Cammi, R.; Pomelli, C.; Ochterski, J. W.; Martin, R. L.; Morokuma, K.; Zakrzewski, S. Dapprich, A. D. Daniels, M. C. Strain, O. Farkas, D. K. Malick, A. D. Rabuck, K. Raghavachari, J. B. Foresman, J. V. Ortiz, Q. Cui, A. G. Baboul, S. Clifford, J. Cioslowski, B. B. Stefanov, G. Liu, A. Liashenko, P. Piskorz, I. Komaromi, R. L. Martin, D. J. Fox, T. Keith, M. A. Al-Laham, C. Y. Peng, A. Nanayakkara, M. Challacombe, P. M. W. Gill, B. Johnson, W. Chen, M. W. Wong, C. Gonzalez and J. A. Pople, Gaussian Inc., Pittsburgh, PA, 2003.
- (4) A. P. Scott and L. Radom, *J. Phys. Chem.*, 1996, **100**, 16502-16513
- (5) N. M. O'Boyle, A. L. Tenderholt, K. M. Langner, *J. Comp.Chem.*, 2008, **29**, 839-845
- (6) R. K. Dennington, T.; Millam, J.G. Schaftenaar, J. H. Noordik, *J. Comp. Mod. Design*, 2000, **14**, 123-134

# APPENDIX D

## **Spiropyran-Terthiophene Multi- Modal Molecular Switches: Photochromic, Acidochromic and Electrochromic Properties**

**Publication status: Manuscript in preparation.**

**M. Zanoni**, K. Wagner, R. Byrne, S. Gambhir, P. Wagner, G. G. Wallace, D. L. Officer and D. Diamond, "Spiropyran-Terthiophene multi-modal molecular switches: photochromic, halochromic and electrochromic properties", *in preparation*, (2013).

## D-1 Synthesis of the New Spiropyran (BSPe) and Spiropyran-Terthiophene Moieties (BSP6 and BSP7)

### Preparation of BSPe

1',3',3'-trimethylspiro(chromene-2,2'-indolin)-6-yl acetate (**BSPe**) was synthesized according to the following procedure: all glassware washed using 1M NaOH in EtOH and dried overnight in a drying cabinet. 1-(2-hydroxyethyl)-3,3-dimethylindoline-6'-hydroxylspiropyran (**BSP5**) (0.44 g, 1.1 mmol) was dissolved in acetic anhydride (75 ml, 0.79 mmol) and the brown mixture stirred until the spiropyran crystals were completely dissolved at 30 °C. After this, 5 drops of concentrated H<sub>2</sub>SO<sub>4</sub> were carefully added waiting each time for the bubbles to disappear. The mixture was allowed to reach 70 °C and it was stirred for 2 hr. The reaction was quenched with a saturated aqueous solution of NaHCO<sub>3</sub> until no further reaction was observed. The mixture was then extracted with 30 ml of DCM, dried over MgSO<sub>4</sub> and concentrated under reduced pressure. The crude mixture was then purified through silica gel column chromatography with a step gradient of ethyl acetate/hexane 1 : 1 (v/v) to reach DCM/hexane 3 : 1 (v/v). After drying under reduced pressure, the desired product was isolated as dark red oil (0.27 g, 61%). <sup>1</sup>H NMR (400 MHz, CDCl<sub>3</sub>): δ 1.23 (6H, s, C3-CH<sub>3</sub>), 2.19 (3H, s, N-CH<sub>3</sub>), 2.64 (3H, s, CO-CH<sub>3</sub>), 5.63 (1H, d, J = 10 Hz, H3 Pyr), 6.45 (1H, d, J = 7.72 Hz, Ar-H), 6.70 (1H, d, J = 3.76 Hz, Ar-H), 6.72 (1H, m, J = 7.64, Ar-H), 6.77 (1H, dd, J = 0.84 Hz, 7.4 Hz, Ar-H), 6.99 (1H, dd, J = 0.86 Hz, 7.22 Hz, Ar-H), 7.10 (1H, dd, J = 1.22 Hz, 7.6 Hz, Ar-H), 7.20 (1H, ddd, J = 1.22 Hz, 15.22 Hz, Ar-H+C=O). <sup>13</sup>C NMR (400 MHz, CDCl<sub>3</sub>): δ 18.5 (C[CH<sub>3</sub>]<sub>2</sub>), 20.5 (O-CH<sub>3</sub>), 30.6 (N-CH<sub>3</sub>), 52 (C[CH<sub>3</sub>]<sub>2</sub>-backbone), 106.6, 117.8, 125.9, 127.6, 137.4, 148.9 (C-indoline aromatic), 115.4, 116.6, 121, 121.2, 121.4, 127, 142.8, 151.2, 169 (C-pyran). Electronic spectrum (Acetonitrile) λ<sub>max</sub> nm: 294, 458.

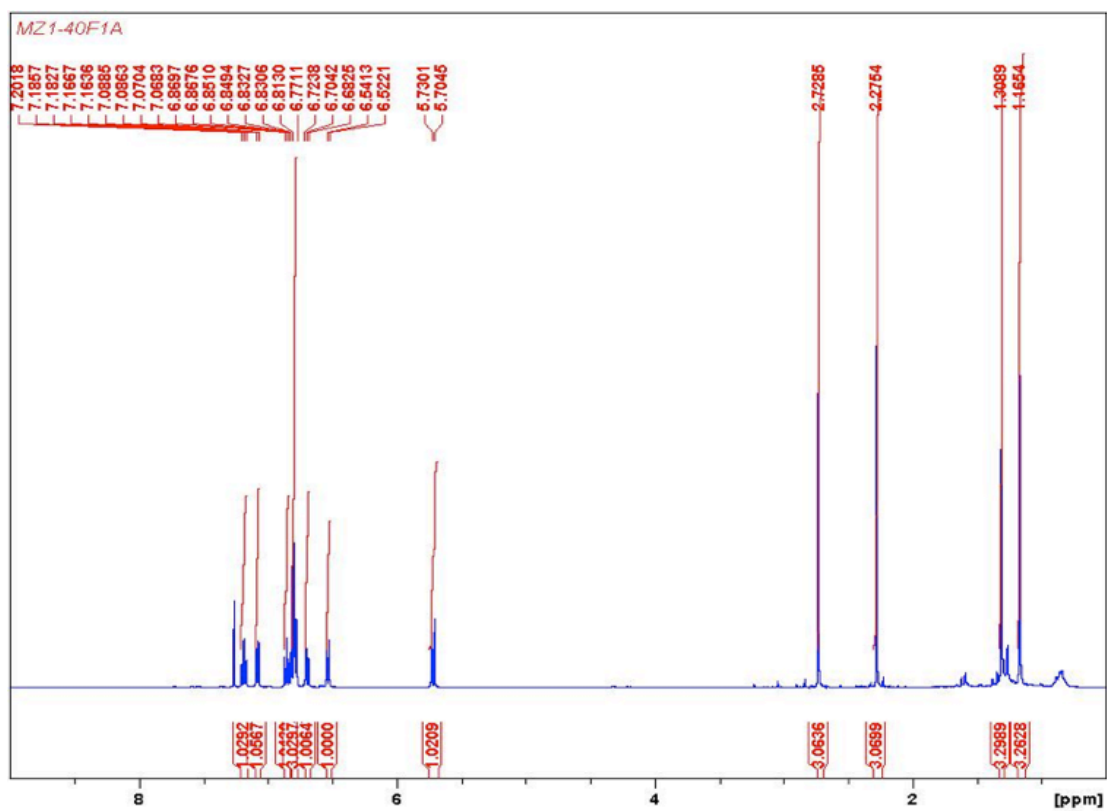


Figure D1:  $^1\text{H}$  NMR spectra of BSPe using a Bruker 400 MHz in  $\text{CDCl}_3$ .

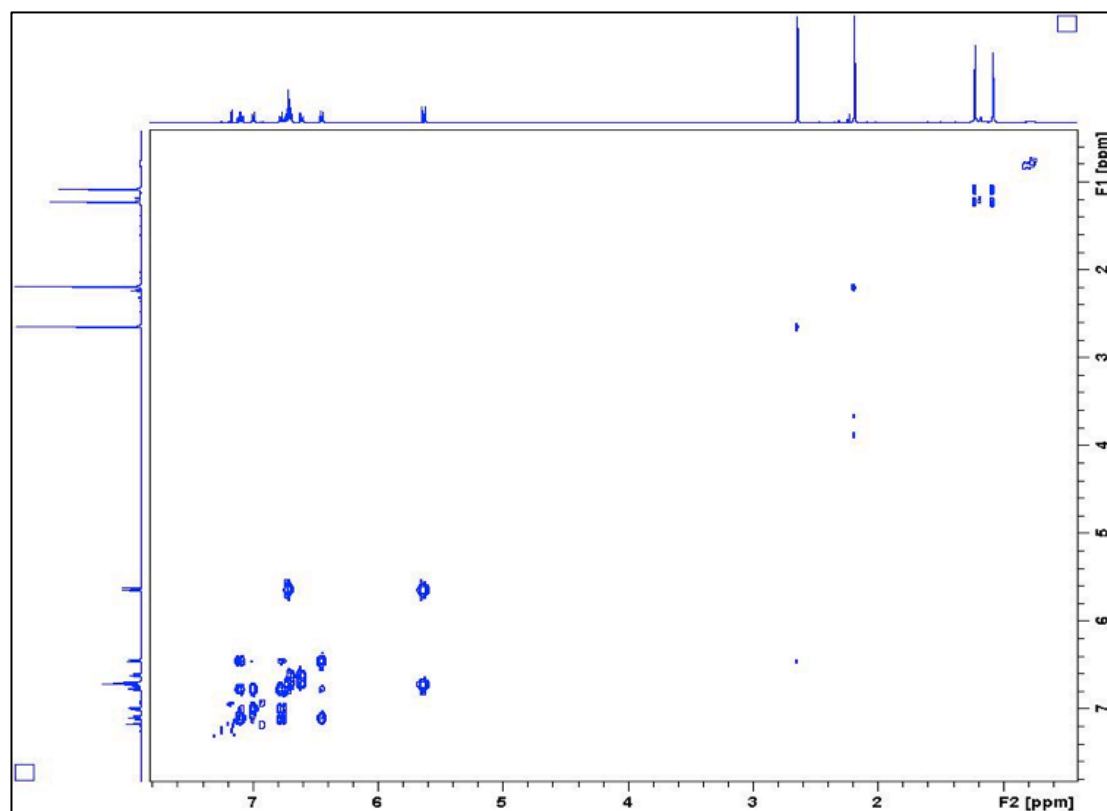
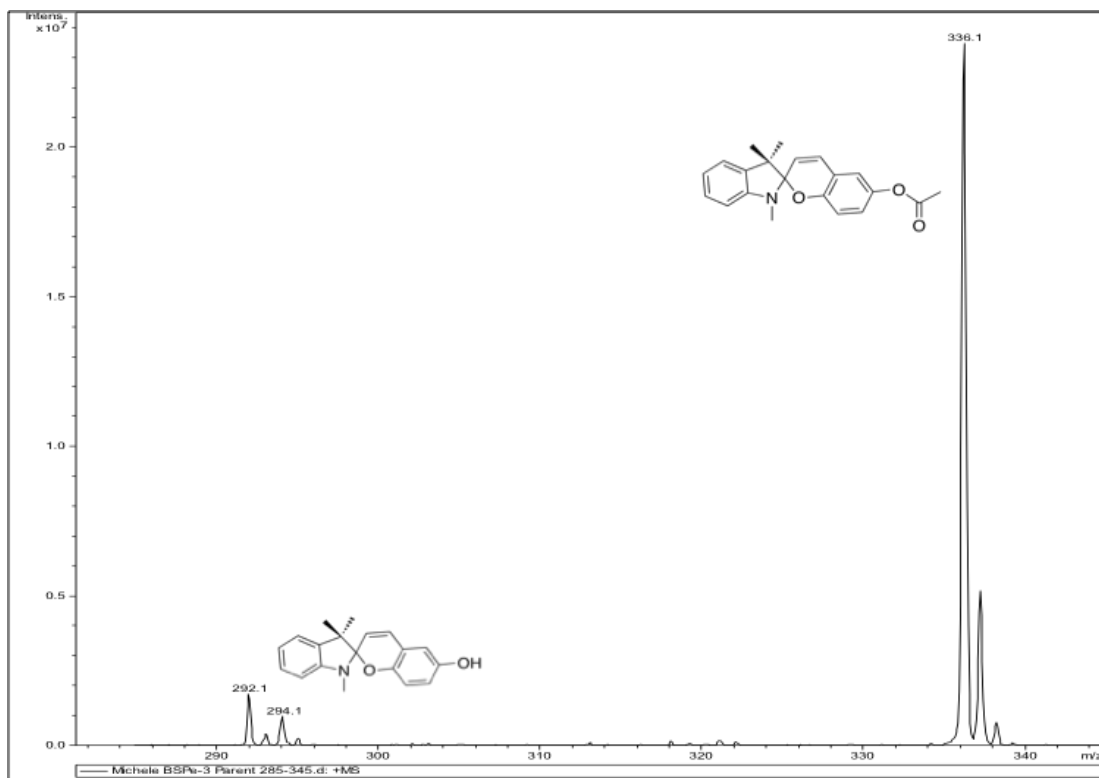


Figure D2: COSY spectra of BSPe using a Bruker 400 MHz in  $\text{CDCl}_3$ .



**Figure D3:** High resolution mass spec of BSPe.

### Synthesis of BSP6 and BSP7

4,4''-Didecyloxy-2,2':5',2''-terthiophene-3'-acetic acid (**AcTTh**) and 4,4''-Didecyloxy-2,2':5',2''-terthiophene-3'-carboxylic acid (**CbTTh**) were synthesized according to the procedure previously reported.<sup>7,42</sup>

1',3',3'-trimethylspiro(chromene-2,2'-indolin)-6-yl-4,4''-bis(decyloxy)-(2,2':5',2''-terthiophene))-3'-acetate (**BSP6**) and 1',3',3'-trimethylspiro[chromene-2,2'-indolin]-6-yl-4,4''-bis(decyloxy)-(2,2':5',2''-terthiophene))-3'-carboxylate (**BSP7**) were synthesized following this procedure: **TTh** (0.09 g, 0.145 mmol), dicyclohexylcarbodiimide (DCC) (0.03 g, 0.143 mmol) and 4-dimethylaminopyridine (0.0013 g, 0.011 mmol) were dissolved in DCM (12 ml) at 0 °C. 1-(2-hydroxyethyl)-3,3-dimethylindoline-6'-hydroxylspiropyran (**BSP5**) (0.04 g, 0.11 mmol) dissolved in DCM (10 ml) was added drop wise over 30 mins to the stirring solution. After **BSP5** was completely added, the reaction mixture was allowed to reach 20 °C. After a further 90 minutes, 50% of the DCM was removed under reduced pressure, cold ether (10 ml) was added to precipitate the urea salt of DCC. This precipitate was removed by filtration and the volume was reduced to give a dark brown oil, which was purified on a silica column, eluting with DCM. The resulting product was a brown-yellowish oil, with a final yield of 74% (0.078 g) for **BSP6** and 72% (0.074 g) for **BSP7**.

Analytical characterization for **BSP6**:  $^1\text{H}$  NMR (400MHz,  $\text{CDCl}_3$ ):  $\delta$  7.127 (m, 1H), 7.07 (1H, s, TTh-H4'), 7.011 (m, 1H), 6.87 (1H, d,  $J = 1.7$  Hz, H3); 6.824 (m, 5H), 6.665 (1H, d,  $J = 8$  Hz, H6), 6.466 (1H, d,  $J = 12$  Hz, H5), 6.251 (d,  $J=8$  Hz, 1H), 6.12 (1H, d,  $J = 1.7$  Hz, H5''), 5.656 (1H, d,  $J = 12$  Hz, H4), 3.94 (m, 4H, 2OCH<sub>2</sub>), 3.77 (2H, BSP-COO-CH<sub>2</sub>), 2.648 (3H, s, N-CH<sub>3</sub>), 1.718 (m, 4H),  $\delta$  1.394 (6H, s, indoline 2xCH<sub>3</sub>), 1.81-0.86 (m, 16CH<sub>2</sub>, 2CH<sub>3</sub>).

$^{13}\text{C}$  NMR (100 MHz):  $\delta$  161.46, 157.74, 157.31, 152.13, 148.15, 143.57, 143.27, 136.68, 135.61, 133.97, 131.69, 128.93, 127.64, 126.73, 126.06, 122.54, 121.81, 121.52, 120.29, 119.42, 119.19, 116.95, 115.64, 106.84, 104.44, 100.44, 97.27, 70.27, 70.28, 51.84, 49.27, 34.95, 33.97, 31.92, 29.73, 29.58, 29.40, 29.35, 29.21, 28.98, 26.04, 25.86, 25.63, 25.47, 24.97, 24.72, 22.72, 20.21, 14.16.

FT-IR (film)  $\nu_{\text{max}}/\text{cm}^{-1}$  2927 (s), 2855 (s), 1761 (s), 1535 (s), 1485 (s), 1467 (m), 1362 (s), 1175 (w), 1111 (s), 1023 (s), 945 (s), 820 (s). Electronic spectrum (Acetonitrile)  $\lambda_{\text{max}}$  nm: 297, 358, 471.

Analytical characterization of **BSP7**:  $^1\text{H}$  NMR (400MHz,  $\text{CDCl}_3$ ):  $\delta$  7.14 (m, 2H), 6.97 (1H, dd,  $J = 4$  Hz, 20Hz, 16Hz), 6.678 (1H, d,  $J = 8$ Hz), 6.714 (m, 3H), 6.60 (1H, d,  $J=8$ Hz), 6.441 (1H, d,  $J=12$ Hz), 6.176 (1H, d,  $J = 1.7$  Hz, H5''), 6.06 (1H, d,  $J = 4$ Hz, H4), 5.60 (1H, d,  $J = 12$  Hz, H4'), 3.94 (m, 4H, 2OCH<sub>2</sub>), 2.648 (3H, s, N-CH<sub>3</sub>), 1.718 (m, 4H), 1.394 (6H, s, indoline 2xCH<sub>3</sub>), 1.81-0.86 (m, 16CH<sub>2</sub>, 2CH<sub>3</sub>).

$^{13}\text{C}$  NMR (100 MHz): 169.5, 168.2, 156.65, 156.6, 151.05, 147.07, 142.41, 135.33, 133.91, 132.17, 131.76, 129.54, 129.09, 128.64, 127.81, 126.58, 125.16, 124.27, 121.21, 120.45, 119.28, 119.09, 118.15, 118.10, 118.05, 117.65, 115.35, 115.24, 114.52, 105.78, 103.37, 97.21, 95.60, 69.25, 69.23, 50.77, 33.84, 30.87, 29.89, 29.28, 28.69, 28.55, 28.37, 28.36, 28.31, 28.20, 27.90, 25.02, 25.00, 24.79, 21.67, 19.13, 13.21. FT-IR (film)  $\nu_{\text{max}}/\text{cm}^{-1}$  2927 (s), 2855 (s), 1737 (s), 1528 (s), 1485 (m), 1375 (s), 1178 (s), 1105 (s), 948 (s). Electronic spectrum (Acetonitrile)  $\lambda_{\text{max}}$  nm: 371, 469, 300.

## D-2 Reagents and Analytical techniques

1-(2-hydroxyethyl)-3,3-dimethylindoline-6'-hidroxylspiropyran (identifier: **BSP5**) was purchased from Acros Organics, and used without further purification. Acetic Anhydride and concentrated sulphuric acid were obtained from Sigma Aldrich, and stored in a dry environment under N<sub>2</sub>. Dry DCM was purchased from Sigma Aldrich, Ireland and used as received. Dicyclohexylcarbodiimide and dimethylaminopyridine

were obtained from Sigma Aldrich, and stored in a desiccator under N<sub>2</sub>. All other solvents were Sigma Aldrich HPLC grade and used as received. Tetrabutylammonium perchlorate (TBAP) was obtained from Sigma Aldrich, Ireland and used without further purification. Optically transparent ITO (Indium Tin Oxide) coated glass were ordered from Delta Technologies, Limited, resistivity R<sub>s</sub> = 4-8 Ω. All other reagents were purchased from Sigma Aldrich, and stored appropriately.

The ultraviolet source for the photoisomerisation processes was a Photo Chemical Reactors LTD (<http://www.photochemicalreactors.co.uk>) 16 W, Hg lamp. The white light was a LMI-6000 LED Illuminator equipped with a double gooseneck fibre optic. UV-vis spectra and spectroelectrochemistry were acquired with a Varian CaryWinUV 50 probe instrument. FT-IR spectra were recorded with a Perkin Elmer Spectrum GX on a solid surface. All electrochemical experiments were performed with a CH-instrument Electrochemical Analyser potentiometer. The <sup>1</sup>H NMR and <sup>13</sup>C NMR experiments were performed using a Bruker 400 MHz by dissolving the samples in CDCl<sub>3</sub> at 298 K. The in house built UV/white light LED array employed has been described elsewhere.<sup>49</sup>

### D-3 Analytical methods for the protonation experiments

For the studies of the kinetic and thermodynamic protonation, 10<sup>-4</sup> M stock solutions of **BSP6** and **BSP7** were prepared in acetonitrile. The volumetric flasks were then wrapped in aluminium foil, bubbled with N<sub>2</sub> and stored in a dark environment. A 10<sup>-1</sup> M stock solution of HCl was prepared in deionised water; the flask was sealed and stored at 293 K.

The protonation over time measurements were performed as follows:

- The absorbance spectrum of each spiropyran solution (3 ml, 10<sup>-4</sup> M) was taken.
- The solution of spiropyran was spiked with 100 μl HCl (10<sup>-1</sup> M), to give a final HCl concentration of 3.2 x 10<sup>-3</sup> M.
- Absorbance spectra were collected with a time frame of 300 s and the analysis of each molecule was run for a maximum time of 3600 s.

The kinetics of protonation were measured according to the following method:

- The UV-vis instrument was set to measure the absorbance at the λ<sub>max</sub> of the protonated MCH of each spiropyran derivative and the spontaneous formation of the thermodynamically favoured protonation **BSP+H<sup>+</sup>⇒MCH<sup>+</sup>** was measured at 5 K increments from 283 to 303 K over a period of 1 hour (5 acquisitions for each derivative, n = 3).

- The samples (3.2 ml) were placed in a thermostatically controlled UV-vis cuvette and 100  $\mu$ l  $10^{-1}$  M HCl added to give a final HCl concentration of  $3.2 \times 10^{-3}$  M. The samples were stirred continuously for the entire duration of the experiment..
- Each experiment was stopped after 60 minutes.

The reversibility tests were studied using the following procedure:

- A quartz cuvette containing 3 ml of spiropyran ( $10^{-4}$  M) solution was placed in the UV-Vis spectrophotometer and the temperature thermostatted at 293 K.
- An in-house fabricated dual wavelength UV ( $\lambda_{\text{max}} = 365$  nm) and white light ( $\lambda > 470$  nm) LED array light source<sup>49</sup> was attached at the top of the cuvette with the minimum space necessary for the pipette tip containing the acid solution to pass. This arrangement fixes the source/sample distance over the entire set of experiments, and allows the samples to be illuminated at the selected wavelength from above.
- After the addition of the acid solution (same concentration and volume as per the kinetics experiments), the spectra were gathered for 1hr.
- Every 10 minutes, the illuminating wavelength was alternately changed from UV to white light and a spectrum collected.

## D-4 Kinetics of protonation

To determine the kinetics of protonation for **BSPe**, **BSP6** and **BSP7** the following processes were studied at 293 K in acetonitrile in the presence of HCl ( $3.2 \times 10^{-3}$  M):

- Rate of formation of **MCH<sup>+</sup>** from **BSP** induced solely by the presence of acid in the same chemical environment in the dark.
- Rate of formation of **MCH<sup>+</sup>** from **BSP** facilitated by illumination at 365 nm in presence of acid.
- Rate of reversion of **MCH<sup>+</sup>** to **BSP**, under white light illumination.

These experiments, along with the other de-activation results here presented, were facilitated by the in-house built LED system.<sup>49</sup> The light can be independently switched by an external command: once the device is immobilized on top of the cuvette (constant illumination path length in both the conditions and for all the solutions), the operator can remotely decide which type of light (UV or VIS) illuminates the solution and therefore which process will be triggered.

## D-5 Kinetics and thermodynamic analysis

The thermal formation first order kinetic curves were modelled using equation (D1):

$$\ln \frac{[A]}{[A_0]} = -kt \quad (D1)$$

Where,  $[A]$  = absorption at time  $t$ ,  $[A_0]$  = absorption at 0 seconds,  $k$  = rate constant and  $t$  = time (s).

The Arrhenius equation (D2) was used to plot the linear temperature dependence of the rate constant for **BSP+H<sup>+</sup>⇒MCH<sup>+</sup>** thermal formation and estimate the activation energy ( $E_a$ ) and the pre-exponential factor  $A$ .

$$\ln k = E_a / RT + \ln A \quad (D2)$$

where  $k$  = rate constant ( $s^{-1}$ ),  $E_a$  = Activation energy ( $kJ mol^{-1}$ ),  $R$  = gas constant ( $J mol^{-1} K^{-1}$ ),  $T$  = temperature (K) and  $A$  = pre-exponential factor ( $s^{-1}$ ).

Following the generalised **BSP+H<sup>+</sup>⇒MCH<sup>+</sup>** system, the Eyring equation (D3) was used to determine the thermodynamic properties of the transition state equilibrium of activation ( $K^\ddagger$ ), entropy of activation ( $\Delta S^\ddagger$ ), and the enthalpy of activation ( $\Delta H^\ddagger$ ). A derivative of this equation, eqn (D4), can be used to derive the equilibrium of activation ( $K^\ddagger$ ):<sup>50-52</sup>

$$\ln(k / T) = -\Delta H^\ddagger / RT + \ln(k / h) + \Delta S^\ddagger / R \quad (D3)$$

$$k = (k_B T / h) K^\ddagger \quad (D4)$$

where  $k$  = rate constant of the forward reaction,  $T$  = temperature (K),  $\Delta H^\ddagger$  = enthalpy of activation,  $\Delta S^\ddagger$  = entropy of activation,  $R$  = gas constant,  $k_B$  = Boltzmann constant and  $h$  = Planck's constant.

Thermodynamic activation properties such as  $\Delta S^\ddagger$ ,  $\Delta H^\ddagger$  and  $K^\ddagger$  for each MCH<sup>+</sup> derivative were calculated using the Eyring equation. Equation (D5) was used to calculate the Gibbs free energy of activation ( $\Delta G^\ddagger$ ).

$$\Delta G^\ddagger = \Delta H^\ddagger - T \Delta S^\ddagger \quad (D5)$$

where  $\Delta G^\ddagger$  = Gibbs free energy of activation ( $kJ mol^{-1}$ ),  $\Delta H^\ddagger$  = enthalpy of transition state ( $kJ mol^{-1}$ ),  $T$  = temperature (K) and  $\Delta S^\ddagger$  = entropy of the transition state ( $J K^{-1} mol^{-1}$ ).

## D-6 Electropolymerization and Electrochemical experiments

**pBSP6** and **pBSP7** films were electrochemically grown on optically transparent ITO (Indium Tin Oxide) coated glass (Delta Technologies, Limited, resistivity  $R_s = 4-8 \Omega$ ) by cyclic voltammetry from a solution in acetonitrile containing 0.1 M Tetrabutylammonium perchlorate (TBAP) and the monomers at a concentration of 8 mM. Pt mesh and Ag/Ag<sup>+</sup> electrodes were used as the counter electrode and quasi-reference electrode, respectively. The half-wave potential was measured for 1 mM ferrocene,  $E_{1/2} = 0.165$  V, vs. Ag/AgCl reference electrode. Solutions were degassed prior the measurements. Cyclic voltammetry experiments were performed on electrochemically grown films on the ITO immersed in a  $10^{-1}$  M solution of TBAP in dry acetonitrile.

## D-7 Conductivity measurement

4 point resistivity meter (JANDEL Model RM2), with spacing in square array 0.635 mm, was used in conductivity measurements. **pBSP6** and **pBSP7** was electrochemically grown on optically transparent ITO-coated glass by chronoamperometric deposition at constant potential 0.8 V during 1 hour. The polymer was than peeled off the electrode and the conductivity measurement was performed on the freestanding film.

## D-8 Electrochemistry and spectroelectrochemistry of BSPe

For cyclic voltammetry (CV) measurements a  $10^{-4}$  M solution of **BSPe** was prepared in a 0.1 M solution of TBAP in acetonitrile. 10 ml of this solution were placed in an electrochemical cell equipped with an Ag/Ag<sup>+</sup> electrode (reference electrode), a Pt minigrad (counter electrode) and a Pt wire (working electrode). In situ spectroelectrochemical measurements were performed using a quartz cuvette, covered with a Teflon cap equipped with a Pt mini grid working and auxiliary electrode and Ag wire as pseudo reference electrode. The solution was an aliquot of the same stock used for the CV.

## D-9 UV-vis spectroelectrochemistry of the polymers

In situ spectroelectrochemical measurements were performed using a quartz cuvette covered with a customized Teflon cap equipped with a Pt mini grid counter electrode and Ag wire pseudo reference electrode. The potential was held at the indicated voltage for three minutes while the spectra were obtained.

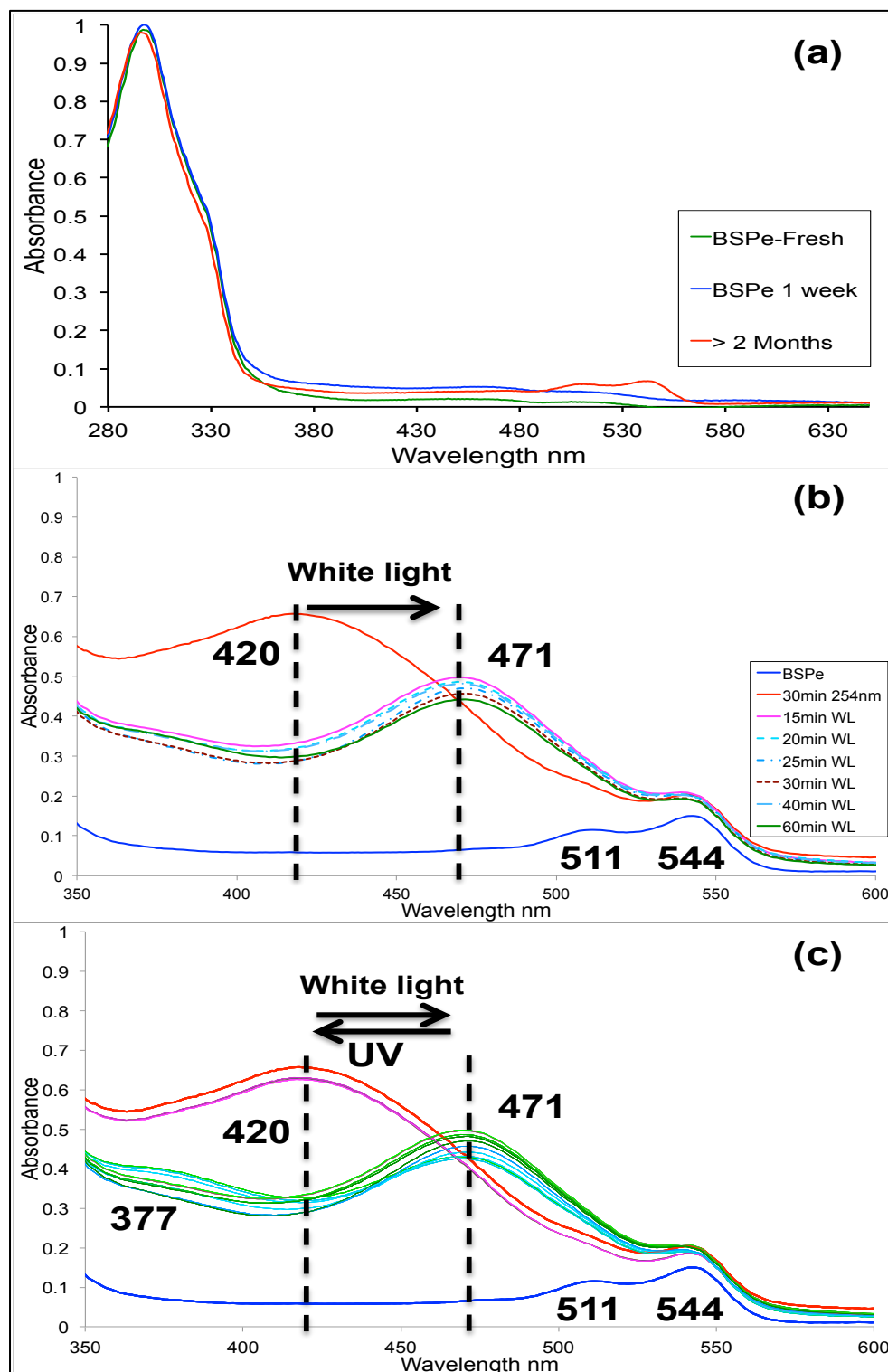
## **D-10 Photochemistry of pBSP6 and pBSP7**

The polymer films were analysed as follows: 3 freshly prepared films of each material were reduced at -400 mV. Each sample was soaked in acetonitrile in a quartz cuvette and the spectrum was acquired. The polymer film inside the cuvette was illuminated with a 254 nm UV light for 60 minutes and the relative spectrum obtained. The substrate was then exposed to the white light source and a spectrum obtained every 15 minutes. The same procedure was repeated for all the films.

## **D-11 Atomic force microscopy (AFM) and scanning electron microscopy (SEM)**

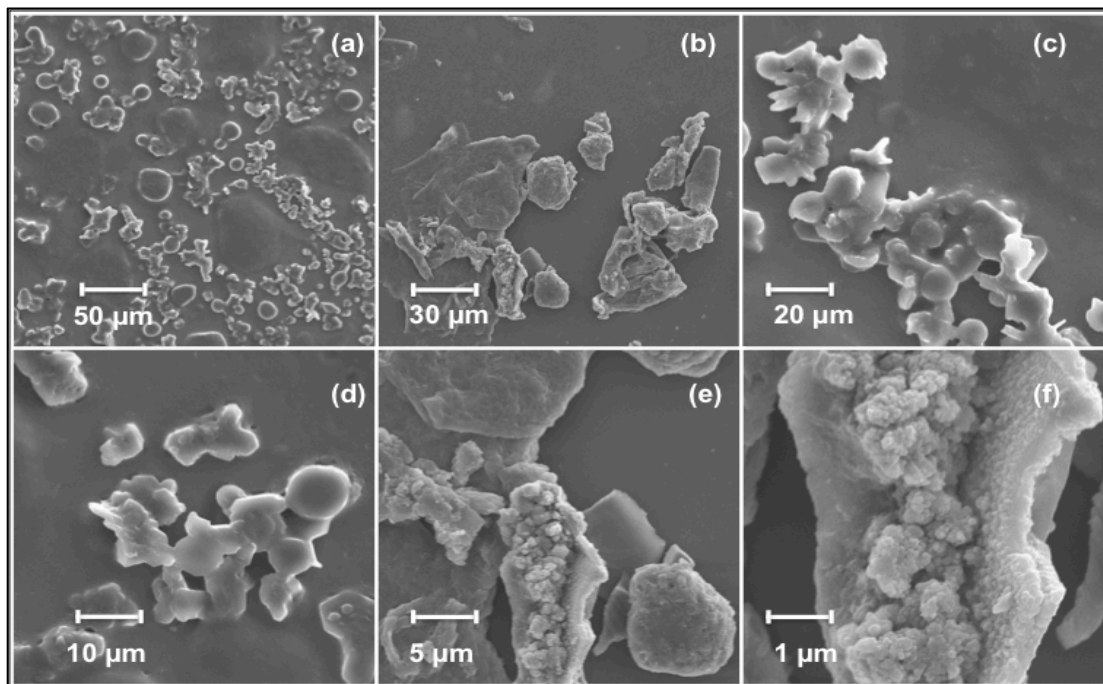
**pBSP6** and **pBSP7** films for SEM and AFM analysis were electrodeposited on ITO by applying a constant potential (0.8 V) for 1 minute and then oxidized or reduced at different constant potentials as described in the text. A Jeol7500 field emission scanning electron microscope (FESEM) was used for the SEM experiments. AFM images of the polymer films were obtained with a JPK Nanowizard®II BioAFM (JPK Instruments, Germany). AC mode images were taken in air using NSC MikroMasch silicon nitride cantilevers ( $k \approx 40$  N/m).

## D-12 UV-vis Characterization of BSPe $10^{-4}$ M in Acetonitrile



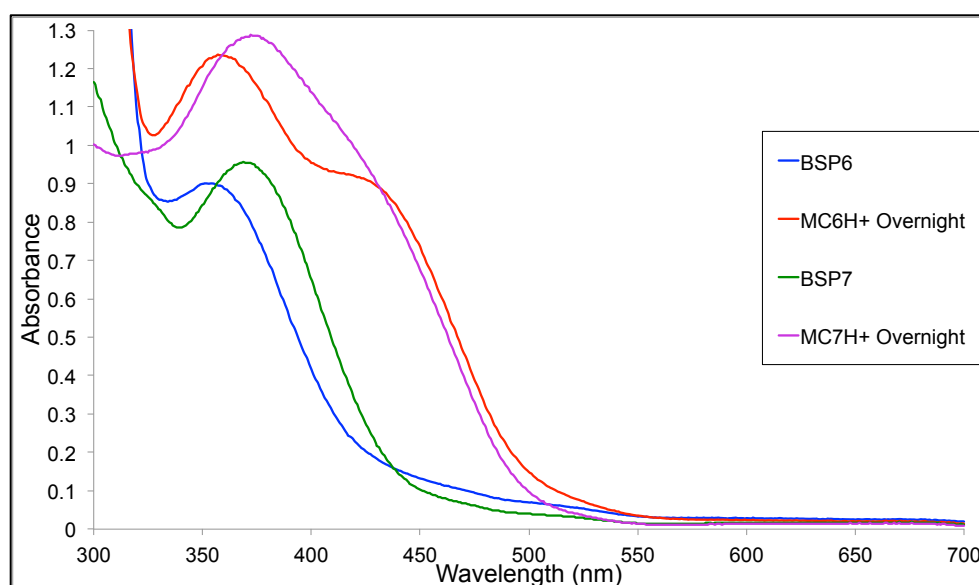
**Figure D4:** (a) UV-vis monitoring of the progressive formation of BSPe aggregates from a  $10^{-4}$  M solution in Acetonitrile over time. (b) UV-vis switching experiment on BSPe  $10^{-4}$  M solution in Acetonitrile. BSPe (blue line); MCE (red line) generated after 15 minutes of 254 nm UV light; resulting MCE-aggregates (pink line) after 15 minutes of white light illumination; dashed lines and the solid green line are the resulting white light induced irreversible aggregated species. (c) Repeated cycles of 254 nm UV light and white light (30 cycles x 5 minutes each) on a  $10^{-4}$  M solution of BSPe in acetonitrile at room temperature.

## D-13 UV-vis Overnight Protonation of BSP6 and BSP7 $10^{-4}$ M in Acetonitrile



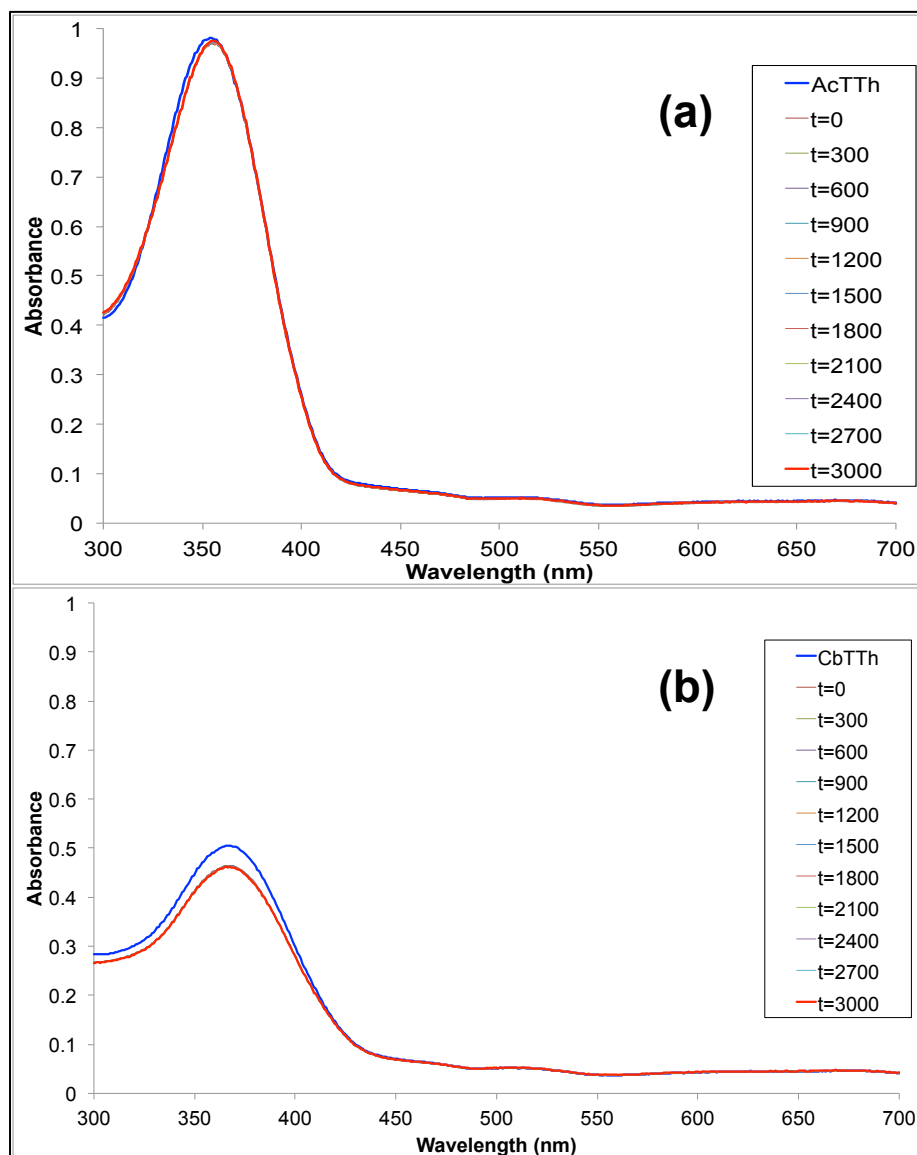
**Figure D5:** (a)-(f) Different SEM magnification of **BSPe** aggregates all formed upon illumination with UV light (254 nm) and white light (5 minutes each) of a  $10^{-4}$  M solution in acetonitrile. The samples were dried under white light illumination and  $N_2$  flow for 30 minutes at room temperature.

## D-14 UV-vis Overnight Protonation of BSP6 and BSP7 $10^{-4}$ M in Acetonitrile

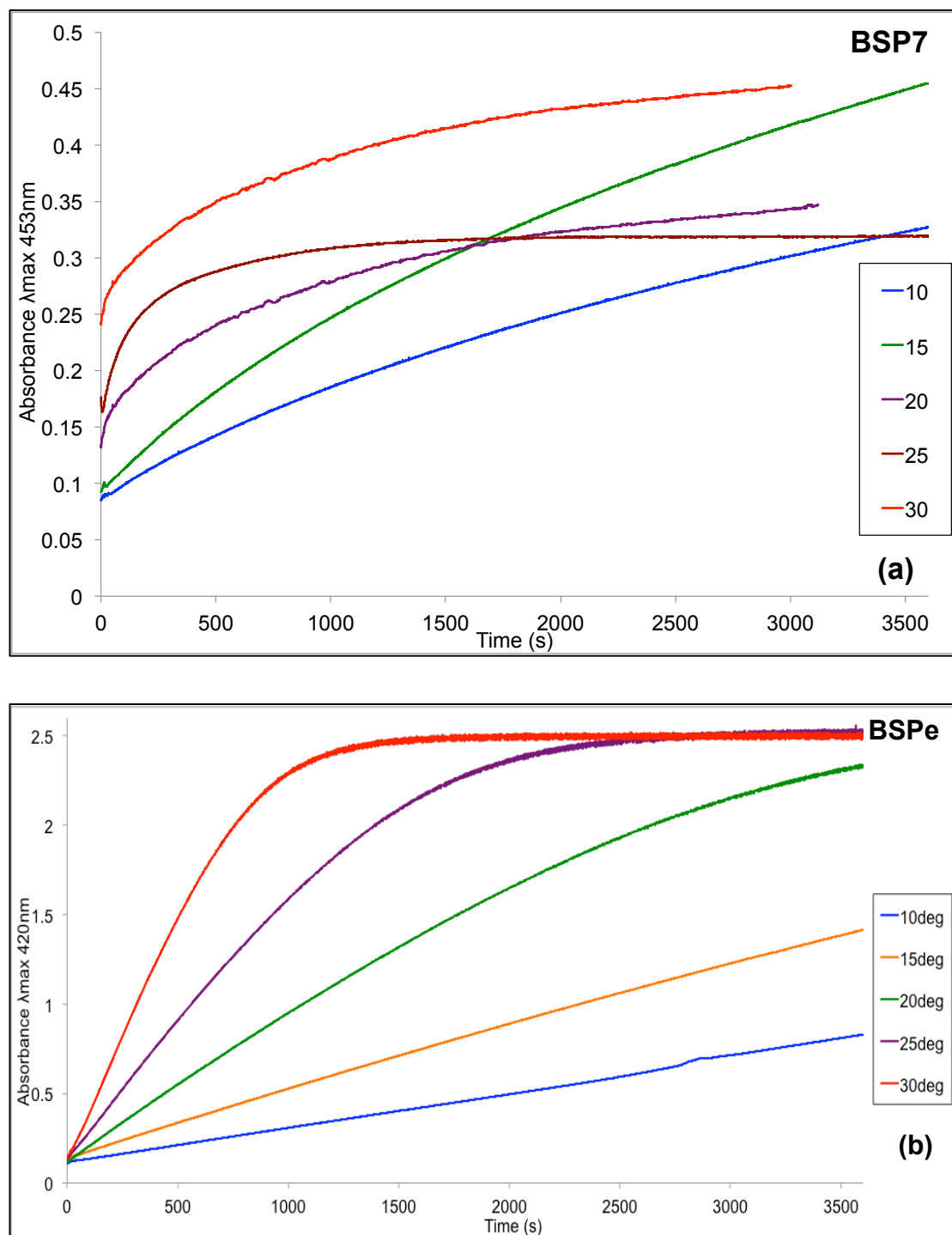


**Figure D6:** Overnight protonation study of 3 ml  $10^{-4}$  M solutions of **BSP6** and **BSP7** with addition of 100  $\mu$ l of HCl (0.1 M).

## D-15 Protonation Experiment of AcTTh and CbTTh



**Figure D7:** Protonation study of the free standing monomers **AcTTh** and **CbTTh** both diluted up to  $10^{-4}$  M in Acetonitrile and added of  $100\mu\text{l}$  of  $\text{HCl}$  0.1 M.

**D-16 Kinetics of Protonation for BSP7 and BSPe**

**Figure D8:** (a) Kinetics of protonation in the range of temperature of 283-303 K of BSP7. (b) Kinetics of protonation in the range of temperature of 283-303 K of BSPe

## D-17 UV-vis Spectral Response at Constant Wavelength of pBSP6, pBSP7 and pAcTTh

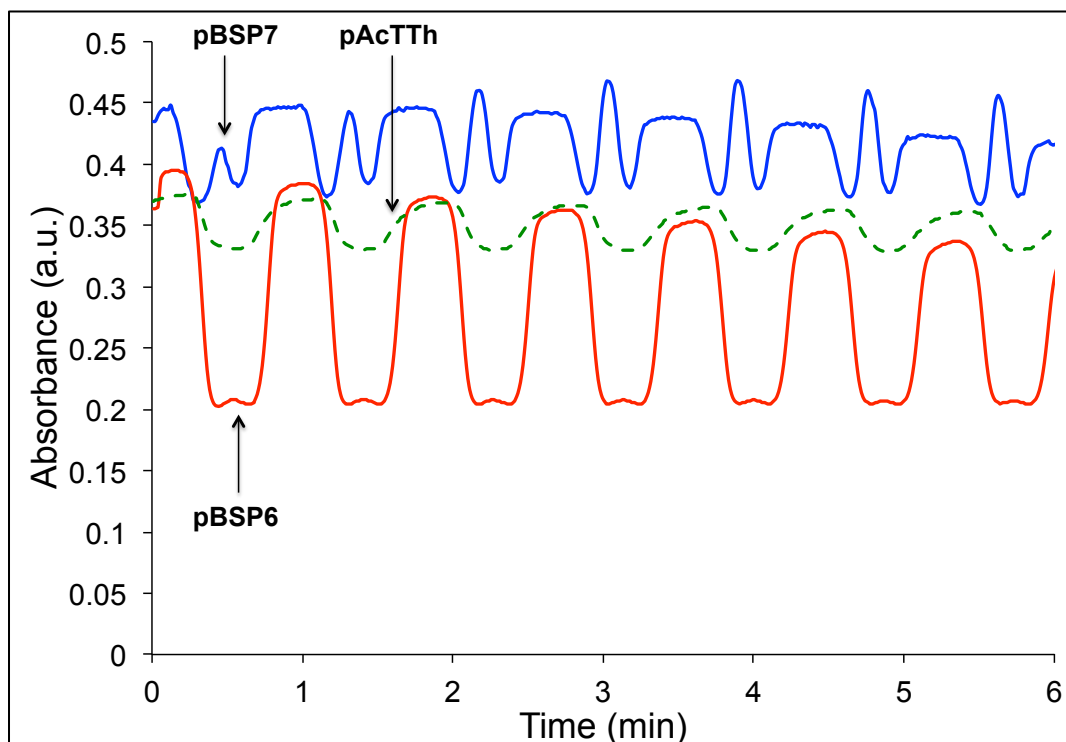


**Figure D9:** UV-vis spectra obtained at constant wavelength for pBSP6 ( $\lambda_{\max}$  508 nm), pBSP7 ( $\lambda_{\max}$  510 nm), and pAcTTh ( $\lambda_{\max}$  569 nm) electrochemically polymerized on ITO by cyclic voltammetry from 0 V to 0.75 V in 0.1 M TBAP in Acetonitrile. The potential was cycled between -0.4 V and +1 V.

## D-18 Photochemical Actuation of pBSP6

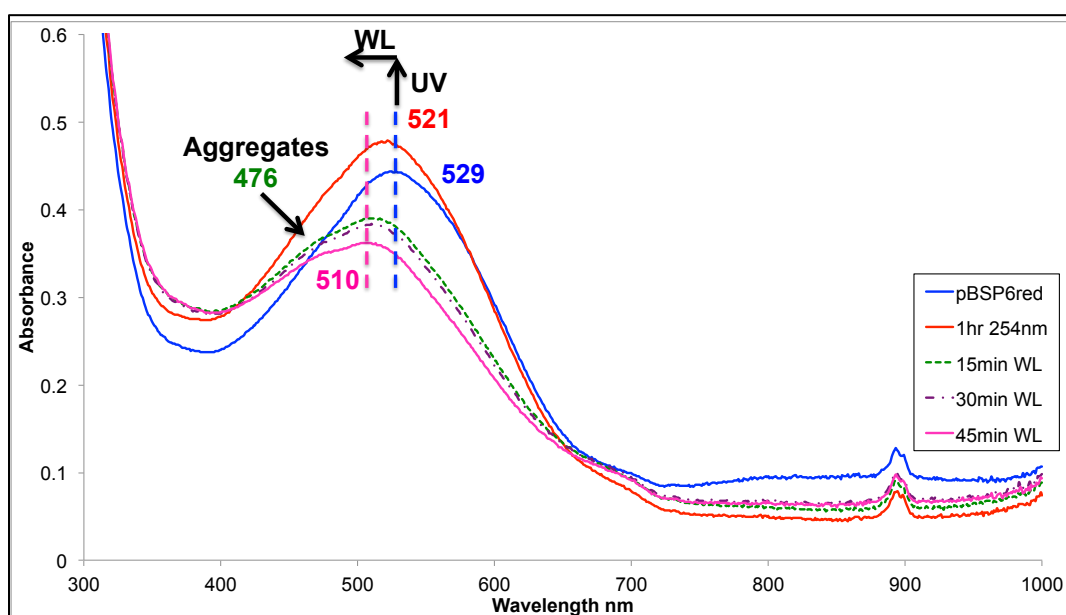


**Figure D10:** Photo-Actuation of pBSP6 (red line) after illumination with a 254 nm UV lamp and back isomerization process (dashed lines and solid pink line) induced by white light illumination.

## D-19 SEM Pictures of pBSP7

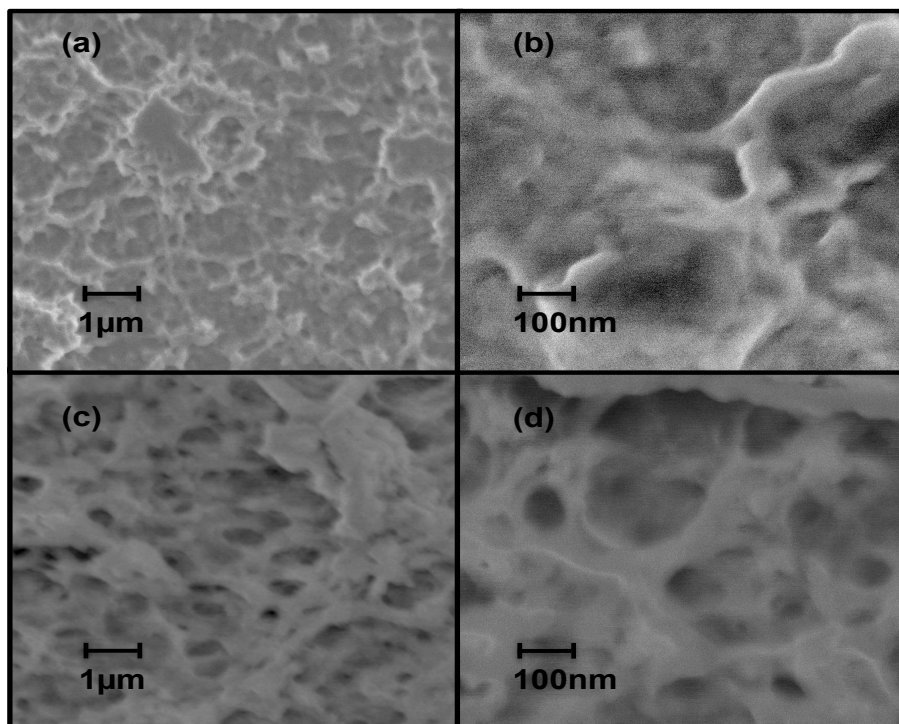


**Figure D11:** SEM pictures of **pBSP7** after stimulation at constant potential, at -0.4 V for 3 minutes (a) and (b) and at +1.0 V (c) and (d) for 3 minutes.

## D-20 AFM Pictures of pBSP7

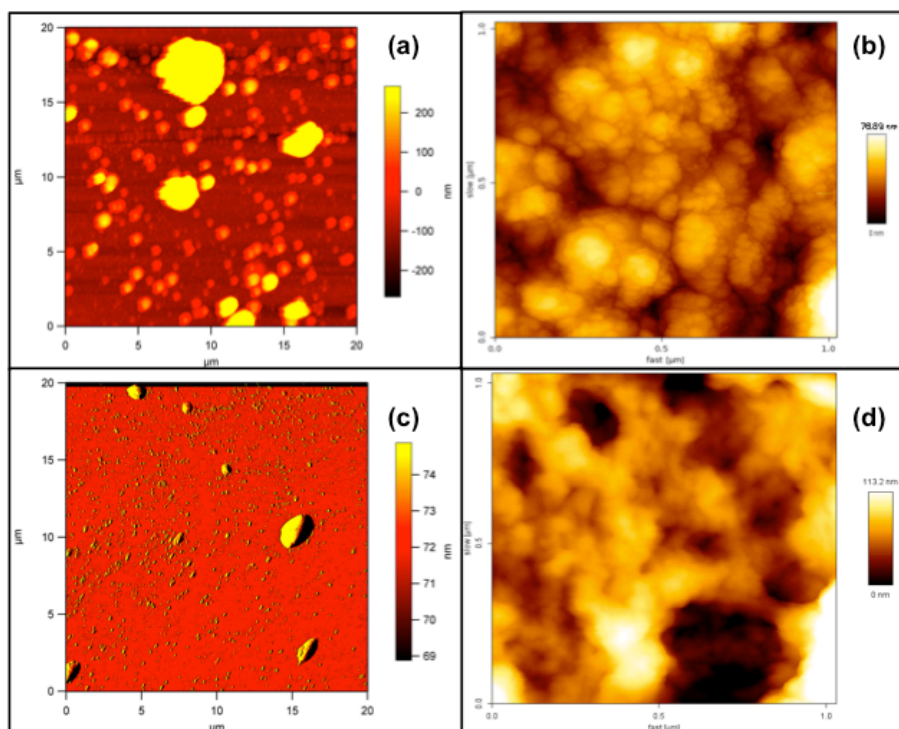


**Figure D12:** AFM pictures of **pBSP7** after stimulation at constant potential, at -0.4 V for 3 minutes (a) and (b) and at +1.0 V for 3 minutes (c) and (d).